Appendixes A through G are supplemental to *NCHRP Research Report 1018: Zone of Intrusion Envelopes Under MASH Impact Conditions for Rigid Barrier Attachments* (NCHRP Project 22-34, "Determination of Zone of Intrusion Envelopes under MASH Impact Conditions for Barrier Attachments"). The full report can be found by searching on the report title on the National Academies Press website (www.nap.edu).

## Appendix A. Crash Test Database

# Table A-1. Crash Test Database

| Barrier | Ref. no. | Report no. | | Test information | | | | Test conditions | | | | Suspension damage | Tire deflation | Deflection | | ZOI (in.) (ms) | Vehicle ZOI component |
|---|---|---|---|---|---|---|---|---|---|---|---|---|---|---|---|---|---|
| | | | | Agency Test no. | Article | Barrier height (in.) | MASH designation no. | Impact point | Impact speed (mph) | Impact angle (deg) | IS value (kip-ft) | | | Dynamic (in.) | Working width (in.) | | |
| Jersey | 1 | TRP-03-177-06 | Performance Evaluation of the Permanent New Jersey Safety Shape Barrier - Update to NCHRP 350 Test No. 3-10 | MwRSF 2214-NJ-1 | Jersey PCB | 32 | 3-10 | 221.7 in. DS of US end | 60.3 | 26.1 | 56.8 | None | RF | N/A | 19.1 | N/A | RF hood |
| | 2 | 13th International LS-DYNA Users Conference | Crash Test and Simulation Comparisons of a Pickup Truck and Small Car Oblique Impacts into a Concrete Barrier | TTI RF 476460-1 | Jersey barrier | 32 | 3-11 | N/A | 62.6 | 25.2 | 119.9 | Unknown | Unknown | 0 | 0 | N/A | RF fender and side |
| | 3 | NCHRP22-20(2) Final Report | Design Guidelines for Test Level 3 (TL-3) Through Test Level 5 (TL-5) Roadside Barrier Systems Placed on Mechanically Stabilized Earth (MSE) Retaining Wall | TTI 478130-1 | Barrier atop MSE retaining wall | 42 | 5-12 | 37.5 ft DS of US end | 49.4 | 15.1 | 438.3 | Unknown | Unknown | N/A | 180 | N/A | RF of cab, RS of trailer |
| | 4 | FHWA TX-13 0-6646-1 | Signs on Concrete Median Barriers | TTI 466462-1 | Spread tube sign support on median barrier | 32 | 3-11 | 42.5 in. US of support | 61.6 | 25 | 114.4 | Right upper/lower ball joints and A-arms, the right frame rail, left rear U-bolts, and drive shaft deformed | RF | 0 | 0 | 20.4 | RF hood |
| | | | | TTI 466462-2a | Bracket and sacrificial pin sign support on median barrier | 32 | 3-11 | 34.2 in. US of sign support | 63.2 | 25 | 119.1 | Right upper/lower ball joints and A-arms, and right frame rail deformed | RF, RR, LR | 0 | 0 | 14.2 | RF hood |
| | | | | TTI 466462-3 | Chute channel sign support on median barrier | 32 | 3-11 | 34.7 in. US of support | 62.9 | 24.4 | 118.8 | RF frame rail and right upper/lower A-arms deformed | RF | 0 | 0 | 25.9 | RF hood |
| | | | | TTI 466462-4 | Slotted 10 BWG sign Support on median barrier | 32 | 3-11 | 43.0 in. US of support | 62.5 | 25.8 | 124 | RF upper/lower A-arms and right frame rail deformed | RF | 0 | 89 | 20.6 | RF hood |
| | 5 | 401761-SBG1 | MASH Test 5-12 of the Schock ComBAR Parapet | TTI 401761-SBG1 | Schock ComBAR parapet | 41.3 | 5-12 | 33.5 ft DS of US end | 50.5 | 15.6 | 488.4 | None | No | N/A | 108 | N/A | RF of cab, RS of trailer |
| | 6 | TRP-03-224-10 | Dynamic Evaluation of a Pinned Anchoring System for New York State's Temporary Concrete Barriers - Phase II | MwRSF NYTCB-5 | Pinned temporary barrier | 32 | 3-11 | 4 ft - 3.2 in. US of CL of joint 4-5 | 64.3 | 26.2 | 138 | Right rear tire disengaged | No | 20.5 | 32.5 | N/A | RS |
| | 7 | 510605-RYU1 | MASH Test 5-12 on the Ryerson/Pultrall Parapet | TTI 510605-RYU1 | Ryerson/Pultrall parapet | 41.3 | 5-12 | 36 in. US of joint | 49.1 | 14.6 | 407.9 | Front axle and tie rods, RF spring, U-bolts, and shock, right frame rail deformed | RF | 0 | 54 | N/A | RS of cab, RS of trailer |
| | 8 | b226 | FHWA Eligibility Letter b226 | PTI 2011_11 | Conti Enterprises half-shaped bridge rail | N/A | 3-11 | 5.1 ft from the joint 3-4 | 61 | 24.1 | 102.5 | Unknown | Unknown | 0.5 | N/A | N/A | Unknown |
| | 9 | TRP-03-338-17 | Performance Evaluation of New Jersey's PCB with a Pinned Configuration and Grouted Toes | MwRSF NJPCB-1 | PCB with pinned configuration and grouted toes | 32 | 3-11 | 49 1/16 in. US of joint 4-5 | 62.6 | 24.7 | 114.9 | LF (impact) tire disengaged | No | 13.5 | 37.5 | 11.7 (100) | Hood |
| | 10 | TRP-03-340-17 | Performance Evaluation of New Jersey's PCB with a Bolted Configuration and Grouted Toes | MwRSF NJPCB-2 | PCB with bolted configuration and grouted toes | 32 | 3-11 | 45 13/16 in.US of joint 4-5 | 62.6 | 24.5 | 112.6 | None | LF | 4.9 | 24 | 10.2 (76) | Grille and bumper |
| | 11 | TRP-03-373-17 | Performance Evaluation of New Jersey's PCB with a Back-Side Pinned Configuration and Grouted Toes | MwRSF NJPCB-6 | PCB with back-side pinned configuration and grouted toes | 32 | 3-11 | 45 11/16 in. US of joint 4-5 | 62.9 | 25.1 | 119 | LF (impact) wheel partially disengaged | No | 15.2 | 41 | 20.6 (106) | Hood |
| | 12 | TRP-03-374-17 | Performance Evaluation of New Jersey's PCB with a Traffic-Side Pinned Configuration and Grouted Toes | MwRSF NJPCB-7 | PCB with traffic-side pinned configuration and grouted toes | 32 | 3-11 | 46.4 in. US of joint 4-5 | 62.8 | 25.2 | 119.5 | None | LF | 11.4 | 35.4 | 16.7 (98) | Hood |
| F-shape | 13 | 510602-JJH8 | MASH Test 3-11 on the Easi-Set Industries J-J Hooks/MASH Proprietary Barrier Pinned to Asphalt | TTI 510602-JJH8 | Median barrier | 32 | 3-11 | 4.6 ft US of joint 8-9 | 63 | 24.6 | 114.5 | Left frame rail and upper/lower A-arms deformed | LF | 8.8 | 32 | N/A | LF |
| | 14 | 510602-JJH9 | MASH Test 3-11 on the Easi-Set Industries J-J Hooks/MASH Proprietary Bolt-Down Barrier System | TTI 510602-JJH9 | Median barrier | 32 | 3-11 | 4.1 ft US of joint 3-4 | 62.5 | 25 | 114.5 | Left frame rail and upper/lower A-arms deformed | LF | 5.9 | 27.5 | N/A | LF |

Table A-1. Crash Test Database (continued)

| Barrier | Ref. no. | Report no. | | Test information | | | | Test conditions | | | | Suspension damage | Tire deflation | Deflection | | ZOI (in.) (ms) | Vehicle ZOI component |
|---|---|---|---|---|---|---|---|---|---|---|---|---|---|---|---|---|---|
| | | | | Agency Test no. | Article | Barrier height (in.) | MASH designation no. | Impact point | Impact speed (mph) | Impact angle (deg) | IS value (kip-ft) | | | Dynamic (in.) | Working width (in.) | | |
| F-shape | 15 | 690900-IND2 | MASH Test 3-11 of the Indiana Anchored Temporary Concrete Barrier with Wedge Anchor Studs | TTI 690900-IND2 | Indiana anchored temporary barrier with wedge anchor studs and modified top connectors | 31 | 3-11 | 4.7 ft US of joint 8-9 | 62.7 | 25.3 | 121.1 | Both impact-side tires partially disengaged | No | 11.9 | 28.1 | N/A | LS |
| | 16 | 690900-IND3 | MASH Test 3-11 of the Indiana Anchored Temporary Concrete Barrier with Wedge Anchor Studs and Modified Top Connection | 690900-IND3 | Indiana anchored temporary barrier with wedge anchor studs and modified top connectors | 31 | 3-11 | 43 in. US of joint 8-9 | 62.5 | 26.1 | 126.9 | LS tires and rims, left lower A-arm, and LR U-bolts, springs, and doors damaged | LF | 13.3 | 30.1 | N/A | LS |
| | 17 | TRP-03-386-19 | Crash Testing Evaluation of the WisDOT Tied-Down Portable Concrete Barrier | MwRSF WITD-1 | WISDOT anchored PCB | 32 | 3-11 | 44.3 in. US of joint 8-9 | 62.0 | 25.6 | 119.7 | RR (impact) tire disengaged | RF | 14.3 | 36.8 | 14.9 (74) | Hood |
| | 18 | FHWA TX-17 0-6946-1 | MASH Evaluation of TxDOT Roadside Safety Features - Phase I | TTI 469467-5-1 | TxDOT CSB(7)-10 pinned to concrete | 32 | 3-11 | 4.4 ft US of joint 2-3 | 63.5 | 24.8 | 119.4 | RR (impact) tire partially disengaged | RF | 24.6 | 42.5 | N/A | RS |
| Single-slope | 19 | NCHRP22-20(2) Final Report | Design Guidelines for Test Level 3 (TL-3) Through Test Level 5 (TL-5) Roadside Barrier Systems Placed on Mechanically Stabilized Earth (MSE) Retaining Wall | TTI 478130-2 | TL-4 MSE wall | 36 | 4-12 | 60 in. US of joint 5-6 | 58.5 | 15.2 | 173.3 | Unknown | Unknown | 0.9 | N/A | N/A | LS of box |
| | 20 | TRP-03-356-16 | Development of the Manitoba Constrained-Width, Tall Wall Barrier | MwRSF MAN-1 | Manitoba constrained width, tall wall bridge rail | 49.25 | 5-12 | 18.1 in. US of open joint | 51.7 | 15.2 | 490 | LS support beams under trailer deformed | No | 2 | 37.4 | 29.5 | RF of cab, RF of trailer |
| | 21 | CA17-2654 | Compliance Crash Testing of the Type 60 Median Barrier, Test 140MASH3C16-04 | Caltrans 140MASH3C16-04 | CA type 60 median barrier | 36 | 3-10 | 21 ft DS of US end anchor | 61.2 | 25.7 | 58.1 | None | No | 0 | 0 | N/A | N/A |
| | 22 | FHWA TX-15 9-1002-15-3 | Crash Test and Evaluation of Restrained Safety-Shape Concrete Barriers on Concrete Bridge Deck | TTI 490027-2-1 | Single-slope barrier restrained on concrete deck | 42 | 4-12 | 4.7 ft DS of joint 2-3 | 58.6 | 15.6 | 184 | Left frame rail, LF springs and U bolts damaged | LF, LR | 7.1 | 58.7 | 137.5 | LS of cab and box |
| | 23 | FHWA TX-12 9-1002-5 | Determination of Minimum height and Lateral Design Load for MASH Test Level 4 Bridge Rails | TTI 420020-9b | TxDOT single-slope traffic rail | 36 | 4-12 | 24 ft DS of US end | 57.2 | 16.1 | 186.3 | Left frame rail, front axle, front U-bolts and springs, front tie rod, steering rod, LR U-bolts and springs, and drive shaft deformed | RF | 0 | 63.6 | N/A | LS of cab and box |
| | 24 | FHWA TX-17 0-6946-1 | MASH Evaluation of TxDOT Roadside Safety Features - Phase I | TTI 469467-3-1 | TxDOT single-slope barrier with 1-in. ACP overlay | 42 | 4-12 | 25 ft - 2 in. DS of US end | 56.5 | 15.8 | 175 | None | RF | 1 | 72.9 | 154.8 | LS of box |
| | 25 | 405160-13-1 | Development and Testing of a Concrete Barrier Design for use in Front of Slope of MSE Wall | TTI 405160-13-1 | Single-slope barrier offset 2 ft from 1.5H:1V slope | 32 | 3-11 | 62 in. US of joint 2-3 | 63.1 | 24.2 | 110.8 | Right upper A-arm, right tie rod end, and sway bar deformed | No | 5.6 | 19.6 | N/A | RS |
| | 26 | FHWA/TX-11/9-1002-3 | MASH Test 3-11 of the TxDOT Single-slope Bridge Rail (Type SSTR) on Pan-formed Bridge Deck | TTI 420020-3 | TxDOT pan-formed bridge rail | 36 | 3-11 | 5.2 ft US of joint | 63.8 | 24.8 | 120.6 | RS wheels disengaged, right upper/lower ball joints, RF frame rail and upper/lower A-arms, RR axle damaged | Disengaged | 0 | 10 | N/A | RF fender |
| | 27 | b249 | FHWA Eligibility Letter b249 | TTI 510602-EWP1 | Gravix impact wall | 36 | 4-12 | 6 ft DS of barriers 5 and 6 | 57.3 | 15.7 | 176.8 | Unknown | Unknown | N/A | N/A | 101.1 | LS of cab and box |
| | 28 | TRP-03-388-18 | MASH TL-3 Evaluation of the Unreinforced, Single-slope Concrete Median Barrier | MwRSF OSSB-1 | Single-slope barrier | 43 | 3-11 | 51.2 in. US of joint 2-3 | 62.8 | 24.9 | 116.3 | Left frame horn buckled near suspension and LF bumper mount plate bent | LF | 1 | 28 | 10.8 (68) | Hood |
| | 29 | TRP-03-415-19 | Development of a MASH TL-4 Concrete Bridge Rail with Considerations for Future Raodway Overlays | MwRSF 4CBR-1 | TL-4 optimized bridge rail | 36 | 4-12 | 300 in. DS of bridge deck end | 57.6 | 15.975 | 186.3 | Unknown | Unknown | 1 | 53.7 | 55.4 (828) | Back of box |
| | 30 | TTI 0-6946-R2 | MASH Evaluation of TxDOT Roadside Safety Features - Phase 2 | TTI 469468-6-1 | TXDOT 42-in. single-slope median barrier with top-mounted luminaire | 42 | 4-12 | 10.4 ft US of luminaire | 57.2 | 14.5 | 152 | None | No | 0 | 80.5 | N/A | Box |
| | 31 | TRP-03-194-07 | Development of TL-5 Vertical Faced Concrete Median Barrier Incorporation Head Ejection Criteria | MwRSF TL5CMB-2 | Median barrier | 42 | NCHRP 350 5-12 | 30.0 ft DS of US end | 52.8 | 15.4 | 522.9 | Damage to front axle, broken U-bolt axle, RF spring bolts disengaged, damage to shock absorber and RF spring | LF | 1.5 | 74.6 | N/A | RF end of tractor, RS of trailer |

# Table A-1. Crash Test Database (continued)

| Barrier | Ref. no. | Report no. | | Test information | | | | Test conditions | | | | Suspension damage | Tire deflation | Deflection | | ZOI (in.) (ms) | Vehicle ZOI component |
|---|---|---|---|---|---|---|---|---|---|---|---|---|---|---|---|---|---|
| | | | | Agency Test no. | Article | Barrier height (in.) | MASH designation no. | Impact point | Impact speed (mph) | Impact angle (deg) | IS value (kip-ft) | | | Dynamic (in.) | Working width (in.) | | |
| Vertical | 32 | TRP-03-220-09 | Development and Testing of New Vertical-Faced Temporary Concrete Barrier for Use on Composite Panel Bridge Decks | MwRSF KSFRP-1 | Temporary barrier on FRP composite bridge deck | 32 | 3-11 | 4 ft - 3.3 in. US of joint 2-3 | 61.1 | 25.9 | 119.3 | Right upper control arm fractured, RF steel rim severely deformed with tears and significant crushing | No | 4.4 | 20.4 | N/A | LF hood |
| | 33 | FHWA TX-15 9-1002-15-5 | Crash Test and Evaluation of the TxDOT T224 Bridge Rail | TTI 490025-2-2 | TxDOT 224 bridge rail | 42 | 5-10 | 4.2 ft US of post no. 4 | 62.6 | 25.1 | 57 | RF strut and tower deformed | No | None | 16.5 | N/A | N/A |
| | | | | TTI 490025-2-3 | | 42 | 5-11 | 3.9 ft DS of post 3 | 64.3 | 24.8 | 123 | RF rail and RF upper/lower A-arms, and right upper/lower ball joints deformed | No | None | 16.5 | N/A | RF hood |
| | | | | TTI 490025-2-1 | | 42 | 5-12 | 2.0 ft DS of joint | 50.5 | 14.1 | 404 | Front axle pushed rearward, right tie rod and U-bolts and RF shock and mount deformed | No | 2.1 | 38.5 | N/A | RF hood, LS of trailer |
| | 34 | FHWA TX-14 9-1002-12-13 | MASH Test 3-11 of the TxDOT T222 Bridge Rail | TTI 490024-2-1 | TxDOT T222 bridge rail | 32.75 | 3-11 | 51 in. US of splice 1-2 | 64.4 | 25.5 | 129.8 | None | No | 2.1 | 13.2 | None | LF hood |
| | 35 | FHWA TX-17 0-6946-1 | MASH Evaluation of TxDOT Roadside Safety Features - Phase I | TTI 469467-1-1 | TxDOT vertical wall | 36 | 4-12 | 5 ft US of expansion control joint | 55.5 | 15 | 154 | None | RF | 2.2 | 67 | 104.6 | LS box |
| | 36 | FHWA-RD-96-199 | NCHRP Report 350 Compliance Test 5-12 of the 1.07-m Vertical Wall Bridge Railing | TTI 405511-2 | Vertical Wall bridge rail | 42 | NCHRP 350 5-12 | 17.4 ft DS of US end | 49.8 | 14.5 | 428.7 | U-bolts and shocks damaged | RF | 0 | N/A | N/A | RS of trailer |
| | 37 | 475350-1 | Design of Roadside Barrier Systems Placed on MSE Retaining Walls | TTI 475350-1 | TxDOT type T211 | 32 | 3-11 | 4.3 ft US of 4th joint | 63.2 | 25.6 | 123.4 | Left upper A-arm, left outer tie rod end, left frame rail and rear axle deformed and left upper ball joint broken | LF | 0.8 | 0 | N/A | LF fender, LS cab and tailgate |
| | 38 | Eligibility Letter b285 | FHWA Eligibility Letter b285 | TTI 607451-1 | Pulaski skyway bridge parapet | 44 | 4-12 | 5.1 ft US of open joint | 57.4 | 15.3 | 169 | Unknown | Unknown | 4.4 | 20.1 | N/A | LF of cab and box |
| | | | | TTI 607451-2 | | 44 | 4-11 | 4.2 ft US of open joint | 62.5 | 24 | 109 | Unknown | Unknown | 1 | 17 | N/A | LF of cab |
| | | | | TTI 607451-3 | | 44 | 4-10 | 4.2 ft US of open joint | 62.5 | 25 | 57 | Unknown | Unknown | 0.5 | 16.5 | N/A | N/A |
| | 39 | FHWA TX-12 9-1002-7 | MASH Test 3-11 on the 5-Inch Cast in Place Deck Barrier Anchors | TTI 420021-5 | TxDOT 5-in. CIPD barrier anchors, T223 open bridge rail | 32 | 3-11 | 54.5 in. US of expansion joint | 62.5 | 26.3 | 119.7 | RF (impact) wheel disengaged | No | 0.9 | 16 | N/A | RF hood |
| | 40 | TTI 0-6946-R2 | MASH Evaluation of TxDOT Roadside Safety features - Phase 2 | TTI 469468-2-1 | C412 bridge rail | 42 | 5-12 | 1.2 ft DS of joint | 50.8 | 15 | 464 | None | No | 1.2 | 86.7 | N/A | Box |
| | 41 | TTI 0-6946-R2 | MASH Evaluation of TxDOT Roadside Safety features - Phase 2 | TTI 469468-3-1 | C411 bridge rail | 42 | 2-10 | 2.7 ft US of 30th parapet window | 44.2 | 23.9 | 26.2 | None | No | 0 | 12 | N/A | Hood |
| | | | | TTI 469468-3-2 | | 42 | 2-11 | 2.2 ft US of 14th parapet window | 45 | 24.4 | 57.9 | None | No | 0 | 12 | N/A | N/A |
| | 42 | TRP 03-420-19 | Crash Testing and Evaluation of the HDOT 34-in. Tall Aesthetic Concrete Bridge Rail | MwRSF H34BR-1 | Hawaii 34-in. aesthetic bridge rail | 34 | 3-10 | 3.6 ft US of expansion joint 3-4 | 62.3 | 25.7 | 59.2 | None | No | 0.3 | 10 | N/A | Hood |
| | | | | MwRSF H34BR-2 | | 34 | 3-11 | 4.3 ft US of expansion joint 3-4 | 64.1 | 25.7 | 126.4 | None | RF | 0.2 | 22.2 | N/A | Hood |
| | 43 | TRP-03-148-05 | Development, Testing, and Evaluation of NDOR's TL-5 Aesthetic Open Concrete Bridge Rail | MwRSF ACBR-1 | Nebraska aesthetic concrete bridge rail | 42 | NCHRP 350 5-12 | Midspan between posts 3 and 4 | 49.5 | 16.3 | 508.8 | Left shock and leaf springs disengaged, bottom shock mount and right-side axle disengaged | RR | 11.2 | 75.4 | N/A | RS of cab and trailer |
| Steel and combination rails | 44 | FHWA CA-15-2181 | Compliance Crash Testing of the Type 732SW Bridge Rail | Caltrans 130MASH3P13-01 | Type 732SW bridge rail | 32 (parapet) 48 (handrail) | 3-11 | 22.2 ft DS of US end | 62.7 | 24.8 | 117 | Unknown | RF | 1 | N/A | N/A | RS |
| | | | | Caltrans 110MASH3C14-01 | | 32 (parapet) 48 (handrail) | 2-10 | 27.2 ft DS of US end | 44.1 | 24.3 | 26.3 | None | RF | 0 | N/A | N/A | N/A |
| | 45 | 17-06870_TL5 | MASH TL-5 Steel Bridge Rail for Suspension Bridges | TTI 603911-1 | TBTA steel bridge rail | 42 | 5-10 | 3.1 ft US of splice 4-5 | 62.5 | 24.7 | 55 | Unknown | Unknown | 1.5 | 15.5 | N/A | N/A |
| | | | | TTI 603911-2 | | 42 | 5-11 | 4.3 ft US of splice 4-5 | 64.3 | 24.8 | 123 | Unknown | Unknown | 2 | 15.8 | N/A | RS |
| | | | | TTI 603911-3 | | 42 | 5-12 | 6.0 in. DS of splice 4-5 | 49.9 | 15.1 | 450 | Unknown | Unknown | 2 | 62 | N/A | RS of cab and trailer |
| | 46 | 9-1002-15-2 | MASH TL-4 Evaluation of the TxDOT Type C2P Bridge Rail | TTI 490026-4-1 | TxDOT type C2P bridge rail | 42 | 4-10 | 45 in. US of post 11 | 63 | 25.7 | 60 | None | LF | 0.8 | 14 | N/A | N/A |
| | | | | TTI 490026-4-2 | | 42 | 4-11 | 47.5 in. US of post 6 | 62.9 | 24.5 | 115 | None | LF | 2.5 | 14 | N/A | LS |
| | | | | TTI 490026-4-3 | | 42 | 4-12 | 63 in. US of post 6 | 58.4 | 15.3 | 176 | None | LF | 11.4 | 62.3 | N/A | RS of box |

# Table A-1. Crash Test Database (continued)

| Barrier | Ref. no. | Report no. | | Test information | | | | Test conditions | | | | Suspension damage | Tire deflation | Deflection | | ZOI (in.) (ms) | Vehicle ZOI component |
|---|---|---|---|---|---|---|---|---|---|---|---|---|---|---|---|---|---|
| | | | | Agency Test no. | Article | Barrier height (in.) | MASH designation no. | Impact point | Impact speed (mph) | Impact angle (deg) | IS value (kip-ft) | | | Dynamic (in.) | Working width (in.) | | |
| Steel and combination rails | 47 | 9-1002-12-1 | MASH Test 3-11 on T131RC Bridge Rail | TTI 490022-1 | TxDOT T131RC bridge rail | 36 | 3-11 | 5 ft US of post 6 | 63 | 24.7 | 115.5 | RF upper/lower ball joints pulled out of sockets. Tie rod, right upper/lower A-arms, right frame rail deformed | RR | N/A | N/A | N/A | RS mirror |
| | 48 | 690900-GEC7-9 | MASH TL-4 Evaluation of the Lake Pontchartrain Causeway Dual-Rail Bridge Rail (46-in. Tall; Option B1) | TTI 690900-GEC7a | Lake Pontchartrain causeway design B1 | 46 | 4-12 | 4.7 ft US of joint 6-7 | 58.2 | 16 | 191 | None | LF | 19.6 | 70.5 | N/A | LF cab, LS of box |
| | | | | TTI 690900-GEC8 | | 46 | 4-10 | 3.8 ft US of joint 18-19 | 61.5 | 24.8 | 54 | None | RF | 1.5 | 7.8 | N/A | Unknown |
| | | | | TTI 690900-GEC9 | | 46 | 4-11 | 3.7 ft US of joint 12-13 | 62.2 | 25 | 116 | RF (impact) wheel disengaged | RR | 8.2 | 31 | N/A | RS |
| | 49 | 690900-GEC1-3 | MASH TL-4 Evaluation of the Lake Pontchartrain Causeway Single-Rail Bridge Rail (46-Inch Tall; Option A) | TTI 690900-GEC1 | Lake Ponchartrain causeway single rail | 39 | 4-12 | 59 in. US of joint | 57.5 | 15.2 | 166.5 | LF (impact) wheel disengaged | LR | 6.9 | 14.1 | N/A | LF of cab, LS of box |
| | | | | TTI 690900-GEC2 | | 39 | 4-11 | 59.5 in. US of joint | 63.4 | 25 | 120.5 | None | No | 3.1 | 11.3 | N/A | LS |
| | | | | TTI 690900-GEC3 | | 39 | 4-10 | 43.5 in. US of joint | 61.4 | 25 | 54.6 | None | No | 0.7 | 10 | N/A | LS |
| | 50 | DOI 10.1080/13588265. 2014.937558 | Int. Journal of Crashworthiness - Impact Performance Evaluation of MASH TL-4 Bridge Barrier | TTI 4-10 | PosBarrier-B | 53.1 | 4-10 | 72.8 in. US of post 12 | 62.4 | 25.6 | 58.3 | LF (impact) wheel disengaged | No | 1.5 | 16.3 | N/A | N/A |
| | | | | TTI 4-11 | | 53.1 | 4-11 | 80 in. US of post 9 | 63.9 | 25.3 | 124.6 | LF (impact) wheel disengaged | No | 2.2 | 19.7 | N/A | LS |
| | | | | TTI 4-12 | | 53.1 | 4-12 | 66.3 in. US of post 5 | 57.9 | 14.2 | 147.9 | Left upper/lower A-arms, left frame rail deformed and tie rod end broken | RF | 3 | 19.3 | N/A | LS of box |
| | 51 | FHWA TX-12 9-1002-12-2 | MASH TL-3 Testing and Evaluation of a Steel Brige Rail with Pickets | 490022-2 | TxDOT picket rail | 36 | 3-10 | 3.7 ft US of Post 9 | 62 | 24.9 | 53.4 | None | RF, LR | 0.9 | 10.7 | N/A | N/A |
| | | | | TTI 490022-3 | | 36 | 3-11 | 5.0 ft US of post 4 | 61.6 | 24.2 | 107 | RF frame rail and RF upper/lower A-arms deformed | RF | 2.8 | 10.4 | N/A | LF fender |
| | 52 | TM-9-1002-1 | TxDOT T131 Bridge Rail | TTI 420021-2 | TxDOT T131 bridge rail | 33 | 3-10 | 4.5 ft US of post 3 | 60 | 25.1 | 52.3 | None | No | 4.8 | 13.7 | N/A | N/A |
| | 53 | Eligibility Letter b286 | FHWA Eligibility Letter b286 | Safet Tech. BG1716 | BarrierGuard 800 MDS | 36.1 | 3-10 | 58.1 ft DS of end | 62.2 | 25 | 56.6 | Unknown | Unknown | 7.4 | 26.4 | N/A | N/A |
| | | | | Safe Tech. BG1615 | | | 3-11 | 58.1 ft DS of end | 63.1 | 25 | 113.3 | Unknown | Unknown | 18.5 | 39.7 | N/A | N/A |
| | 54 | TTI 0-6946-R2 | MASH Evaluation of TxDOT Roadside Safety features - Phase 2 | TTI 469468-1-1 | TxDOT C402 bridge rail | 42 | 4-10 | 3.6 ft US of last open joint in parapet | 62.6 | 25 | 57 | Unknown | Unknown | N/A | 12.5 | 24 | N/A |
| | | | | TTI 469468-1-2 | | 42 | 4-11 | 4.3 ft US of second open joint in parapet | 62.7 | 25.3 | 120 | Unknown | Unknown | 1.1 | 16.5 | 46 | LF fender and hood |
| | | | | TTI 469468-1-3 | | 42 | 4-12 | 5.0 ft US of first open joint in parapet | 56.9 | 15 | 160 | Unknown | Unknown | N/A | 63.9 | 144.5 | LF of cab, LS of box |
| | 55 | TRP-03-408-19 | Iowa DOT Combination Bridge Separation Barrier with Bicycle Railing | MwRSF IBBR-1 | Iowa bicycle bridge rail | 24 (parapet) 48 (handrail) | 2-11 | 49.4 in. US of post 4 | 45.3 | 25.3 | 63.8 | Unknown | Unknown | 3.8 | 38.8 | 21.7 (72) | Grille and bumper |
| | 56 | TRP-03-410-19 | Development Of A Mash Test Level 4 Steel, Side-Mounted, Beam-And-Post, Bridge Rail | MwRSF STBR-2 | Steel, side-mounted, beam-and-post bridge rail | 36 | 4-11 | 19.3 in. US of post 8 | 64.5 | 24.6 | 120.3 | None | No | 7 | 19 | N/A | Hood |
| | 57 | | | MwRSF STBR-3 | | 39 | 4-10 | 50.5 in US of splice 6-7 | 62 | 24.8 | 54.5 | None | LF | 2.9 | 15.2 | N/A | Hood |
| | 58 | | | MwRSF STBR-4 | | 36 | 4-12 | 53.2 in. US of splice 6-7 | 56.4 | 14.7 | 151.9 | None | No | 7.9 | 87.7 | N/A | Box |
| | 59 | TTI 0-6946-R2 | MASH Evaluation of TxDOT Roadside Safety features - Phase 2 | TTI 469468-4-1 | T1W bridge rail | 32 | 3-10 | 3.9 ft US of curb joint | 61.9 | 24.8 | 55 | None | LF | 1.1 | 15.3 | N/A | N/A |
| | | | | TTI 469468-4-2 | | 32 | 3-11 | 5.0 ft US of deck/curb joint | 62 | 25 | 115 | None | No | 13 | 19.3 | N/A | Hood/door |
| Transitions and other | 60 | TRP-03-318-15 | MASH TL-4 Crash Testing and Evaluation of the Restore Barrier | MwRSF SFH-1 | Low maintenance, energy-absorbing median barrier | 38.5 | 4-11 | 41.2 in. US of the joint 5-6 | 63.4 | 24.8 | 118.6 | LF control arm disengaged | LF, LR | 11.2 | 35.5 | N/A | N/A |
| | | | | MwRSF SFH-2 | | 38.5 | 4-10 | 8.3 in. US of joint 7-8 | 64.3 | 24.8 | 58.3 | None | LF, LR | 7.3 | 28.8 | N/A | N/A |
| | | | | MwRSF SFH-3 | | 38.5 | 4-12 | 55.75 in. US of joint 5-6 | 56.5 | 14.9 | 154.4 | None | LR | 15.1 | 60.2 | N/A | Box |

Table A-1. Crash Test Database (continued)

| Barrier | Ref. no. | Report no. | | Test information | | | | Test conditions | | | | Suspension damage | Tire deflation | Deflection | | ZOI (in.) (ms) | Vehicle ZOI component |
|---|---|---|---|---|---|---|---|---|---|---|---|---|---|---|---|---|---|
| | | | | Agency Test no. | Article | Barrier height (in.) | MASH designation no. | Impact point | Impact speed (mph) | Impact angle (deg) | IS value (kip-ft) | | | Dynamic (in.) | Working width (in.) | | |
| Transitions and other | 61 | FHWA TX-12 9-1002-8 | Development of a MASH TL-2 Guardrail-to-Bridge Rail Transition Compatible with 31-inch guardrail | TTI 420021-4 | W-to-thrie-to-bridge rail single-slope transition | 36 (parapet) 31 (beam) | 2-21 | 55 in. US of parapet | 43.7 | 25.8 | 61.5 | None | LF | 5.7 | 15.8 | N/A | LF hood |
| | 62 | | | TTI 420021-6 | | 36 (parapet) 31 (beam) | 2-20 | 5.9 ft US of post 9 | 43.5 | 26.4 | 30.2 | None | RF, LF | 14.4 | 31.2 | N/A | N/A |
| | 63 | | | TTI 420021-7 | | 36 (parapet) 31 (beam) | 2-20 | 4 ft US of bridge rail end | 43.5 | 24.4 | 26.1 | None | LF | 3.4 | 11.7 | N/A | N/A |
| | 64 | TRP-03-208-10 | Development of a Temporary Concrete Barrier to Permanent Concrete Median Barrier Approach Transition | MwRSF TCBT-1 | Temporary-to-permanent barrier transition | 42 | 3-21 | 56.4 in. US of US barrier end | 62.5 | 24.7 | 114.1 | RF upper/lower control arms severely damaged | No | 2.6 | 24.9 | N/A | RF |
| | 65 | Eligibility Letter b281 | FHWA Eligibility Letter b281 | TTI 690902-PCL1 | Transition from Jersey to offset cross-bolted F-shape with message sign mounted on back side | 44.3 | 3-20 | 34.6 in. US of barrier 7 | 62.4 | 25.1 | 57.5 | Unknown | Unknown | 1.2 | 8.7 | N/A | N/A |
| | 66 | TRP-03-367-19 | 34-in. Tall Thrie Beam AGT To Concrete Buttress | MwRSF 34AGT-1 | 34-in. tall thrie beam AGT | 34 (rail) 39 (buttress) | 3-21 | 27.5 in. US of post 18 | 62.2 | 24.7 | 113 | LF (impact) wheel disengaged | LF | 11 | 26.4 | 14.5 (92) | Hood |
| | 67 | | | MwRSF 34AGT-2 | | 34 (rail) 39 (buttress) | 3-20 | 2 in. US of post 18 | 62.1 | 25.5 | 57.7 | None | LF | 2.7 | 19.9 | 6.3 (72) | Hood |
| | 68 | TRP-03-369-19 | Development of a Standardized End Buttress for Approach Guardrail Transitions | MwRSF AGTB-2 | Standardized buttress for AGT | 31 (rail) 36 (buttress) | 3-21 | 86.1 in. US of end buttress | 62.7 | 25.4 | 124.8 | RR (impact) wheel disengaged, RF lower shock mount disengaged, RF and RR steering knuckle assemblies disengaged | LF | 5.4 | 26 | 17.6 (84) | Hood |

# Appendix B. Agency Survey and Results

## B-1 Project Background

MwRSF is the primary contractor on NCHRP Project 22-34, "Determination of Zone of Intrusion Envelopes Under the MASH Impact Conditions for Barrier Attachments." Zone of intrusion (ZOI) envelopes are in AASHTO's current *Roadside Design Guide* (RDG) to assist transportation agencies in locating attachments on or near rigid roadside barriers or bridge rails. The existing envelopes were developed based on reviewing crash tests conducted according to *NCHRP Report 350*. In 2009, MASH became the new crash testing standard for roadside hardware, and test vehicles and some impact conditions were updated. Thus, there is a need to re-evaluate ZOI envelopes using current MASH crash tests.

## B-2 Purpose of Survey

The research team needs information from state DOTs on rigid barrier usage at various MASH test levels, available in-service performance evaluation (ISPE) data related to rigid barriers and/or attachments near barriers, and any updates in your rigid barrier standards and specifications from what is available online.

For the purposes of this survey, we are referring to "rigid barriers" as systems that would deflect minimally under MASH impact conditions: permanent concrete barriers or bridge rails, anchored temporary concrete barriers, and robust steel barriers and bridge rails. "Attachments" may be objects placed on top of or behind a barrier, including signs, luminaires, overhead sign structures, noise walls, debris fences, or other support structures. Many existing rigid barrier systems your agency uses may have been evaluated to prior standards (*NCHRP Report 350* or prior). This survey is specifically targeting MASH barriers you may be in the process of or will be transitioning to in the future. Please answer the survey questions in relation to MASH barriers.

1. When considering where to place an object behind or above a rigid barrier, do you use the ZOI criteria from Section 5.5.2 in the RDG?

   ☐ Yes

   ☐ No

2. If you do not use the ZOI criteria from the RDG, can you provide further discussion on how you select crashworthy hardware and determine the location of attachments when they are located behind or above a rigid barrier?

3. For MASH test levels 2 through 5, what are the barrier shapes and minimum and maximum rail heights of concrete barriers or concrete bridge rails your agency uses, or plans to use in the near future?

   Min. height: _____ Max. height: _____

   ☐ Single-slope

   ☐ Jersey

☐ F-shape

☐ Vertical

☐ Open concrete rail

☐ Low-profile

4. For MASH test levels 2 through 5, what are the minimum and maximum rail heights of steel bridge rail or combination concrete/steel bridges your agency uses, or plans to use in the near future

   Min. height: _____ Max. height: _____

5. Has your agency conducted any ISPEs, or plan to do so in the near future, regarding fixed objects or attachments placed on or near barriers or the performance of rigid barriers in general?

   ☐ Yes; please describe

   ☐ No, but planning to in the future; please describe

   ☐ No

6. Is your agency familiar with any specific crashes that involved a fixed object hazard located with the ZOI of a barrier?

   ☐ Yes; please describe

   ☐ No

7. Are there any other comments regarding ZOI envelopes or fixed object hazards placed within the ZOI you would like to provide?

8. Has your agency updated, or in the process of updating, standard plans and specifications from what is available on your agency's website?

   ☐ Yes; please describe

   ☐ No

**B-3 Question 1**

*When considering where to place an object behind or above a rigid barrier, do you use the ZOI criteria from Section 5.5.2 in the* RDG*?*

Most states use RDG ZOI guidelines, as shown in Figure B-1.

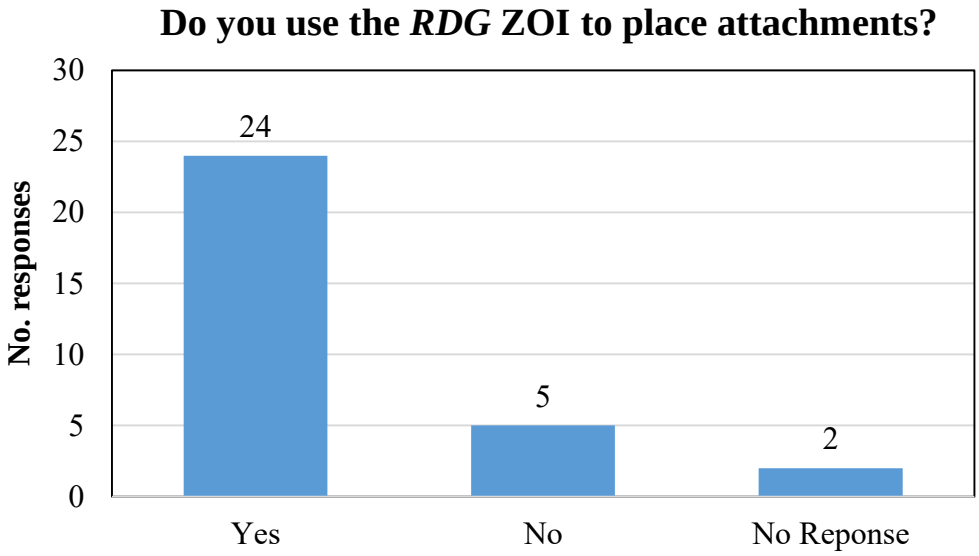


Figure B-1. Question 1 Results

**B-4 Question 2**

*If you do not use the ZOI criteria from the RDG, can you provide further discussion on how you select crashworthy hardware and determine the location of attachments when they are located behind or above a rigid barrier?*

Five states reported they do not use RDG ZOI guidelines when locating attachments near barriers:

- We strive hard to avoid mounting fixed objects on barrier. When necessary, we widen the barrier locally and attach box beam on the upper portion of the face to limit lean and climb.

- The answer is yes and no. For most objects the ZOI is considered per the RDG. On occasion when there is no option the zone is ignored and the engineer is responsible for determining if objects within the zone are structurally sound under impact. The exact value of this impact load is not known. We are considering including the ZOI criteria or a variation in our *Roadway Design Manual*.

- Design Manual offers guidance for determining the location of attachments such as bridge lighting, sign structures, and sound barrier walls. Attachments located behind barriers require crashworthy hardware installations that provide minimum deflection distance between the rear face of the barrier and the front face of the attachment.

- Historically, attachments and hardware have been selected and placed based on their demand (i.e., as close to a barrier or on top of a barrier as needed).

- Currently the only requirement for ZOI criteria within our Standards is for structure column protection. Signs and luminaire are placed on top of barrier only in median applications. Right shoulder applications, these devices are placed at a minimum, beyond the deflection distance of the chosen barrier system when room is available.

**B-5 Question 3**

*For MASH test levels 2 through 5, what are the barrier shapes and minimum and maximum rail heights (in in.) of concrete barriers or bridge rails your agency uses, or has plans to use in the near future?*

Single-slope concrete barriers at all test levels were most common and Jersey barriers were least common, as shown in Figure B-2. Individual responses to Question 3 are shown in Figure B-3 through Figure B-6.

MASH TL-2 concrete barrier heights ranged from 14 to 54 in., with 32 and 42 in. the most common. Seven states reported they did not use MASH TL-2 concrete barriers and two did not respond. MASH TL-3 concrete barrier heights ranged 26 from 57 in., with 32 to 54 in. the most common. Two states reported they did not use MASH TL-3 concrete barriers and one did not respond. MASH TL-4 concrete barrier heights ranged from 32 to 90 in., with 32 to 54 in. the most common. MASH TL-5 concrete barrier heights ranged from 41 to 90 in., with 41 to 54 in. the most common. One state reported they did not use MASH TL-5 concrete barriers and five did not respond.

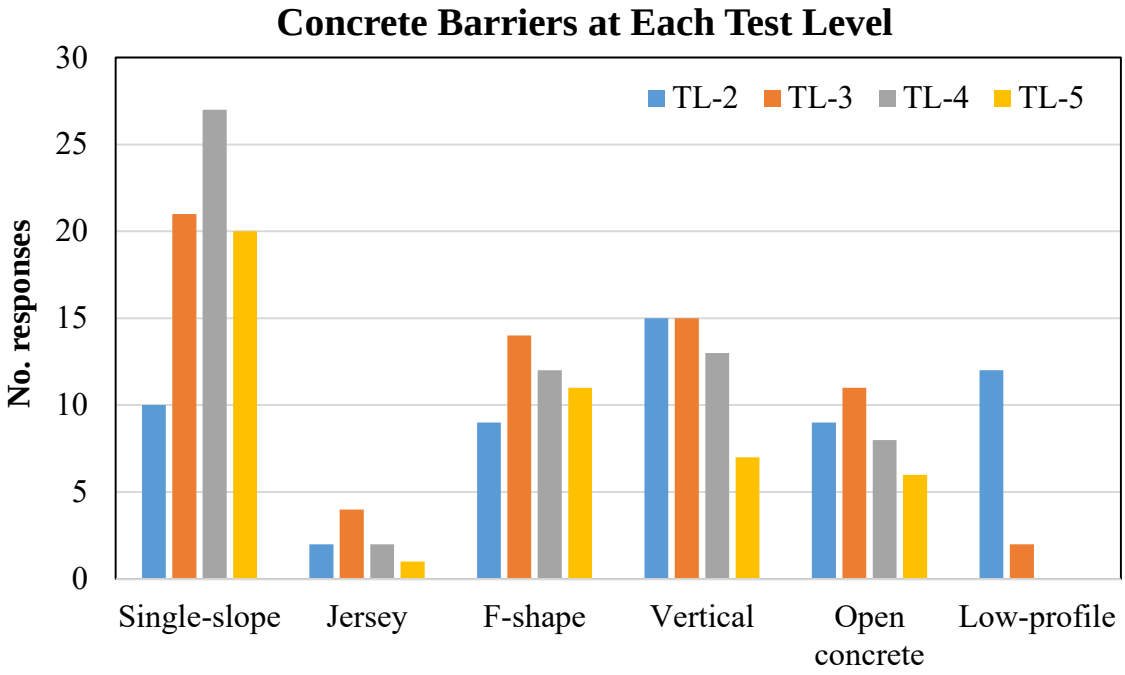


Figure B-2. Question 3 Results, Barrier Shape

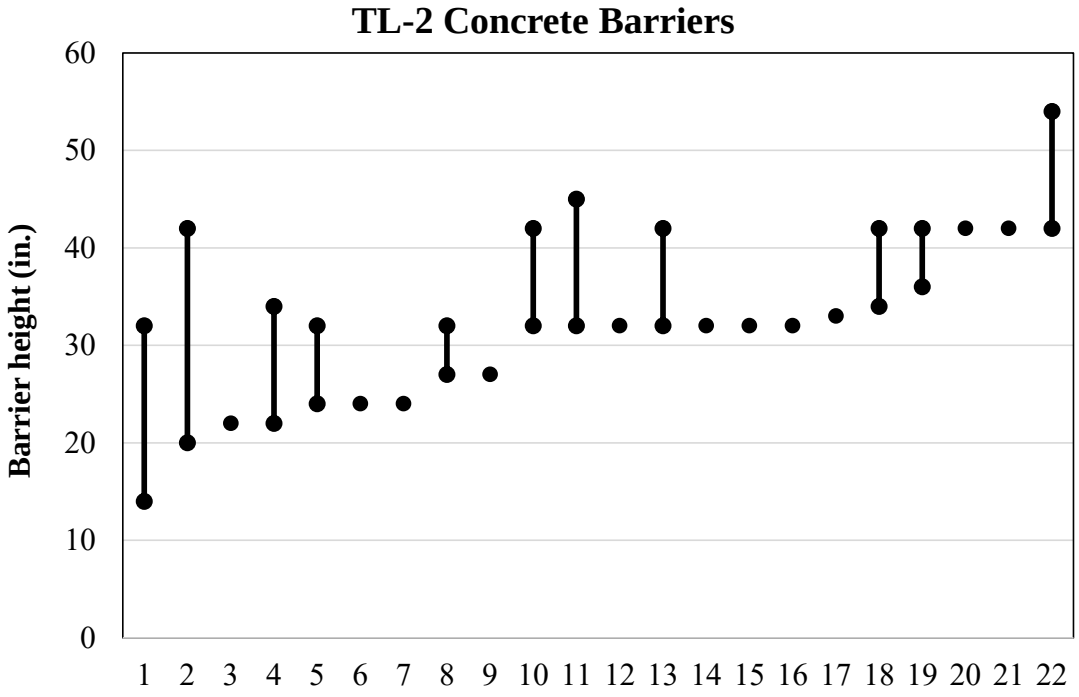


Figure B-3. Question 3 Results, MASH TL-2

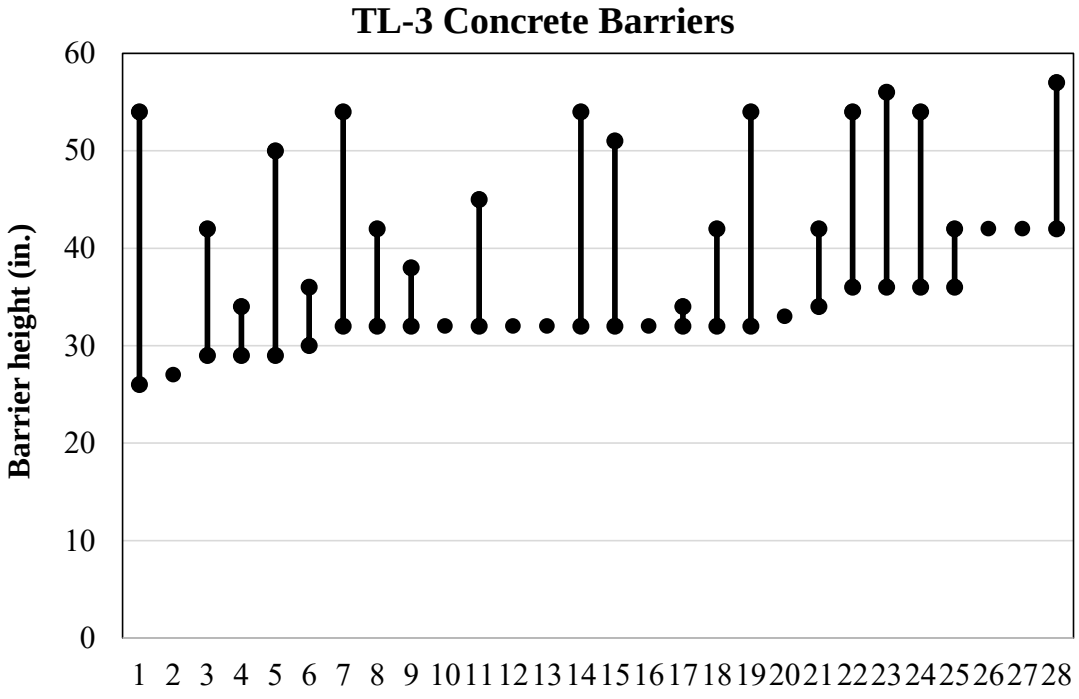


Figure B-4. Question 3 Results, MASH TL-3

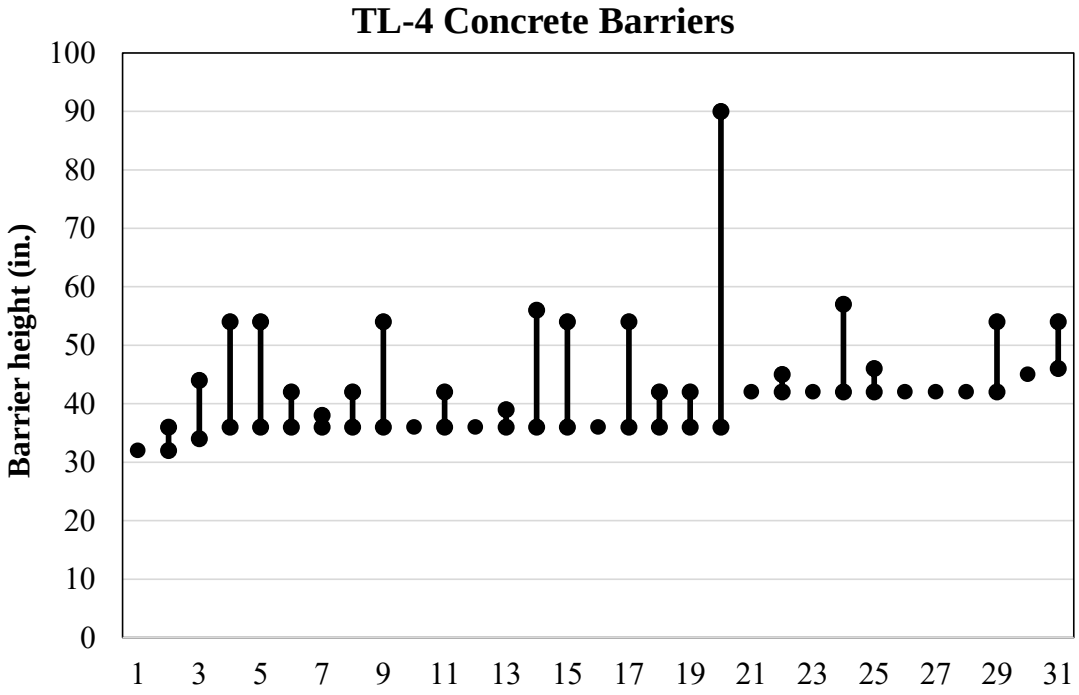


Figure B-5. Question 3 Results, MASH TL-4

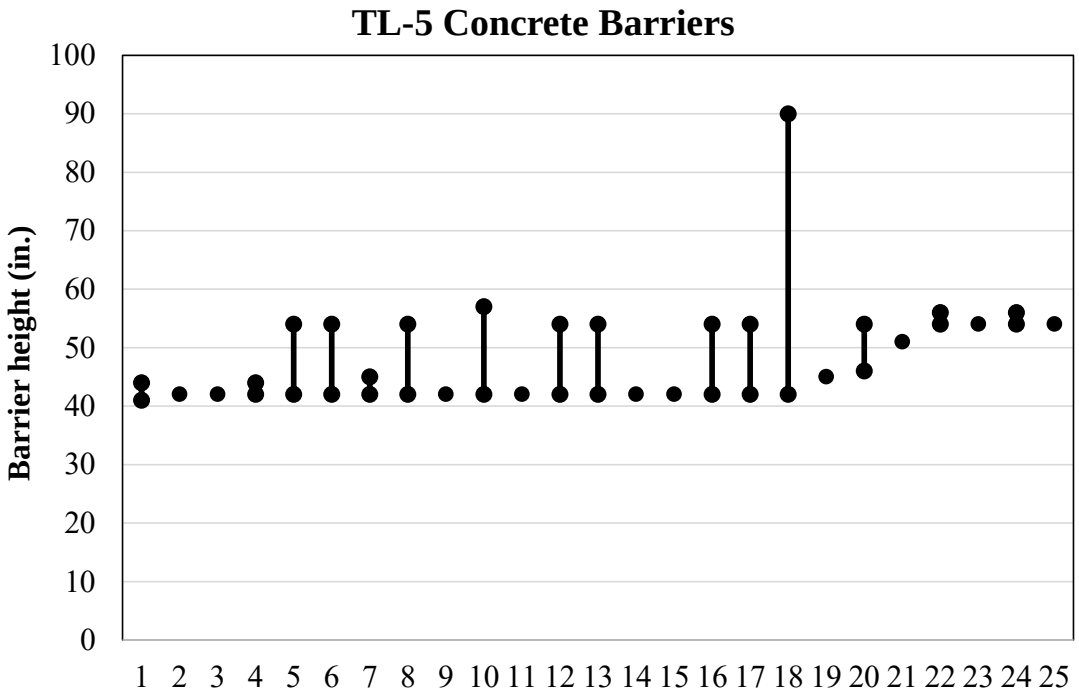


Figure B-6. Question 3 Results, MASH TL-5

**B-6 Question 4**

*For MASH test levels 2 through 5, what are the minimum and maximum rail heights (in in.) of steel bridge rail or combination concrete/steel bridge rails your agency uses, or plans to use in the near future?*

Barrier shape was not included as steel and combination bridge rails vary significantly across states. Thus, steel barrier shapes were garnered from state DOT standard plans. Responses to Question 4 are shown in Figure B-7 through Figure B-10.

MASH TL-2 steel barrier heights ranged from 24 to 54 in., with 31 to 42 in. the most common. Five states reported they did not use MASH TL-2 rigid steel barriers and fifteen did not respond. MASH TL-3 steel barrier heights ranged from 27 and 56 in., with 31 to 42 in. the most common. Five states reported they did not use MASH TL-3 rigid steel barriers and eleven did not respond. MASH TL-4 steel barrier heights ranged from 32 to 56 in., with 36 to 42 in. the most common. Six states reported they did not use MASH TL-4 rigid steel barriers and five did not respond. MASH TL-5 steel barrier heights ranged from 42 and 54 in., with 42 to 50 in. the most common. Eight states reported they did not use MASH TL-5 rigid steel barriers and twelve did not respond.

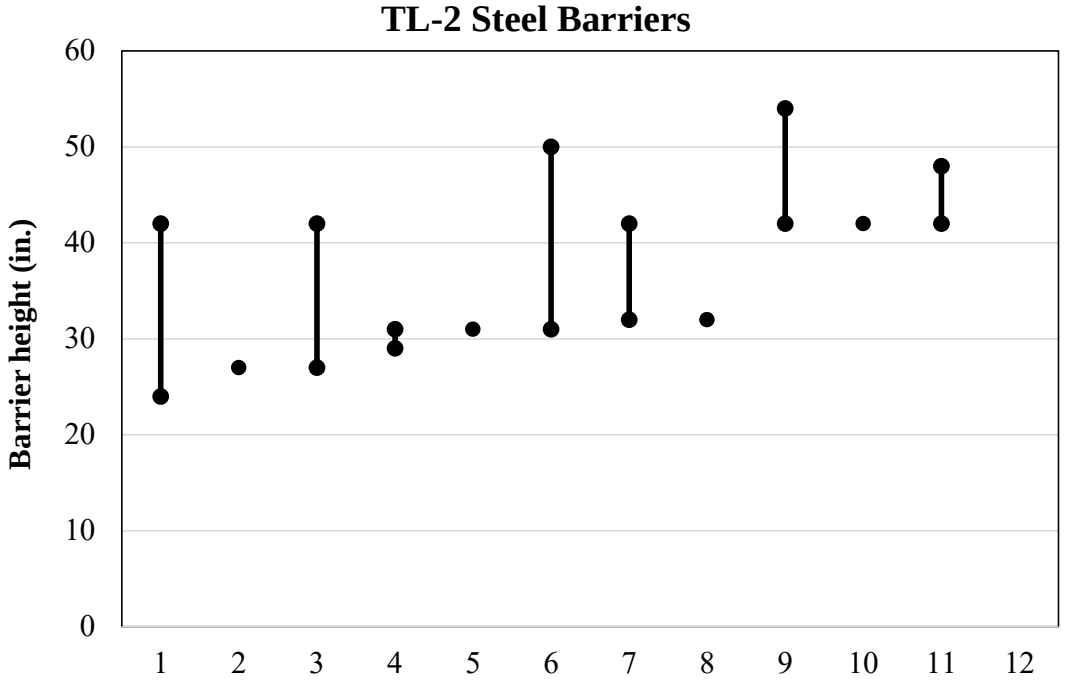


Figure B-7. Question 4 Results, MASH TL-2

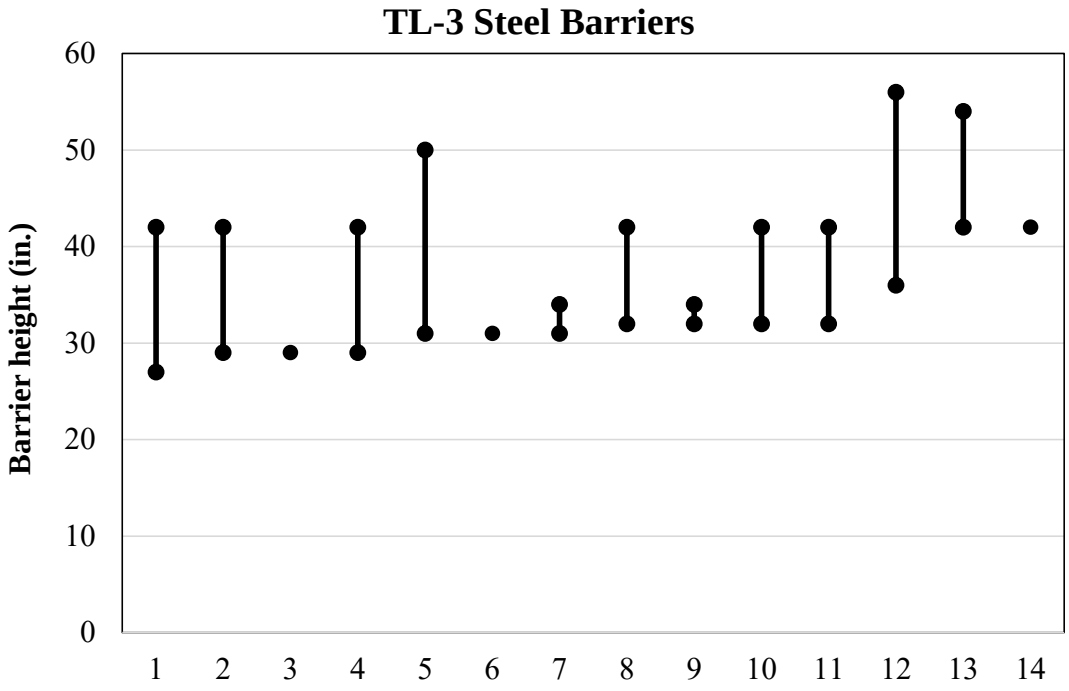


Figure B-8. Question 4 Results, MASH TL-3

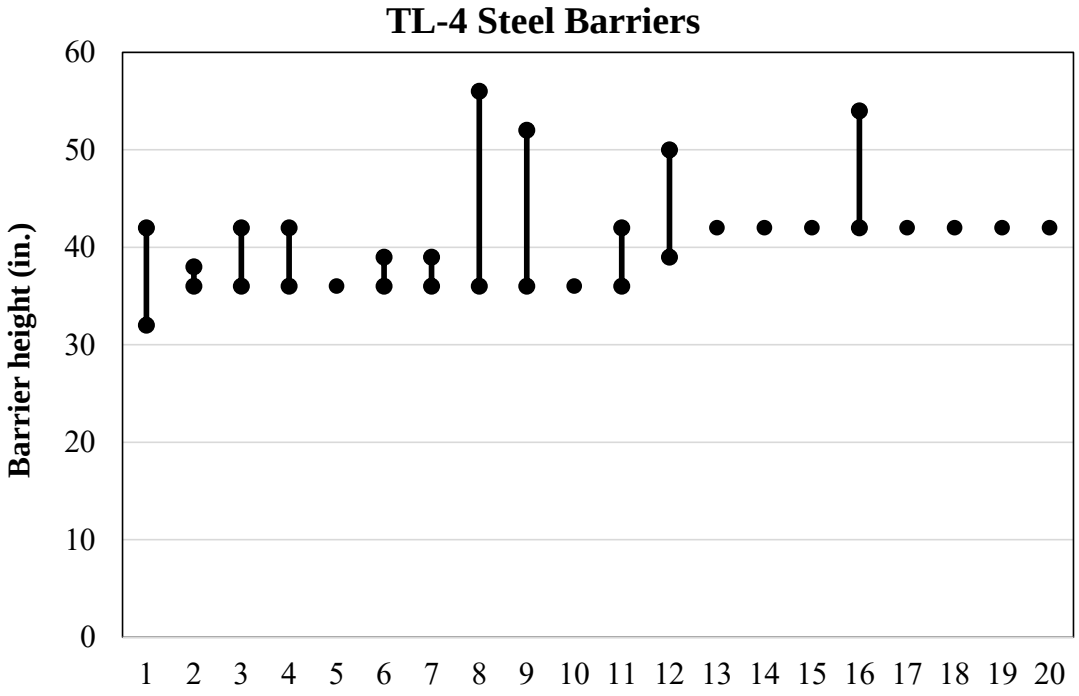


Figure B-9. Question 4 Results, MASH TL-4

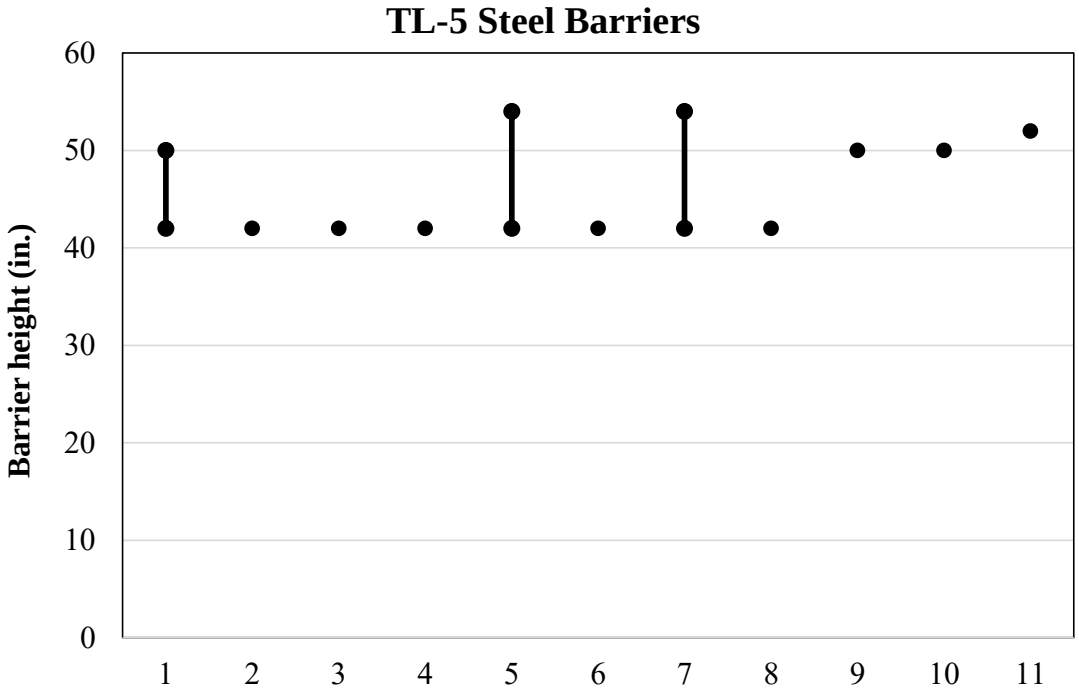


Figure B-10. Question 4 Results, MASH TL-5

**B-7 Question 5**

*Has your agency conducted any ISPEs, or does your agency plan to do so in the near future, regarding (a) fixed objects or attachments placed on or near barriers or (b) performance of rigid barriers in general?*

Responses to Question 5 are shown in Figure B-11. Three states had conducted ISPEs and six had not but planned to in the future. Twenty-one states had not conducted any ISPEs. Comments provided were:

- Data-gathering parties are in too many organizationally isolated agencies to permit a reasonable study.
- We are in the preliminary stages of looking into this matter.
- We have no formal or ongoing program to evaluate the performance of rigid barriers. Only observations after an accident.
- No for (a), yes for (b). PA Bridge Barrier was crash tested successfully by TTI to MASH TL-5. Total height is 50 in. with 24 in. of base concrete and two steel rails mounted on top. PA Type 10M Bridge Barrier was crash tested successfully by TTI to MASH TL-4. Total height is 39 in. with 17 in. of base concrete and two steel rails mounted on top. PA Structure Mounted Guide Rail will be crash tested by TTI for MASH TL-3 compliance. Total height is 31⅜ in. with W-beam guide rail at 31 in. above finished grade and mounted on top with height of 8 in.

- Our usage is so low, it wouldn't render useful results.
- We are interested in using light pole, noise wall and chain link fence behind barriers without impact issue.
- Planning to use the guidance from NCHRP Project 22-33 for ISPEs when it is complete.
- Joint Transportation Research Program (JTRP) SPR-3705 Performance Assessment of Road Barriers in Indiana. The research included concrete barriers as well as other barrier types (previously summarized in Section 2.5.1).
- We have started a tagging program with police agencies for hardware that has been hit by vehicles. Hoping the data gather from this program with help with ISPEs.
- Federal Highway Administration (FHWA) requirement for barrier acceptance.
- We are looking into ISPEs of concrete barrier systems both cast-in-place and portable concrete barrier.
- We are currently working with other NETC states to do simulated crash tests of current steel box beam bridge rails common to member states.

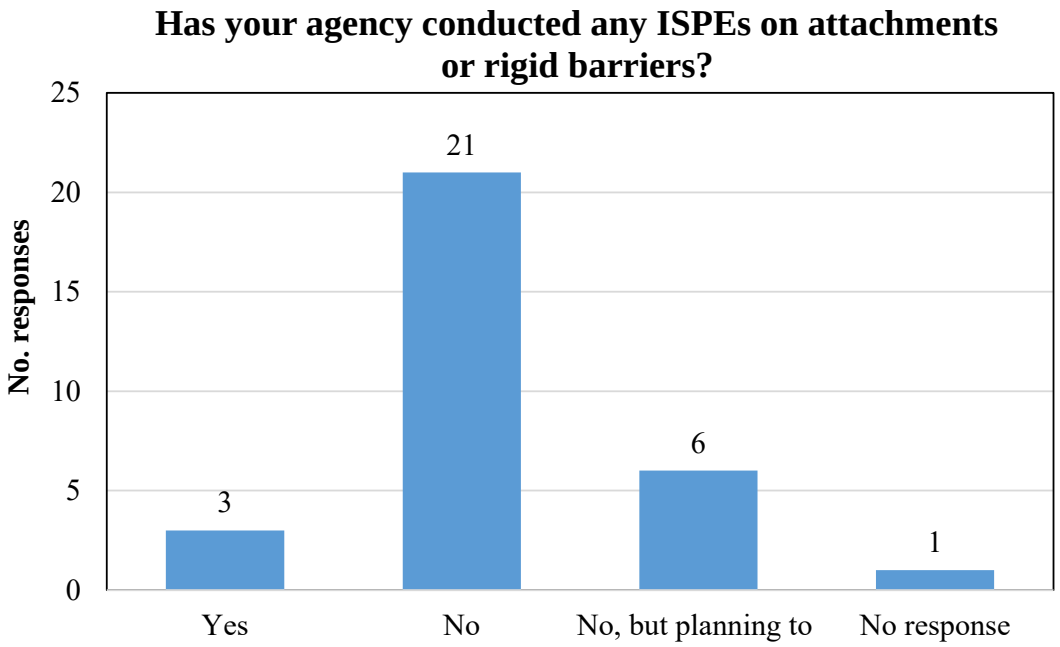


Figure B-11. Question 5 Results

### B-8 Question 6

*Is your agency familiar with any specific crashes that involved a fixed object hazard located with the ZOI of a barrier?*

Five states were familiar with crashes with attachments in the ZOI and 25 were not, as shown in Figure B-12. Additional comments provided were:

- Bridge piers, signs, and light poles are often needed in urban medians, and the barriers are often notched, widened, and/or transitioned to vertical to accommodate these objects. In one instance, an RV tire blew out and the RV struck and leaned into the median barrier, hitting two integrated light poles. The driver's side was torn open, the driver was ejected and killed, and six other occupants were injured. While the median barrier is hit fairly frequently, objects within the ZOI are rarely impacted. In another case, a glare screen support post disengaged during a crash and penetrated the windshield of a car, causing injury to the driver.

- Light poles mounted on top of barriers have not collapsed but have scratches. Noise walls have had similar issues.

- We would be willing to provide accident data, which would be coded as longitudinal barrier. Those would include guardrail, concrete roadside barrier, and bridge rail.

- Overhead sign structures placed on CMB, as shown in Figure B-13, which was a property-damage only crash. MSE wall panel damage - no photos, but this has been a more frequent issue and we are trying to be more proactive at placing new MSE wall abutments beyond the ZOI. There was recently a related NCHRP that discussed LRFD guidance for placement and design for shielding bridge piers.

- Soundwalls have been located at the top of slope just behind cast-in-place 42-in. single-slope barrier where vehicles have impacted the soundwall posts.

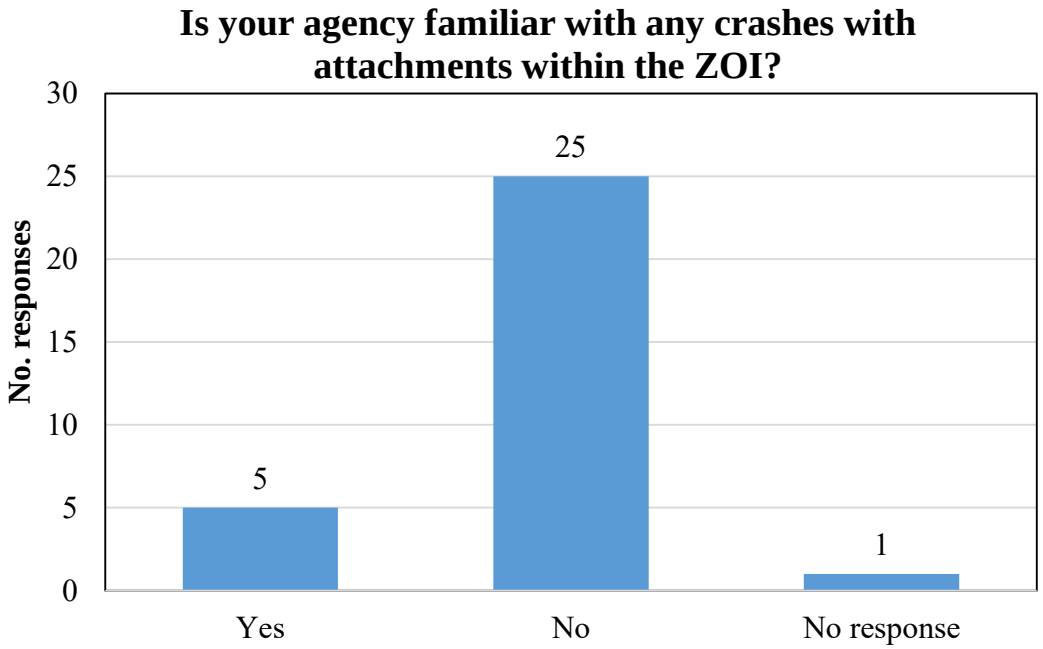


Figure B-12. Question 6 Results

Figure B-13. Overhead Sign Structure Impacted by a Vehicle

**B-9 Question 7**

*Are there any other comments regarding ZOI envelopes or fixed object hazards placed with the ZOI that you would like to provide?*

- Will this research also look at the potential load due to the leaning vehicle? In most cases the majority of load will be transferred through the center of gravity or a rigid section that is caught by the rail. So the portion in the ZOI is expected to be low.
- We try to respect ZOI as best we can. Traffic Engineers sometimes violate this, however.
- There is a need for updated information on MASH ZOI based on testing and real crashes.
- Would like to have ZOI for TL-5 barriers.
- SCDOT is working toward upgrading semi-rigid barriers to TL-5 rigid in front of bridge piers on controlled access routes. Other overhead structures are also a priority. This is happening only through reconstruction projects since rigid barriers affect drainage designs and alter other site conditions. Research continues for non-interstate type sites. Standards have been in place on website since 2016 - drawings search 805-860*.

- We would like to know at what height, for each test level, does ZOI become negligible. Many times, there is not sufficient space to provide setback needed to remove objects from ZOI; therefore, we need to know how tall to make the barrier to avoid ZOI issues.

- In Michigan, ZOI is treated as a "should" condition rather than a "shall" condition. Our preference is to place hazards outside the ZOI, but in some cases this is unavoidable.

- Guidance on evaluating/supporting decisions to place an object in the ZOI would be helpful.

- The envelope put many of our overhead bridge sign structures in jeopardy.

- ZOI should be included in crash test reports.

**B-10 Question 8**

*Has your agency updated, or in the process of updating, your standard plans and specifications from what is available on your agency's website?*

Responses to Question 8 are shown in Figure B-14. Nineteen states had updated or were in the process of updating their standard plans and specifications from what was on their website. Ten states had not updated their standard plans and specifications from what was on their website. Thus, many state DOT plans found previously were likely outdated.

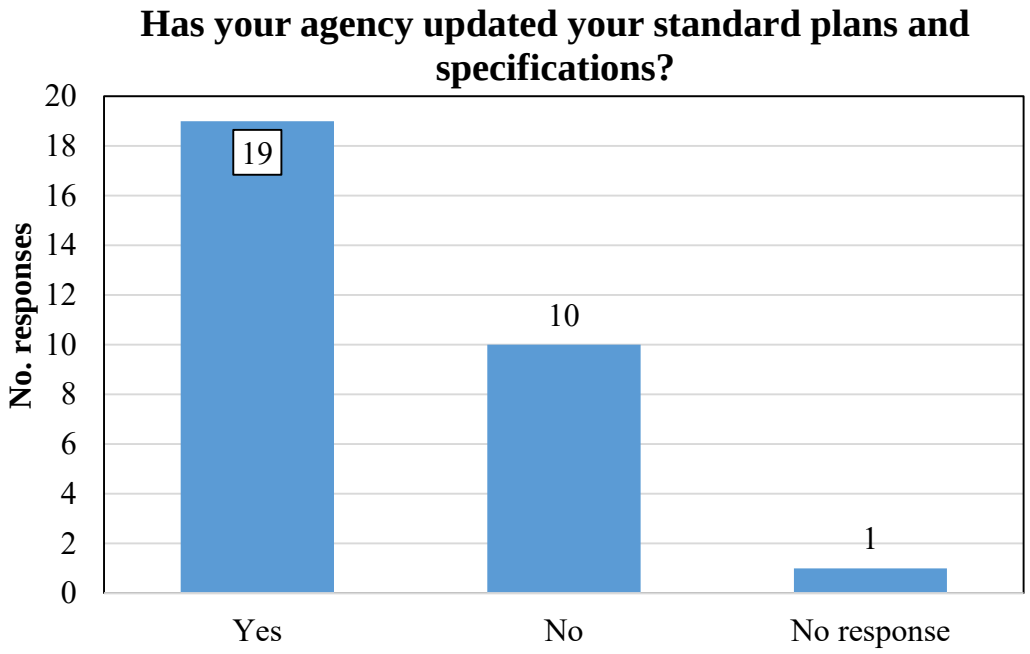


Figure B-14. Question 8 Results

## Appendix C. Preliminary ZOI Envelopes Developed Based on Crash Test Data Review

Preliminary ZOI envelopes for each test level were developed, which formed a rectangle using the vehicle's minimum vertical, maximum vertical, and maximum lateral extents. The preliminary ZOI envelopes were based solely on extents of measurements recorded from video analysis of full-scale crash test data consistent with MASH impact conditions.

### C-1 MASH TL-2

Two MASH TL-2 tests were analyzed, which included MASH test designation nos. 2-10 and 2-11. ZOI envelopes are shown in Figure C-1.

Both tested barriers were concrete parapets with an attached steel handrail, categorized as a steel combination rail. In full-scale crash test no. 110MASH3C14-01 (Her et al. 2017), a small car impacted a 32-in. tall parapet consistent with MASH 2-10 impact conditions and displayed relatively low lateral extent. Test no. IBBR-1 (Bielenberg et al. 2020) was conducted on a 24-in. tall vertical parapet. The steel handrail was contacted in both tests, but it was believed the parapets contributed much more to vehicle redirection than the handrails. Thus, ZOI was measured from the top of the parapet. In test no. IBBR-1, the lateral extent was 22 in., which occurred as the fender began to disengage, wrapped around the steel handrail posts, and continued extending laterally. Without the handrail, maximum lateral extent may have been less. Based on these tests, the maximum lateral and vertical ZOIs are 22 and 57 in., respectively. A preliminary conservative envelope for MASH TL-2 barriers is shown in Figure C-2.

The TL-2 ZOI from *NCHRP Report 350*, shown in Figure 2, extended 12 in. laterally and 78 in. vertically for barriers equal to or taller than 27 in., and extended 28 in. laterally and 78 in. vertically for barriers shorter than 27 in. *NCHRP Report 350* and preliminary MASH ZOI envelopes are compared in Figure C-3.

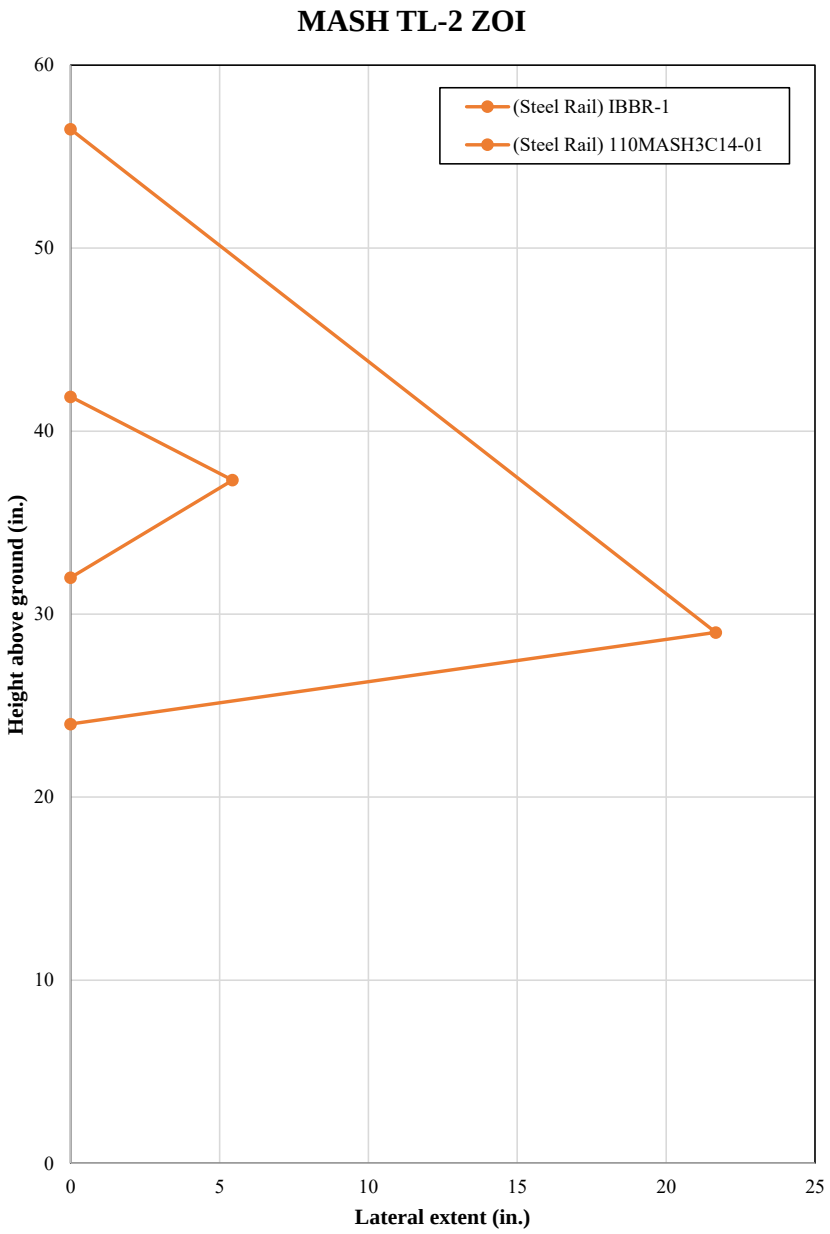


Figure C-1. Preliminary MASH TL-2 ZOI, All Barriers

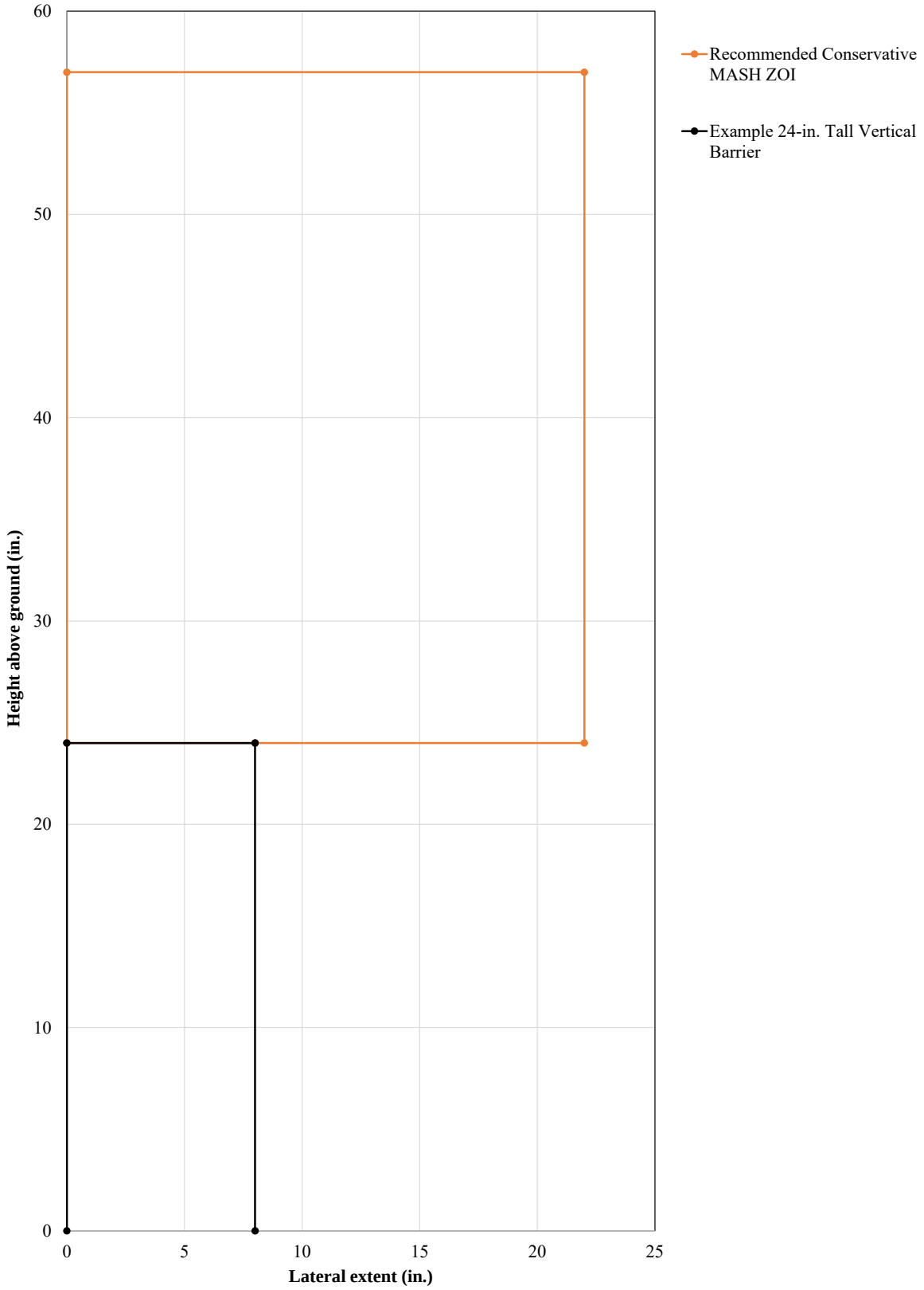


Figure C-2. Preliminary MASH TL-2 Conservative ZOI Envelope

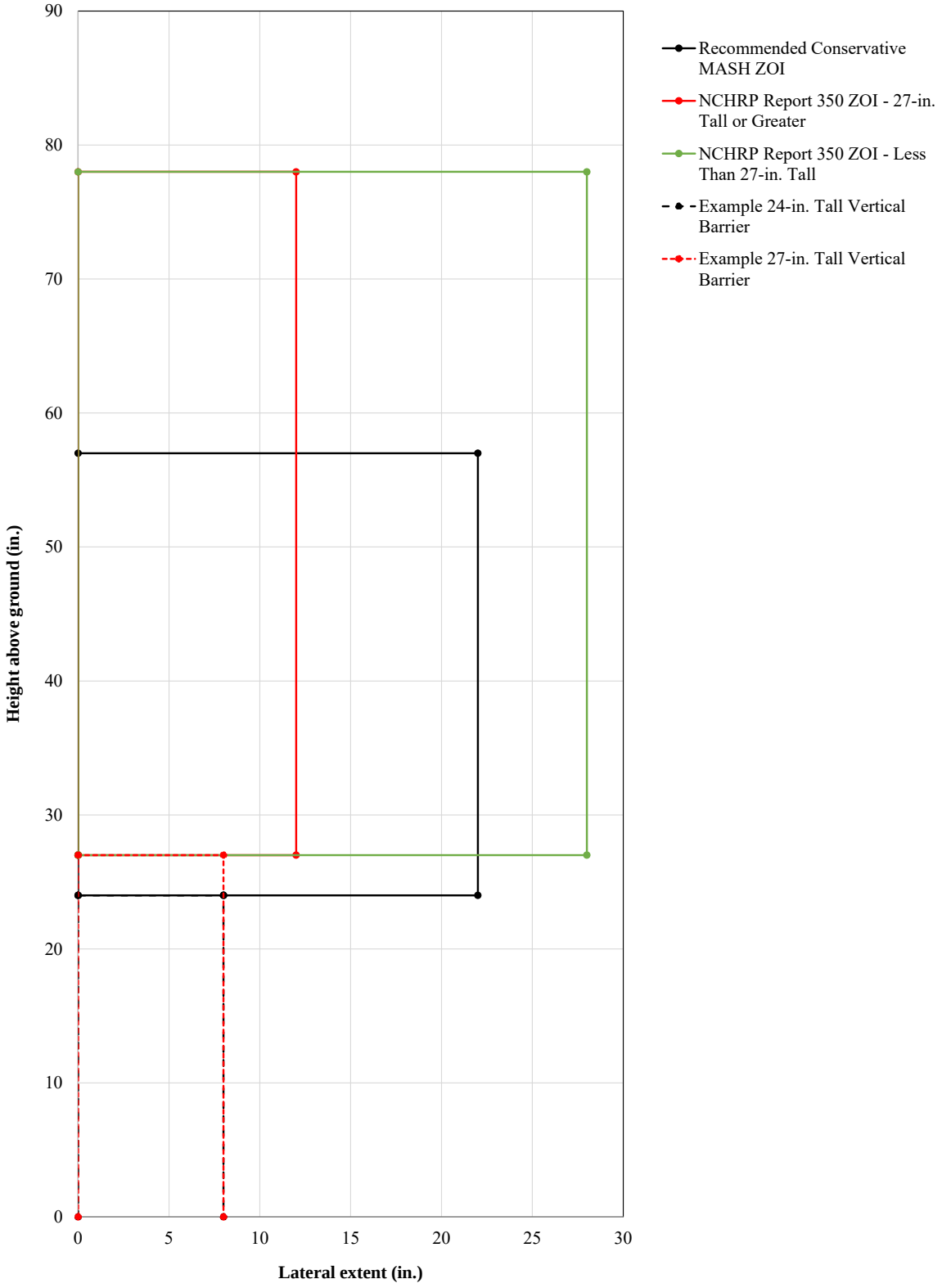


Figure C-3. *NCHRP Report 350* and Preliminary MASH TL-2 ZOI Envelopes

## C-2 MASH TL-3

Thirty-one MASH TL-3 tests were analyzed, which included MASH test designation nos. 3-10, 3-11, 3-20, 3-21, 4-10, 4-11, 5-10, and 5-11, as well as one 2270P simulation of a 36-in. tall single-slope barrier, which displayed similar maximum lateral and vertical extents as the crash tests. ZOI envelopes are shown by barrier height in Figures C-4 through C-8 and by barrier shape in Figures C-9 through C-13.

The lateral extent of the pickup truck in test nos. AGTB-2 (Rosenbaugh et al. 2020) and RF476460-1-4 (Bullard et al. 2010) was considerably farther than other pickup truck testing. Test no. AGTB-2 involved a thrie beam approach guardrail transition to a rigid concrete buttress which deflected a maximum of 5.4 in. It was the lowest rail height in the TL-3 category. Full-scale crash test no. RF476460-1 involved a 32-in. tall Jersey barrier.

In test no. 690900-GEC9 (Williams, Menges, and Kuhn 2015), the rear of the truck bed extended the farthest laterally. However, it was decided a side-swipe motion with a non-critical component did not cause additional risk to vehicle occupants; this assumption was also used in development of the original ZOI envelopes from *NCHRP Report 350* test data (Keller et al. 2003). Thus, this measurement was excluded and only the maximum lateral extent of the front and side of the pickup truck was considered.

Individual data points are not as important as general trends when examining the following figures, though there was not a definite trend between barrier shape and maximum vehicle extent. Most tests and barrier shapes had a maximum lateral ZOI of 12 to 13 in. Some variation occurred within each barrier shape, even for the same barrier height. Lateral extent decreased as barrier height increased, from a maximum of 18 in. with 31- to 33-in. tall barriers to 12 in. for barriers up to 46 in. tall. There was no decrease in lateral extent for barriers taller than 38 in.; 38- to 39-in. tall barriers had a maximum lateral extent of 11 in., while 42- to 46-in. tall barriers had a maximum lateral extent of 12 in. However, few crash tests were conducted on barriers at these heights. The maximum vertical extent was 81 in.

A preliminary conservative envelope for MASH TL-3 barriers is shown in Figure C-14. While 29 in. was believed to be the MASH TL-3 minimum barrier height, as noted in Section 2.8.2, no MASH TL-3 crash tests were conducted on 29-in. tall barriers. Additionally, ZOI measurements were taken on several rigid barriers categorized as "Other and Transitions," but these data points were not included in the preliminary MASH TL-3 envelope since the systems tended to be unique. They were considered in Phase II as needed.

*NCHRP Report 350* and preliminary MASH ZOI envelopes are compared in Figure C-15. The ZOI for *NCHRP Report 350* TL-3 barriers, shown in Figure 3, extended vertically 78 in. for all barriers and extended laterally:

- 18 in. for sloped-face barriers and steel tube bridge rails on curbs
- 24 in. for combination and vertical barriers
- 30 in. for steel tube bridge rails without curbs

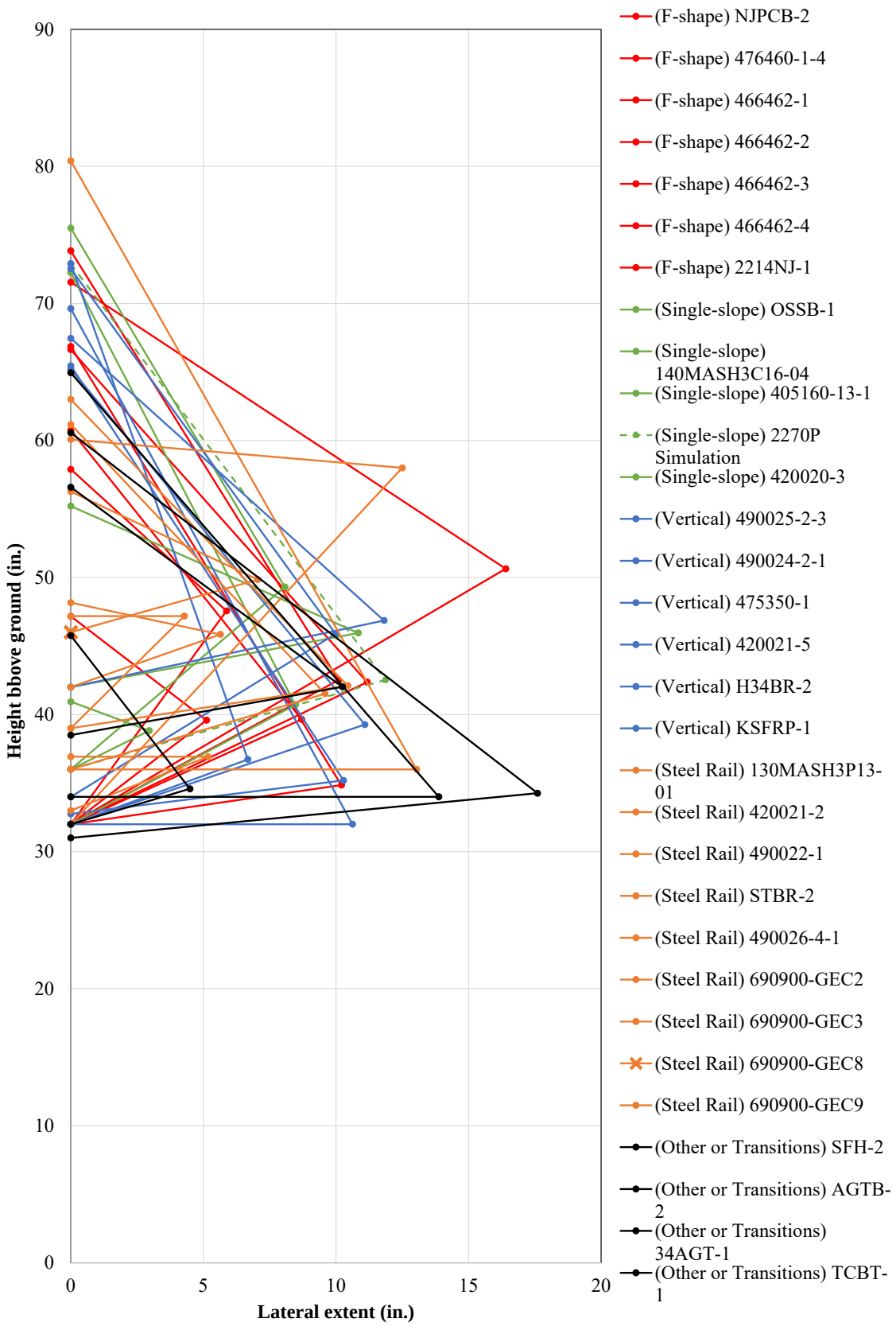


Figure C-4. Preliminary MASH TL-3 ZOI, All Barriers

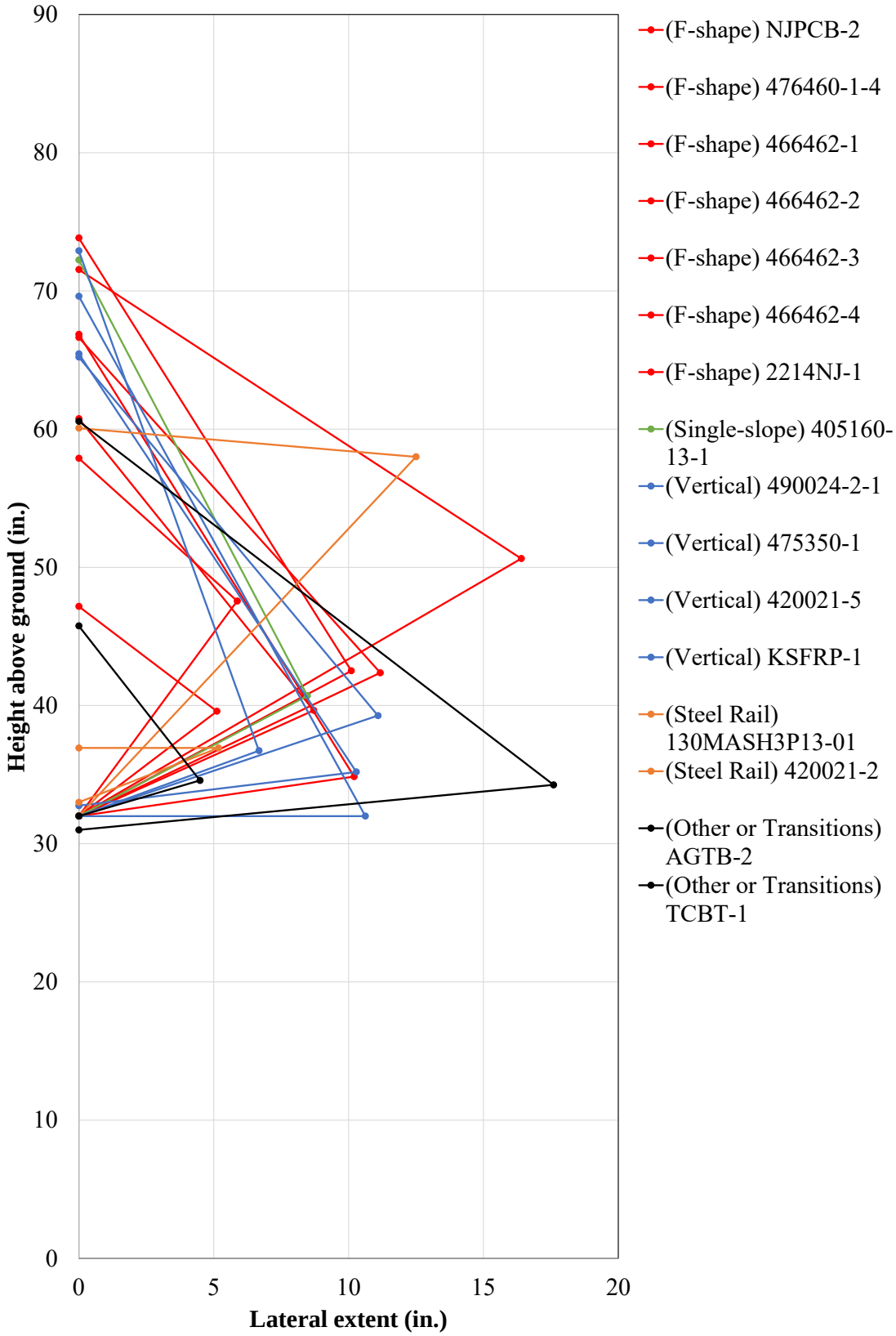


Figure C-5. Preliminary MASH TL-3 ZOI, 31- to 33-in. Tall Barriers

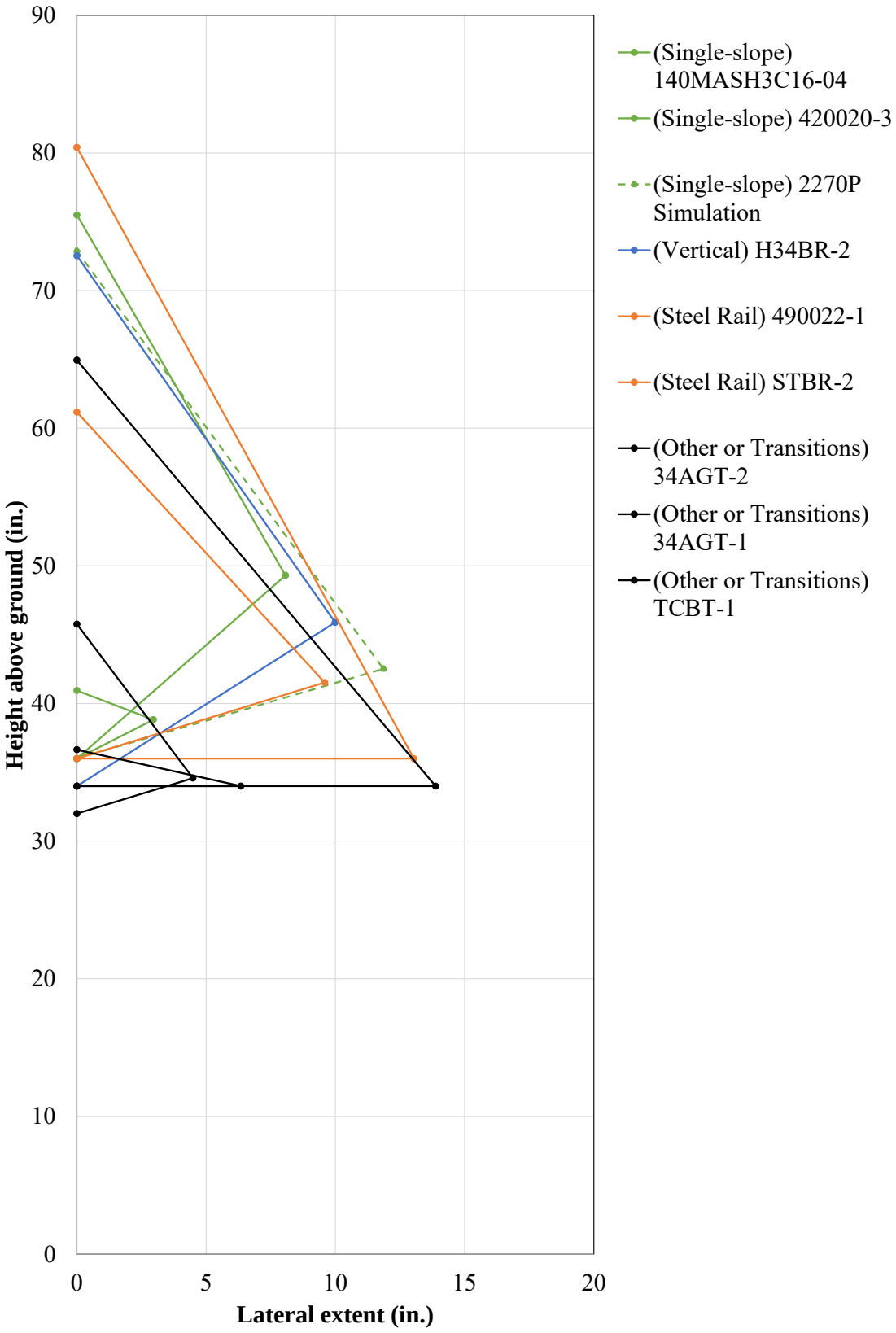


Figure C-6. Preliminary MASH TL-3 ZOI, 34- to 36-in. Tall Barriers

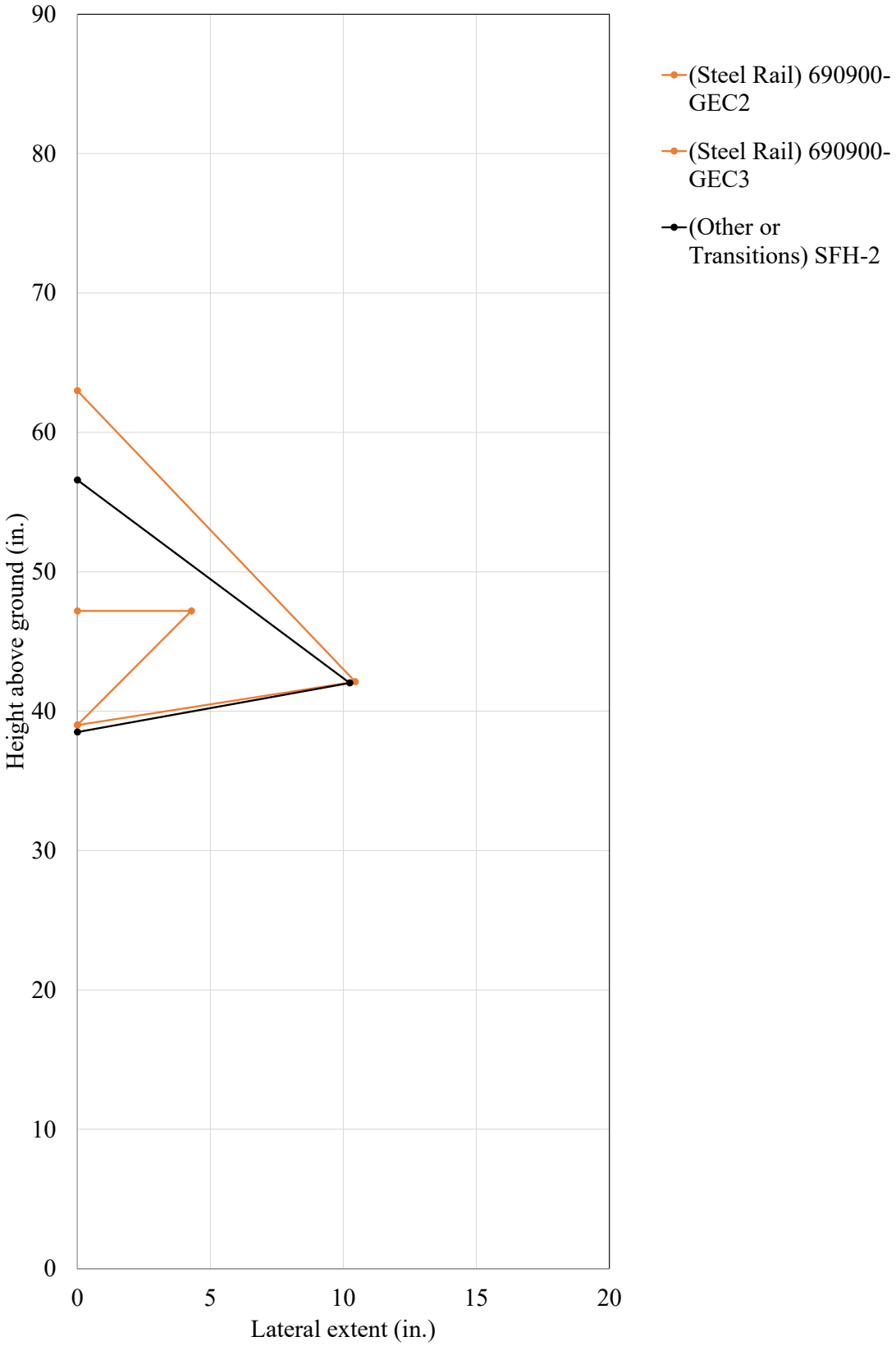


Figure C-7. Preliminary MASH TL-3 ZOI, 38- to 39-in. Tall Barriers

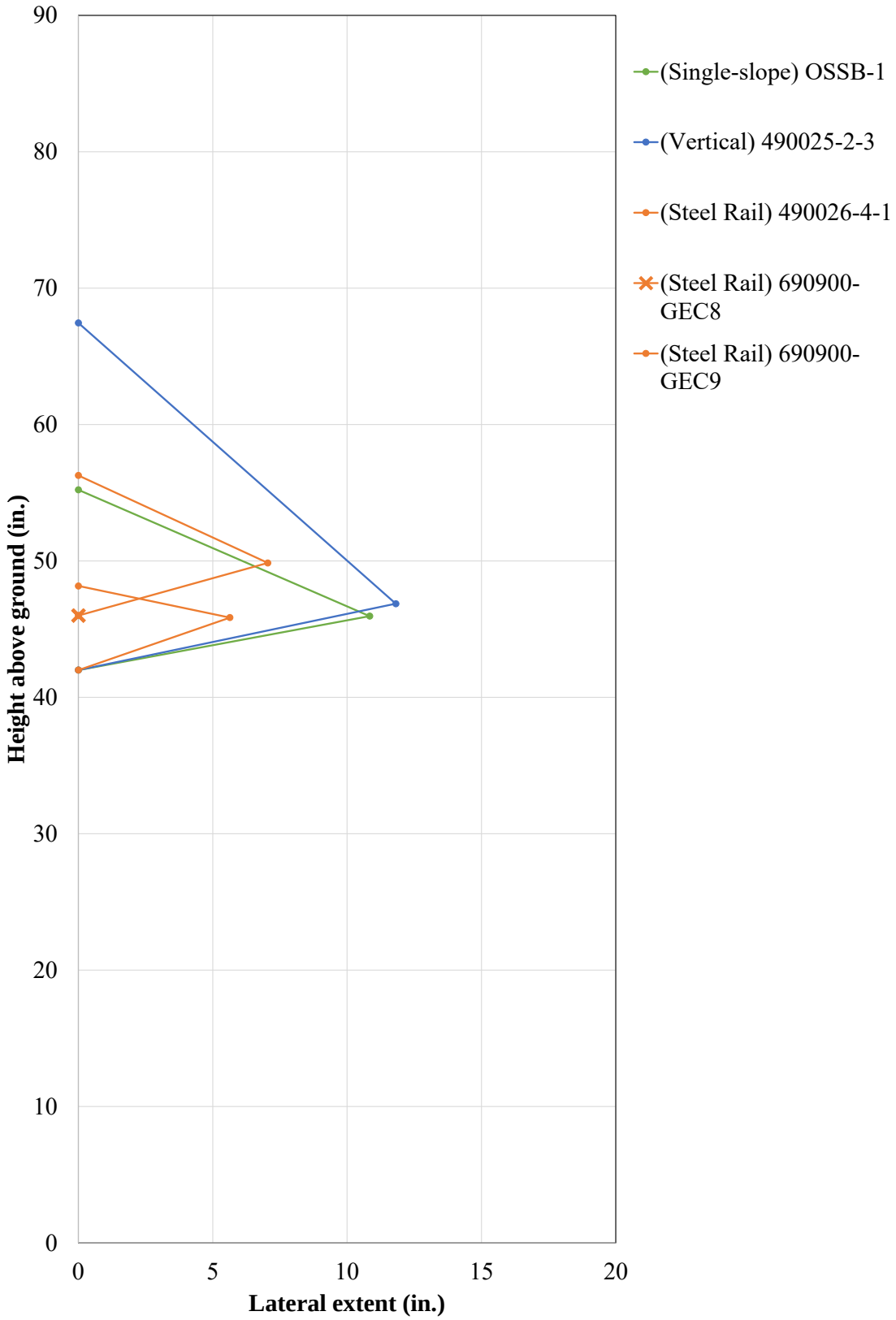


Figure C-8. Preliminary MASH TL-3 ZOI, 42- to 46-in. Tall Barriers

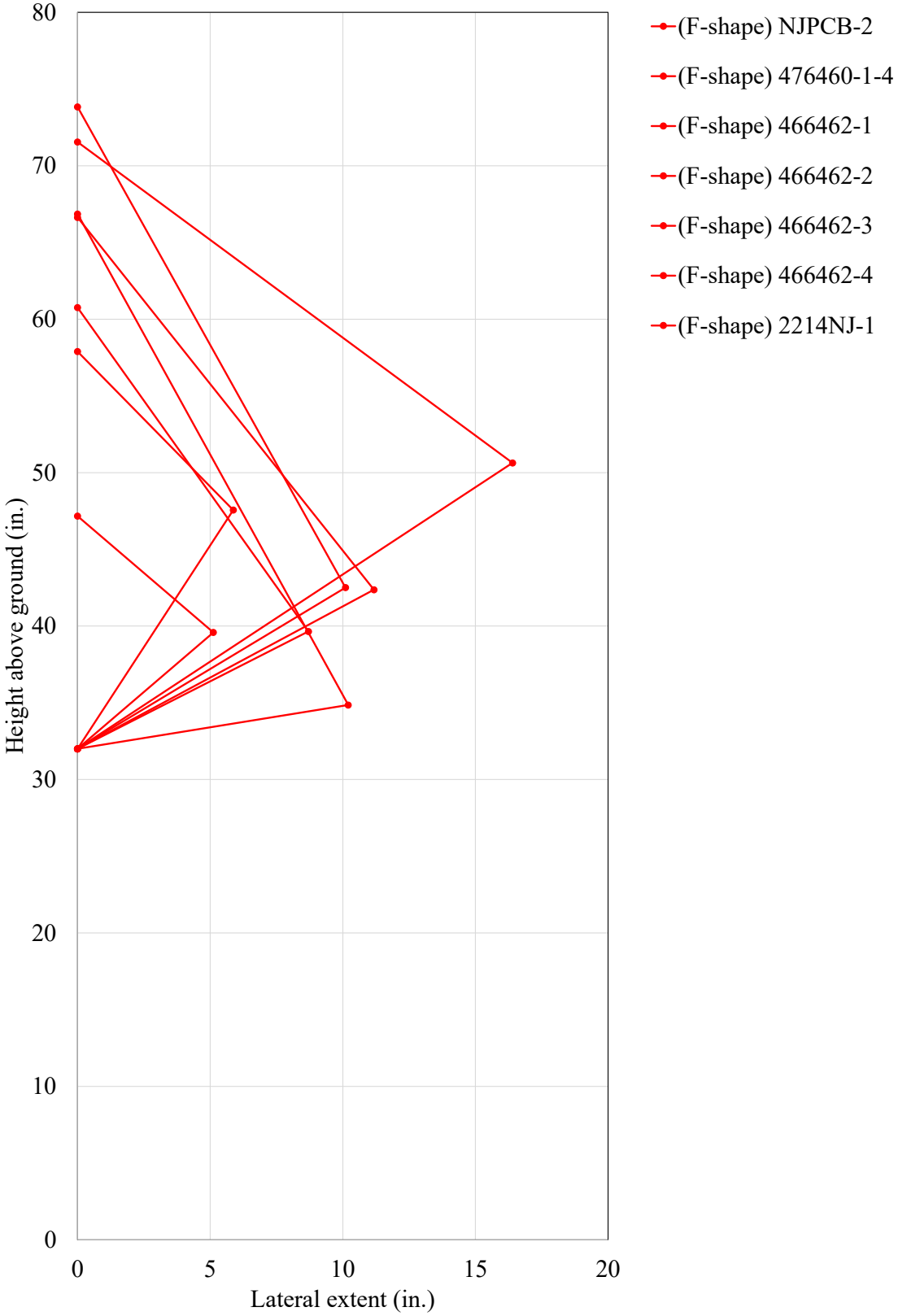


Figure C-9. Preliminary MASH TL-3 ZOI, F-shape Barriers

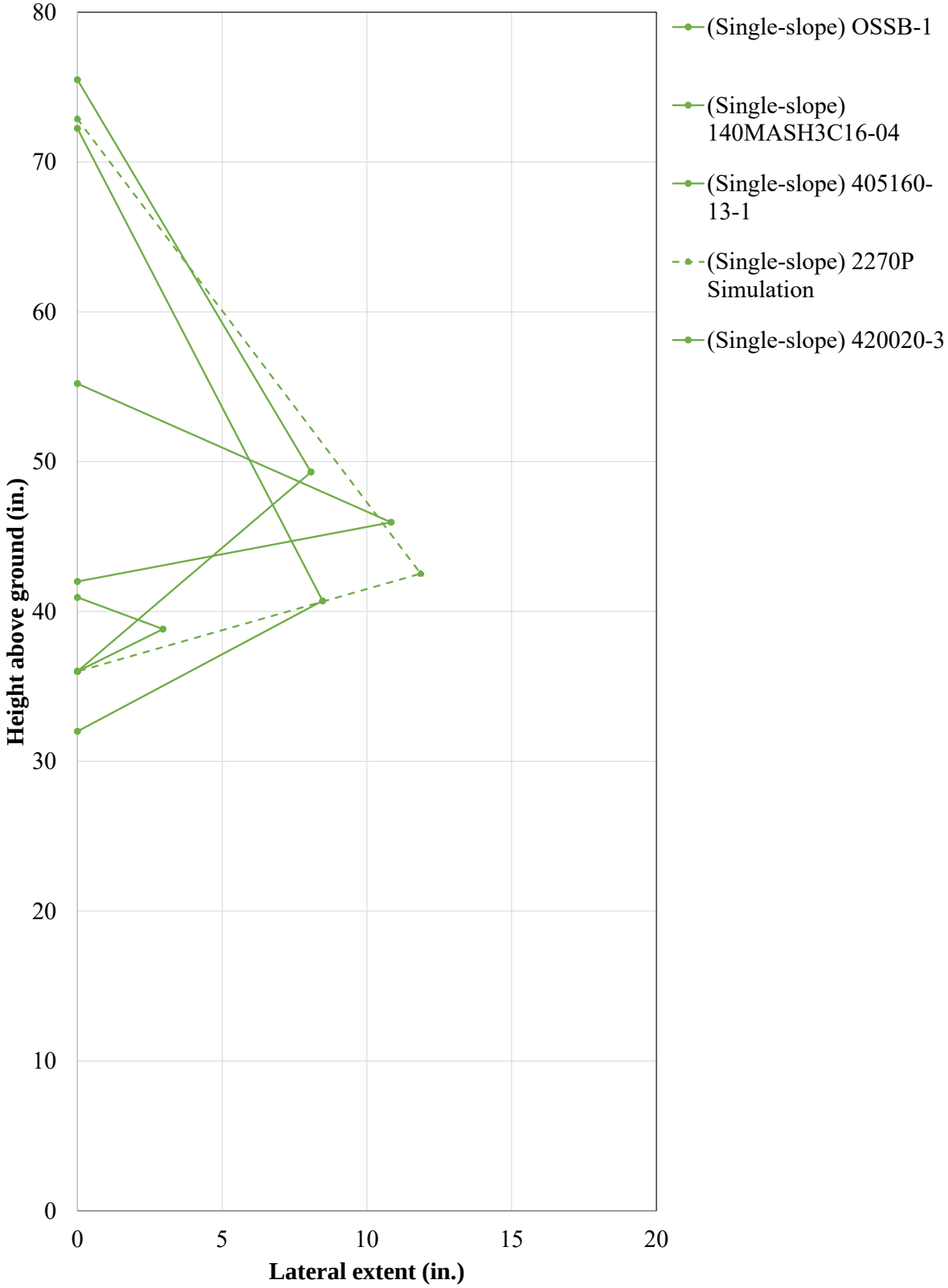


Figure C-10. Preliminary MASH TL-3 ZOI, Single-slope Barriers

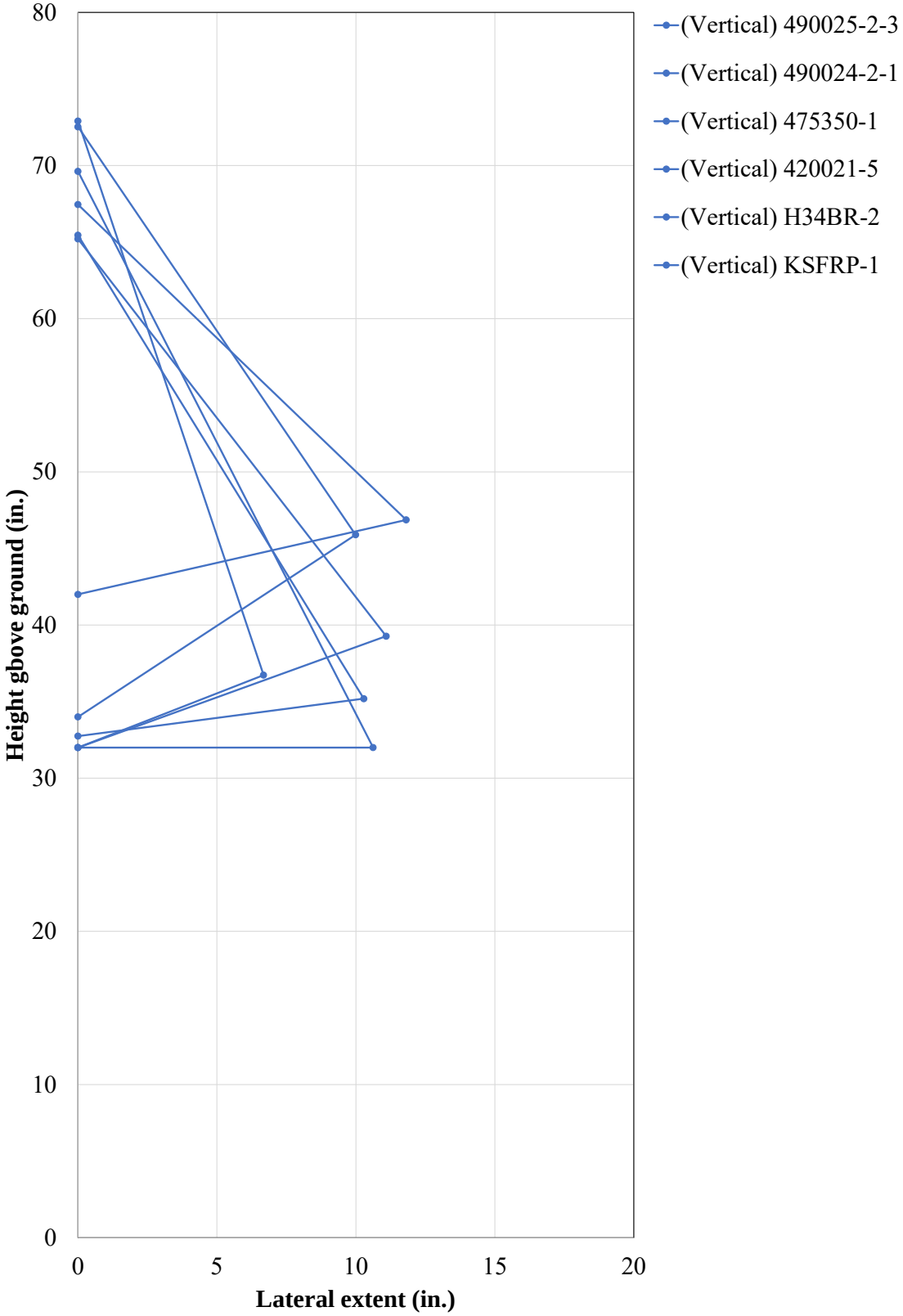


Figure C-11. Preliminary MASH TL-3 ZOI, Vertical Barriers

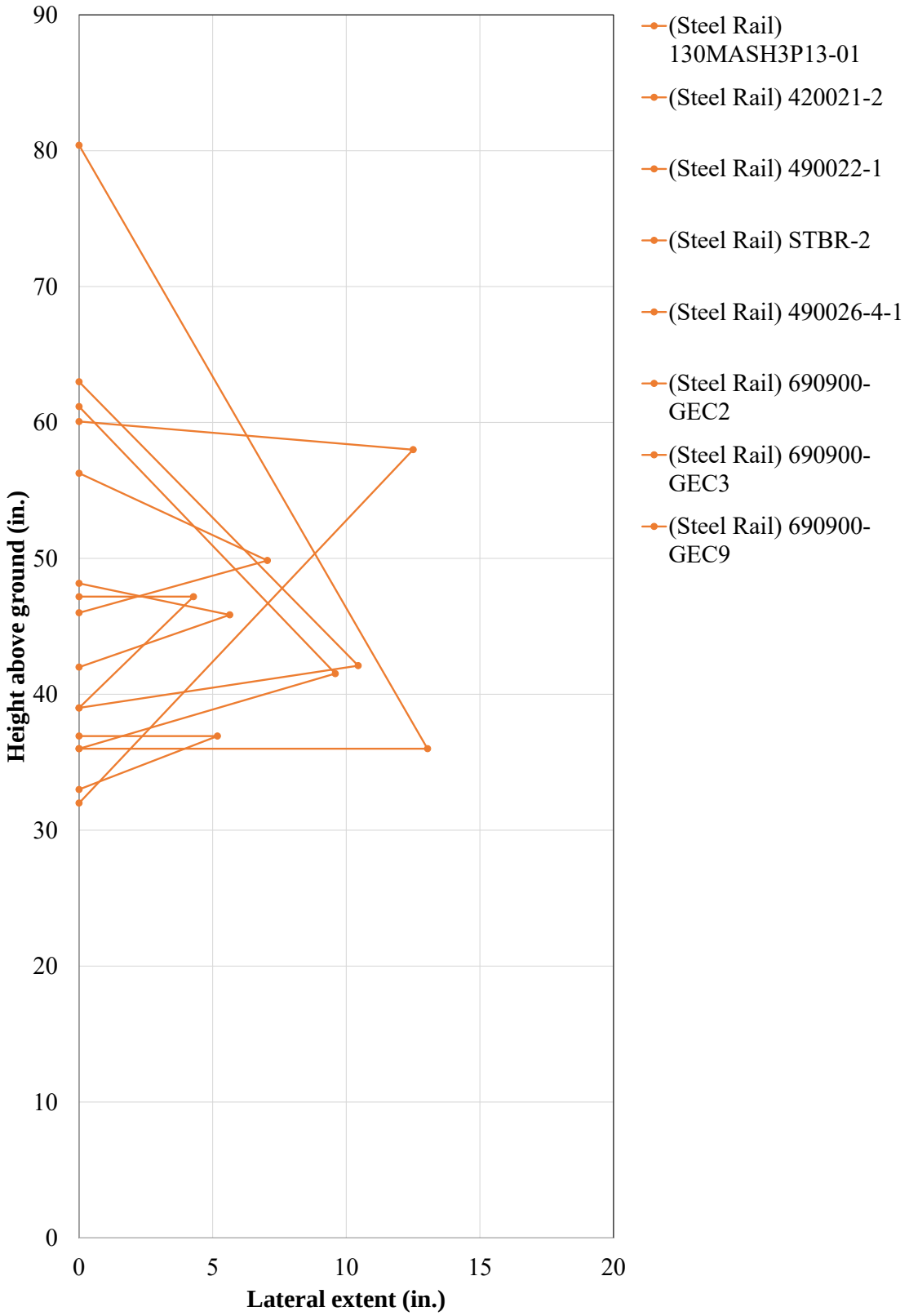


Figure C-12. Preliminary MASH TL-3 ZOI, Steel Rails

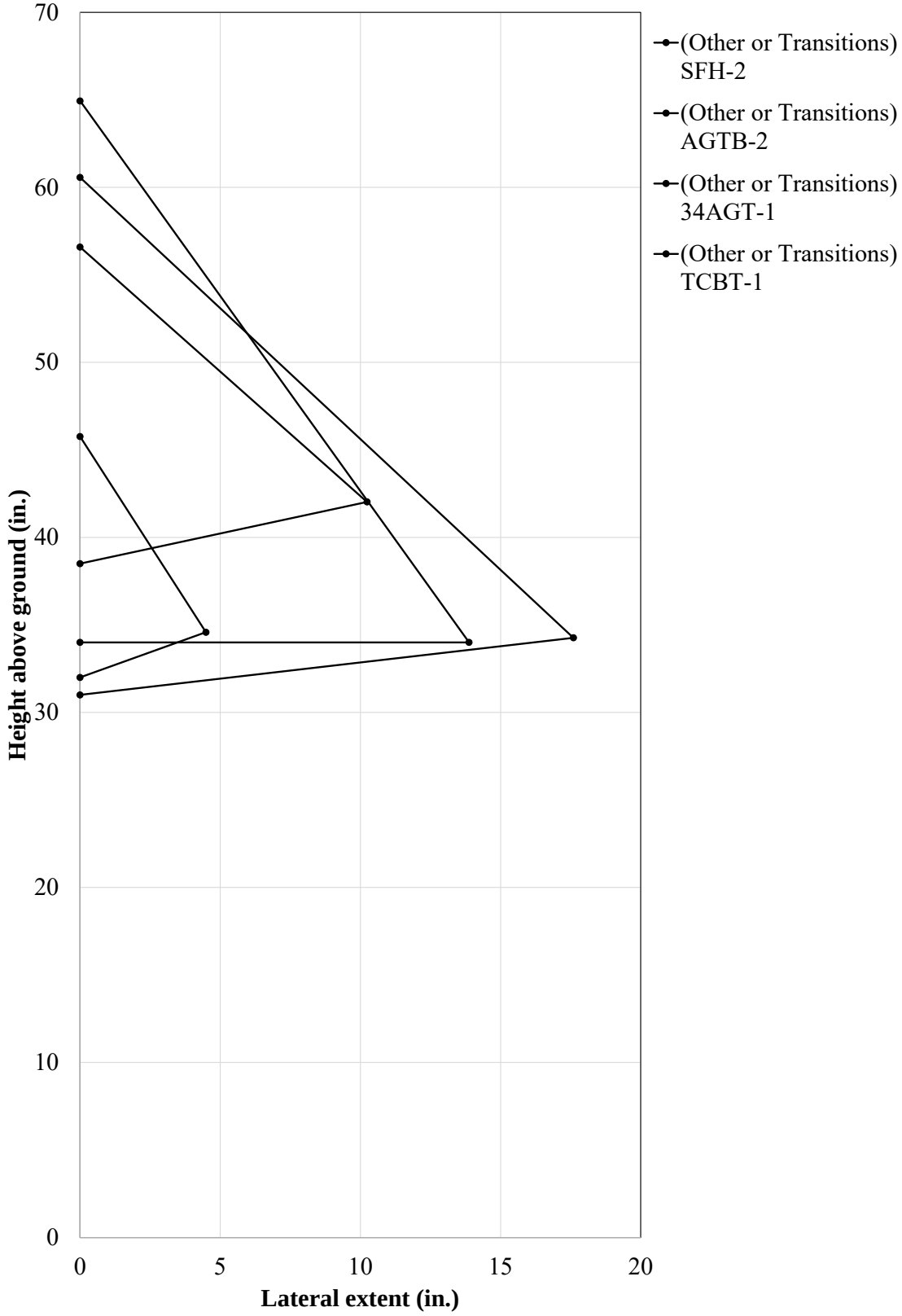


Figure C-13. Preliminary MASH TL-3 ZOI, Other Rigid Barriers or Transitions

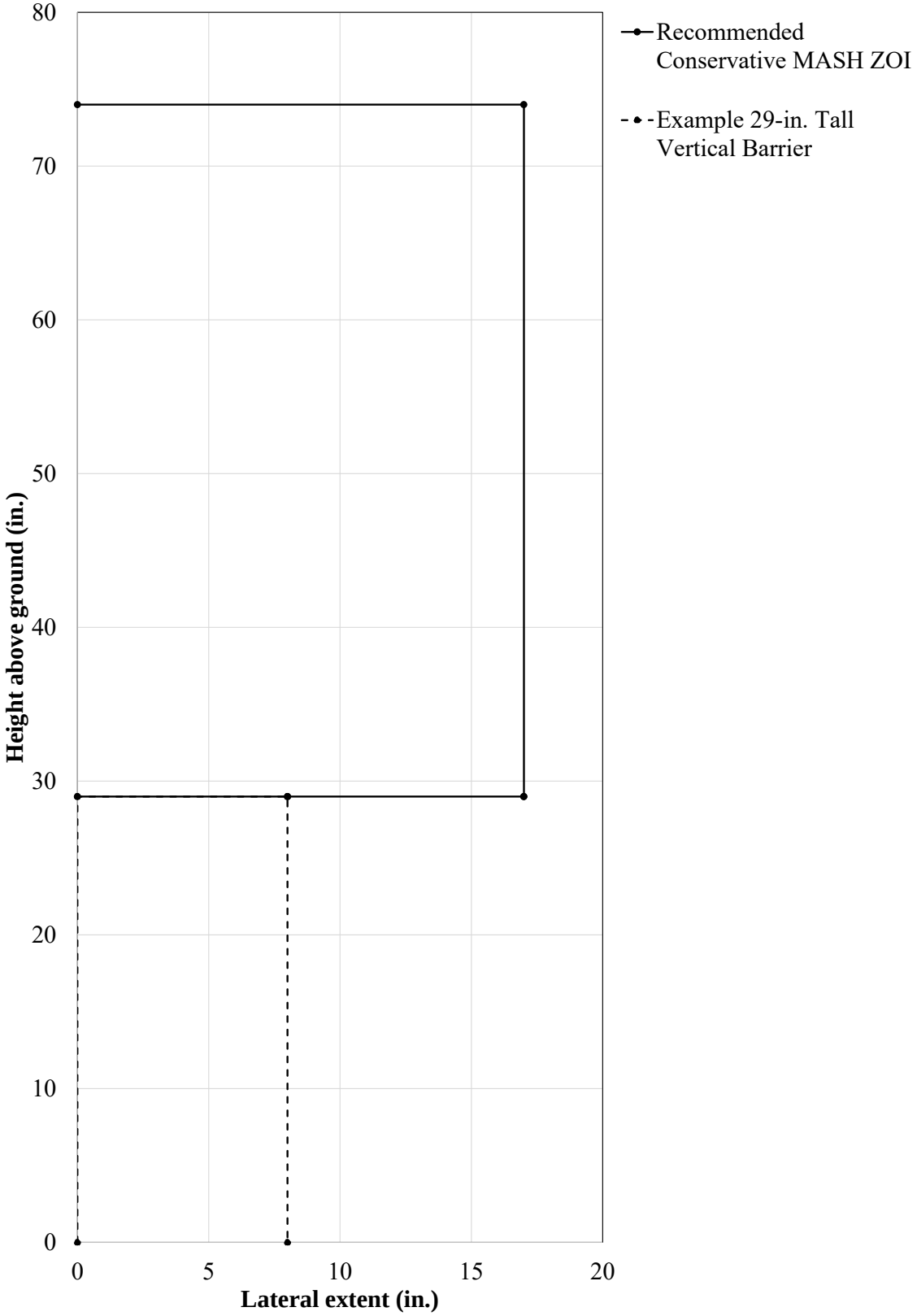


Figure C-14. Preliminary MASH TL-3 Recommended Conservative ZOI Envelope

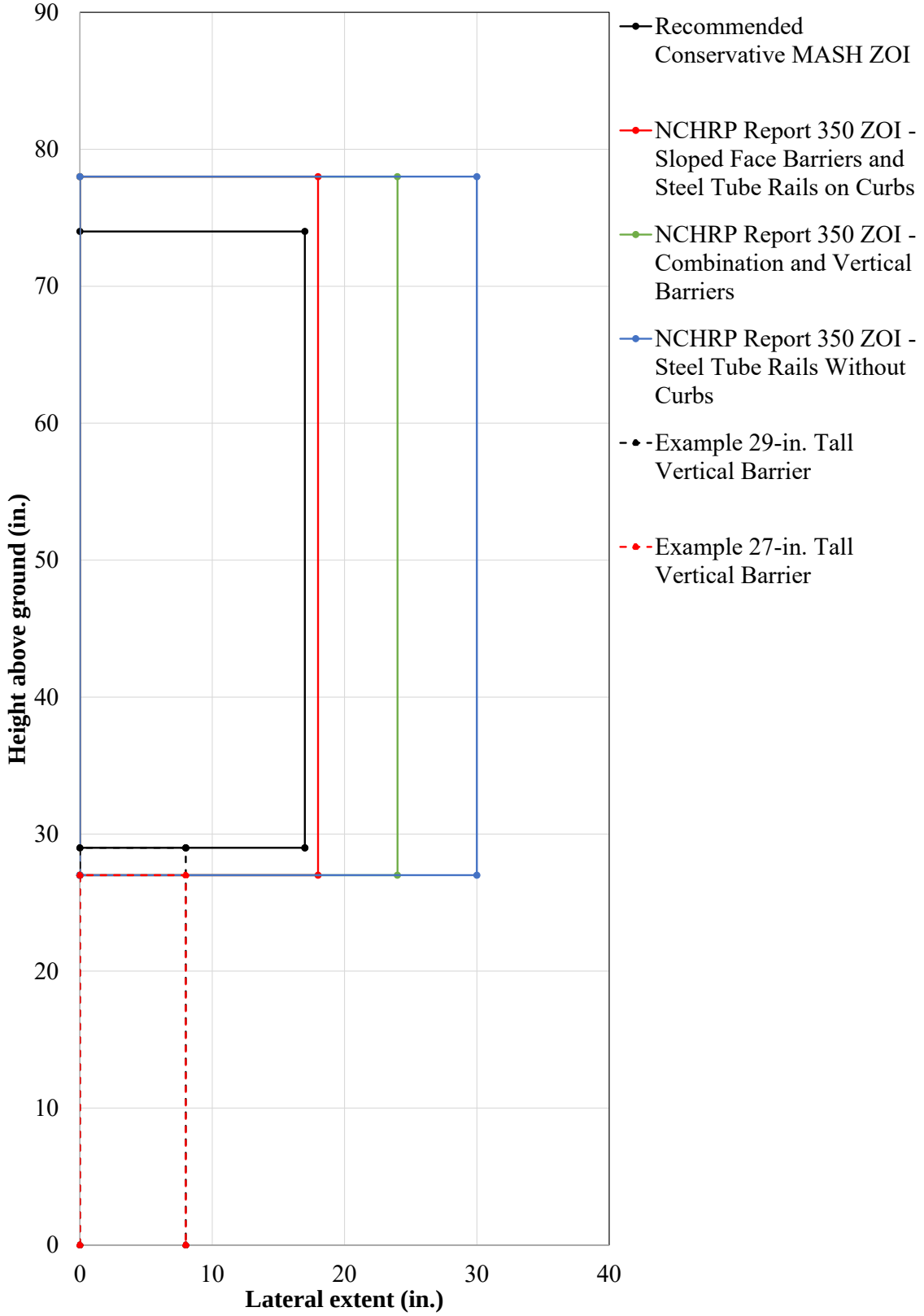


Figure C-15. *NCHRP Report 350* and Preliminary MASH TL-3 ZOI Envelopes

## C-3 MASH TL-4

Eight MASH test designation no. 4-12 tests were analyzed as well as one computer simulation result. ZOI envelopes are shown for the cab in Figures C-16 through C-21 and for the box in Figures C-22 through C-27.

In two crash tests, the box protruded beyond the back of the rail and extended below the top rail surface. Simulation of the 36-in. tall single-slope barrier displayed a similar lateral extent compared to the crash tests, but the vertical extent varied as the simulated box pitched more than seen in crash testing. Thus, further SUT calibration was required in Phase II.

Maximum lateral extent for single-slope, vertical, and steel rail barriers were 81, 62, and 86 in., respectively. Note in test no. STBR-4 (Pena et al. 2020) the SUT rolled on top of the front face of the barrier, which is allowable under MASH criteria. However, this produced a very large lateral extent, and the overall maximum lateral extent would be much less for steel rails if this test were excluded. Maximum lateral extent was 86 and 63 in. for 36- and 42-in. tall barriers, respectively. Thus, shorter barrier heights had larger lateral extents for both the cab and cargo box.

Five single-slope rails had a height of 36 in., and the maximum lateral extent varied from 49.2 to 80.7 in. For MASH TL-4 cab zones, the maximum lateral extents were 36 and 11 in. for 36- and 42-in. tall barriers, respectively. The maximum vertical extent was 161 and 195 in. for 36-and 42-in. tall barriers, respectively. A preliminary conservative MASH TL-4 envelope is shown in Figure C-28, including data from test no. STBR-4.

*NCHRP Report 350* and preliminary MASH ZOI envelopes are compared in Figure C-29. The TL-4 ZOI from *NCHRP Report 350*, shown in Figure C-29, extended:

- 80 in. laterally and 120 in. vertically for the cargo box
- 34 in. laterally and 96 in. vertically for the cab

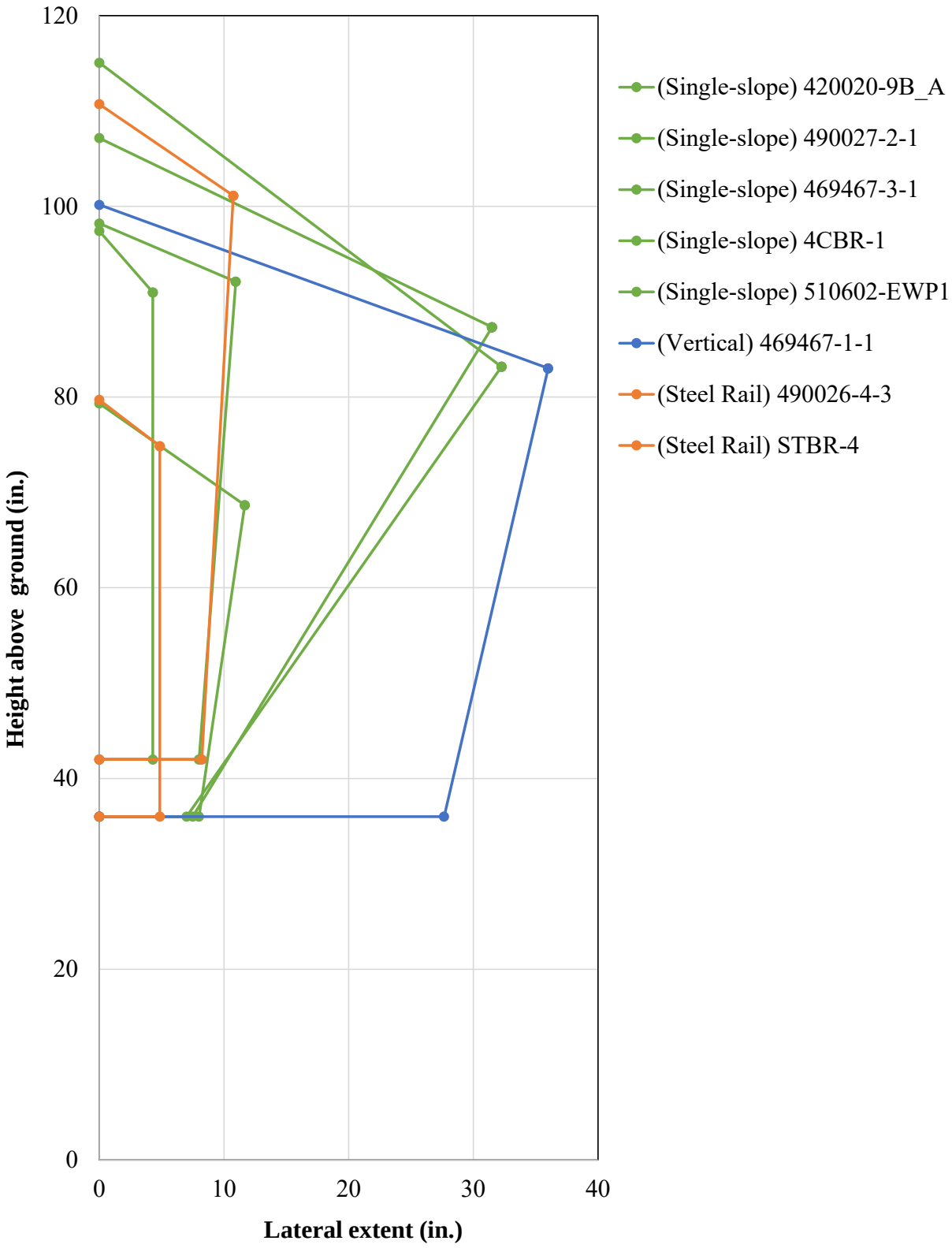


Figure C-16. Preliminary MASH TL-4 Cab ZOI, All Barriers

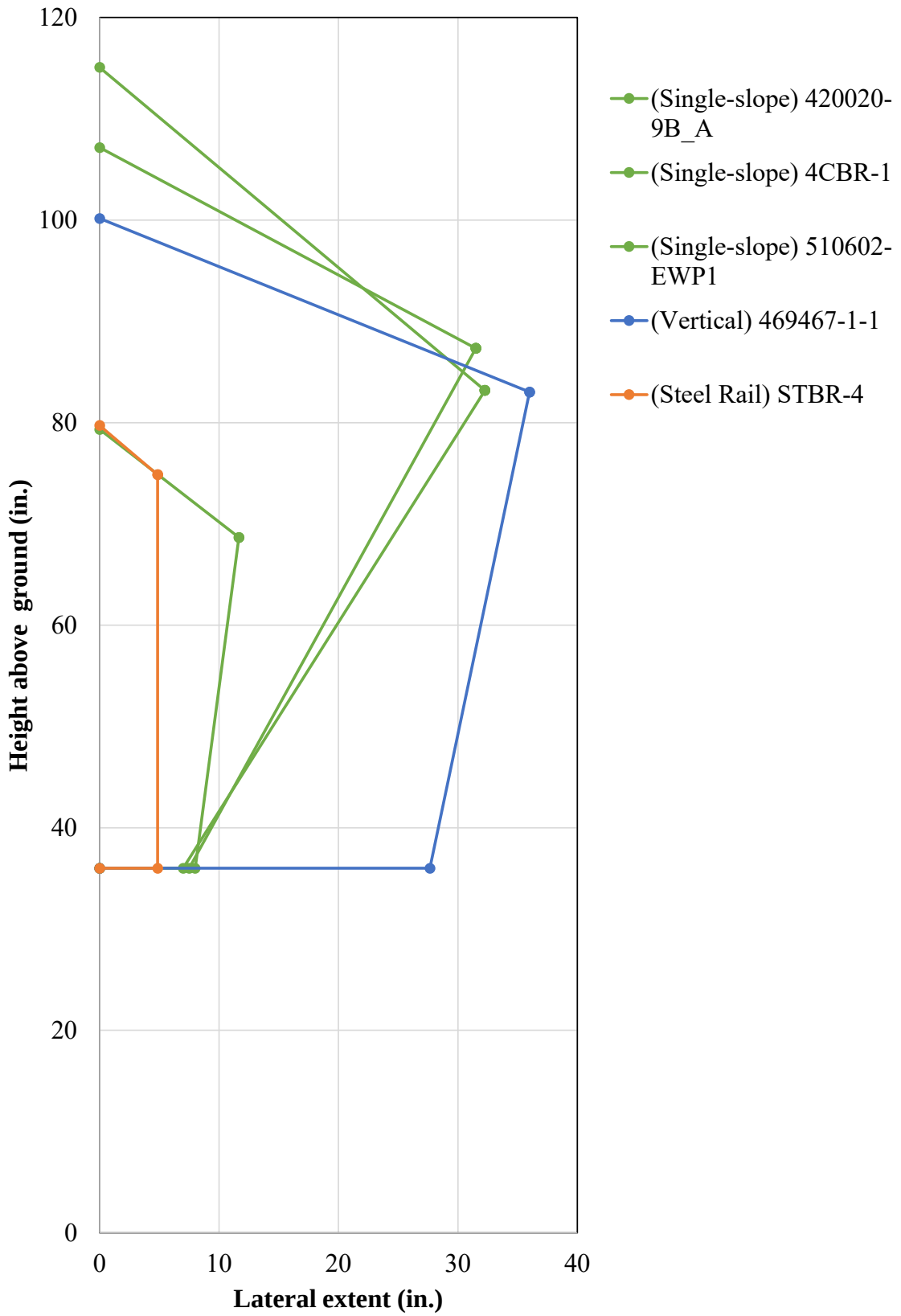


Figure C-17. Preliminary MASH TL-4 Cab ZOI, 36-in. Tall Barriers

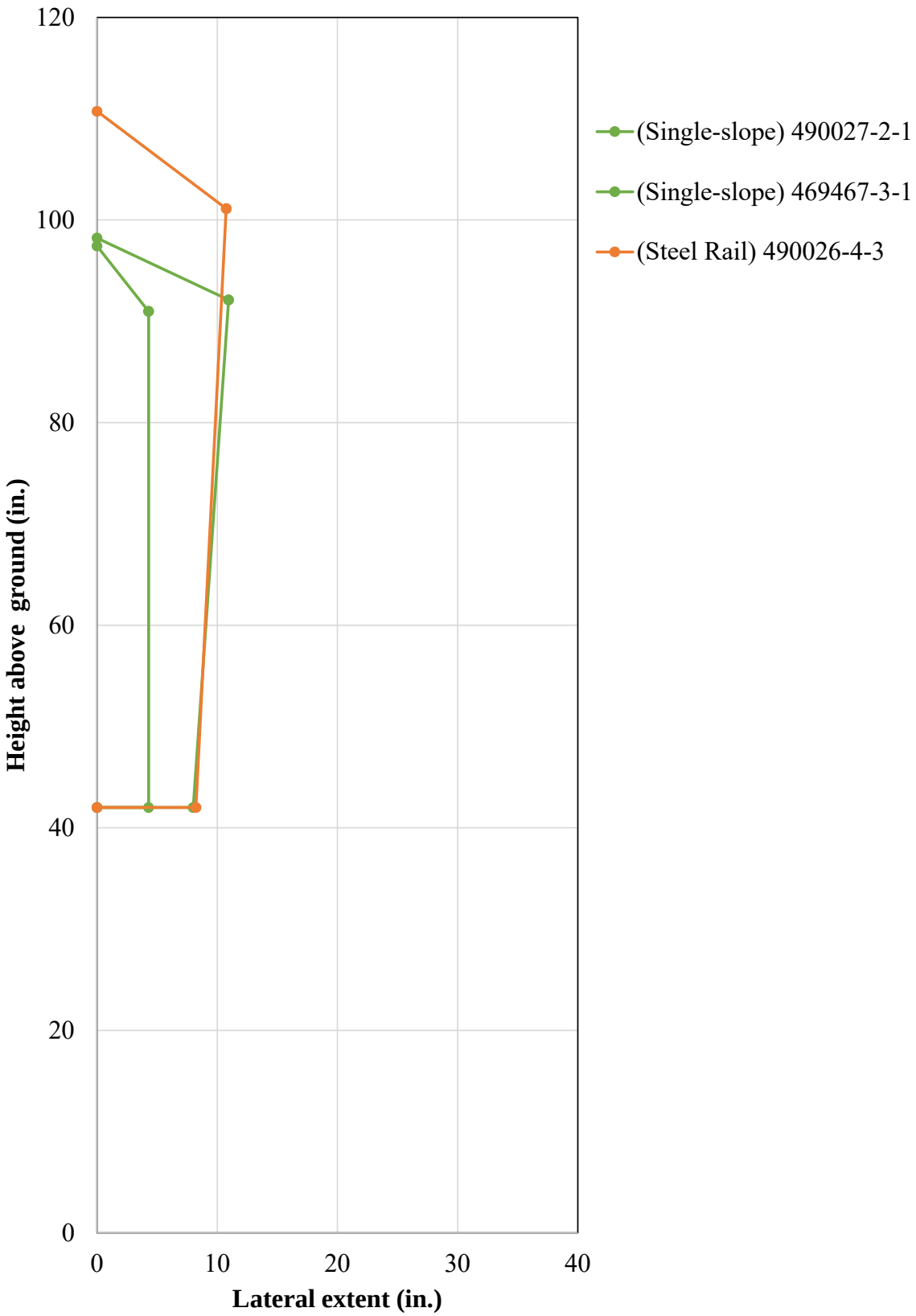


Figure C-18. Preliminary MASH TL-4 Cab ZOI, 42-in. Tall Barriers

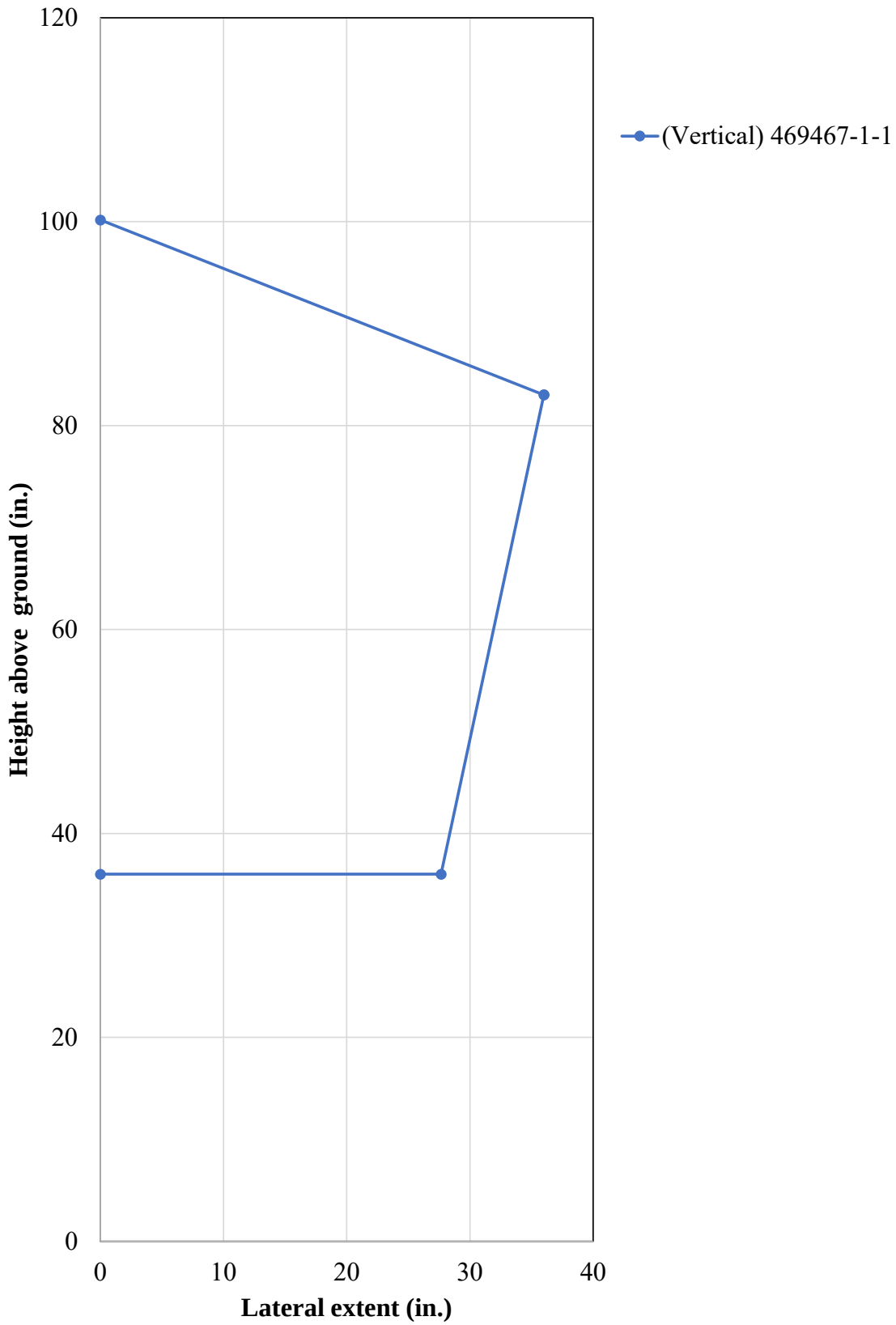


Figure C-19. Preliminary MASH TL-4 Cab ZOI, Vertical Barriers

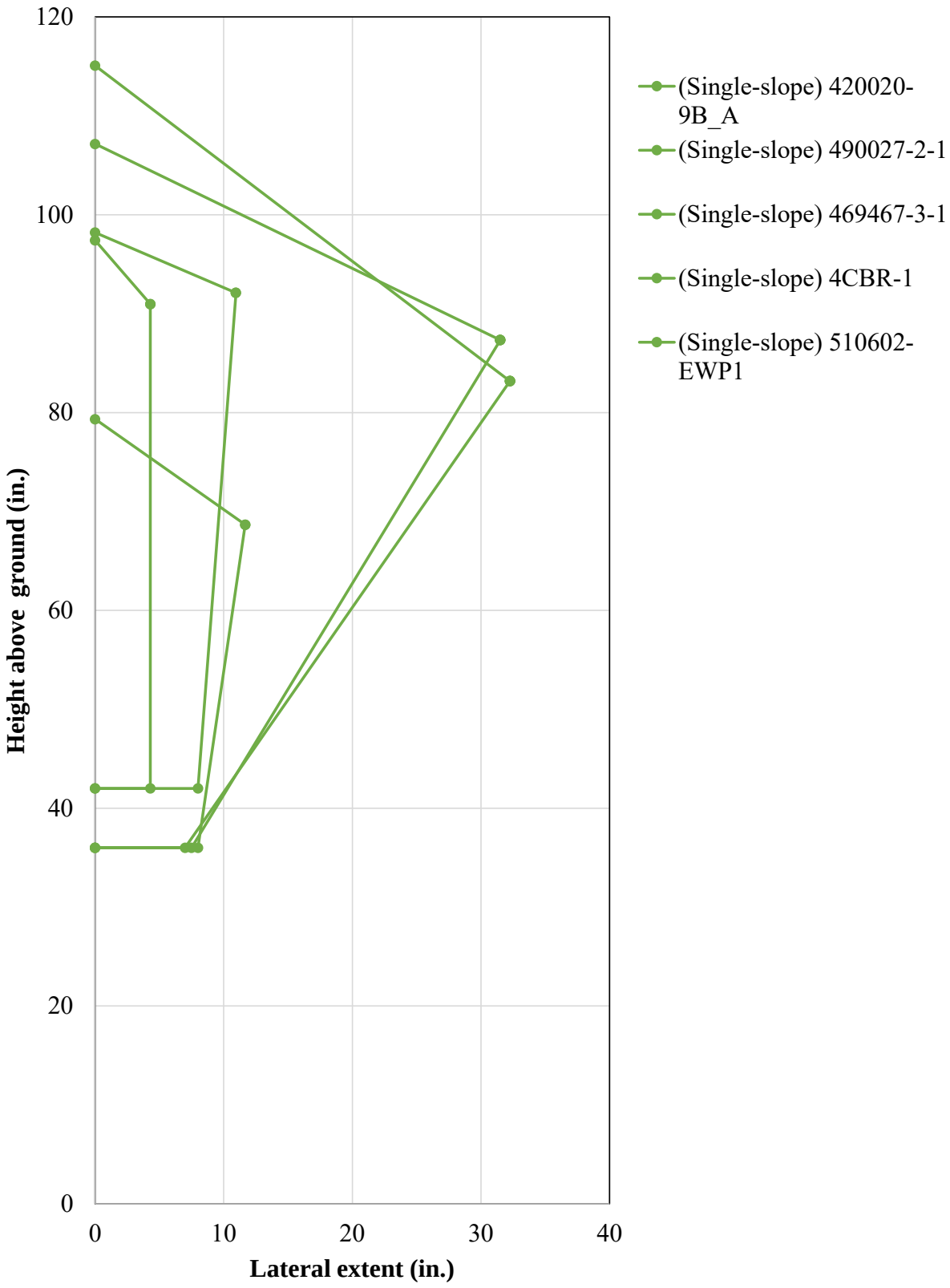


Figure C-20. Preliminary MASH TL-4 Cab ZOI, Single-slope Barriers

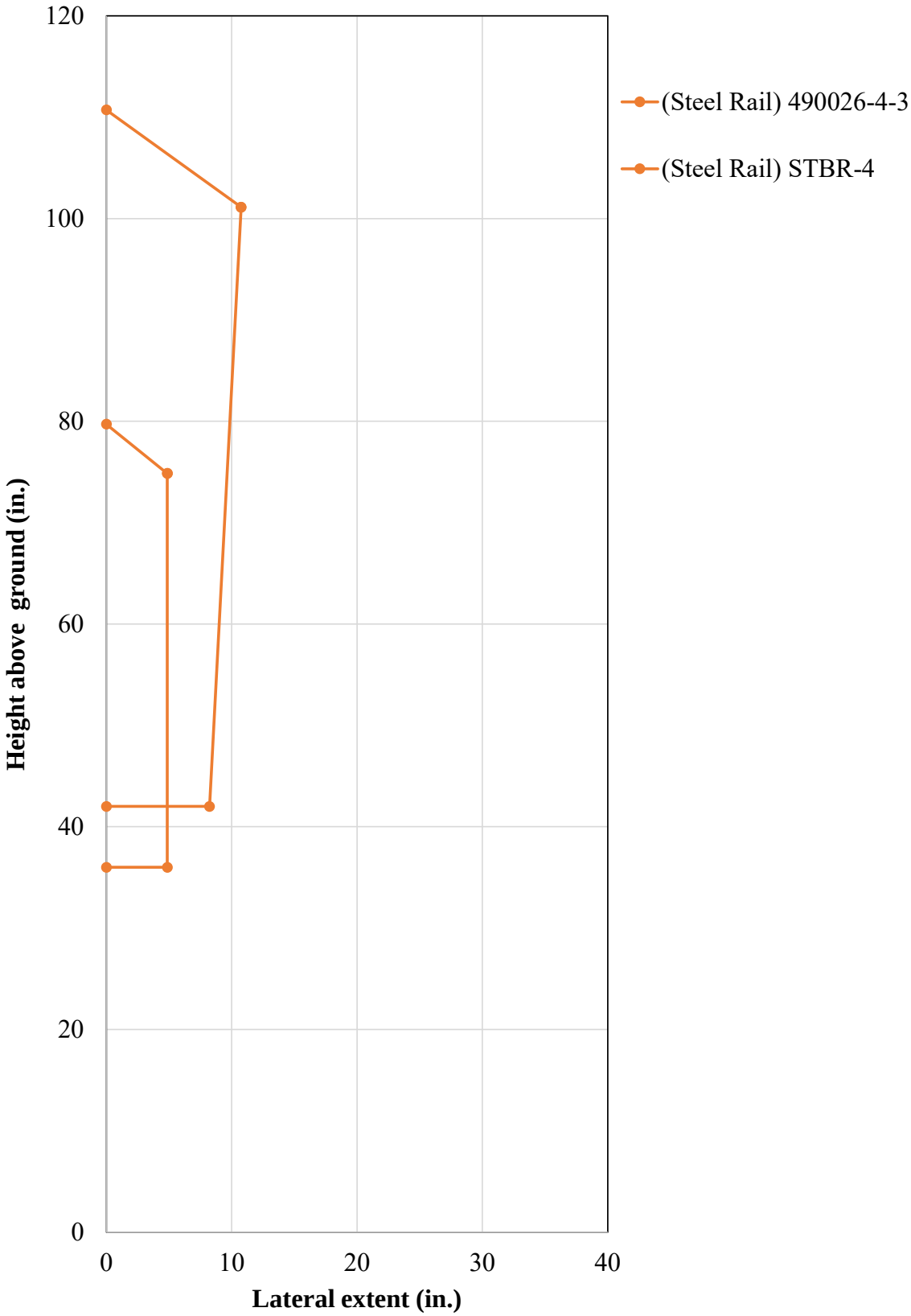


Figure C-21. Preliminary MASH TL-4 Cab ZOI, Steel Rails

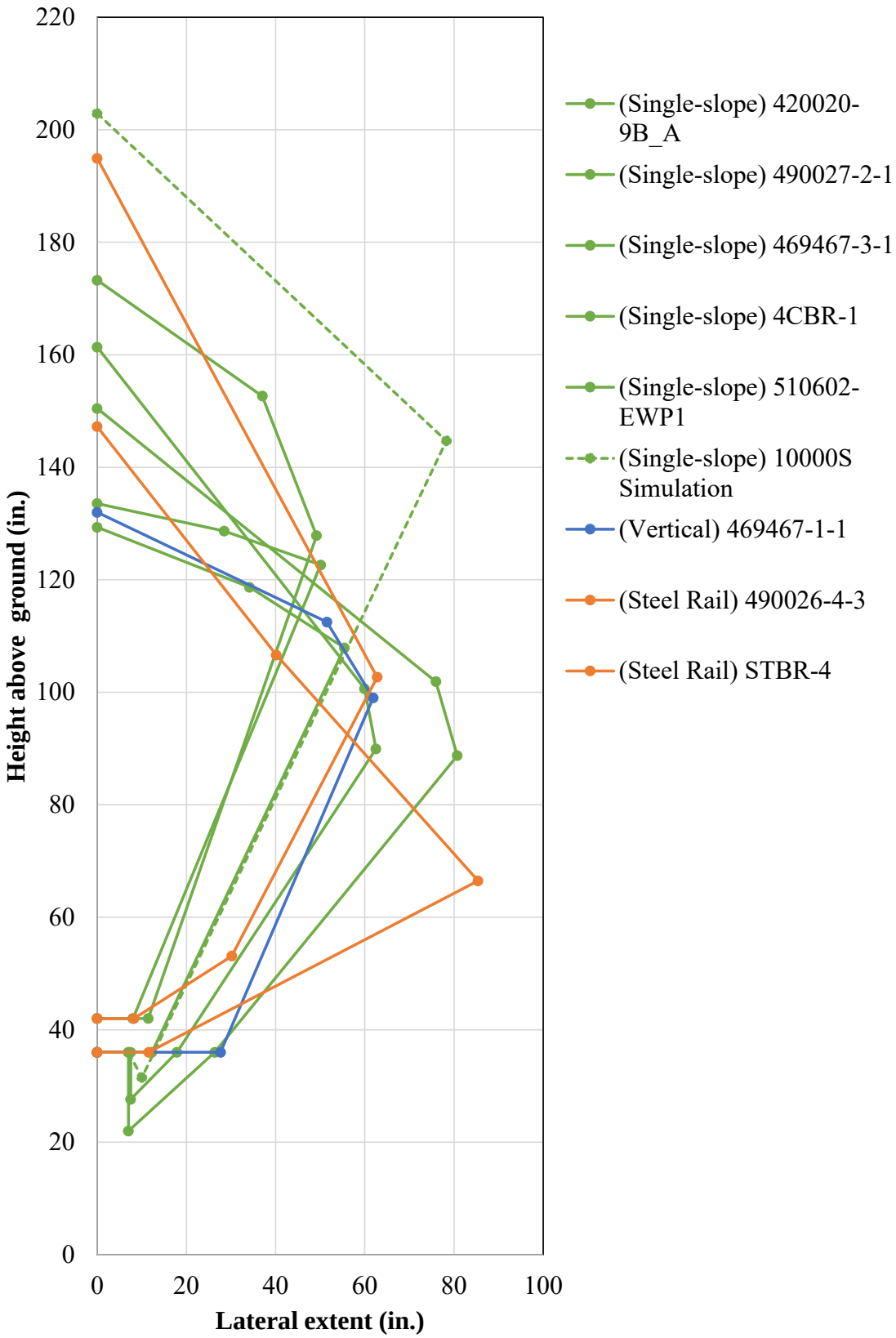


Figure C-22. Preliminary MASH TL-4 Box ZOI, All Barriers

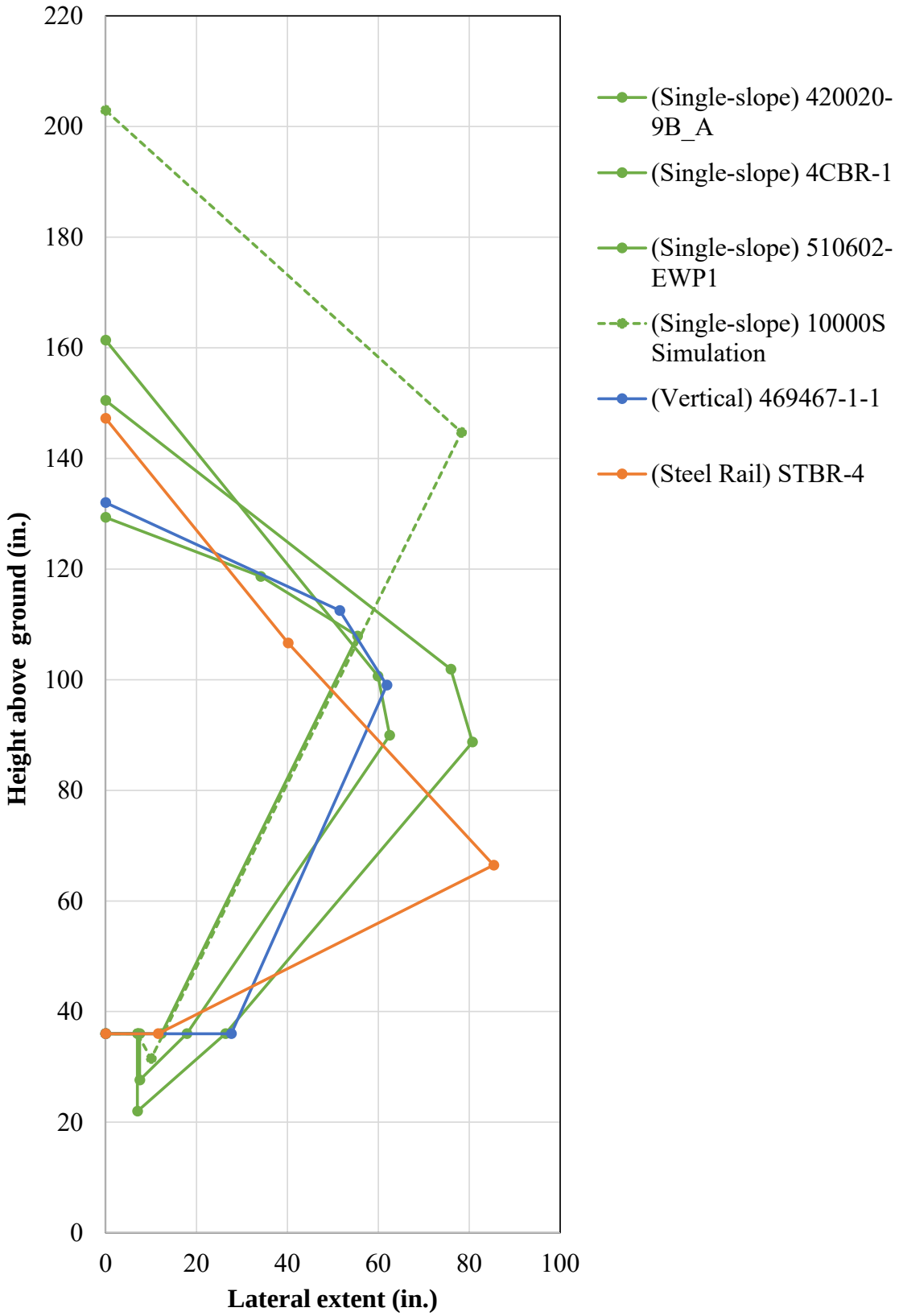


Figure C-23. Preliminary MASH TL-4 Box ZOI, 36-in. Tall Barriers

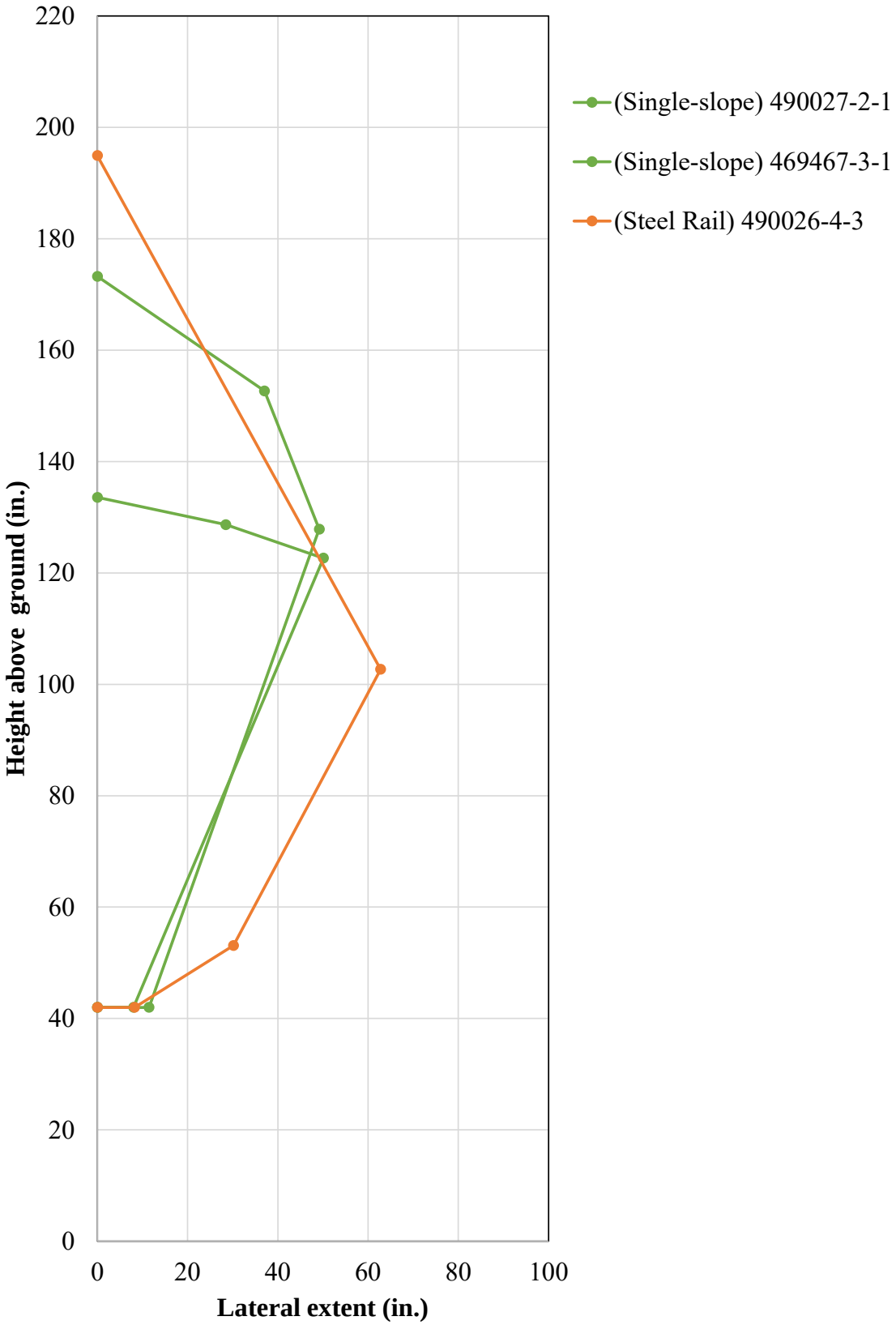


Figure C-24. Preliminary MASH TL-4 Box ZOI, 42-in. Tall Barriers

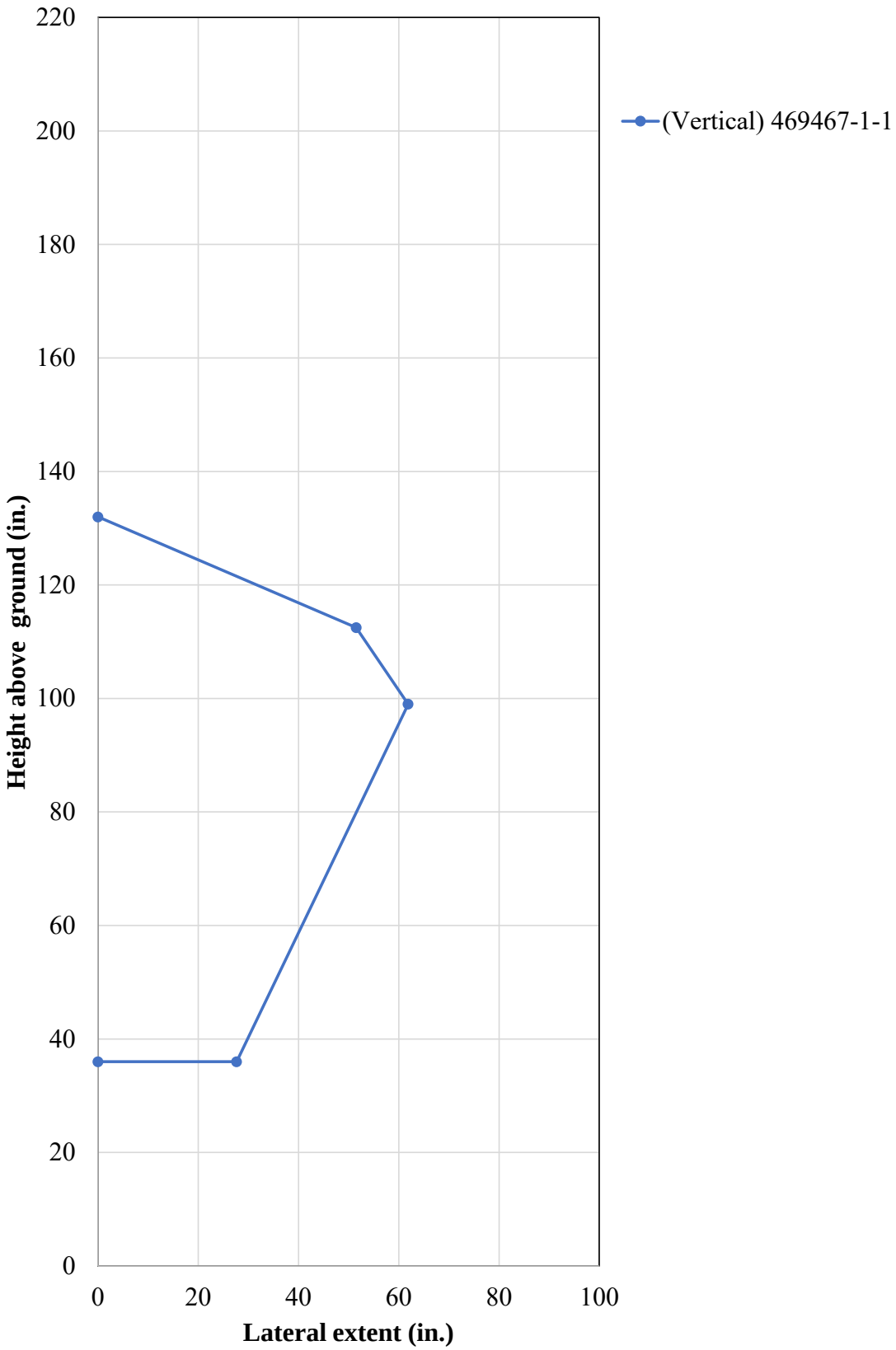


Figure C-25. Preliminary MASH TL-4 Box ZOI, Vertical Barriers

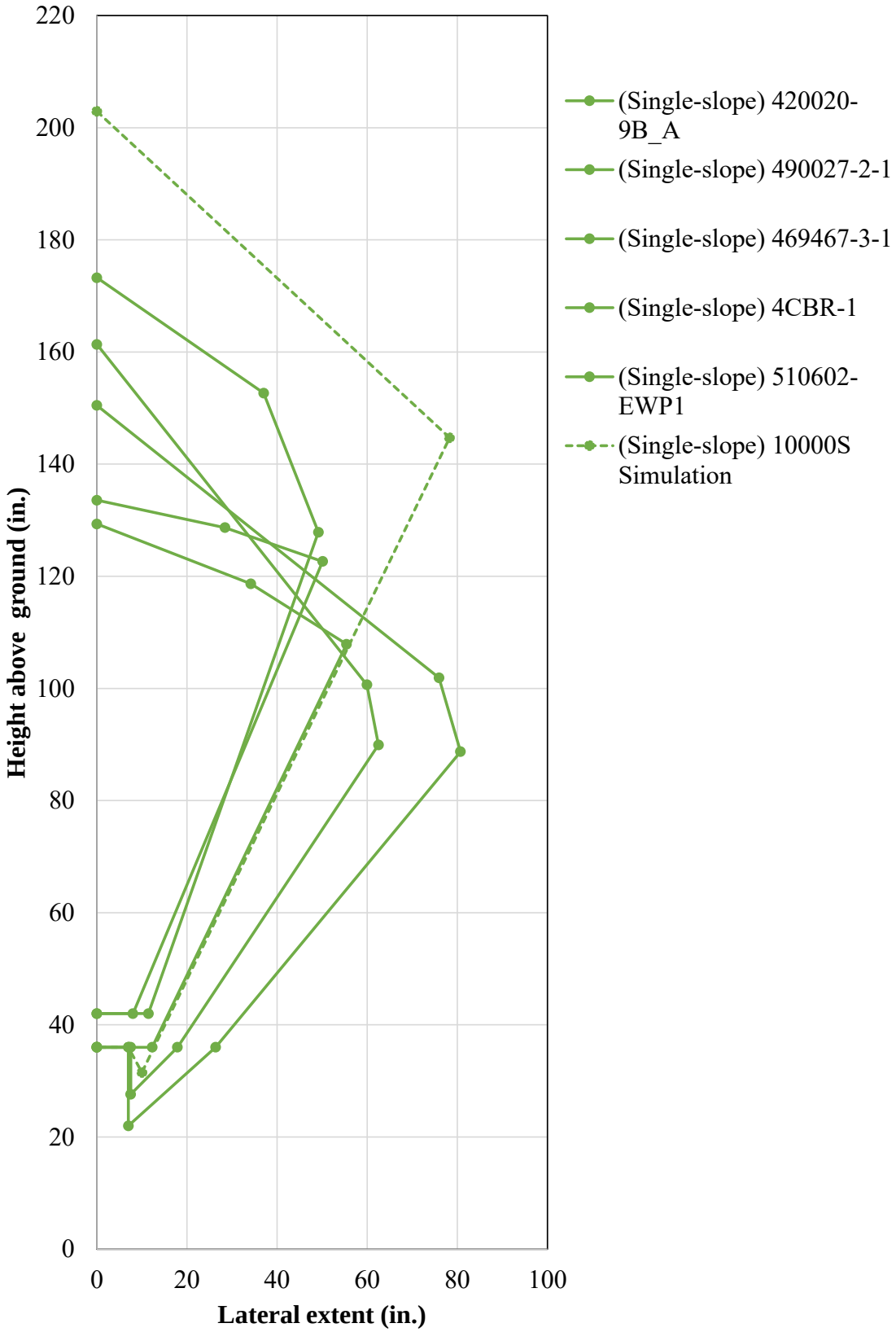


Figure C-26. Preliminary MASH TL-4 Box ZOI, Single-slope Barriers

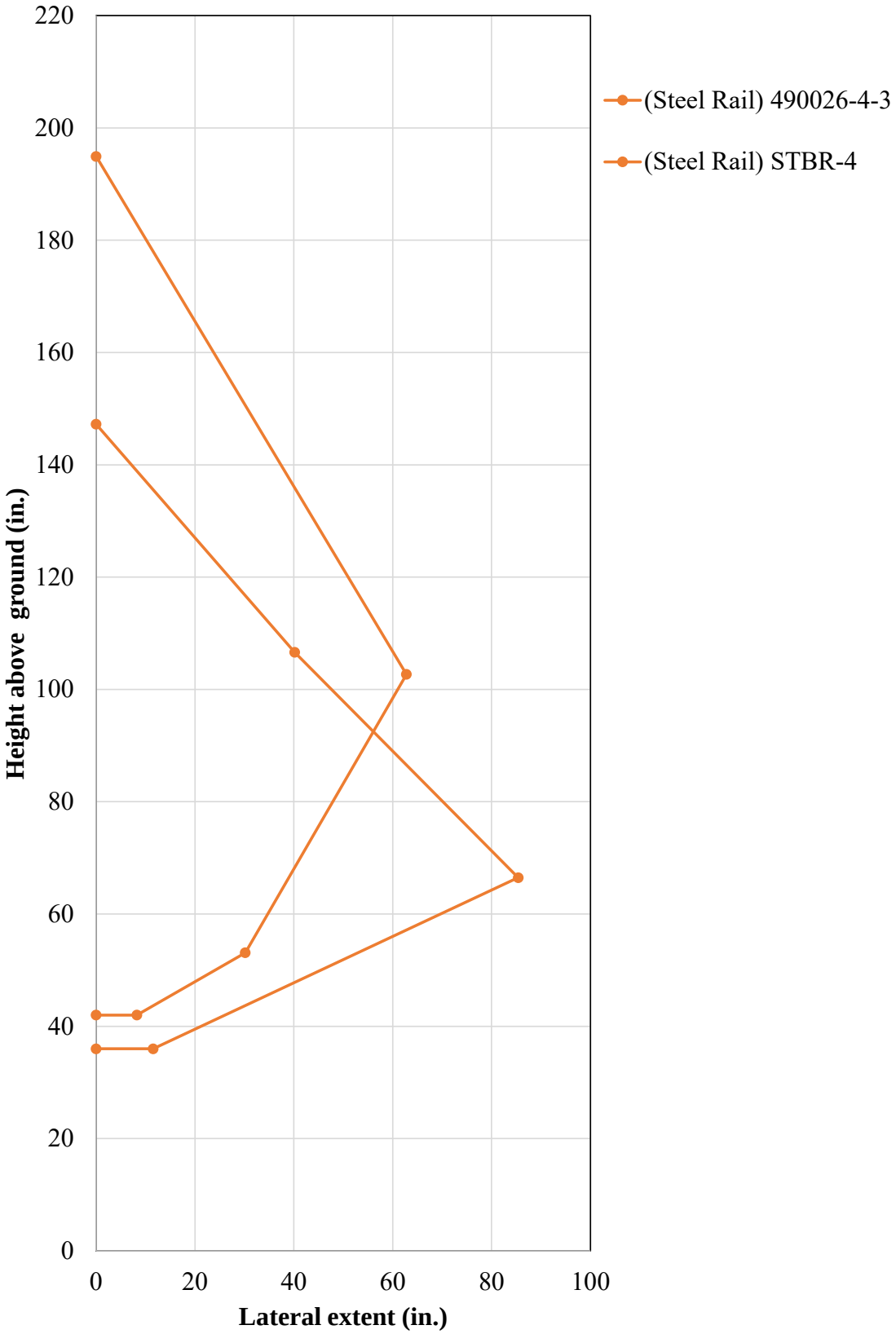


Figure C-27. Preliminary MASH TL-4 Box ZOI, Steel Rails

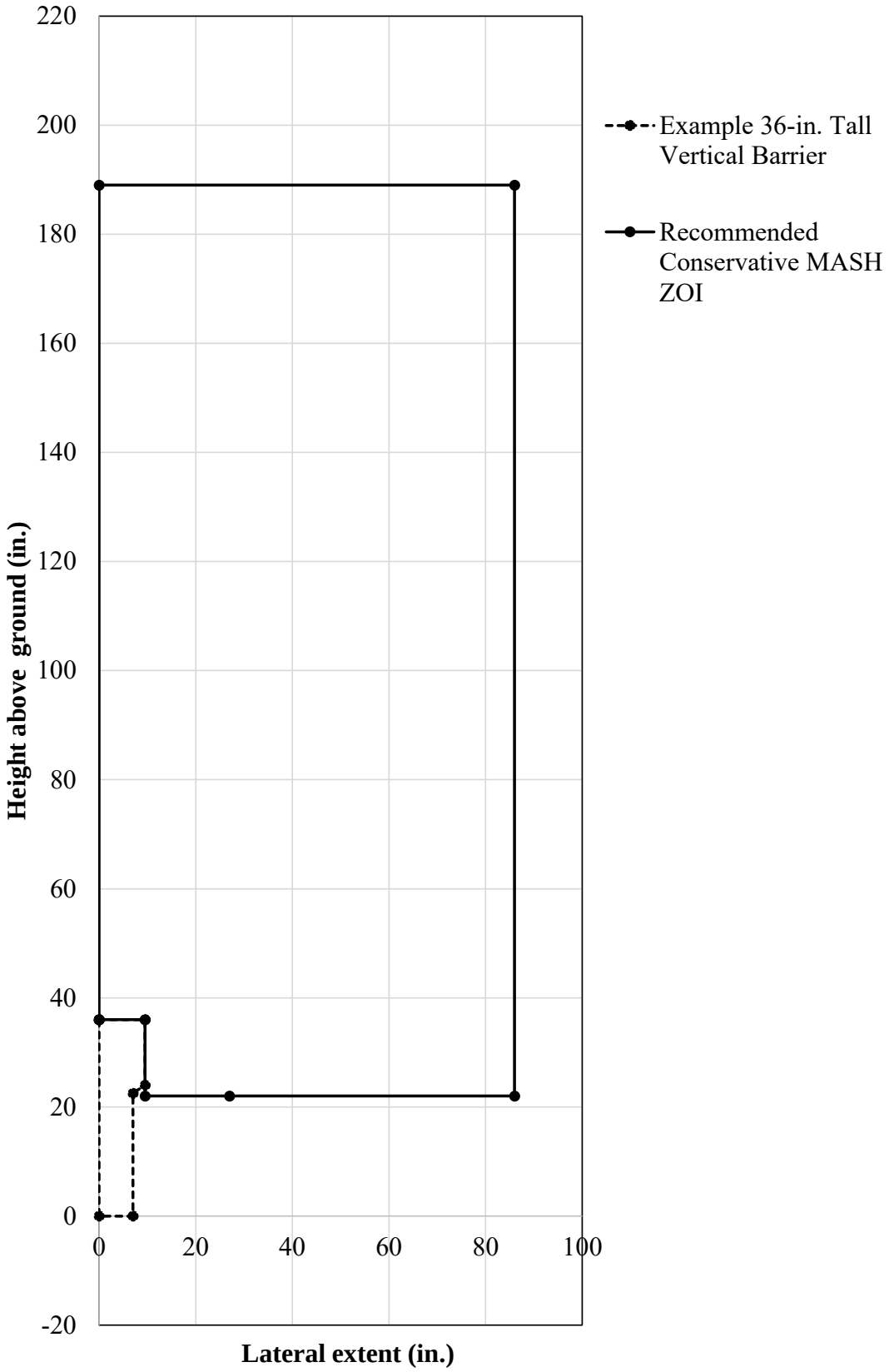


Figure C-28. Preliminary MASH TL-4 Recommended Conservative ZOI Envelope

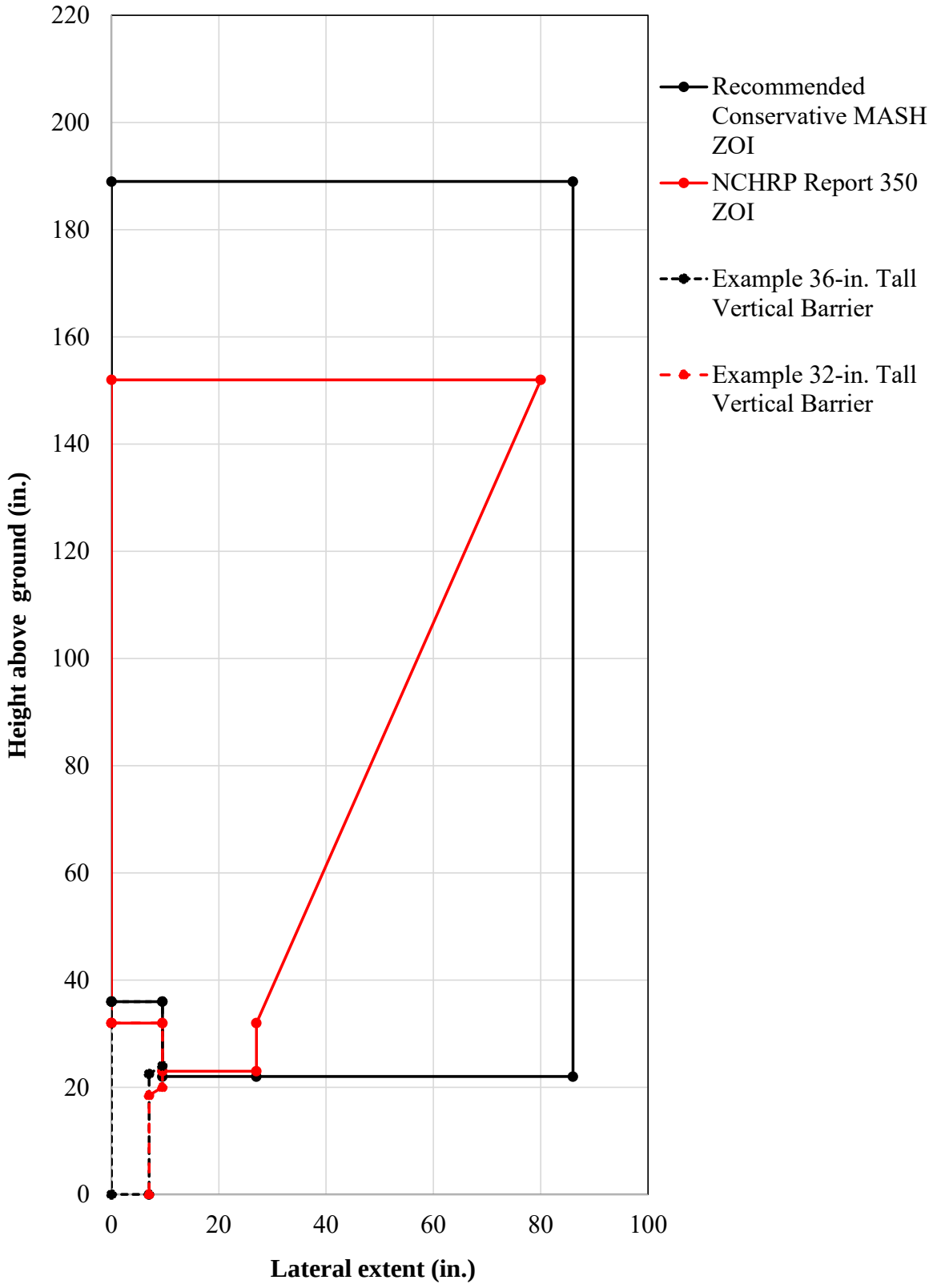


Figure C-29. *NCHRP Report 350* and Preliminary MASH TL-4 ZOI Envelopes

## C-4 MASH TL-5

Six *NCHRP Report 350* and MASH test designation no. 5-12 tests were analyzed. ZOI envelopes are shown for the cab in Figures C-30 through C-35 and for the trailer in Figures C-36 through C-41. Cab extension over the barrier was similar for all TL-5 barriers except test no. TL5CMB-2 (Rosenbaugh, Sicking, and Faller 2007), which displayed reduced cab extension.

Maximum lateral extents for Jersey, single-slope, and vertical barriers were 64, 85, and 74 in., respectively. Note in test no. TL5CMB-2, the ZOI was measured from the top of the barrier, 42 in. above ground. However, the front-top face of the barrier was stepped, so the front face had a lateral step 34 in. above ground. Thus, the ZOI may have been larger in this test as the trailer contacted the barrier at both 34 and 42 in. above groundline, which likely reduced the effective barrier height. While there was some variation in maximum lateral extent based on barrier shape, limited data meant each ZOI for barrier shapes was associated with significant uncertainty.

Five 42-in. tall barriers had a maximum lateral extent of 85 in. The only 49-in. tall barrier had a maximum lateral extent of 22.7 in. This test indicated ZOI may decrease significantly with barrier height at TL-5. The maximum vertical extent was around 140 in. A preliminary conservative MASH TL-5 envelope is shown in Figure C-42. ZOI envelopes were not developed for *NCHRP Report 350*.

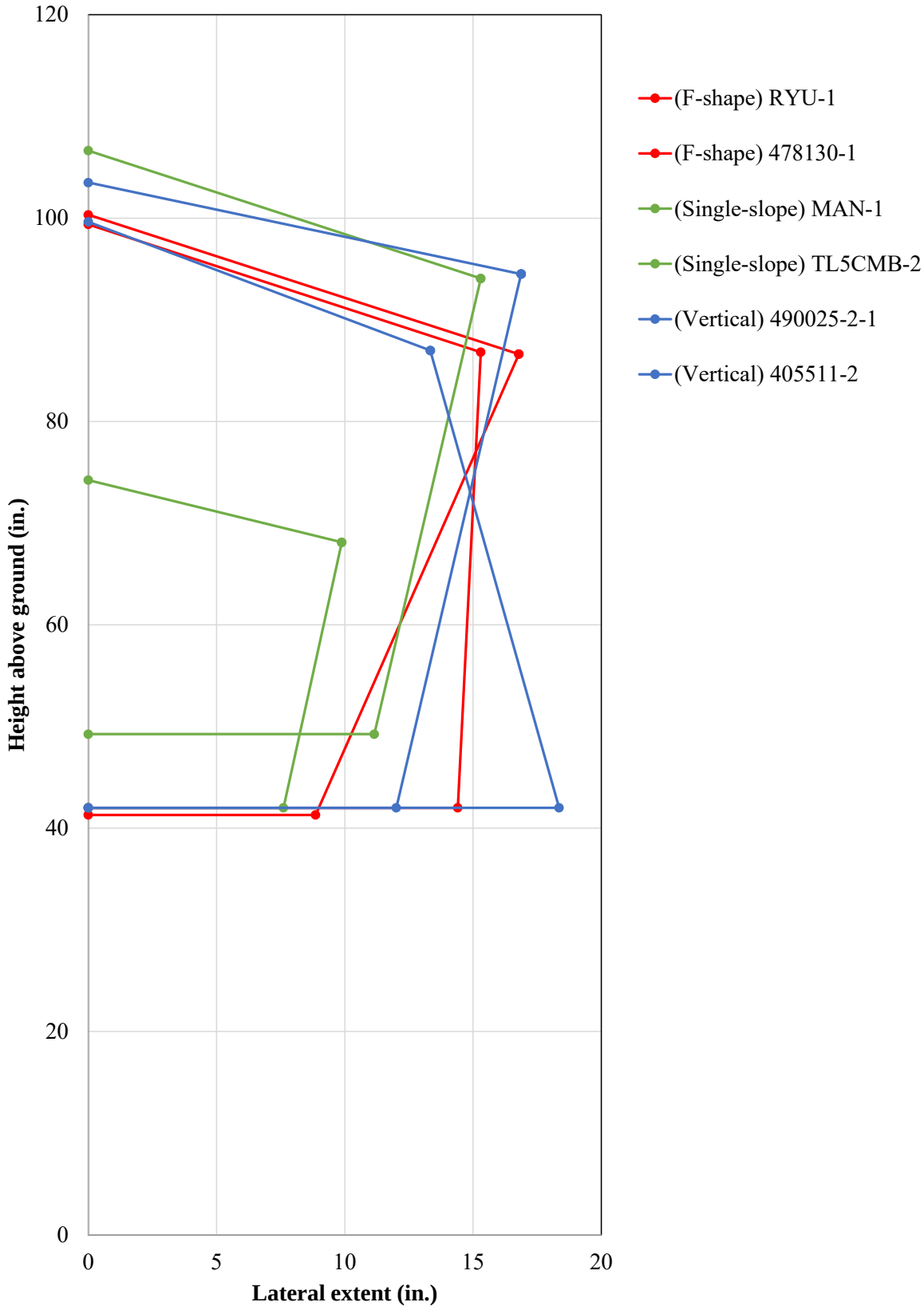


Figure C-30. Preliminary MASH TL-5 Cab ZOI, All Barriers

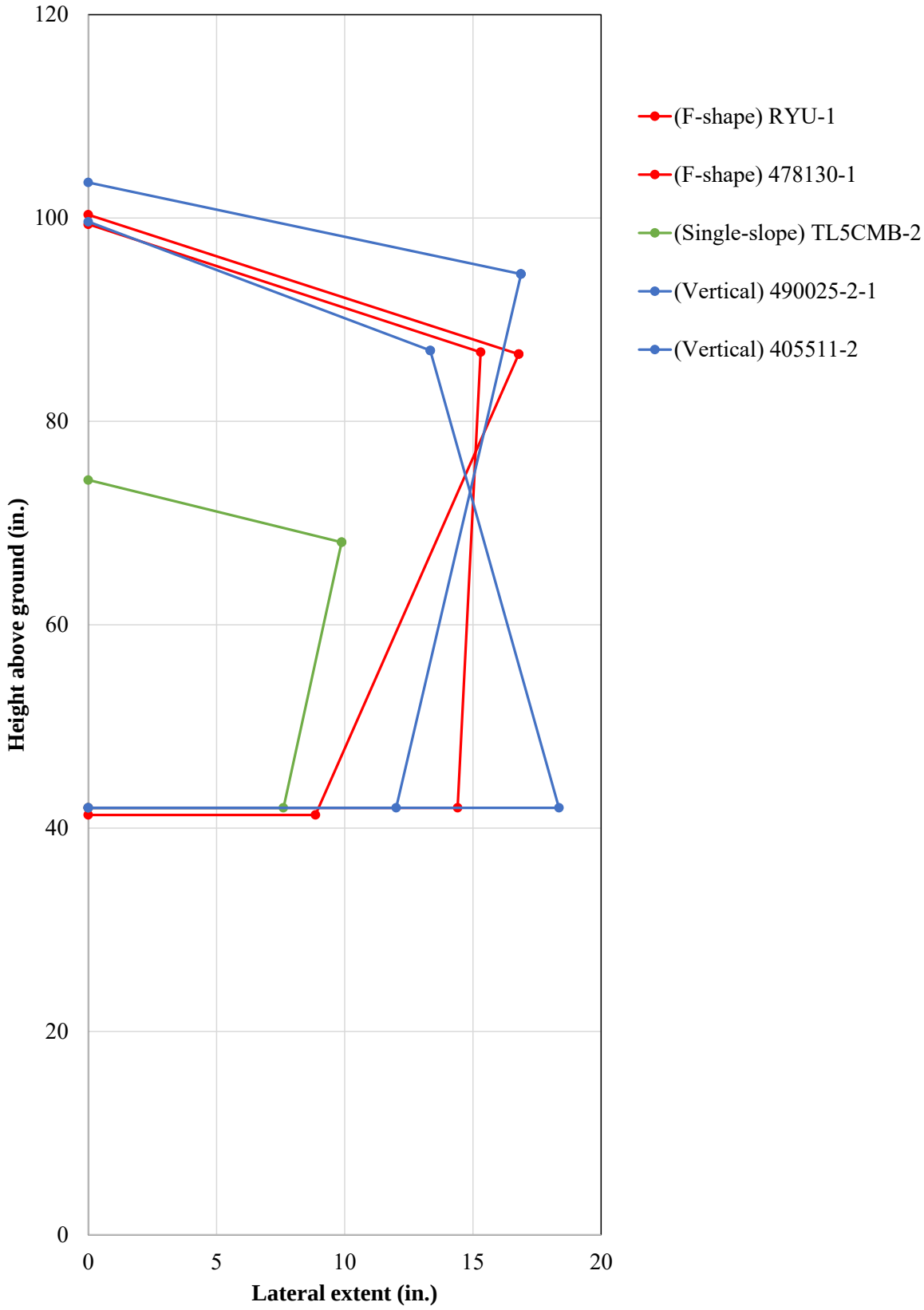


Figure C-31. Preliminary MASH TL-5 Cab ZOI, 42-in. Tall Barriers

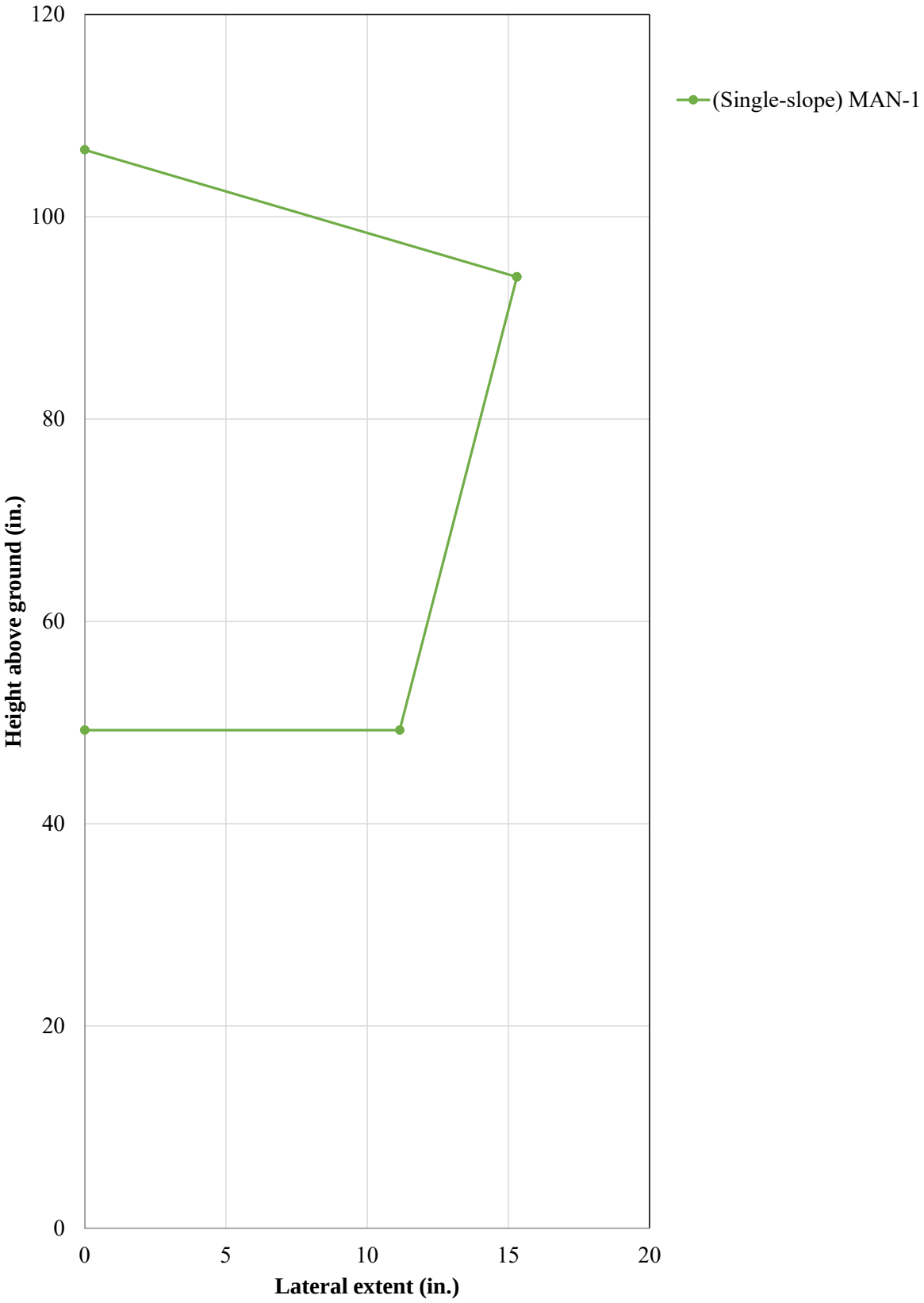


Figure C-32. Preliminary MASH TL-5 Cab ZOI, 49-in. Tall Barriers

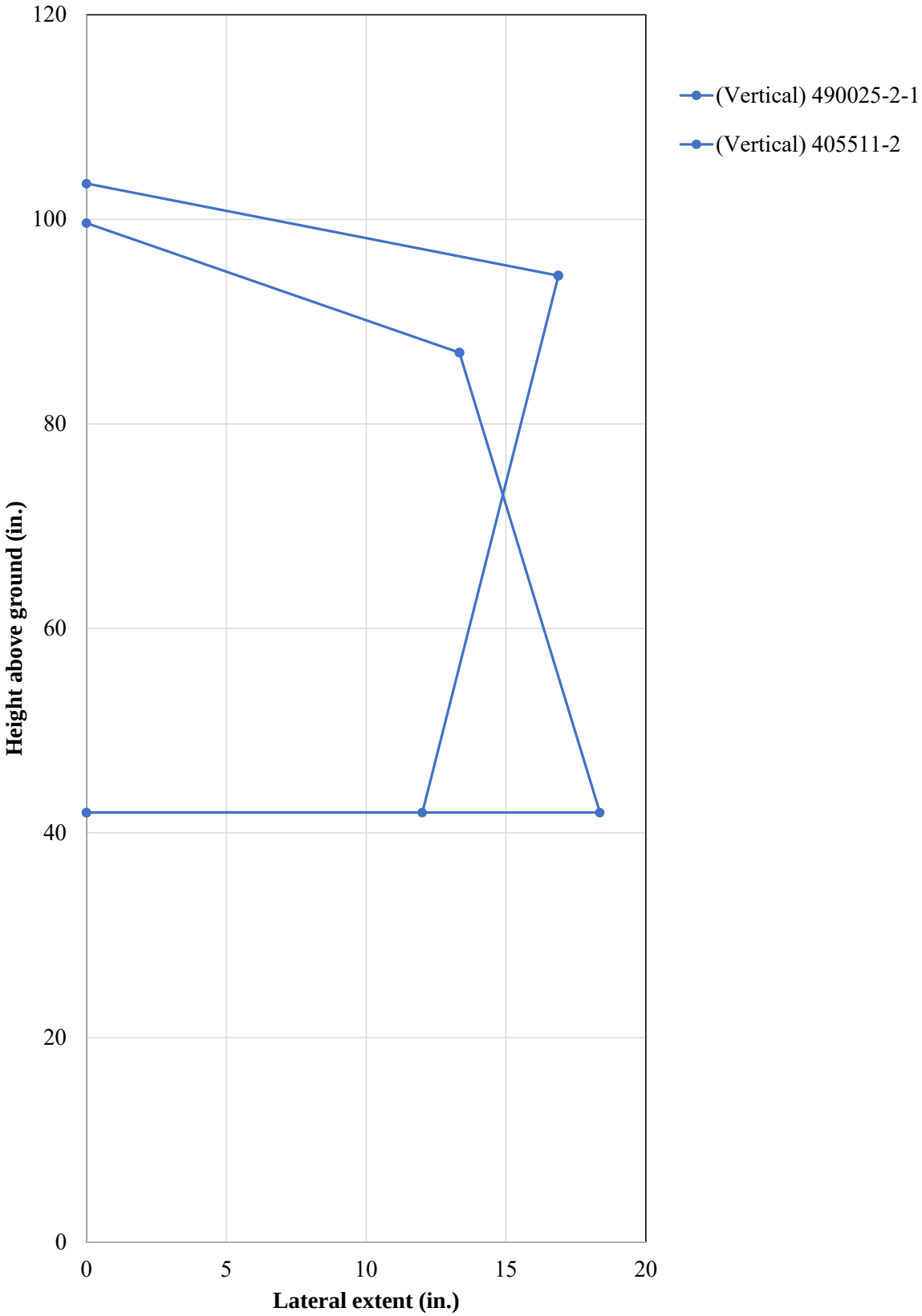


Figure C-33. Preliminary MASH TL-5 Cab ZOI, Vertical Barriers

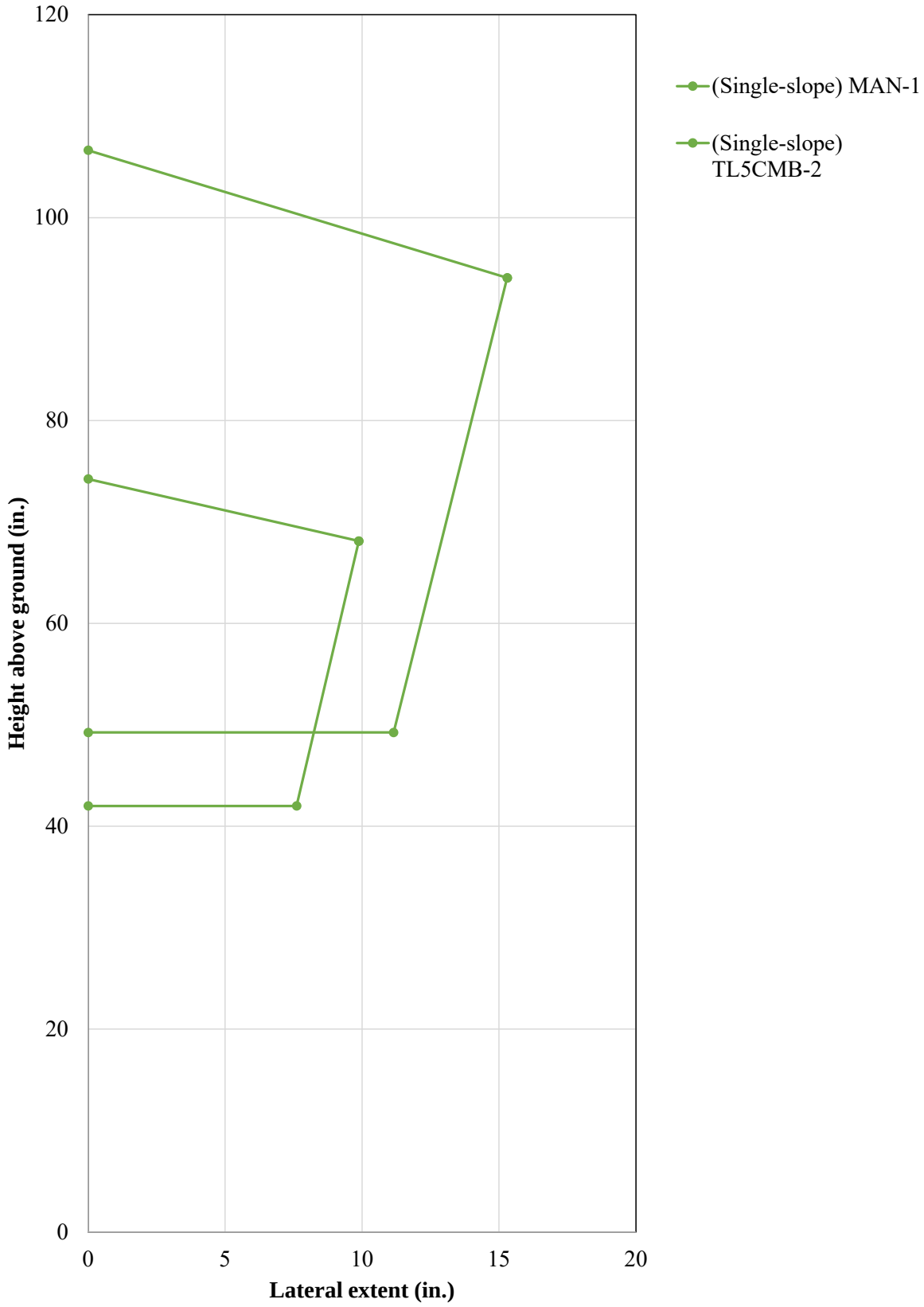


Figure C-34. Preliminary MASH TL-5 Cab ZOI, Single-slope Barriers

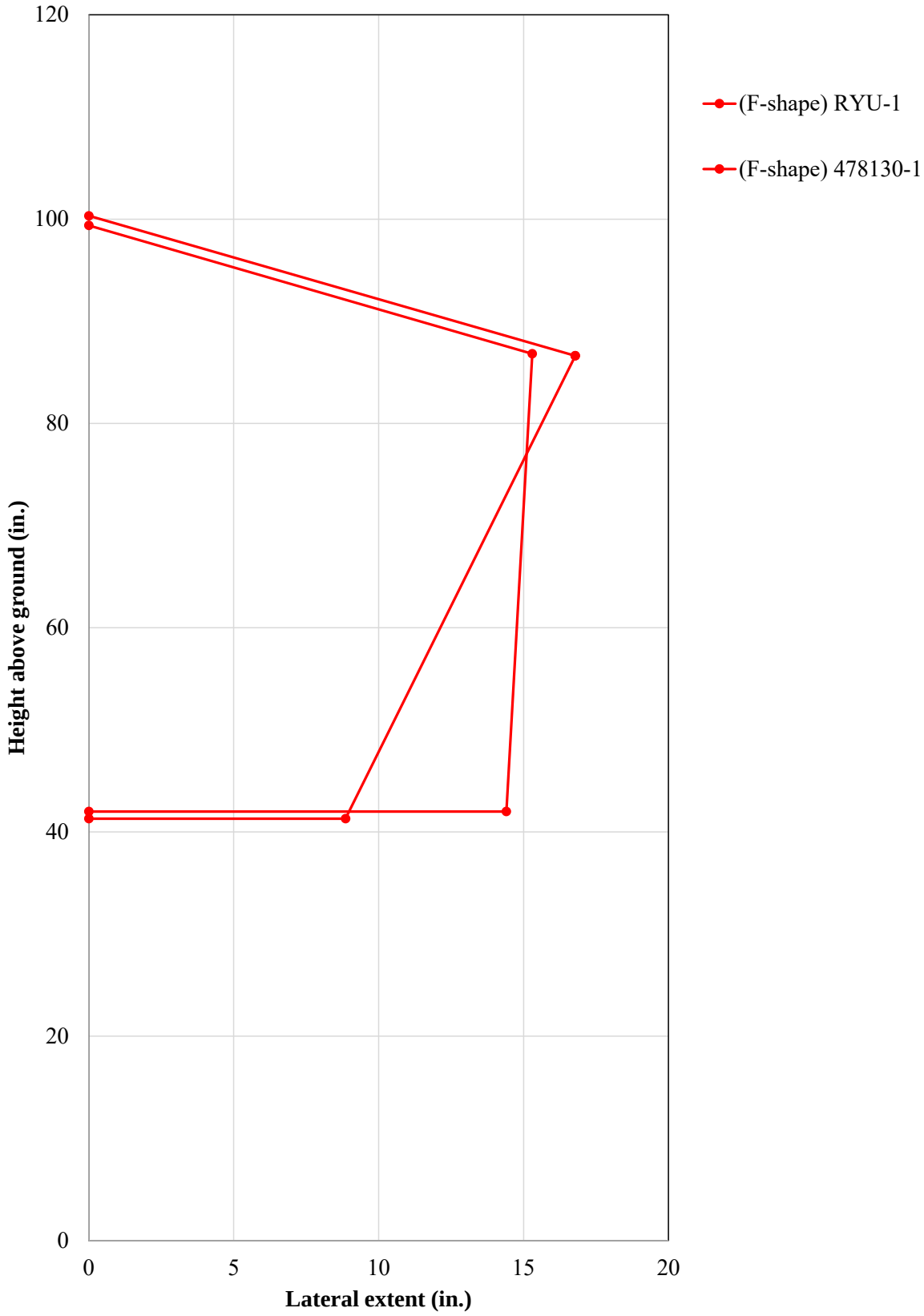


Figure C-35. Preliminary MASH TL-5 Cab ZOI, F-shape Barriers

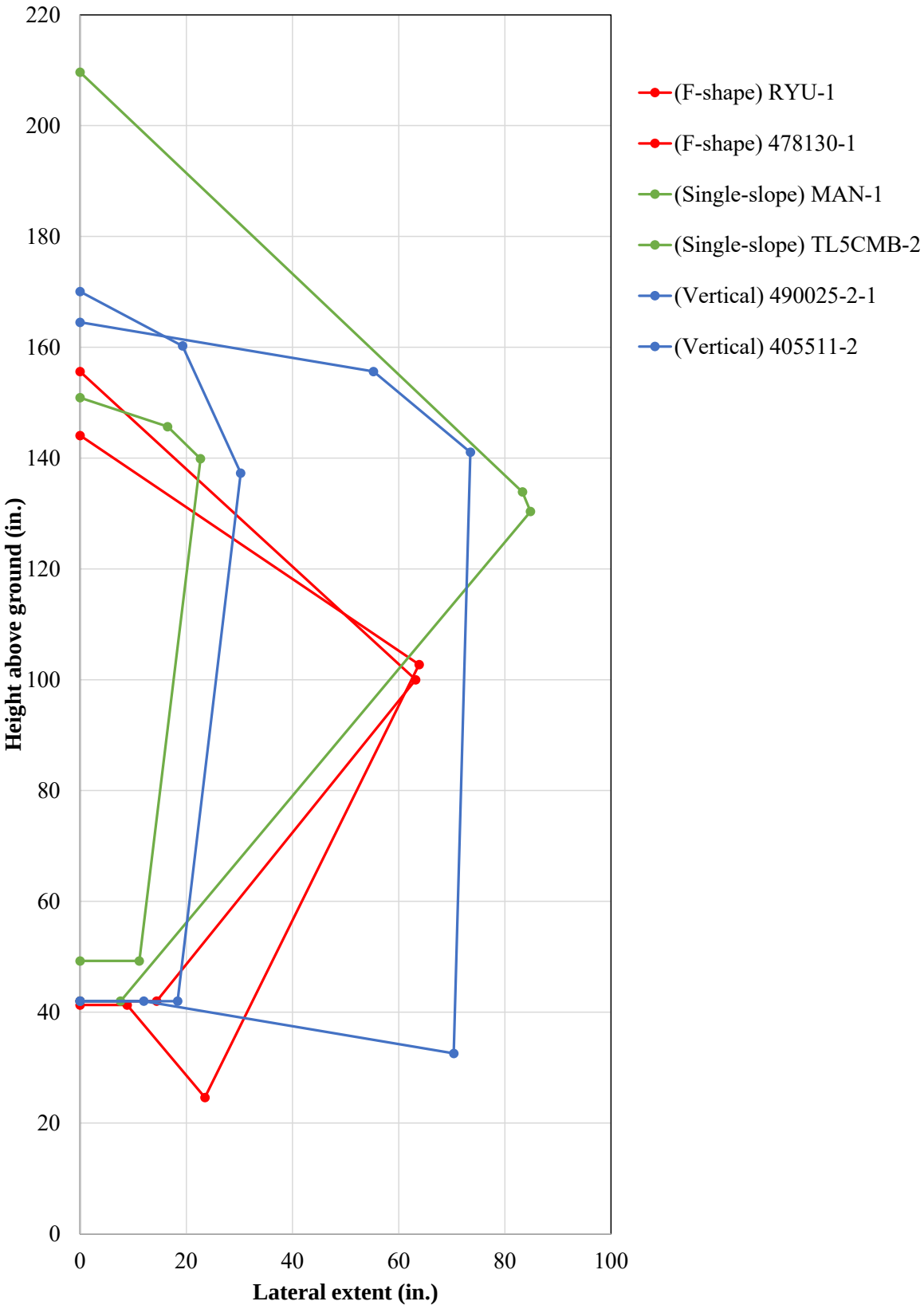


Figure C-36. Preliminary MASH TL-5 Trailer ZOI, All Barriers

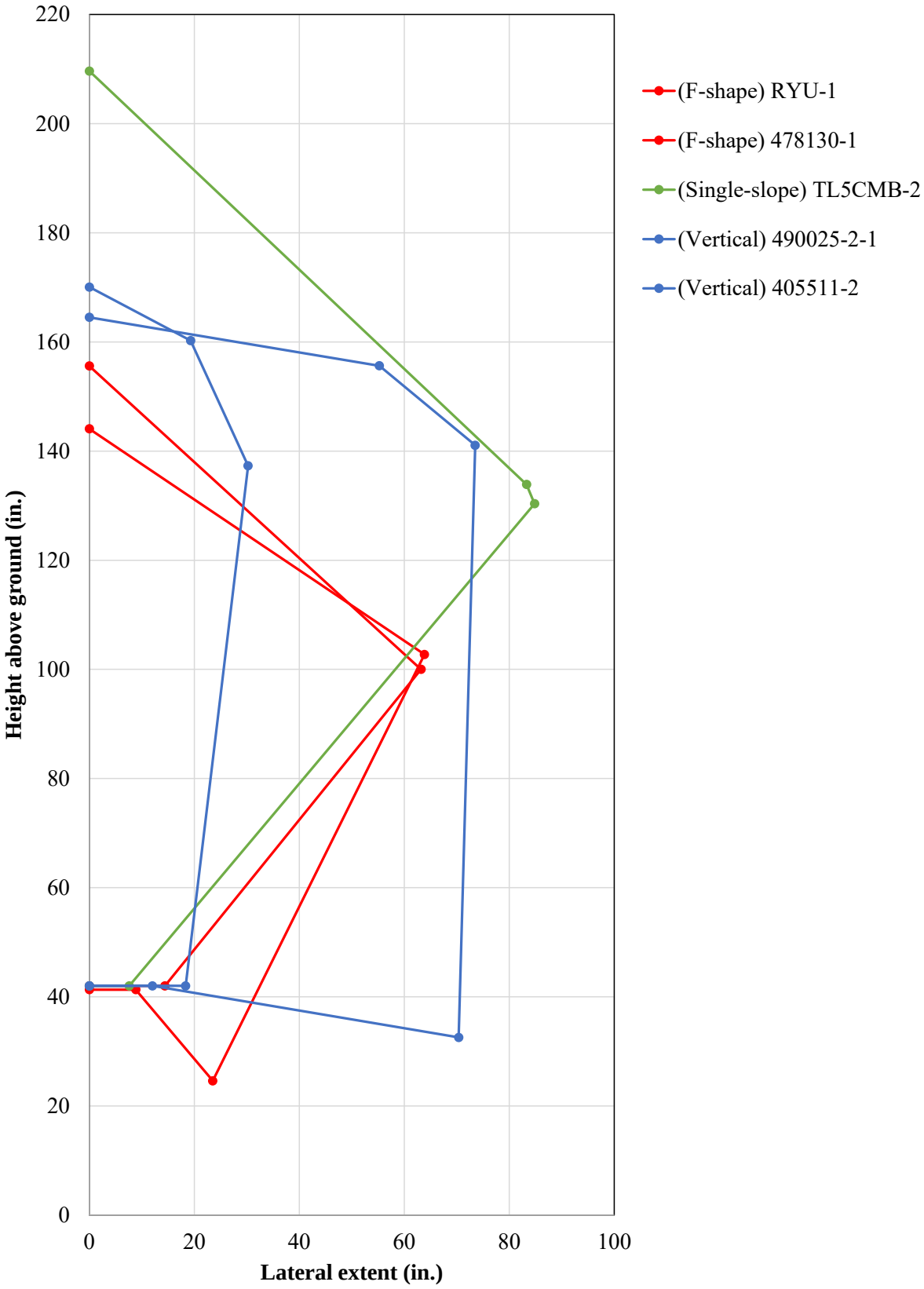


Figure C-37. Preliminary MASH TL-5 Trailer ZOI, 42-in. Tall Barriers

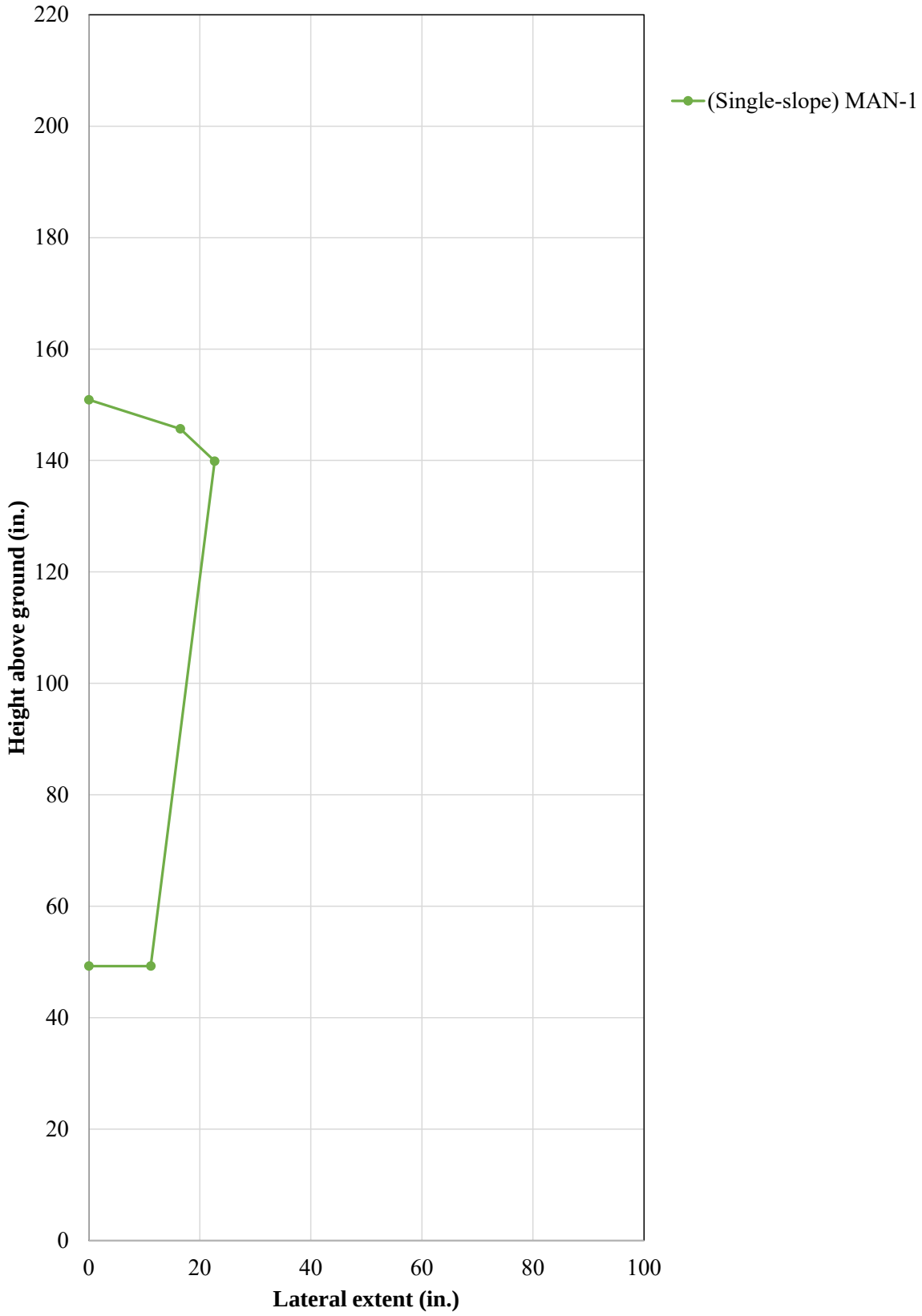


Figure C-38. Preliminary MASH TL-5 Trailer ZOI, 49-in. Tall Barriers

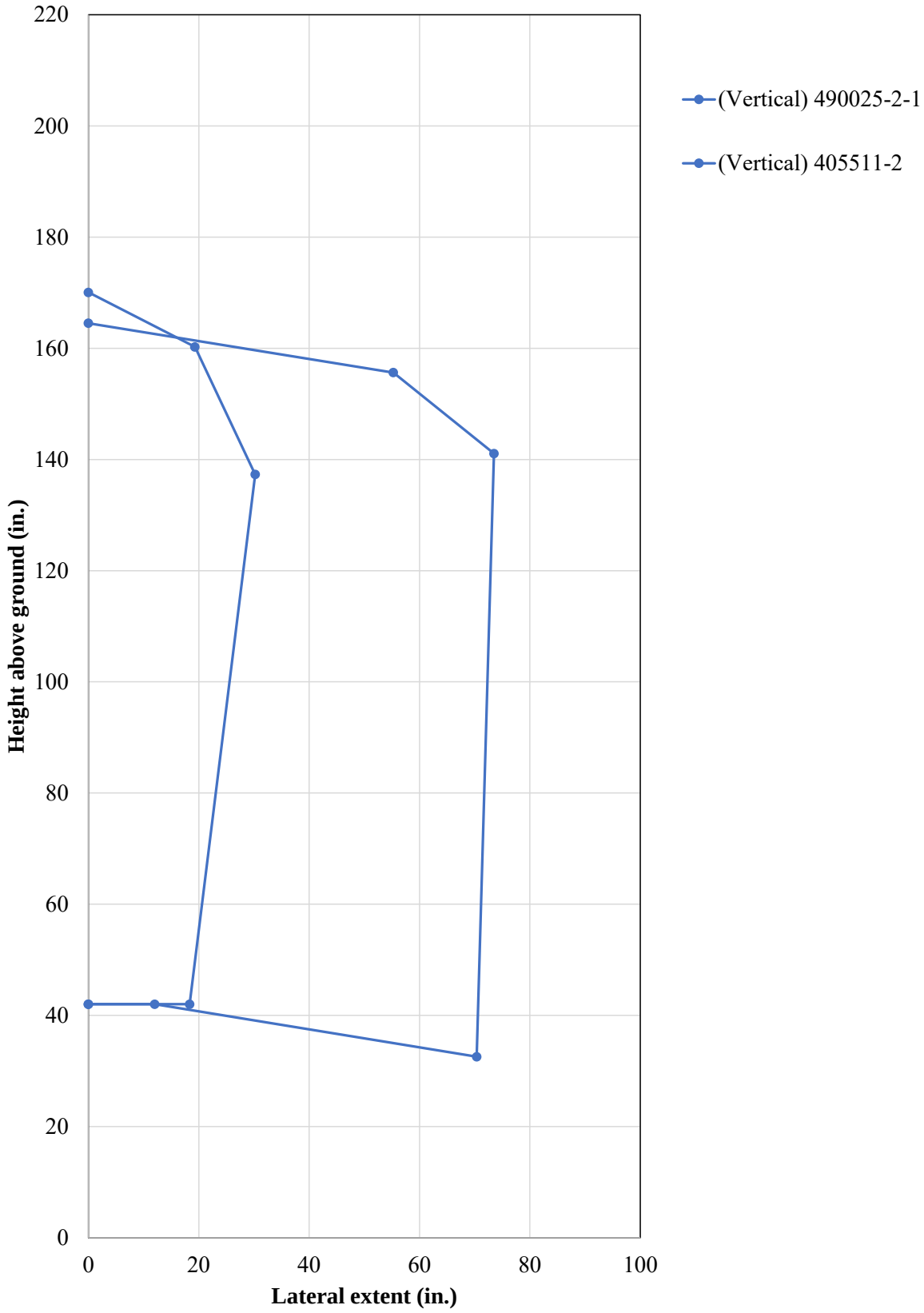


Figure C-39. Preliminary MASH TL-5 Trailer ZOI, Vertical Barriers

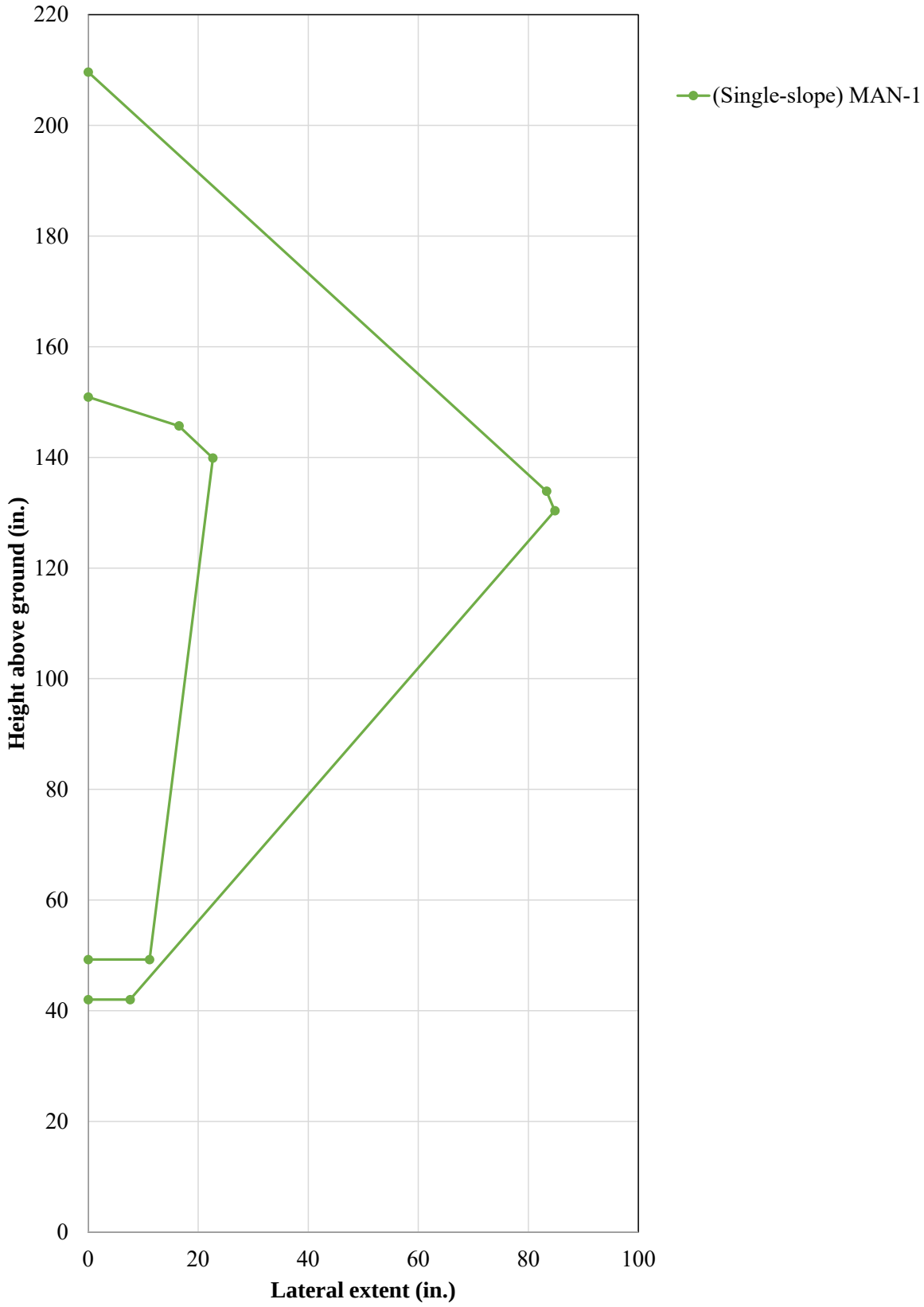


Figure C-40. Preliminary MASH TL-5 Trailer ZOI, Single-slope Barriers

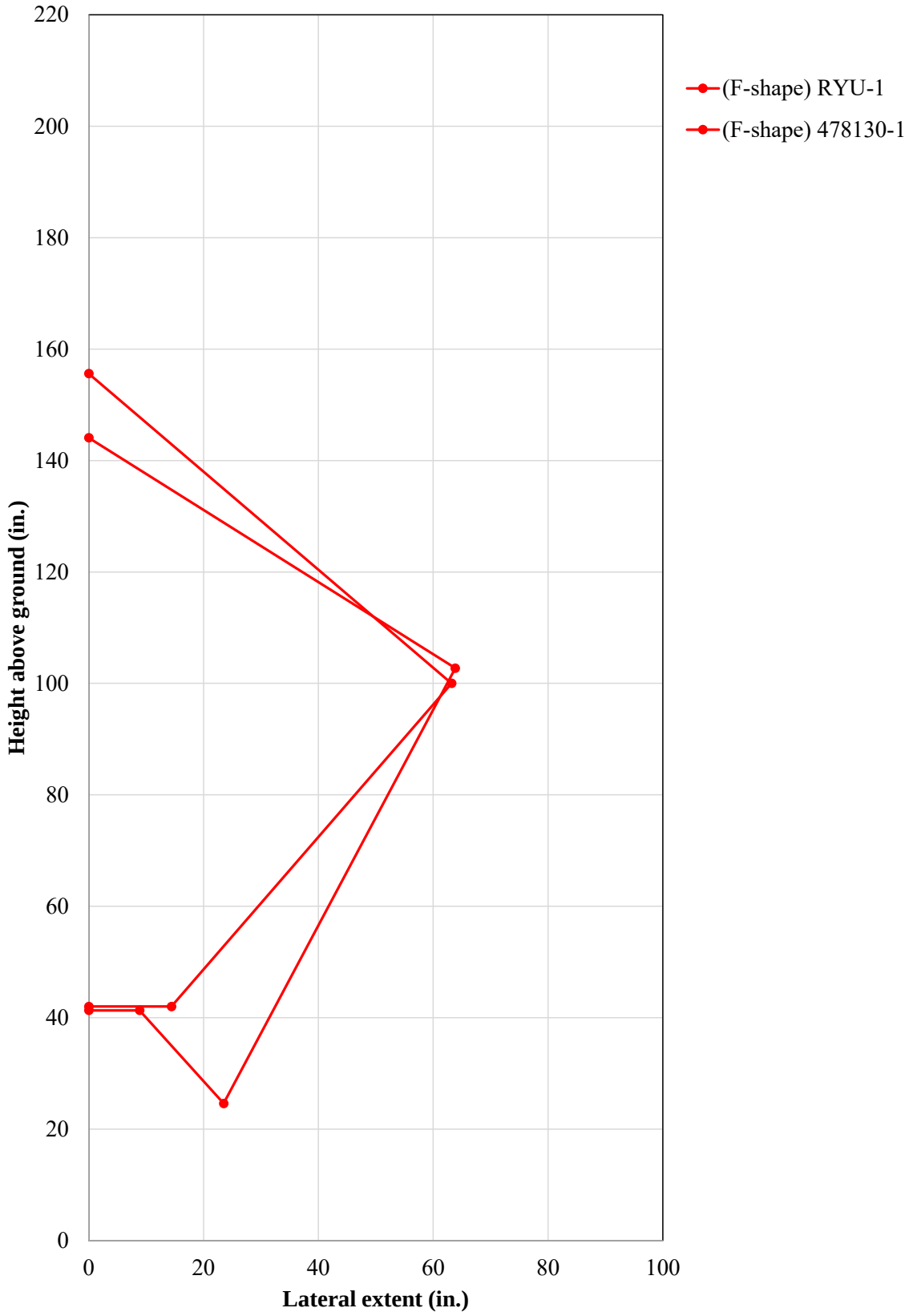


Figure C-41. Preliminary MASH TL-5 Trailer ZOI, F-shape Barriers

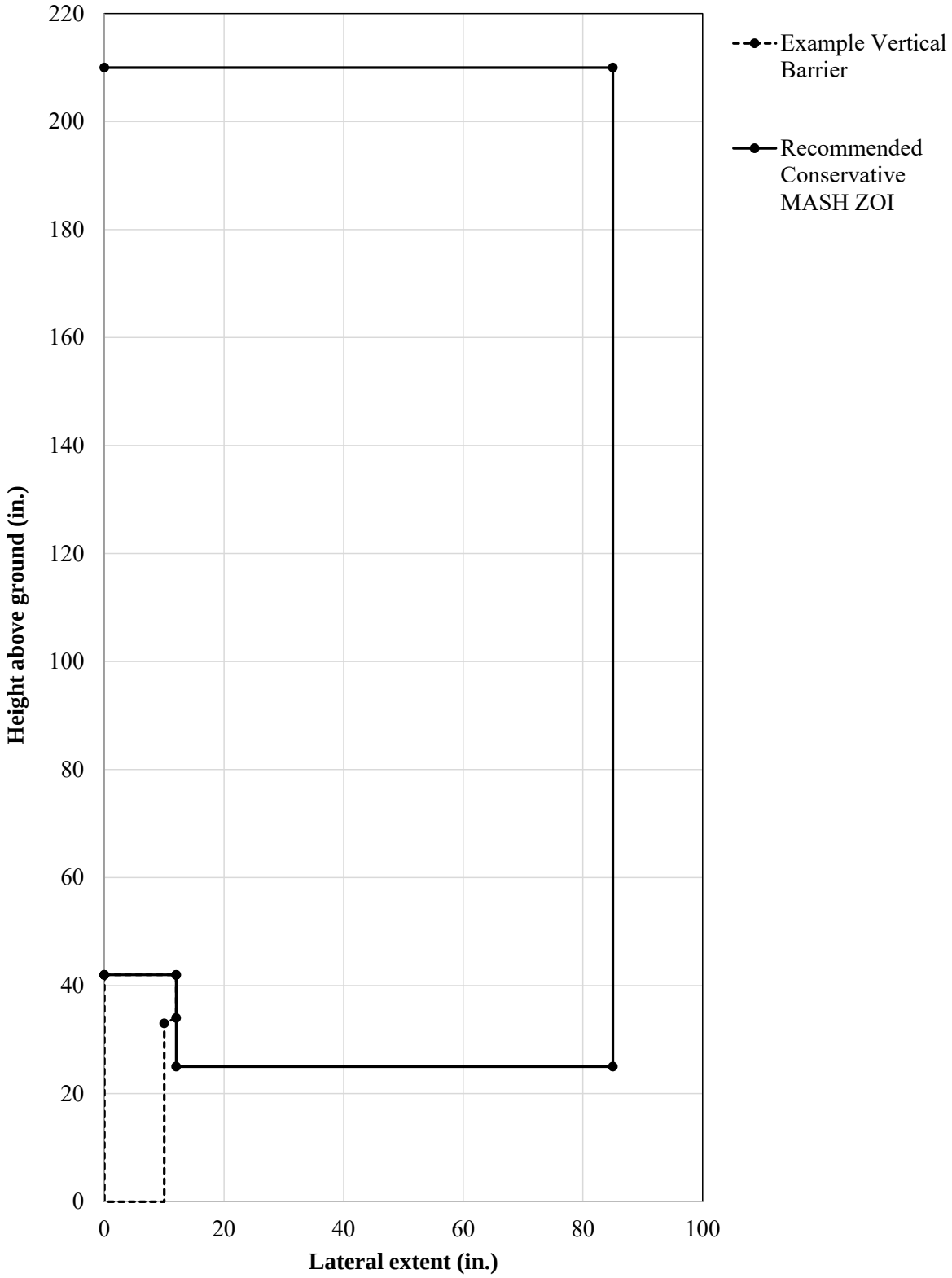


Figure C-42. Preliminary MASH TL-5 Recommended Conservative ZOI Envelope

# Appendix D. RAM Model Preparation and Validation

## D-1 Overview

The first model validated and adjusted as needed was the 2018 RAM 1500 Quad Cab model. Validation was conducted against test nos. IBBR-1, H34BR-2, and OSSB-1 (Bielenberg, Faller, and Ronspies 2018). This appendix discusses efforts to implement, expedite, and improve simulation stability, followed by a discussion of the validation results and model shortcomings.

## D-2 Preparation

The RAM model was repositioned for driver-side impacts at a 25-degree angle, allowing for simple replacement of barrier models for different simulation setups. Accelerations are affected by the recorded location, and therefore the model's accelerometer positioning was adjusted to match the mounting location used in full-scale crash testing. A non-impact, free-rolling vehicle model was defined to have an initial longitudinal velocity and used to conduct a qualitative energy balance check. This ensured the model's energy levels behaved properly in the absence of a rigid barrier impact. All barriers were modeled rigidly with a Belytscho-Tsay element formulation and 15x15 mm shell elements.

## D-3 Stability

The initial RAM model had a dummy in the passenger seat, which later moved to the driver's side to collect additional information during ZOI estimation. However, a number of simulation instabilities were thought to be a potential result of the dummy's inclusion, primarily element snag between the seatbelt and the dummy's torso, as shown in Figure D-1. Since dummy analysis was out of the scope of the project and may have caused model instabilities during simulation, it was removed from the RAM model.

Rubber-bushing hourglassing in the initial RAM model consistently caused error terminations, as shown in yellow in Figure D-2. Element formulation was switched from *fully integrated selective-reduced* to *constant stress solid element* to improve accuracy and reduce instabilities (Hallquist 2007).

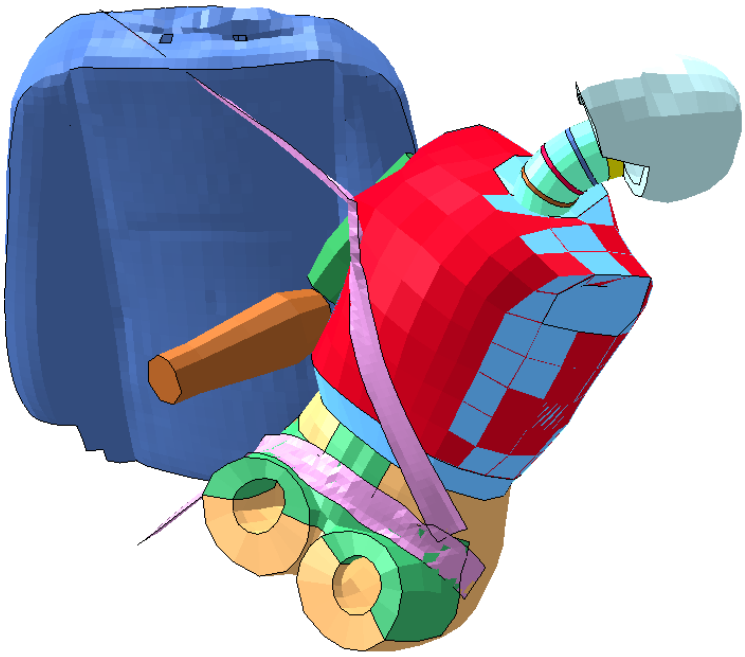

Figure D-1. RAM Model Element Snag on Dummy

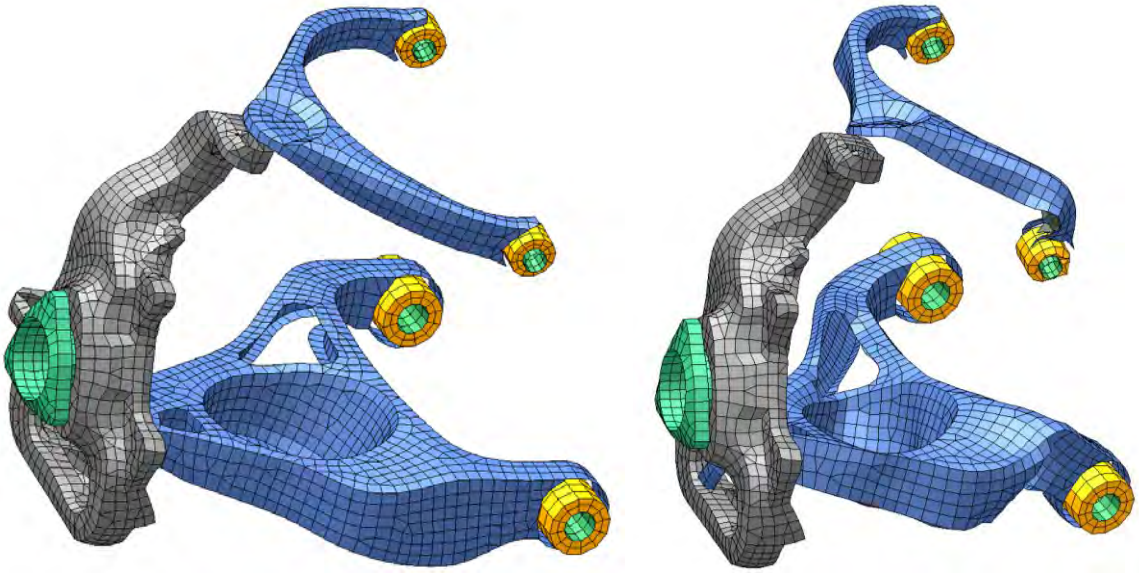

Figure D-2. AM Model Upper Control Arm before and during Impact

## D-4 Friction Selection

Test no. OSSB-1 (Bielenberg, Faller, and Ronspies 2018) was used for friction selection as it included a concrete barrier with a flat, continuous surface and therefore made it simpler to model friction than a combination rail system. Ridedown velocity plots, shown in Figures D-3 and D-4, were studied to select friction values.

Vehicle-barrier static and dynamic friction levels ranged from 0 to 0.3 with 0.1 increments, as shown in Figure D-3. The full-scale longitudinal change in velocity plots fell in between simulations with friction levels of 0.1 and 0.2. Additional models were defined with separate vehicle body-barrier and tire-barrier friction to refine the values; it was expected tire-ground friction would match tire-barrier friction, typically assigned in the range of 0.4 and 0.9 by MwRSF engineers, and would be more accurate than vehicle body-barrier friction. Since friction levels vary depending on the vehicle material interacting with the barrier (e.g., metal and rubber), models were studied with vehicle-barrier friction at 0.1, 0.15, and 0.2, while the tire-barrier friction was set to 0.4. An additional model was simulated with tire-barrier friction set to 0.9; however, this model did not yield proper velocity reduction. Vehicle body-barrier and tire-barrier friction values of 0.1 and 0.4, respectively, provided the best replication of full-scale crash testing. Therefore, validation of all RAM models was conducted with these friction values.

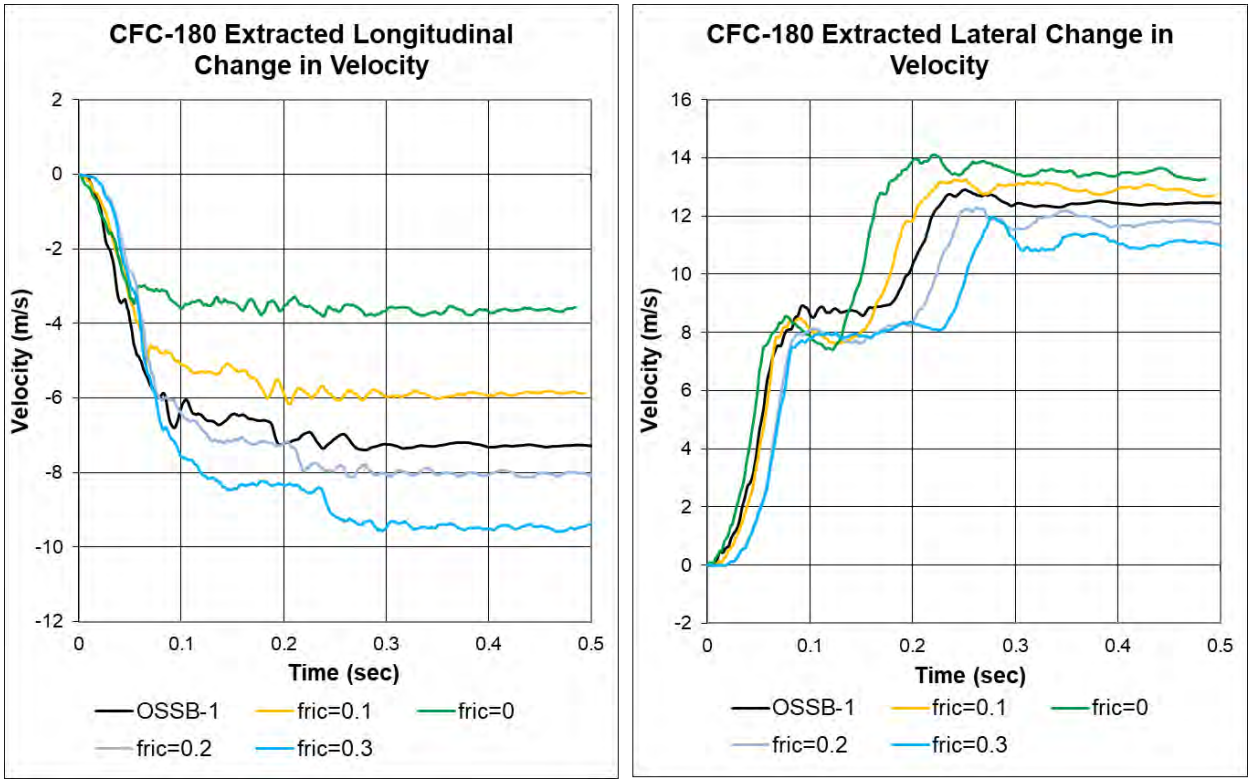


Figure D-3. Velocity Analysis for Varied Vehicle-barrier Friction

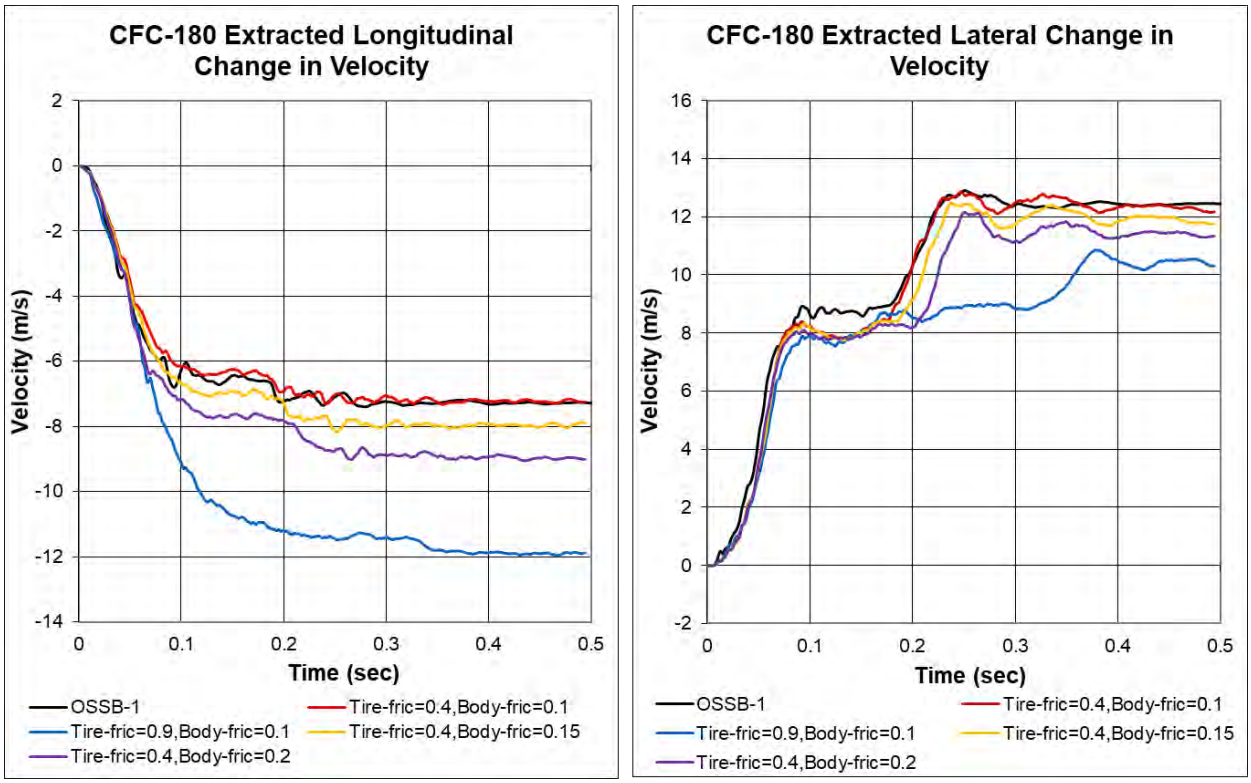


Figure D-4. Velocity Analysis for Varied Tire- and Body-barrier Frictions

## D-5 Validation to Test No. IBBR-1

### D-5.1 Test Setup

In MASH TL-2 full-scale crash test no. IBBR-1 (Bielenberg et al. 2020), a 4,980-lb 2011 RAM 1500 Crew Cab impacted a 48-in. tall vertical barrier with a 24-in. tall parapet at 45.3 mph and a 25.6-degree angle. In simulation, a 5,022-lb 2018 RAM 1500 Quad Cab impacted a 24-in. tall, 10-in. thick vertical barrier at 45.3 mph and 25.0-degree angle. Test vehicle and simulation model dimensions and impact points are compared in Figure D-5.

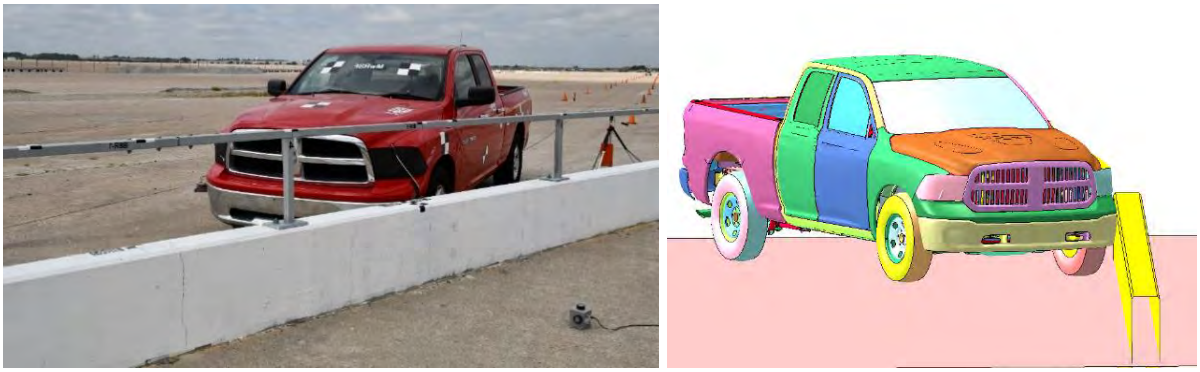

Figure D-5. Test No. IBBR-1 (Bielenberg et al. 2020) and Simulation Vehicles

### D-5.2 ZOI and Key Events

The point of maximum intrusion during simulation is compared to the equivalent time step in test no. IBBR-1 in Figure D-6. The test frame in Figure D-6 was captured prior to the vehicle significantly interacting with the steel rail elements as this rail significantly affected the vehicle's lateral extent. ZOI measurement from the test and simulation had a 26.5 percent relative difference, primarily attributed to the absence of the steel rail in the simulation. Key events are summarized in Table D-1.

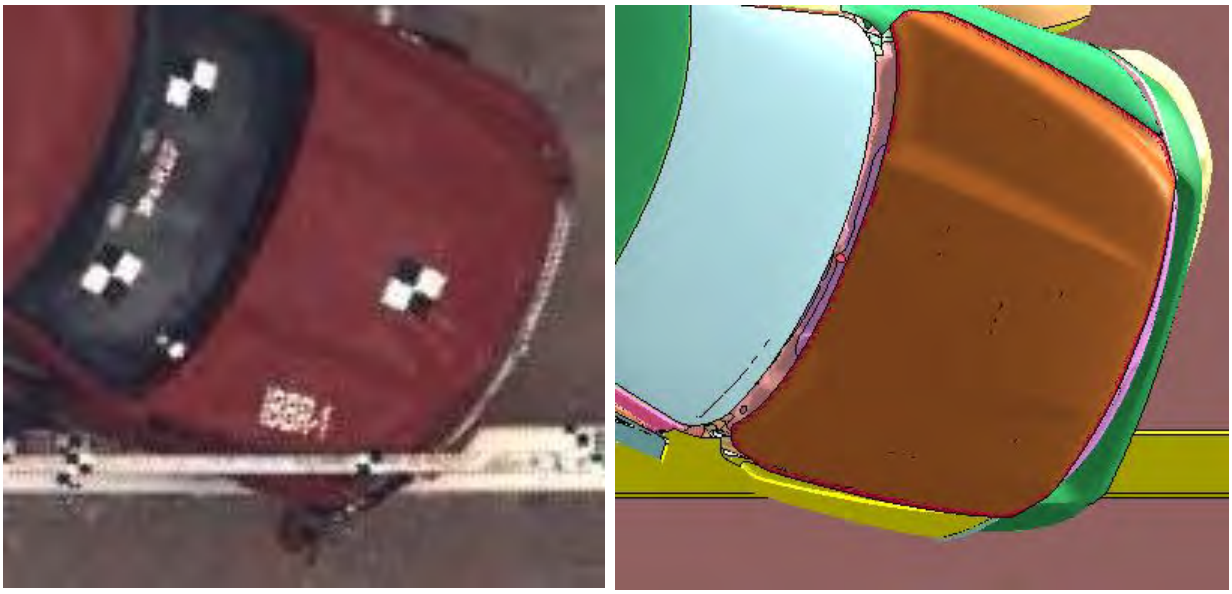

Figure D-6. Maximum Lateral Extent during Test No. IBBR-1 (Bielenberg et al. 2020) and Simulation

Table D-1. Key Events Comparison, Test No. IBBR-1 (Bielenberg et al. 2020) and Simulation

| Event | Test | FEA |
|---|---|---|
| ZOI measurement (in.) | 21.7 | 16.0 |
| ZOI time (ms) | 68 | 85 |
| Parallel time (ms) | 254 | 265 |
| Exit Time (ms) | 383 | 420 |

### D-5.3 Sequential Images

Sequential images of test no. IBBR-1 and the simulation are compared in Figures D-7 through D-12. The simulated vehicle behavior initially compares well to test no. IBBR-1; later in the impact event, the simulated vehicle pitched more and rolled less than the test vehicle, likely due to the absence of the steel rail

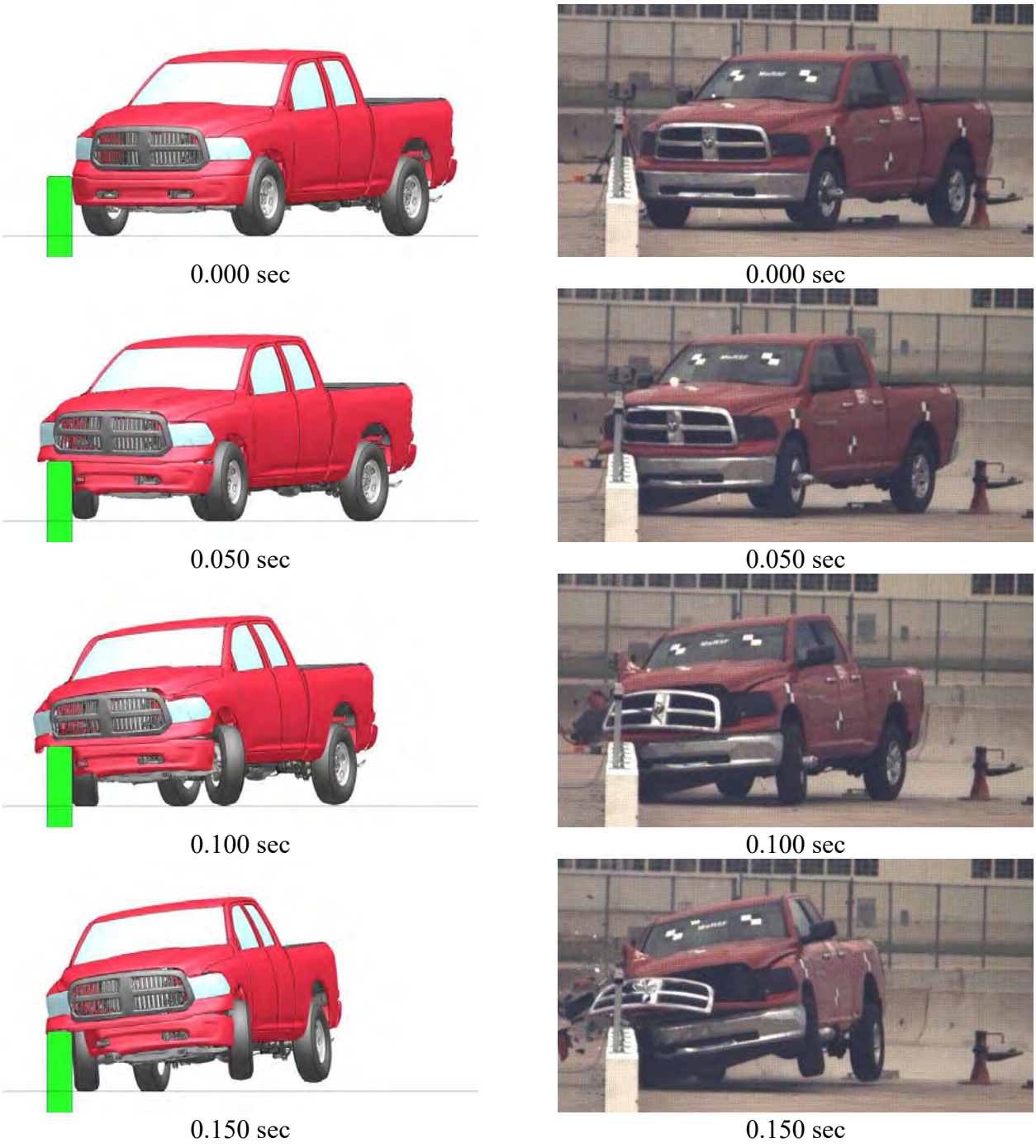


Figure D-7. Test No. IBBR-1 (Bielenberg et al. 2020) and Simulation Downstream Sequential Images

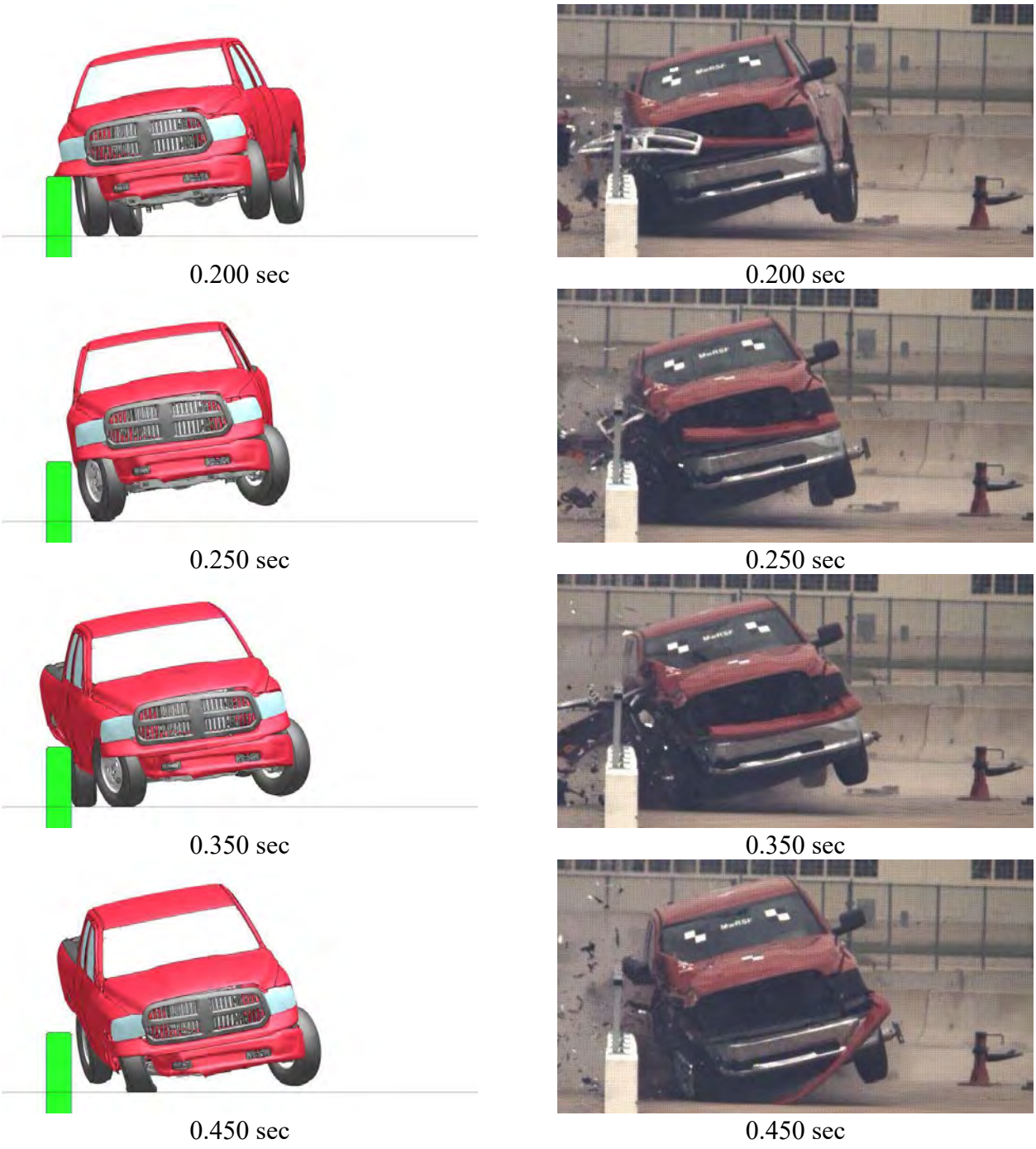


Figure D-8. Test No. IBBR-1 (Bielenberg et al. 2020) and Simulation Downstream Sequential Images

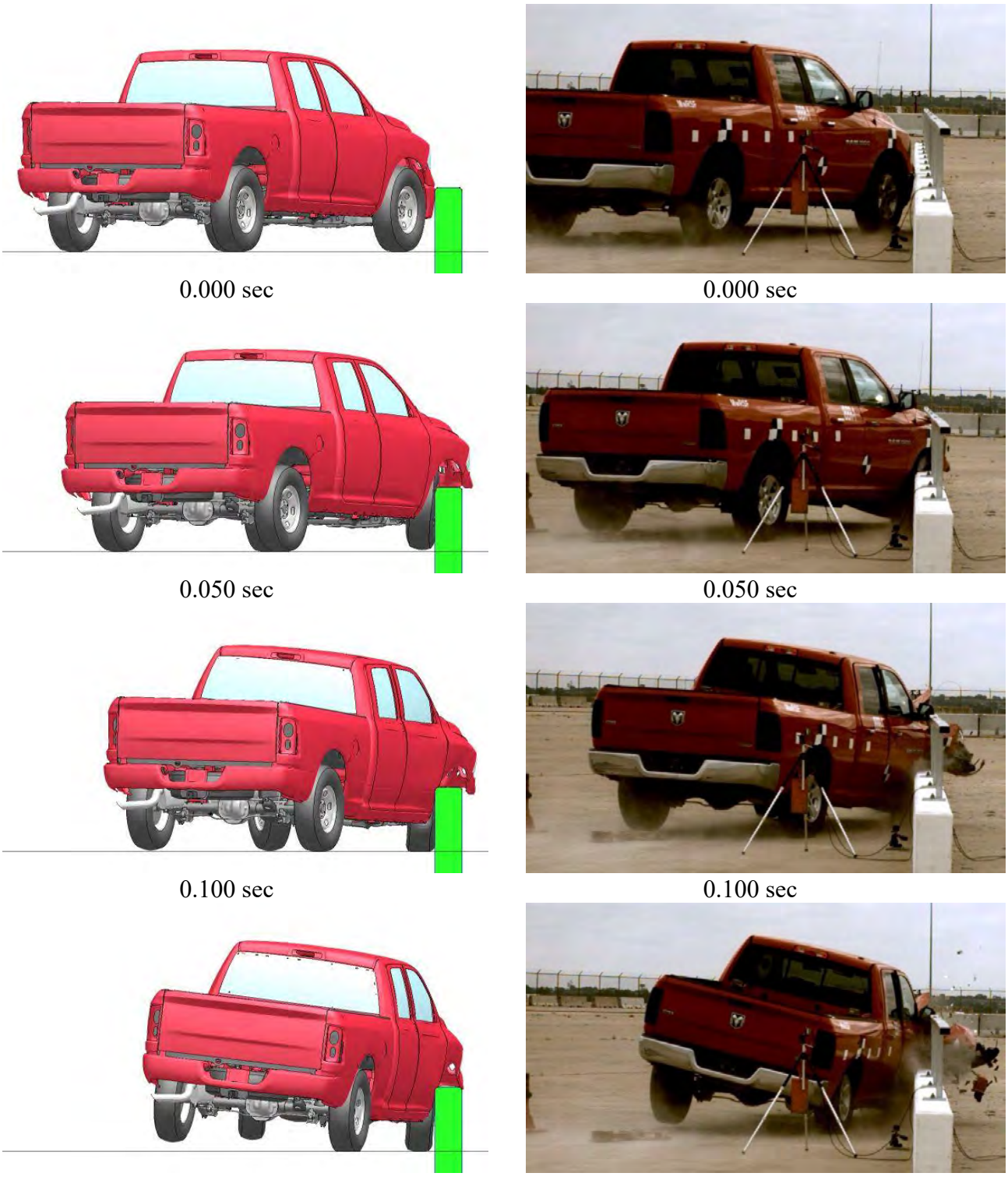


Figure D-9. Test No. IBBR-1 (Bielenberg et al. 2020) and Simulation Upstream Sequential Images

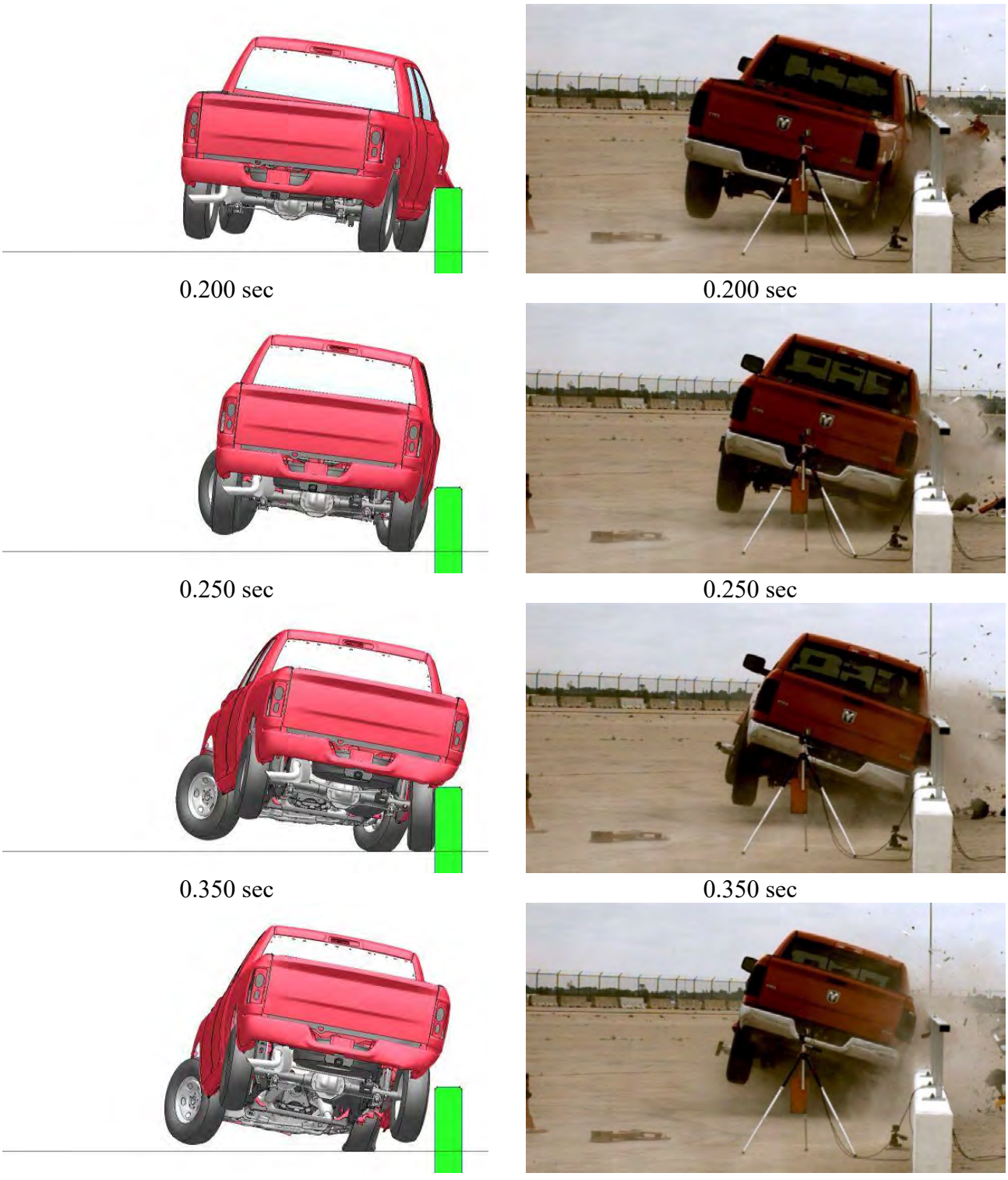


Figure D-10. Test No. IBBR-1 (Bielenberg et al. 2020) and Simulation Upstream Sequential Images (Continued)

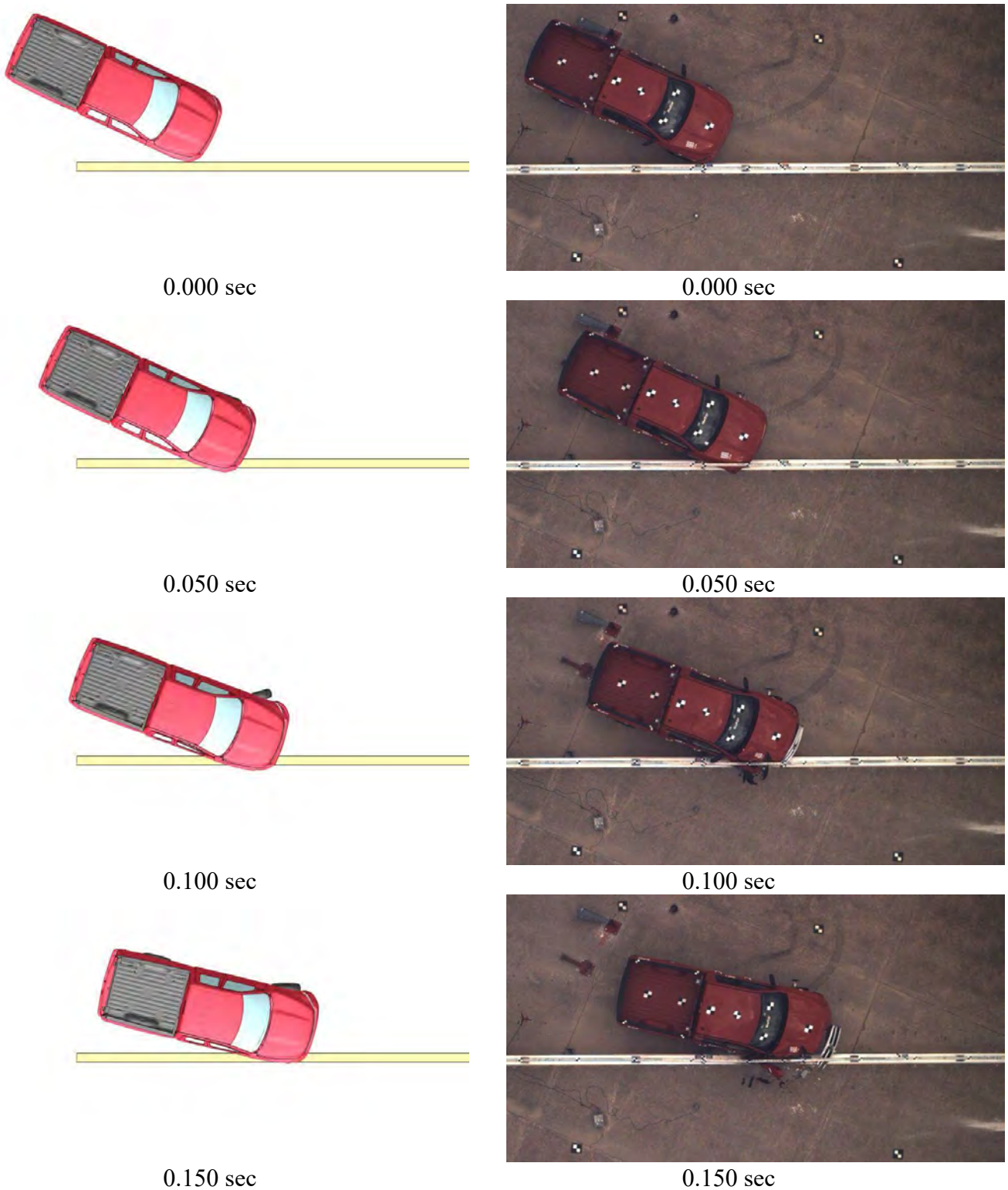


Figure D-11. Test No. IBBR-1 (Bielenberg et al. 2020) and Simulation Overhead Sequential Images

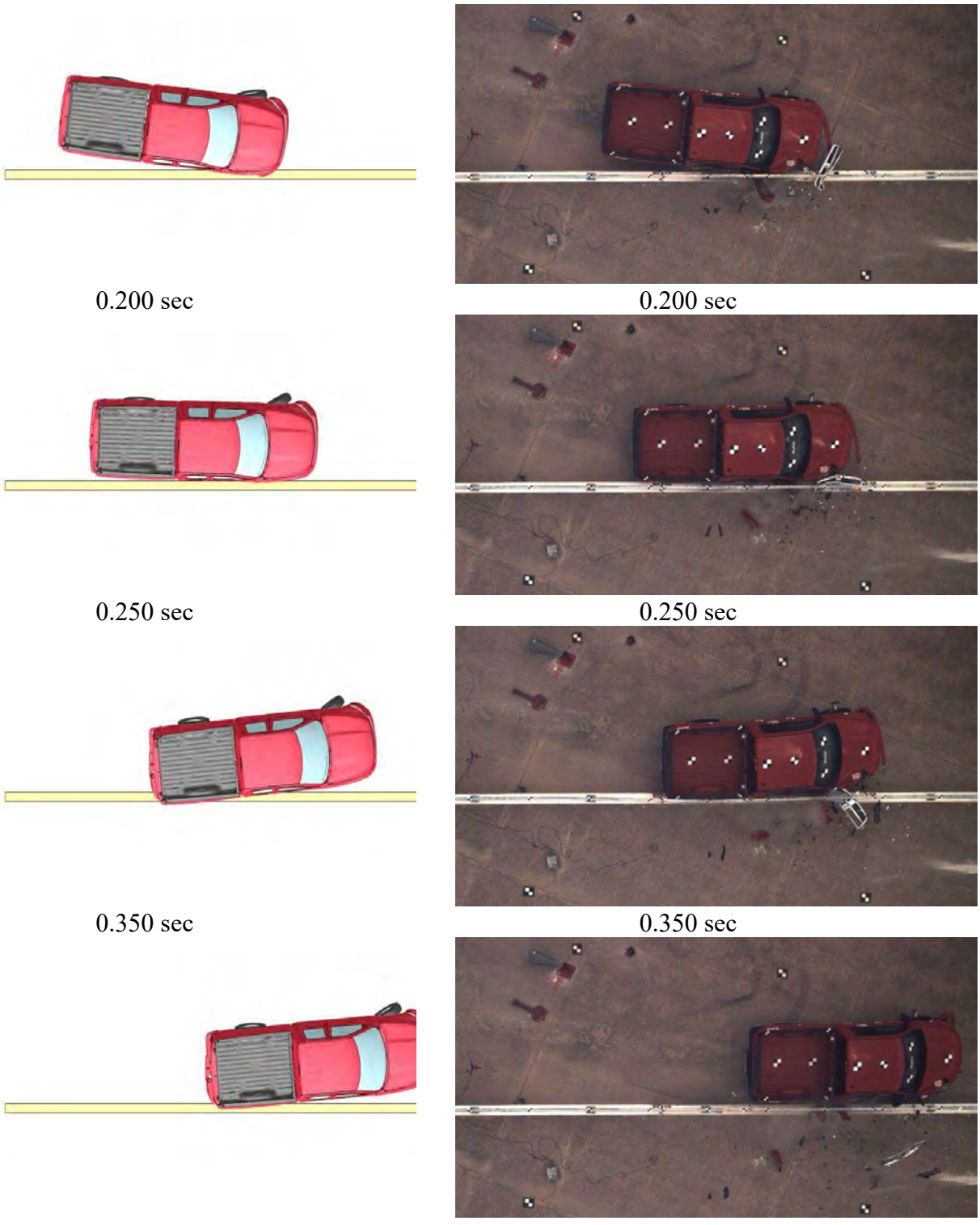


Figure D-12. Test No. IBBR-1 (Bielenberg et al. 2020) and Simulation Overhead Sequential Images

### D-5.4 Time-dependent Data

To validate overall dynamic performance of the crash test and simulation, acceleration, velocity, and displacements were compared, as shown in Figures D-13 through D-15. Accelerations were comparable, providing high confidence in the validation of the vehicle's dynamic ridedown performance.

Euler angles are compared in Figure D-16; yaw and roll were slightly higher in simulation, and pitch was slightly higher in the test due to the absence of a steel rail in simulation. During testing, yaw, pitch, and roll increased abruptly at approximately 0.125 seconds when maximum interaction with the rail occurred. Video analysis suggested snag between the fender, hood, and vertical posts was reduced at this time due to vertical post detachment as the vehicle yawed away from the barrier. The rail element affected the roll, pitch and yaw behavior of the vehicle, which led to inexact replication throughout the later stages of the simulated impact event.

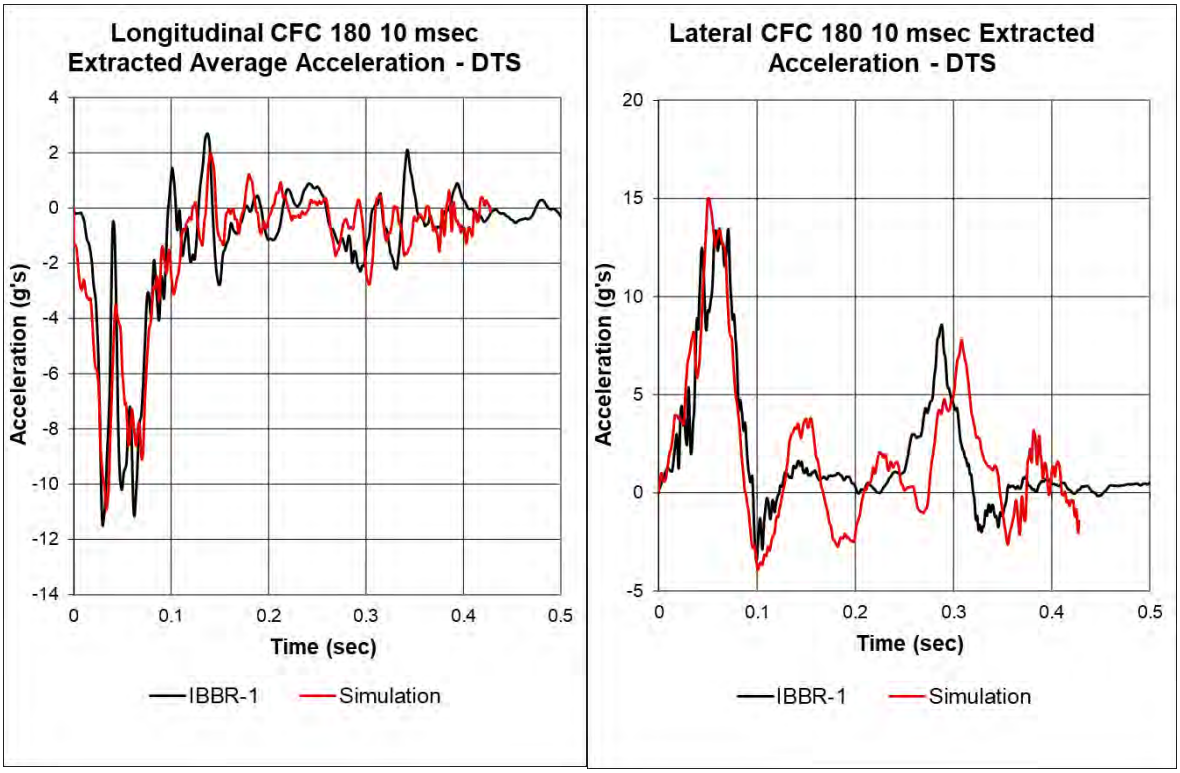


Figure D-13. Test No. IBBR-1 (Bielenberg et al. 2020) and Simulation Acceleration

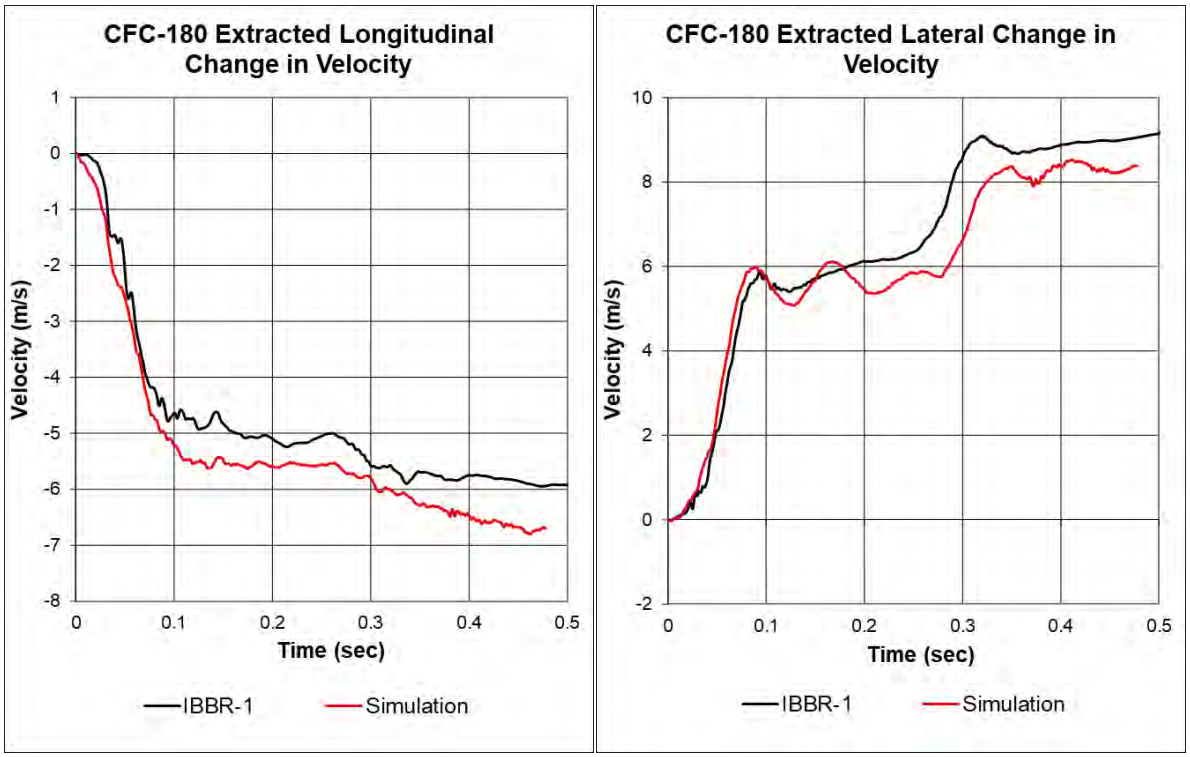


Figure D-14. Test No. IBBR-1 (Bielenberg et al. 2020) and Simulation Velocity

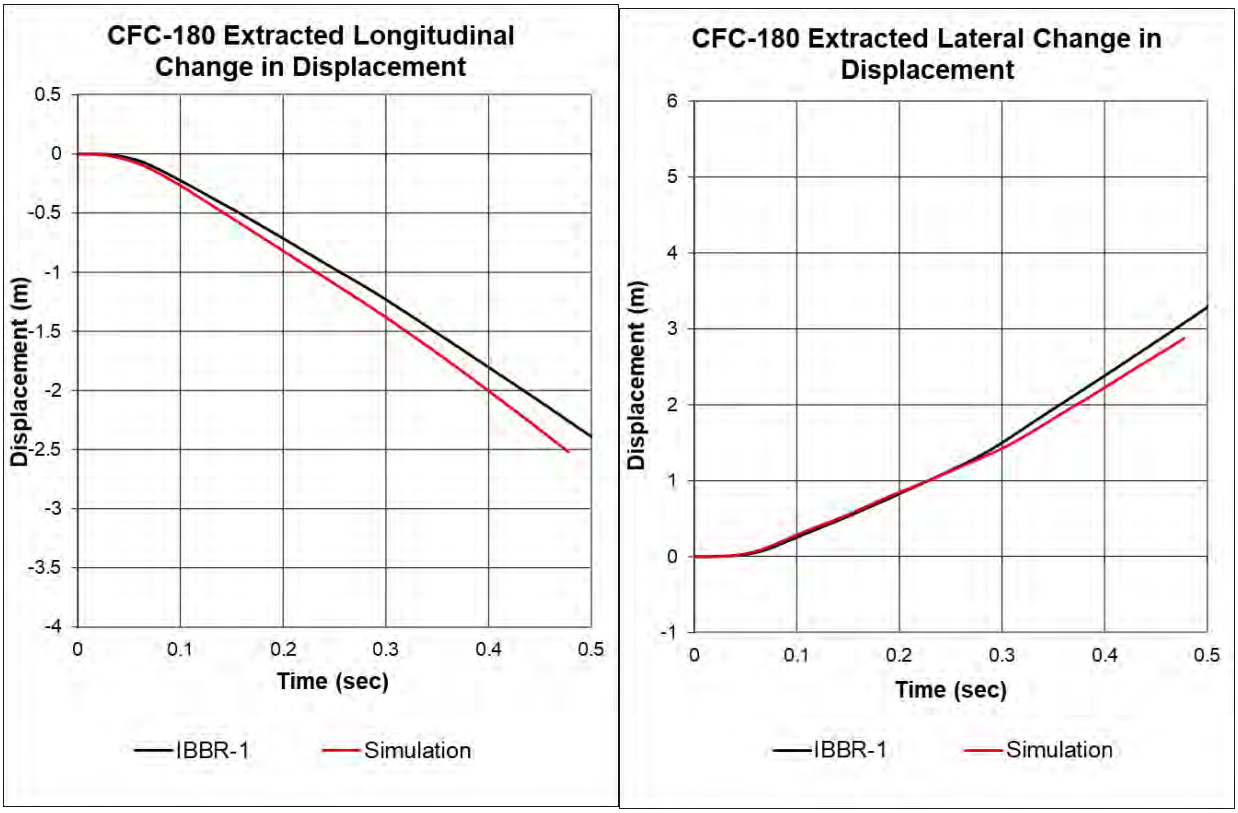


Figure D-15. Test No. IBBR-1 (Bielenberg et al. 2020) and Simulation Displacement

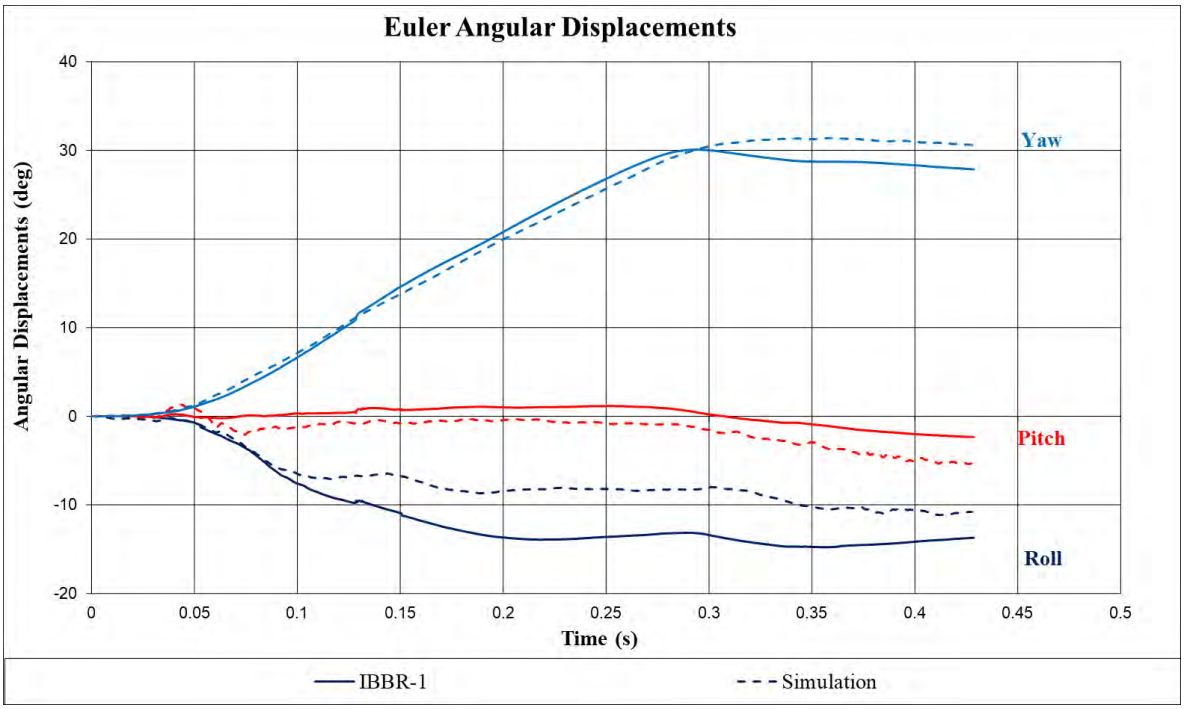


Figure D-16. Test No. IBBR-1 (Bielenberg et al. 2020) and Simulation Euler Angles

## D-5.5 Solution Verification

To determine if the analysis produced a numerically stable result, global verification based on V&V criteria was performed and is summarized in Table D-2. The purpose of this assessment is to ensure simulation results conform to conservation laws of energy, mass, and momentum. This is possible because the analysis was modeled as a closed system, in which the total energy should remain constant and should remain equal to the initial kinetic energy of the vehicle prior to the point of impact. Note hourglass energy does not affect simulation results but is recorded as a standard procedure for future model improvement. In this case, the criteria of the part/material energy did not pass because of high hourglass energy. Parts with high changes in energy were the differential cover and casing, front steel bumper, driver outer door, and front impact-side wheel barrel. The wheel drum failed hourglass criteria after impact and the other parts were deemed to not have a significant effect on results. Thus, they were excluded from evaluation criteria.

Table D-2. Test No. IBBR-1 Simulation Solution Verification

| Verification evaluation criteria | Change (%) | Pass? |
|---|---|---|
| ***Total energy*** of the simulation must not vary more than 10 percent from the beginning of the run to the end of the run | 1.19 | Y |
| ***Hourglass energy*** at the end of the run is less than 5 percent of the total initial energy at the beginning of the run | 1.55 | Y |
| ***Hourglass energy*** at the end of the run is less than 10 percent of the total internal energy at the end of the run | 10.29 | Y |
| The part/material with the most hourglass energy at the end of the run is less than 10 percent of the total internal energy of the part/material at the end of the run | 372.43 | N |
| Mass added to the total model is less than 5 percent of the total model mass at the beginning of the run | 0.09 | Y |
| The part/material with the most mass added had less than 10 percent of its initial mass added | 0.17 | Y |
| The moving parts/materials in the model have less than 5 percent of mass added to the initial moving mass of the model | 0.09 | Y |
| No shooting nodes in the solution | No | Y |
| No solid elements with negative volumes | No | Y |

### D-5.6 Time-history Validation

A quantitative evaluation was based on a comparison of acceleration-time histories collected from the accelerometer readings. The RSVVP program was used to compute Sprague-Geer and analysis of variance (ANOVA) metrics using time-history data from the full-scale test ("true curve") and FEA model ("test curve"). The multi-channel option in RSVVP was used since this option computes metrics for each individual channel as well as for the weighted composite of the combined channels. The data included the x-, y-, and z-acceleration, and the roll, pitch and yaw rates and was filtered in RSVVP using a CFC Class 180 filter.

The TL-3 curves were evaluated over the approximately 0.5-s impact event. The default metric evaluation options in RSVVP were used, which included Sprague-Geers and ANOVA metrics. The default acceptance criteria for these metrics are 40 percent for the Sprague-Geers metrics, 5 percent for the ANOVA mean, and 35 percent for the ANOVA standard deviation of residuals. These acceptance criteria were based on comparison of repeated full-scale crash tests involving small car impacts with a rigid barrier (i.e., uni-body vehicle impact with short impact duration) and were likely too strict for this application, which involves a multi-body vehicle and a relatively long impact event. For this assessment, V&V criteria were used to determine validity, while Sprague-Geers values less than or equal to 55 and standard deviation values less than or equal to 50 were deemed "borderline" acceptable.

#### D-5.6.1 Single-channel Assessment

Sprague-Geers and ANOVA metrics are shown in Table D-3 for x-, y-, and z- acceleration and yaw, roll, and pitch channels using RSVVP. Based on Sprague-Geers metrics, a comparison of the

individual acceleration components indicated the simulation was in good agreement with the test for yaw, roll, x-acceleration, and y-acceleration. The z-acceleration and pitch were in poor agreement with the test. ANOVA metrics indicated the mean residual error and standard deviation of the mean residual error were in agreement with the test for each metric except z-acceleration, which showed poor correlation.

Table D-3. Single-channel Time-history Comparison of Test No. IBBR-1 (Bielenberg et al. 2020) and Simulation

| **Evaluation criteria (time interval [0, 0.4763 s])** | | | | | | | | |
|---|---|---|---|---|---|---|---|---|
| O | ***Sprague-Geers***<br>Values less than or equal to 40 are acceptable | | | | | | | |
| | **Filter: CFC180 Sync.: None** | **RSVVP curve preprocessing** | | | | **M** | **P** | **Pass?** |
| | | **Shift** | | **Drift** | | | | |
| | | **True** | **Test** | **True** | **Test** | | | |
| | X-acceleration | **N** | N | **N** | N | -14.1 | 28.6 | Y |
| | Y-acceleration | **N** | N | **N** | N | 1.8 | 29.3 | Y |
| | Z-acceleration | **N** | N | **N** | N | 170.6 | 48.9 | N |
| | Roll | N | N | N | N | -18.7 | 35.6 | Y |
| | Pitch | N | N | N | N | 70.1 | 46.2 | N |
| | Yaw | N | N | N | N | -6.9 | 12.7 | Y |
| P | ***ANOVA***<br>Both criteria must be met:<br>• Mean residual error must be less than 5 percent of peak acceleration ($\bar{e} \le 0.05 \cdot a_{Peak}$)<br>• Standard deviation of the residuals must be less than 35 percent of peak acceleration ($\sigma \le 0.35 \cdot a_{Peak}$) | | | | | **Mean residual** | **Standard deviation of residuals** | **Pass?** |
| | X-acceleration (peak) | | | | | -0.6 | 12.8 | Y |
| | Y-acceleration (peak) | | | | | 0.7 | 19.5 | Y |
| | Z-acceleration (peak) | | | | | -2.5 | 48.9 | N |
| | Roll | | | | | -0.9 | 6.5 | Y |
| | Pitch | | | | | -0.2 | 6.8 | Y |
| | Yaw | | | | | -0.5 | 3.3 | Y |

### D-5.6.2 Multi-channel Assessment

Since the individual data metrics did not satisfy all acceptance criteria, the multi-channel option in RSVVP was used to calculate weighted Sprague-Geer and ANOVA metrics for the six data channels, as shown in Table D-4. The resulting weight factors computed for each channel indicated the x-acceleration, y-acceleration, roll, and yaw controlled the kinematic behavior of the impact event. The velocity change in the z-direction was insignificant compared to the change in the x- and y-directions and pitch angle magnitudes were negligible compared to yaw. The weighted RSVVP metrics in the multi-channel mode satisfied the acceptance criteria, and therefore the time-history comparison was considered acceptable.

Table D-4. Multi-channel Time-history Comparison of Test No. IBBR-1 (Bielenberg et al. 2020) and Simulation

| **Evaluation criteria (time interval [0 , 0.4763])** | | | | | |
|---|---|---|---|---|---|
| **Multi-channel weights:** Area II method | | X-acceleration: 0.1833<br>Y-acceleration: 0.2791<br>Z-acceleration: 0.0376 | Yaw: 0.2804<br>Roll: 0.1396<br>Pitch: 0.0800 | | |
| O | ***Sprague-Geers***<br>Values less or equal to 40 are acceptable | | **M** | **P** | **Pass?** |
| | | | 14.1 | 28.6 | Y |
| P | ***ANOVA***<br>Both criteria must be met:<br>• Mean residual error must be less than 5 percent of peak acceleration ($\bar{e} \leq 0.05 \cdot a_{Peak}$)<br>• Standard deviation of the residuals must be less than 35 percent of peak acceleration ($\sigma \leq 0.35 \cdot a_{Peak}$) | | **Mean residual** | **Standard deviation of residuals** | **Pass?** |
| | | | -0.63 | 12.82 | Y |

## D-6 Validation to Test No. H34BR-2

### D-6.1 Test Setup

In MASH TL-3 full-scale crash test no. H34BR-2 (Bielenberg 2019), a 5,001-lb 2018 RAM 1500 Crew Cab impacted a 34-in. tall, 10-in. thick vertical barrier at 64 mph and a 25.4-degree angle. In simulation, a 5,022-lb 2018 RAM 1500 Quad Cab impacted a 34-in. tall, 10-in. thick vertical barrier at 63.9 mph and a 25.0-degree angle. Test vehicle and simulation model dimensions and impact points are compared in Figure D-17.

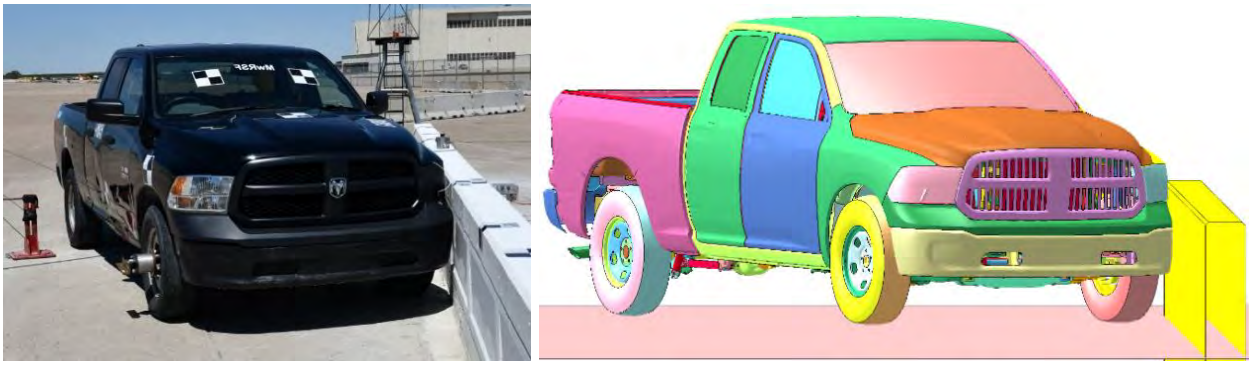

Figure D-17. Test No. H34BR-2 (Bielenberg 2019) and Simulation Vehicles

### D-6.2 ZOI and Key Events

The point of maximum intrusion during simulation is compared to the equivalent time step in test no. H34BR-2 in Figure D-18. ZOI measurement from the test and simulation had a 3.4 percent relative difference. Key events are summarized in Table D-5.

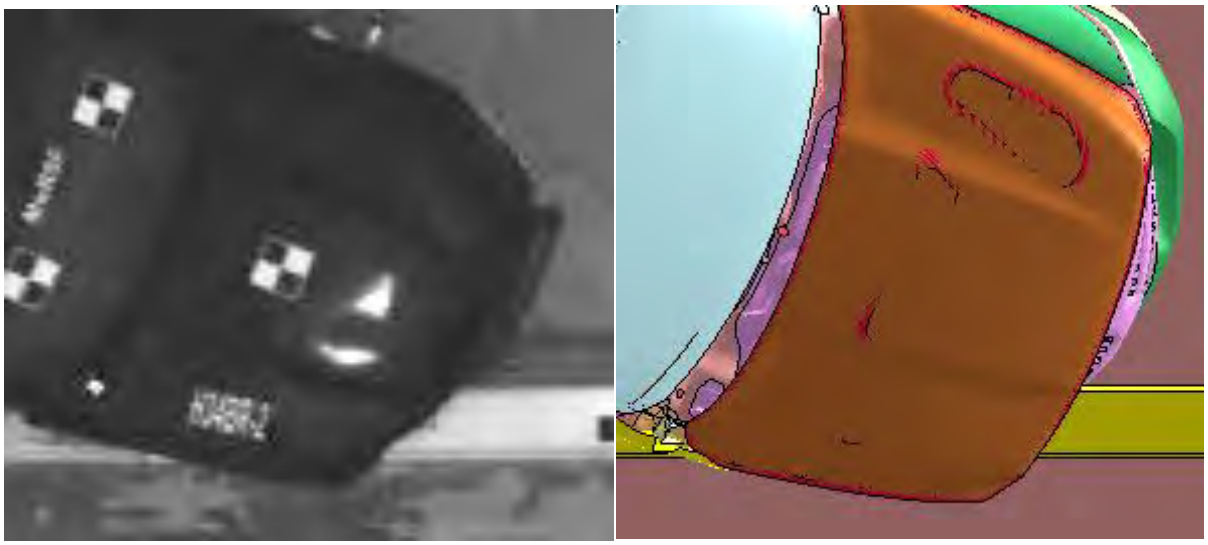

Figure D-18. Maximum Lateral Extent during Test No. H34BR-2 (Bielenberg 2019) and Simulation

Table D-5. Key Events Comparison, Test No. H34BR-2 (Bielenberg 2019) and Simulation

| Event | Test | FEA |
|---|---|---|
| ZOI measurement (in.) | 16.65 | 16.08 |
| ZOI time (ms) | 68 | 75 |
| Parallel time (ms) | 192 | 195 |
| Exit Time (ms) | 408 | 290 |

### D-6.3 Sequentials

Sequential images of test no. H34BR-2 and the simulation are compared in Figures D-19 through D-24. The simulated vehicle behavior was comparable to that of the test vehicle.

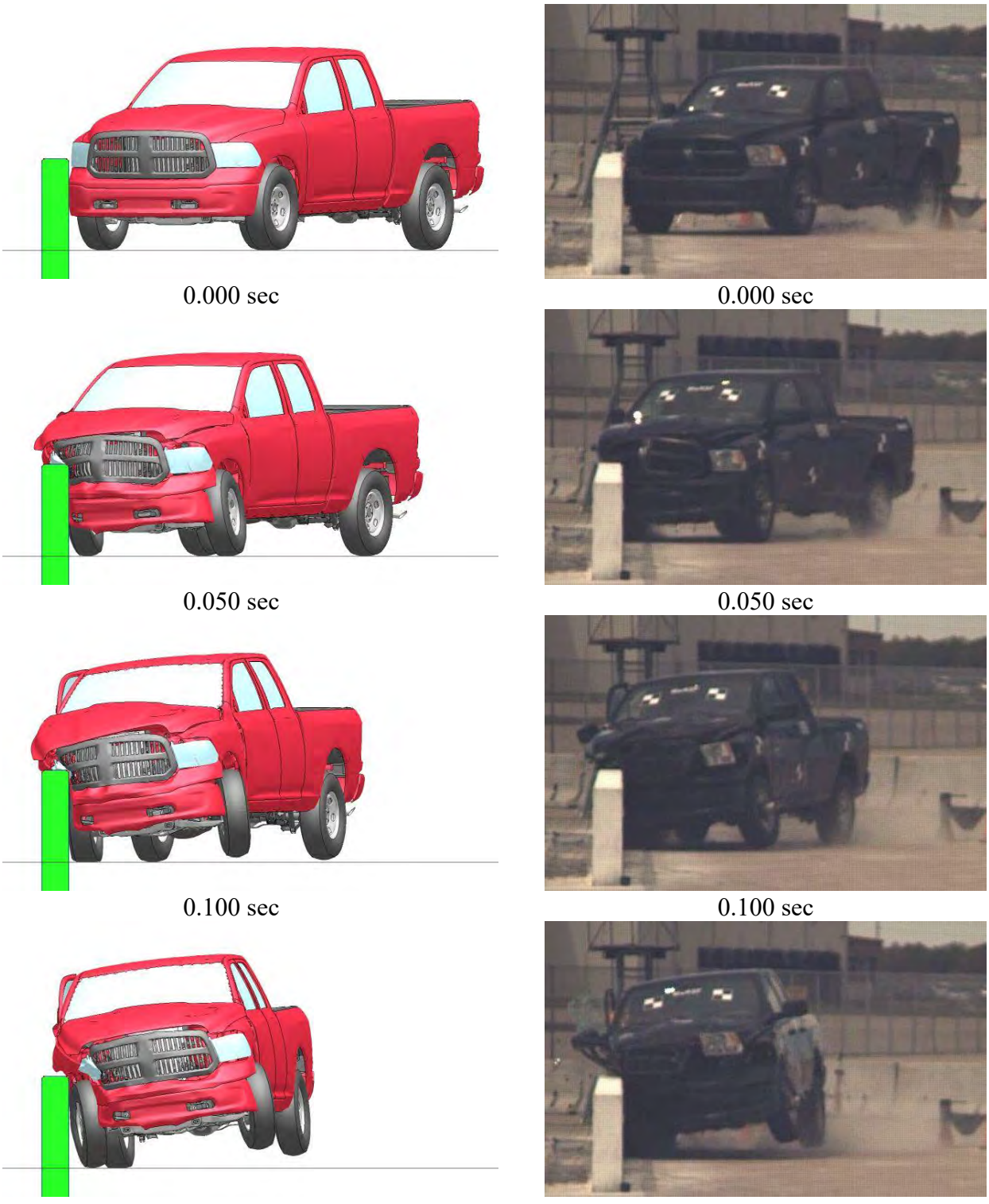


Figure D-19. Test No. H34BR-2 (Bielenberg 2019) and Simulation Downstream Sequential Images


Figure D-20. Test No. H34BR-2 (Bielenberg 2019) and Simulation Downstream Sequential Images (continued)

0.000 sec

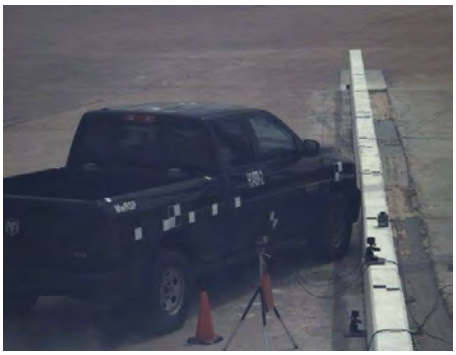

0.000 sec

0.050 sec

0.050 sec

0.100 sec

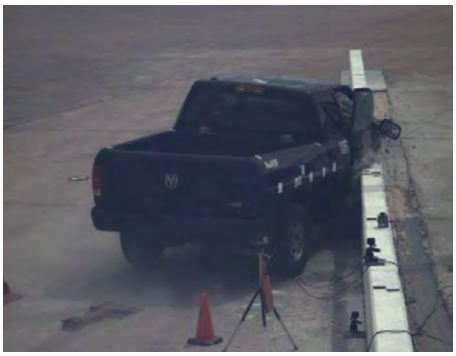

0.100 sec

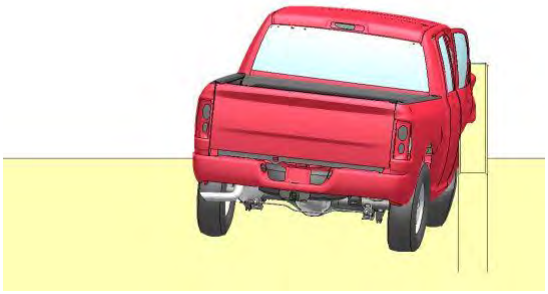

0.150 sec

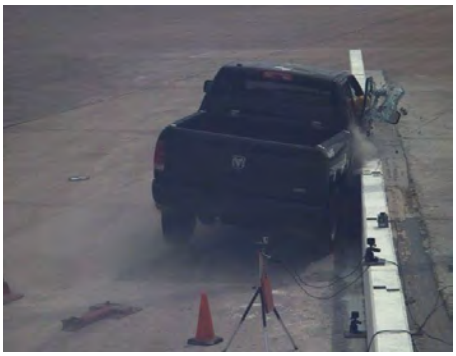

0.150 sec

Figure D-21. Test No. H34BR-2 (Bielenberg 2019) and Simulation Upstream Sequential Images

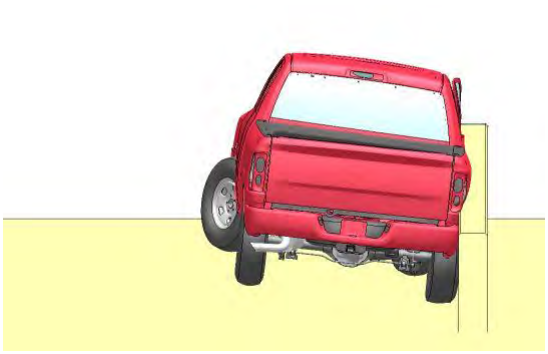

0.200 sec

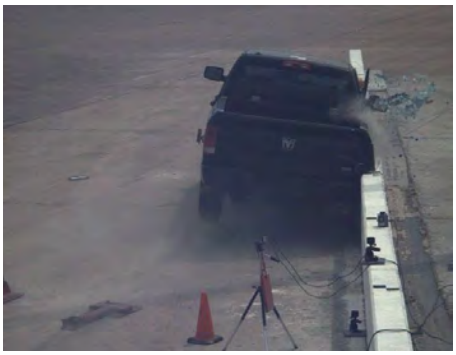

0.200 sec

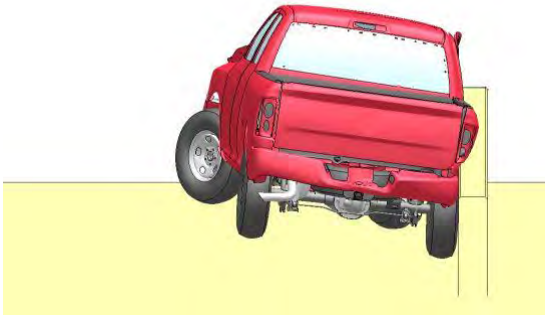

0.250 sec

0.250 sec

0.350 sec

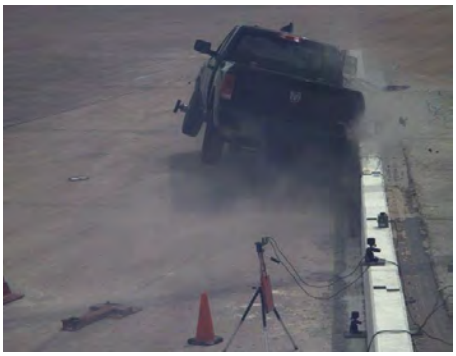

0.350 sec

0.450 sec

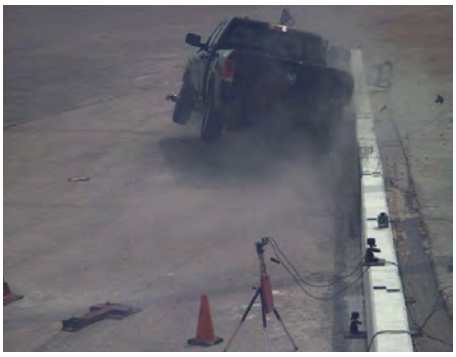

0.450 sec

Figure D-22. Test No. H34BR-2 (Bielenberg 2019) and Simulation Upstream Sequential Images (continued)

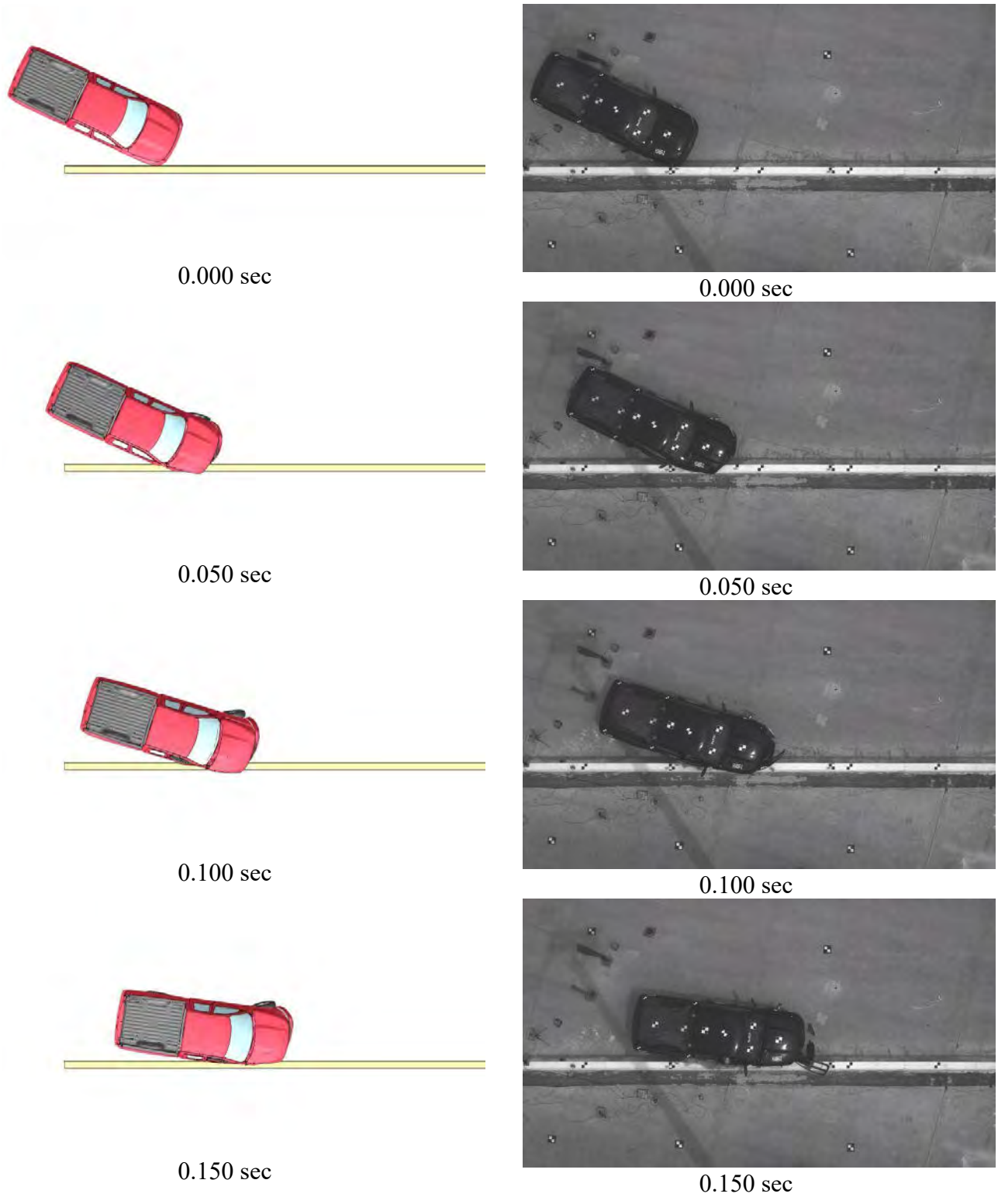


Figure D-23. Test No. H34BR-2 (Bielenberg 2019) and Simulation Overhead Sequential Images

0.200 sec

0.200 sec

0.250 sec

0.250 sec

0.350 sec

0.350 sec

0.450 sec

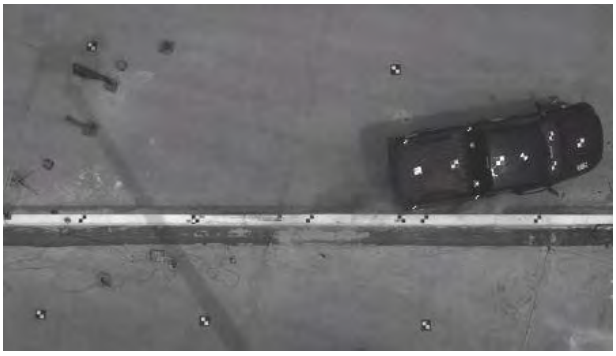

0.450 sec

Figure D-24. Test No. H34BR-2 (Bielenberg 2019) and Simulation Overhead Sequential Images (continued)

## D-6.4 Time-dependent Data

To validate overall dynamic performance of the crash test and simulation, acceleration, velocity, and displacements were compared, as shown in Figures D-25 through D-27. Accelerations were comparable, providing high confidence in the validation of the vehicle's dynamic ridedown performance.

Euler angles are compared in Figure D-28; roll was slightly higher in the test, possibly due to suspension and tire modeling of the RAM model. The wheel is crushed toward the toe pan upon initial impact, and the slight inaccuracy of the tire model may lead to inexact roll and pitch replication later in the simulated impact event.

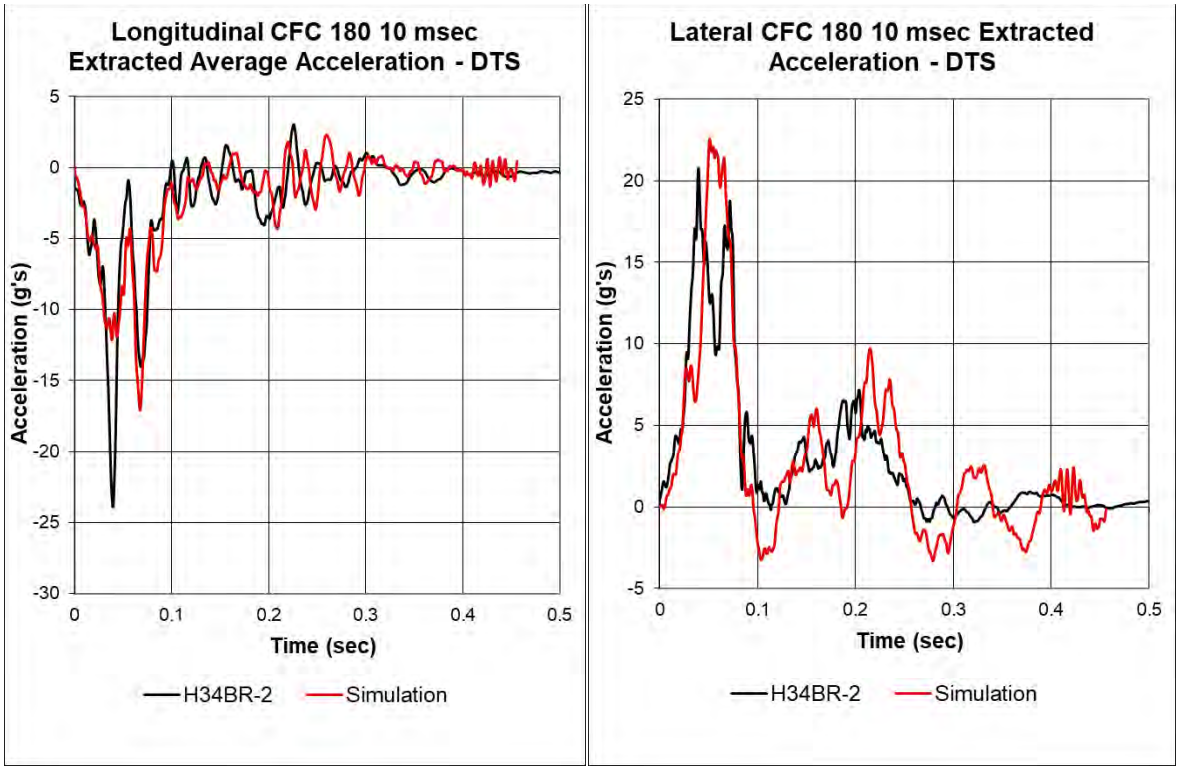


Figure D-25. Test No. H34BR-2 (Bielenberg 2019) and Simulation Acceleration

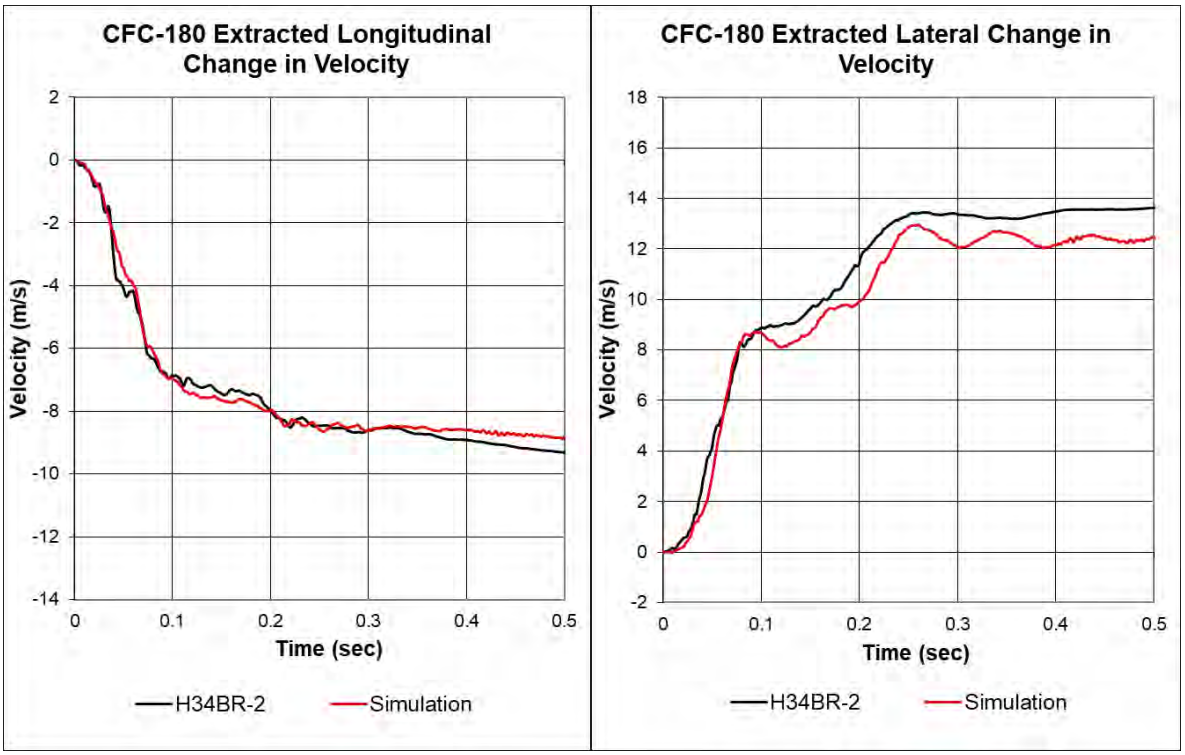


Figure D-26. Test No. H34BR-2 (Bielenberg 2019) and Simulation Velocity

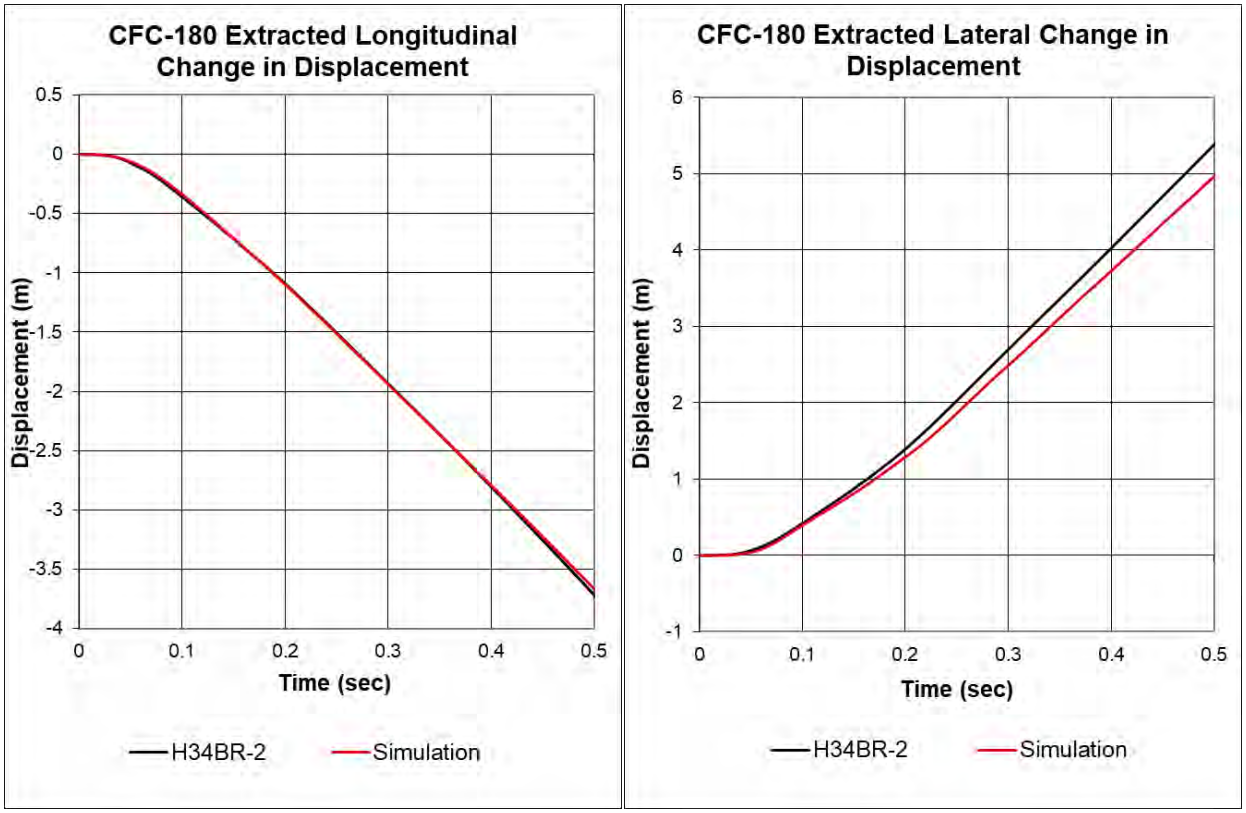


Figure D-27. Test No. H34BR-2 (Bielenberg 2019) and Simulation Displacement

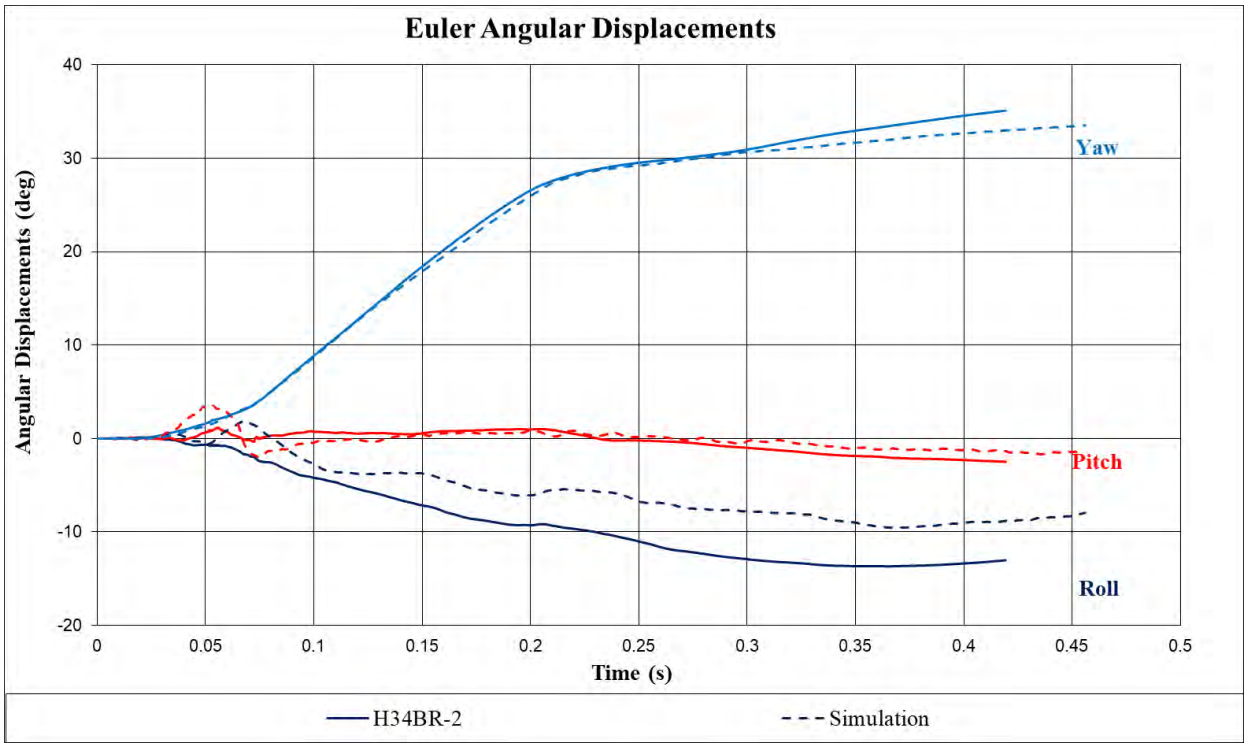


Figure D-28. Test No. H34BR-2 (Bielenberg 2019) and Simulation Euler Angles

## D-6.5 Solution Verification

To determine if the analysis produced a numerically stable result, global verification based on V&V criteria was performed and is summarized in Table D-6. The criterion of the part/material energy did not pass because of high hourglass energy. Parts with high changes in energy were the differential cover, headlight, driver outer door, and plastic bumper cover. These parts were deemed non-critical for energy absorption as they do not have a significant effect on the vehicle's kinematic response. Thus, they were excluded from evaluation criteria.

Table D-6. Test No. H34BR-2 Simulation Solution Verification

| Verification evaluation criteria | Change (%) | Pass? |
|---|---|---|
| ***Total energy*** of the simulation must not vary more than 10 percent from the beginning of the run to the end of the run | 0.83 | Y |
| ***Hourglass energy*** at the end of the run is less than 5 percent of the total initial energy at the beginning of the run | 1.26 | Y |
| ***Hourglass energy*** at the end of the run is less than 10 percent of the total internal energy at the end of the run | 8.71 | Y |
| The part/material with the most hourglass energy at the end of the run is less than 10 percent of the total internal energy of the part/material at the end of the run | 366.99 | N |
| Mass added to the total model is less than 5 percent of the total model mass at the beginning of the run | 0.09 | Y |
| The part/material with the most mass added had less than 10 percent of its initial mass added | 0.22 | Y |
| The moving parts/materials in the model have less than 5 percent of mass added to the initial moving mass of the model | 0.09 | Y |
| No shooting nodes in the solution | No | Y |
| No solid elements with negative volumes | No | Y |

## D-6.6 Time-history Validation

### D-6.6.1 Single-channel Assessment

Sprague-Geers and ANOVA metrics are shown in Table D-7 for x-, y-, and z- acceleration and yaw, roll, and pitch channels using RSVVP. Based on Sprague-Geers metrics, a comparison of the individual acceleration components indicated the simulation was in good agreement with the test for x- and y- acceleration, yaw, and roll. In contrast, the z-acceleration and pitch were in poor agreement with the test. ANOVA metrics indicated the mean residual error and standard deviation of the mean residual error were in agreement with the test for all metrics.

Table D-7. Single-channel Time-history Comparison of Test No. H34BR-(Bielenberg 2019) and Simulation

| Evaluation criteria (time interval [0 , 0.5046 s]) | | | | | | | | |
|---|---|---|---|---|---|---|---|---|
| O | ***Sprague-Geers***<br>Values less than or equal to 40 are acceptable | | | | | | | |
| | **Filter: CFC180 Sync.: None** | **RSVVP curve preprocessing** | | | | **M** | **P** | **Pass?** |
| | | **Shift** | | **Drift** | | | | |
| | | **True** | **Test** | **True** | **Test** | | | |
| | X-acceleration | **N** | N | **N** | N | -20.9 | 30.2 | Y |
| | Y-acceleration | **N** | N | **N** | N | 4.5 | 27 | Y |
| | Z-acceleration | **N** | N | **N** | N | 54.7 | 49.4 | N |
| | Roll | N | N | N | N | 5.7 | 38.6 | Y |
| | Pitch | N | N | N | N | 28.1 | 44.7 | N |
| | Yaw | N | N | N | N | -2.1 | 6.6 | Y |
| P | ***ANOVA***<br>Both criteria must be met:<br>• The mean residual error must be less than 5 percent of peak acceleration ($\bar{e} \le 0.05 \cdot a_{Peak}$)<br>• The standard deviation of the residuals must be less than 35 percent of peak acceleration ($\sigma \le 0.35 \cdot a_{Peak}$) | | | | | **Mean residual** | **Standard deviation of residuals** | **Pass?** |
| | X-acceleration (peak) | | | | | 0.2 | 10.9 | Y |
| | Y-acceleration (peak) | | | | | 0.7 | 14.3 | Y |
| | Z-acceleration (peak) | | | | | -2 | 33.1 | Y |
| | Roll | | | | | -1.5 | 11.3 | Y |
| | Pitch | | | | | 0.5 | 7.3 | Y |
| | Yaw | | | | | 1.3 | 5.1 | Y |

### D-6.6.2 Multi-channel Assessment

Since the individual data metrics did not satisfy all acceptance criteria, the multi-channel option in RSVVP was used to calculate weighted Sprague-Geer and ANOVA metrics for the six data channels, as shown in Table D-8. The resulting weight factors computed for each channel indicated the x- and y-acceleration, roll, and yaw controlled the kinematic behavior of the impact event. The velocity change in the z-direction was negligible compared to the x- and y-directions, and pitch was insignificant compared to yaw. The weighted RSVVP metrics in the multi-channel mode satisfied the acceptance criteria, and therefore the time-history comparison was considered acceptable.

Table D-8. Multi-channel Time-history Comparison of Test No. H34BR-2 (Bielenberg 2019) and Simulation

| Evaluation criteria (time interval [0 , 0.5046 s]) | | | | |
|---|---|---|---|---|
| **Multi-channel weights:** Area II method | X-acceleration: 0.1917<br>Y-acceleration: 0.2803<br>Z-acceleration: 0.028032 | Yaw: 0.3393<br>Roll: 0.0918<br>Pitch: 0.0688 | | |
| O | ***Sprague-Geers***<br>Values less or equal to 40 are acceptable. | **M** | **P** | **Pass?** |
| | | 20.9 | 30.2 | Y |
| P | ***ANOVA***<br>Both criteria must be met:<br>• Mean residual error must be less than 5 percent of peak acceleration ($\bar{e} \leq 0.05 \cdot a_{Peak}$)<br>• Standard deviation of the residuals must be less than 35 percent of peak acceleration ($\sigma \leq 0.35 \cdot a_{Peak}$) | **Mean residual** | **Standard deviation of residuals** | **Pass?** |
| | | 0.21 | 10.85 | Y |

## D-7 Validation to Test No. OSSB-1

### D-7.1 Test Setup

In MASH TL-3 full-scale crash test no. OSSB-1 (Bielenberg, Faller, and Ronspies 2018), a 5,001-lb 2011 RAM 1500 Crew Cab impacted a 42-in. tall, 12-in. thick single-slope barrier at 62.8 mph and a 24.9-degree angle. In simulation, a 5,022-lb 2018 RAM 1500 Quad Cab impacted a 42-in. tall, 12-in. thick single-slope barrier at 62.8 mph and a 24.9-degree angle. Test vehicle and simulation model dimensions and impact points are compared in Figure D-29.

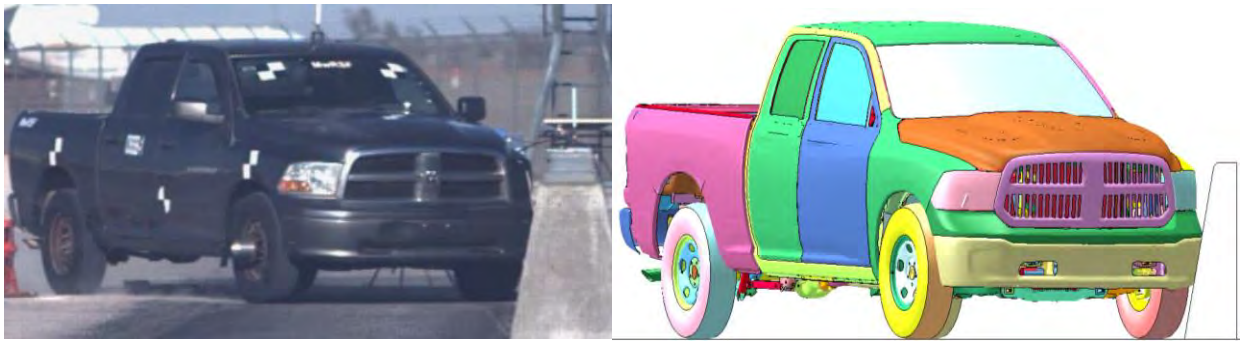

Figure D-29. Test No. OSSB-1 (Bielenberg, Faller, and Ronspies 2018) and Simulation Vehicles

### D-7.2 ZOI and Key Events

The point of maximum intrusion during simulation is compared to the equivalent time step in test no. OSSB-1 in Figure D-30. ZOI measurement from the test and simulation had a 27.3 percent relative difference and a 2.96-in. absolute difference. The simulated model's to replication of the ZOI from full-scale crash testing was deemed acceptable. Key events are summarized in Table D-9.

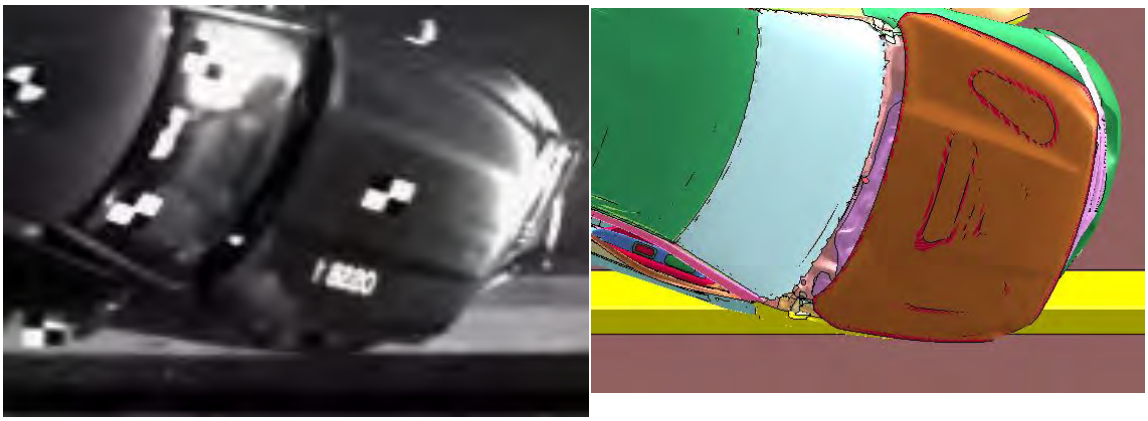

Figure D-30. Maximum Lateral Extent during Test No. OSSB-1 (Bielenberg, Faller, and Ronspies 2018) and Simulation

Table D-9. Key Events Comparison, Test No. OSSB-1 (Bielenberg, Faller, and Ronspies 2018) and Simulation

| Event | Test | FEA |
|---|---|---|
| ZOI measurement (in.) | 10.84 | 7.88 |
| ZOI time (ms) | 70 | 80 |
| Parallel time (ms) | 188 | 185 |
| Exit Time (ms) | 367 | 280 |

**D-7.3 Sequentials**

Sequential images of test no. OSSB-1 and the simulation are compared in Figures D-31 through D-36. The basic simulated vehicle behavior was comparable to that of the test vehicle.

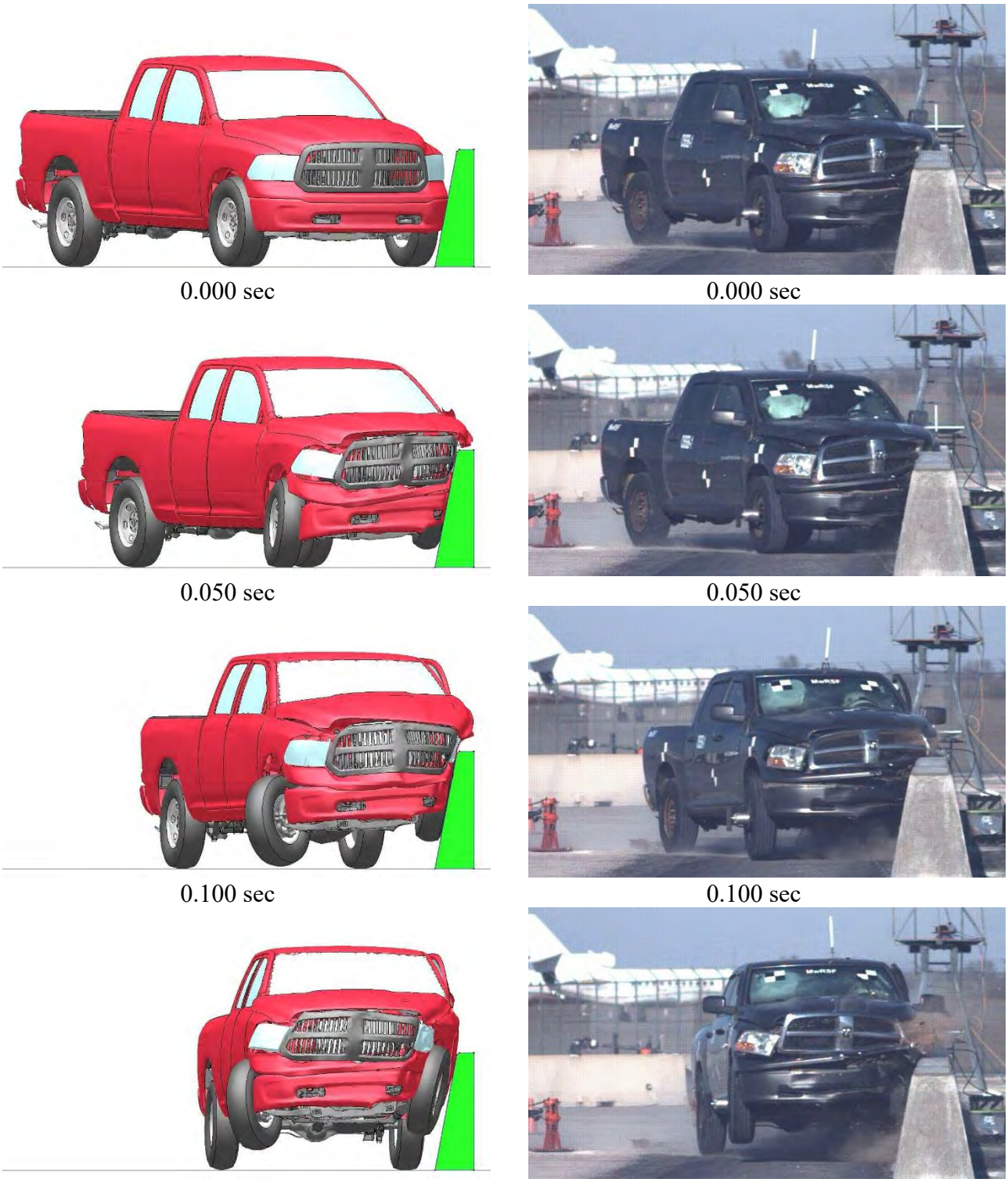


Figure D-31. Test No. OSSB-1 (Bielenberg, Faller, and Ronspies 2018) and Simulation Downstream Sequential Images

0.200 sec

0.200 sec

0.250 sec

0.250 sec

0.350 sec

0.350 sec

0.450 sec

0.450 sec

Figure D-32. Test No. OSSB-1 (Bielenberg, Faller, and Ronspies 2018) and Simulation Downstream Sequential Images (continued)

0.000 sec

0.000 sec

0.050 sec

0.050 sec

0.100 sec

0.100 sec

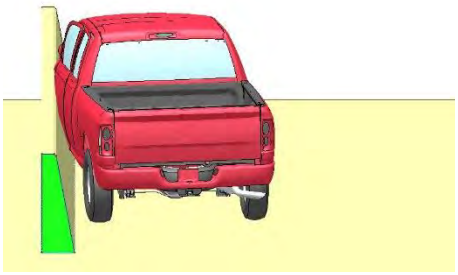

0.150 sec

0.150 sec

Figure D-33. Test No. OSSB-1 (Bielenberg, Faller, and Ronspies 2018) and Simulation Upstream Sequential Images

0.200 sec

0.200 sec

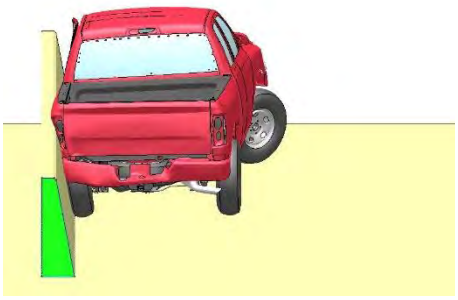

0.250 sec

0.250 sec

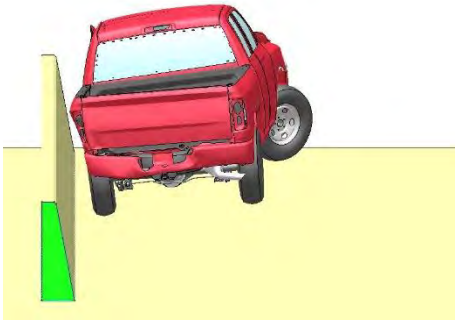

0.350 sec

0.350 sec

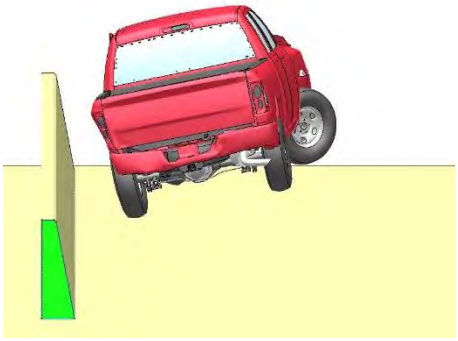

0.450 sec

0.450 sec

Figure D-34. Test No. OSSB-1 (Bielenberg, Faller, and Ronspies 2018) and Simulation Upstream Sequential Images (continued)

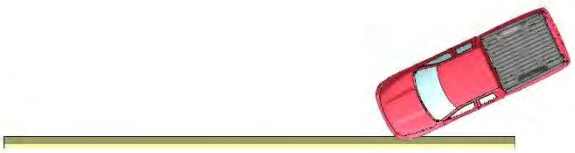

0.000 sec

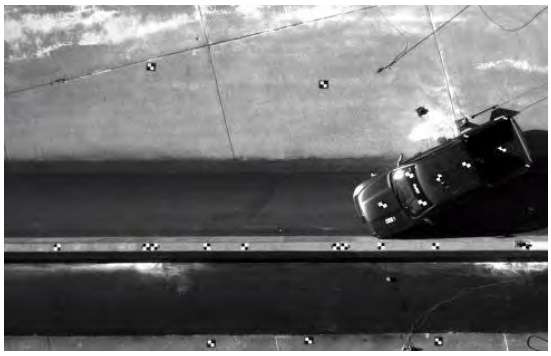

0.000 sec

0.050 sec

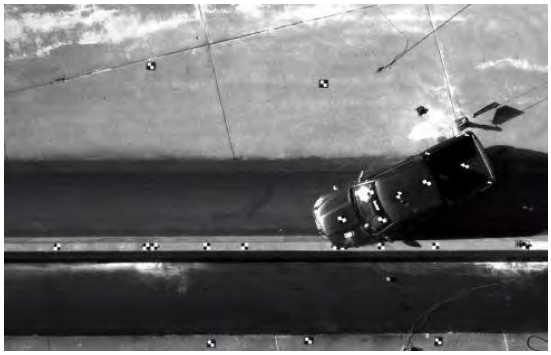

0.050 sec

0.100 sec

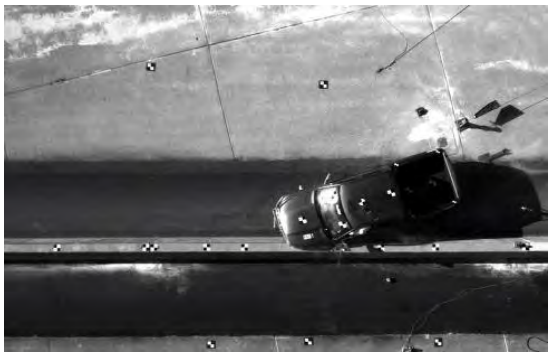

0.100 sec

0.150 sec

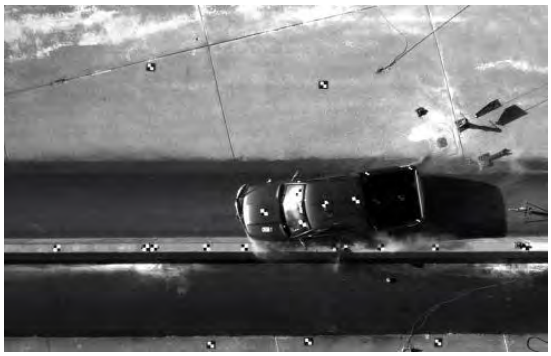

0.150 sec

Figure D-35. Test No. OSSB-1 (Bielenberg, Faller, and Ronspies 2018) and Simulation Overhead Sequential Images

0.200 sec

0.200 sec

0.250 sec

0.250 sec

0.350 sec

0.350 sec

0.450 sec

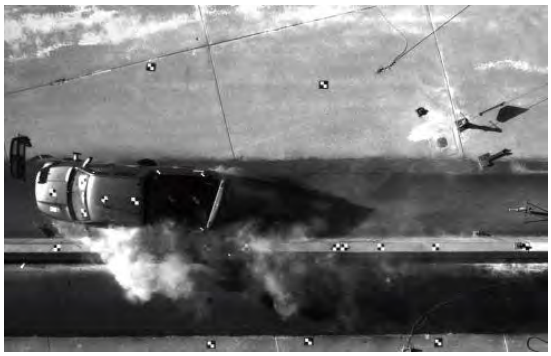

0.450 sec

Figure D-36. Test No. OSSB-1 (Bielenberg, Faller, and Ronspies 2018) and Simulation Overhead Sequential Images (continued)

### D-7.4 Time-dependent Data

To validate overall dynamic performance of the crash test and simulation, acceleration, velocity, and displacements were compared, as shown in Figures D-37 through D-39. A large positive acceleration peak was present at 0.1 seconds in the test data which was not captured by the simulation. This peak appears to have only occurred in Test No. OSSB-1 since it is not as prominent in the previous two pickup truck full-scale crash tests. Accelerations were otherwise comparable, providing high confidence in the validation of the vehicle's dynamic ridedown performance.

Euler angles are compared in Figure D-40; pitch and roll were slightly higher in the test due to minor inaccuracy of suspension and tire models. During the initial simulated impact, the vehicle slightly rolled away from the barrier and pitched upward, affecting the model's ability to replicate roll and pitch thereafter.

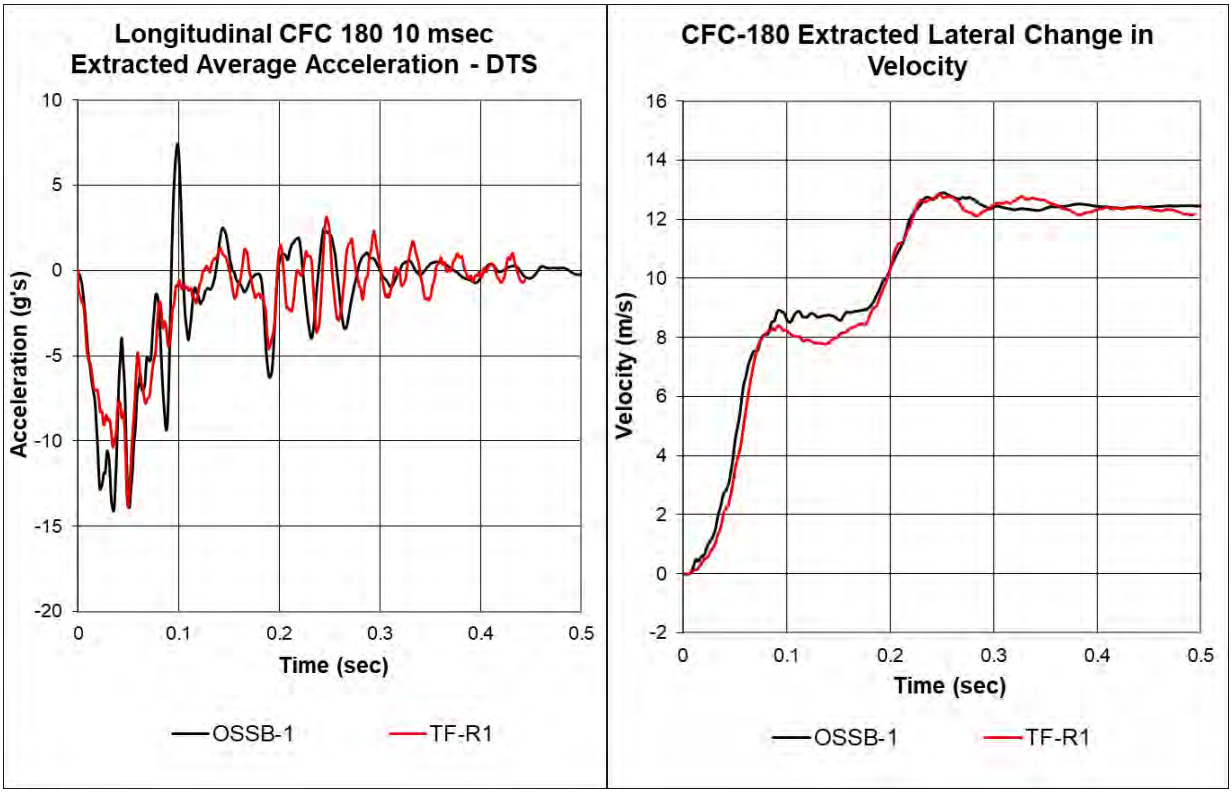


Figure D-37. Test No. OSSB-1 (Bielenberg, Faller, and Ronspies 2018) and Simulation Acceleration

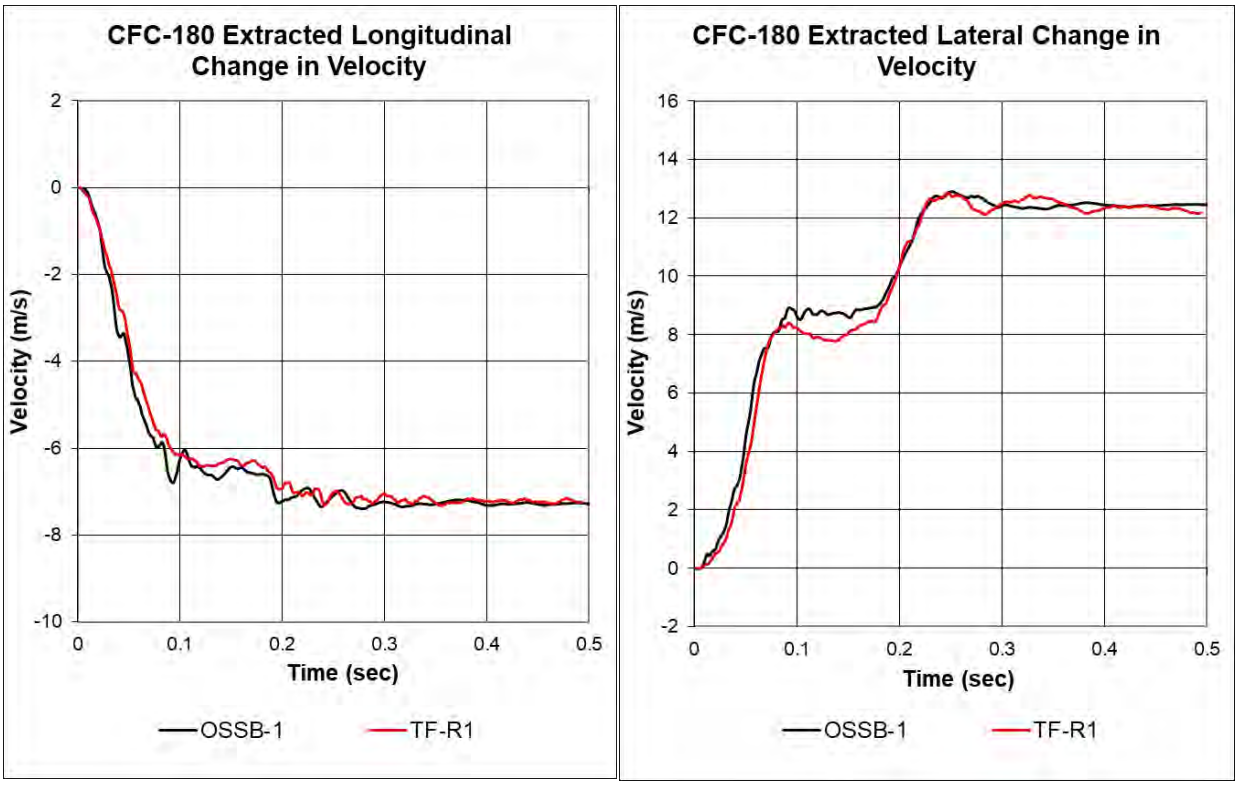


Figure D-38. Test No. OSSB-1 (Bielenberg, Faller, and Ronspies 2018) and Simulation Velocity

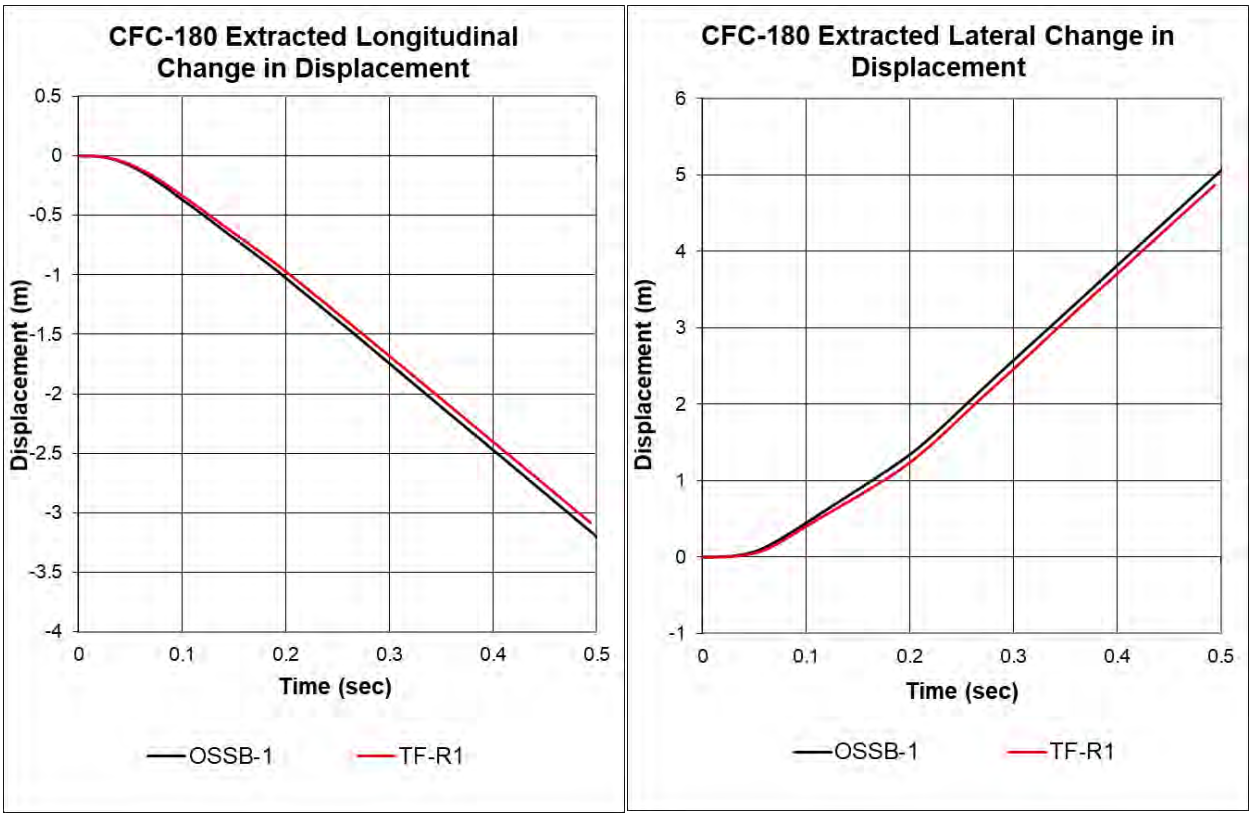


Figure D-39. Test No. OSSB-1 (Bielenberg, Faller, and Ronspies 2018) and Simulation Displacement

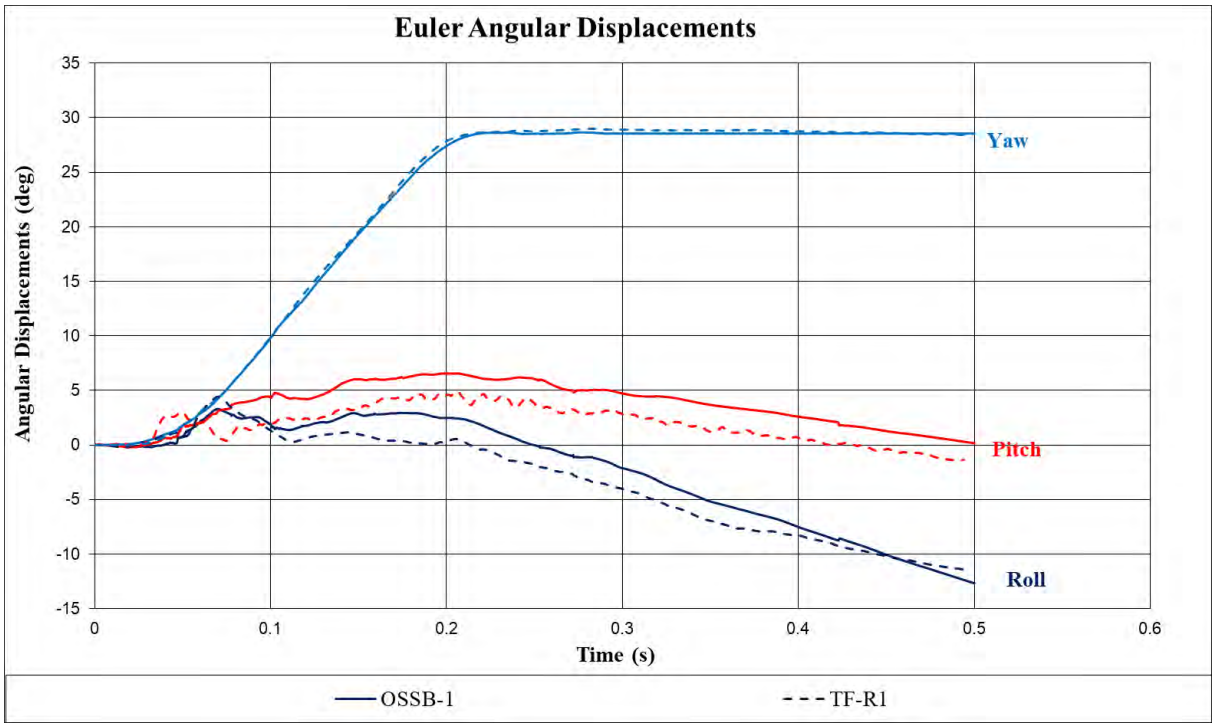


Figure D-40. Test No. OSSB-1 (Bielenberg, Faller, and Ronspies 2018) and Simulation Euler Angles

## D-7.5 Solution Verification

To determine if the analysis produced a numerically stable result, global verification based on V&V criteria was performed and is summarized in Table D-10. The criteria of the part/material energy did not pass because of high hourglass energy. Parts with high changes in energy were the differential cover, driver-side headlight, and driver outer door. These parts were deemed non-critical for energy absorption as they did not have a significant effect on the vehicle's kinematic response. Thus, they were excluded from evaluation criteria.

Table D-10. Table 23. Test No. OSSB-1 Simulation Solution Verification

| Verification evaluation criteria | Change (%) | Pass? |
|---|---|---|
| ***Total energy*** of the simulation must not vary more than 10 percent from the beginning of the run to the end of the run | 1.11 | Y |
| ***Hourglass energy*** at the end of the run is less than 5 percent of the total initial energy at the beginning of the run | 0.88 | Y |
| ***Hourglass energy*** at the end of the run is less than 10 percent of the total internal energy at the end of the run | 6.21 | Y |
| The part/material with the most hourglass energy at the end of the run is less than 10 percent of the total internal energy of the part/material at the end of the run | 337.03 | N |
| Mass added to the total model is less than 5 percent of the total model mass at the beginning of the run | 0.09 | Y |
| The part/material with the most mass added had less than 10 percent of its initial mass added | 0.19 | Y |
| The moving parts/materials in the model have less than 5 percent of mass added to the initial moving mass of the model | 0.09 | Y |
| No shooting nodes in the solution | No | Y |
| No solid elements with negative volumes | No | Y |

## D-7.6 Time-history Validation

### D-7.6.1 Single-channel Assessment

Sprague-Geers and ANOVA metrics are shown in Table D-11 for x-, y-, and z- acceleration and yaw, roll, and pitch channels using RSVVP. Based on Sprague-Geers metrics, a comparison of the individual acceleration components indicated the simulation was in good agreement with the test for yaw, roll, x- acceleration, and y- acceleration. In contrast, the z-acceleration and pitch were in poor agreement with the test. ANOVA metrics indicated the mean residual error and standard deviation of the mean residual error were in agreement with the test for each metric except z-acceleration, which showed poor correlation.

Table D-11. Single-channel Time-history Comparison of Test No. OSSB-1 (Bielenberg, Faller, and Ronspies 2018) and Simulation

| Evaluation criteria (time interval [0, 0.4926 s]) | | | | | | | | |
|---|---|---|---|---|---|---|---|---|
| O | ***Sprague-Geers***<br>Values less than or equal to 40 are acceptable | | | | | | | |
| | **Filter: CFC180 Sync.: None** | **RSVVP curve preprocessing** | | | | **M** | **P** | **Pass?** |
| | | **Shift** | | **Drift** | | | | |
| | | **True** | **Test** | **True** | **Test** | | | |
| | X-acceleration | **N** | N | **N** | N | -15.7 | 25.3 | Y |
| | Y-acceleration | **N** | N | **N** | N | 0.8 | 20.9 | Y |
| | Z-acceleration | **N** | N | **N** | N | 74.2 | 52.4 | N |
| | Roll | N | N | N | N | -29.6 | 36 | Y |
| | Pitch | N | N | N | N | 19.5 | 46 | N |
| | Yaw | N | N | N | N | 1.2 | 6.9 | Y |
| P | ***ANOVA***<br>Both criteria must be met:<br>• Mean residual error must be less than 5 percent of peak acceleration ($\bar{e} \le 0.05 \cdot a_{Peak}$)<br>• Standard deviation of the residuals must be less than 35 percent of peak acceleration ($\sigma \le 0.35 \cdot a_{Peak}$) | | | | | **Mean residual** | **Standard deviation of residuals** | **Pass?** |
| | X-acceleration (peak) | | | | | 0 | 14.8 | Y |
| | Y-acceleration (peak) | | | | | -0.2 | 12.9 | Y |
| | Z-acceleration (peak) | | | | | -3.2 | 51.4 | N |
| | Roll | | | | | 0.3 | 6.6 | Y |
| | Pitch | | | | | -0.4 | 11.5 | Y |
| | Yaw | | | | | -0.1 | 5 | Y |

### D-7.6.2 Multi-channel Assessment

Since the individual data metrics did not satisfy all acceptance criteria, the multi-channel option in RSVVP was used to calculate weighted Sprague-Geer and ANOVA metrics for the six data channels, as shown in Table D-12. The resulting weight factors computed for each channel indicated the x-acceleration, y-acceleration, roll, and yaw controlled the kinematic behavior of the impact event. The velocity change in the z-direction was insignificant compared to the x- and y-directions, and pitch was negligible compared to the yaw and roll. The weighted RSVVP metrics in the multi-channel mode satisfied the acceptance criteria, and therefore the time-history comparison was considered acceptable.

Table D-12. Multi-channel Time-history Comparison of Test No. OSSB-1 (Bielenberg, Faller, and Ronspies 2018) and Simulation

| **Evaluation criteria (time interval [0,0.4926 s])** | | | | |
|---|---|---|---|---|
| **Multi-channel weights:** Area II method | X-acceleration: 0.1747<br>Y-acceleration: 0.2995<br>Z-acceleration: 0.0258 | Yaw: 0.3178<br>Roll: 0.1657<br>Pitch: 0.0165 | | |
| O | ***Sprague-Geers***<br>Values less or equal to 40 are acceptable | **M** | **P** | **Pass?** |
| | | -15.7 | 25.3 | Y |
| P | ***ANOVA***<br>Both criteria must be met:<br>• Mean residual error must be less than 5 percent of peak acceleration ($\bar{e} \le 0.05 \cdot a_{Peak}$)<br>• Standard deviation of the residuals must be less than 35 percent of peak acceleration ($\sigma \le 0.35 \cdot a_{Peak}$) | **Mean residual** | **Standard deviation of residuals** | **Pass?** |
| | | 0 | 14.8 | Y |

## D-8 Discussion

RAM model simulations generally agreed well with each full-scale crash test. Models yielded marginal discrepancies in roll and pitch behavior during initial impact which subsequently led to deviations from test behavior. These discrepancies were attributed to the wheel crush toward the toe pan, indicating there may be deficiencies in how the model's wheel, tire, and suspension components interact with rigid barriers. Although all three validations agreed well with their respective tests, this was not expected to be the case for SUT and tractor-trailer simulation. The RAM model was highly reflective of pickup trucks used in full-scale crash testing, and pickup truck dimensions do not vary significantly. The SUT model, however, was modeled as a 1996 Ford F800 and was not representative of the current vehicle fleet; likewise, SUTs have highly variable dimensions even among comparable model years. It was not reasonable to expect one SUT model to encompass the behavior of each SUT vehicle.

# Appendix E. F800 Model Preparation and Validation

## E-1 Overview

The 1996 F800 SUT model was validated by comparing test vehicle geometry, inertial characteristics, frame and suspension component geometries, and results of simulations with two comparable full-scale crash tests. Validation was conducted against test nos. 4CBR-1 (Rosenbaugh et al. 2021) and 420020-9B (Sheikh, Bligh, and Menges 2011). This appendix discusses efforts to implement, expedite, and improve simulation stability, followed by a discussion of the validation results and model shortcomings.

## E-2 Preparation

The SUT model was repositioned for driver-side impacts at a 15-degree angle, allowing for simple replacement of barrier models for different simulation setups. Accelerations are affected by the recorded location, and therefore the model's accelerometer positioning was adjusted to match the mounting location used in full-scale crash testing. A non-impact, free-rolling vehicle model was defined to have an initial longitudinal velocity and used to conduct a qualitative energy balance check. This ensured the model's energy levels behaved properly in the absence of a rigid barrier impact.

All barriers were modeled rigidly with a Belytscho-Tsay element formulation and 15x15 mm shell elements. Single point constraints were applied to each node to fix the barrier in place.

## E-3 Modifications

Initial simulations using an available SUT model previously evaluated at MwRSF were deemed unacceptable due to many differences between test outcomes and simulations. The following sections describe updates to the model which resulted in improved prediction of ZOI extensions and vehicle dynamic reactions.

### E-3.1 Cargo Box

Preliminary SUT-barrier models revealed problems in the interaction between the cargo box and barrier. As shown in Figure E-1, the cargo box was modeled with a coarse, generic mesh. The cargo box itself consisted of an outer shell attached to bed cross members using spot welds. The bed cross members were connected to the bed rails using constrained nodal rigid bodies. U-bolts attached the bed rails to the truck's frame rails.

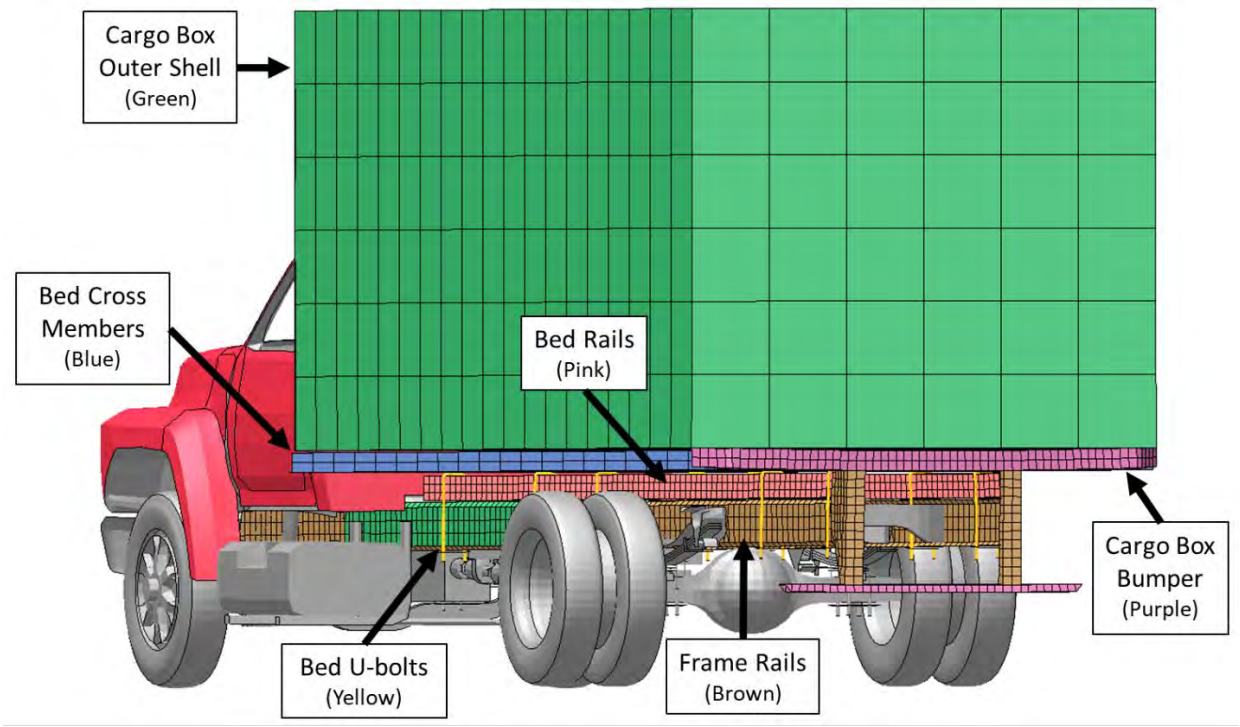


Figure E-1. SUT Cargo Box Components

During preliminary SUT simulation, bed cross members interacted with the barrier and caused snagging and severe mesh distortion, as shown in Figure E-2. At this phase of the research effort, it was expected box parts would interact with barriers more as barrier height increased and potentially cause model stability issues due to the cargo box's coarse mesh.

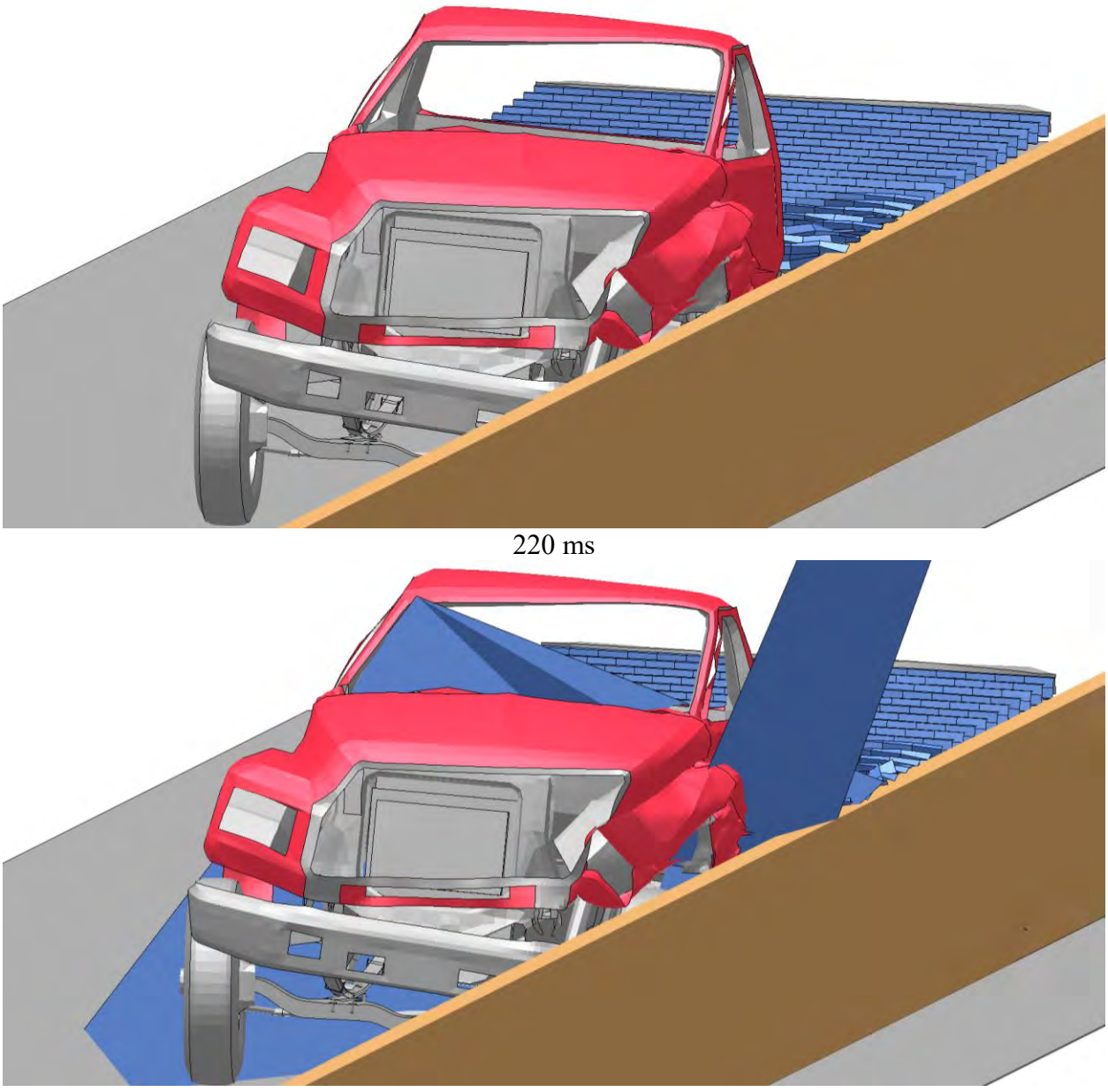

220 ms

230 ms

Figure E-2. Initial SUT Model Node and Element Snagging and Cross Member Distortion

To improve the kinematic reaction of the cargo box assembly and decrease potential for instability, an updated cargo box model developed by Chuck Plaxico (NHTSA n.d.) was implemented in the model, shown in Figure E-3. This model better represented the structure, contacts, and assembly of SUT cargo boxes and could provide better ZOI results at tall barrier heights where major box-barrier interactions occurred. The updated box had a finer mesh and a component covering bed cross members similar to real cargo boxes. When the box was connected to the truck, additional plates were added between the bed and frame rails to replicate what is done in vehicle preparation for full-scale crash testing.

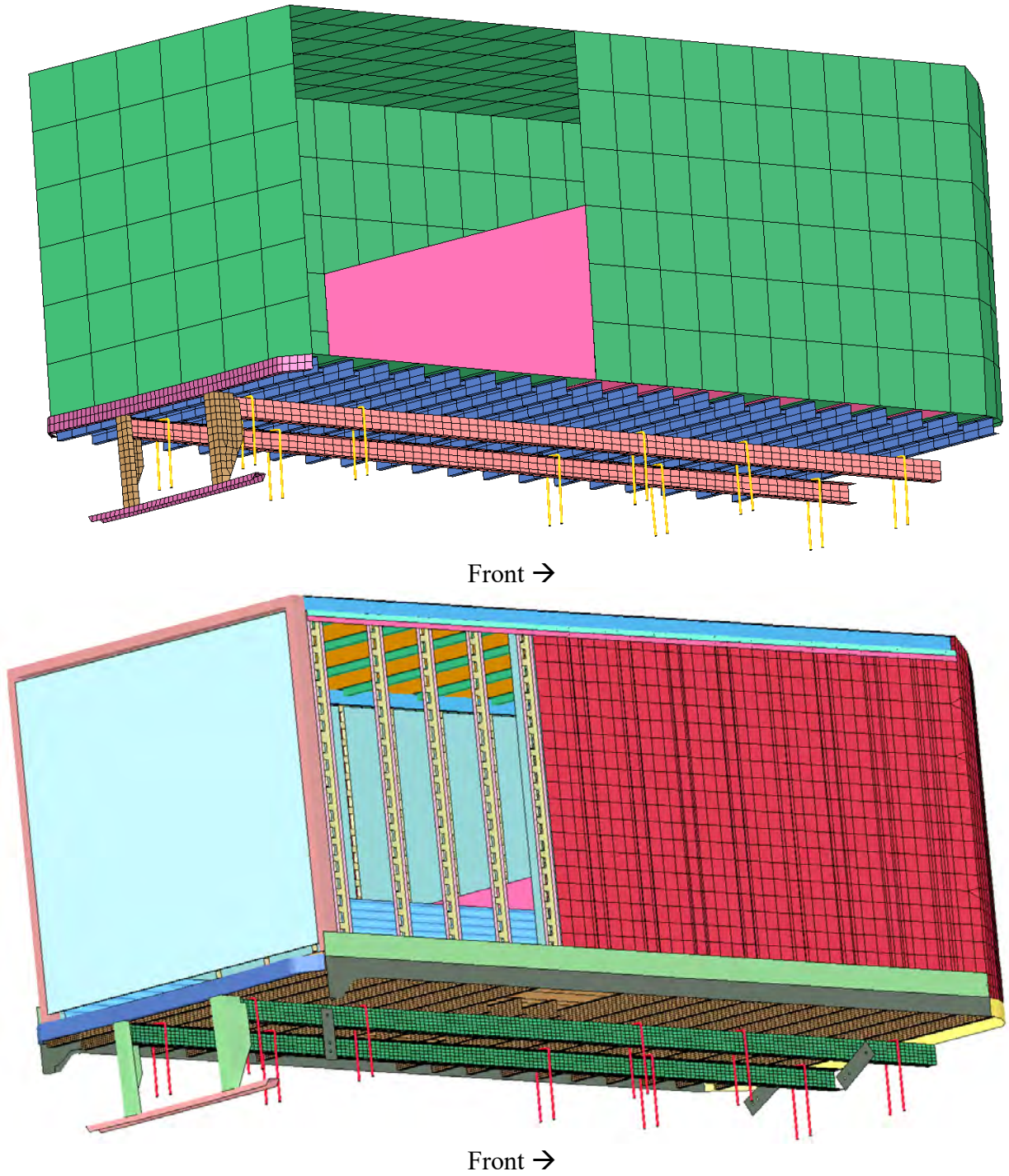


Figure E-3. Original (top) and Plaxico Updated Cargo Box (NHTSA n.d.)

Model stability improved significantly with the updated cargo box. To validate vehicle behavior with the new model, simulations were compared to full-scale test nos. 4CBR-1 (Rosenbaugh et al. 2021) and 4200-20-9b (Sheikh, Bligh, and Menges 2011), conducted on 36-in. tall single-slope, 36-in. tall vertical, and a 42-in. tall single-slope barriers, respectively. However, for barrier heights of 42 in., the simulated truck model did not properly represent the ZOI and the impact-side bottom

edge of the truck was captured by. Note this dimension was not recorded in full-scale crash testing documentation and was determined through video analysis, as shown in Figure E-4. Researchers measured the box height of an un-ballasted SUT at MwRSF's test facility, noting box height typically reduced by ¼ -in. when ballast was installed. The front and rear box corners were 41¾ and 44¼ in. above ground, respectively; both corners on the simulated vehicle were $41\frac{5}{16}$ in. above ground. Therefore, the simulated box was lifted 3 in., expected to provide more conservative ZOI values. Note the simulated box was not pitched forward as it was on the measured vehicle. Lifting the box slightly improved simulation ZOI accuracy.

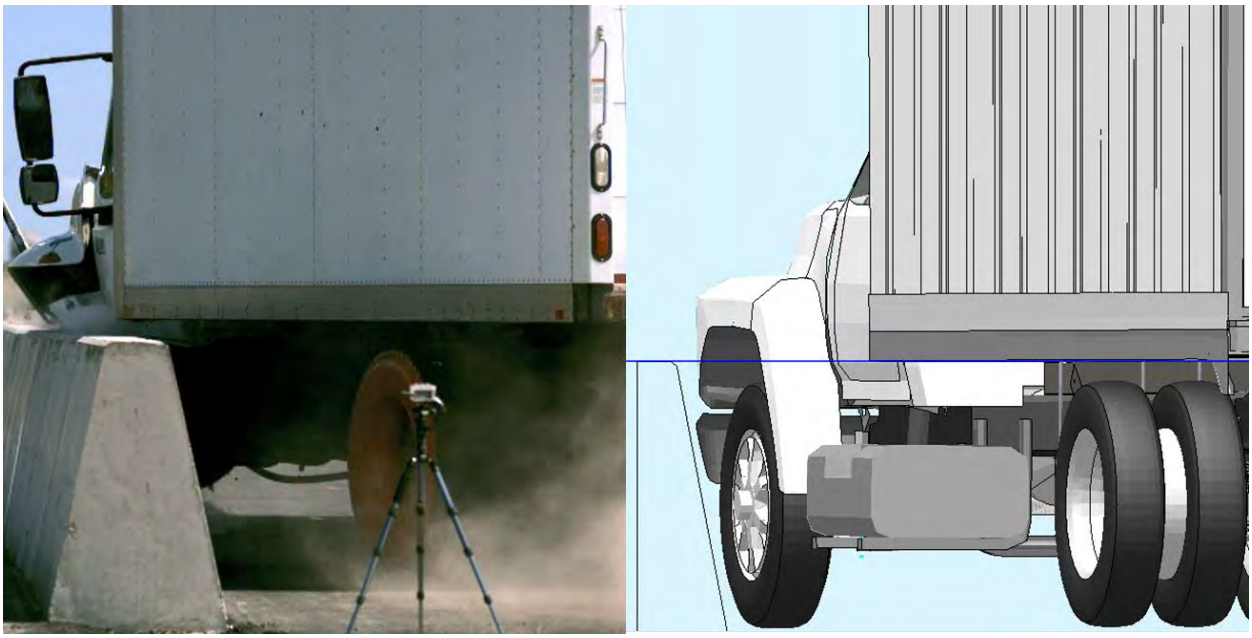

Figure E-4. Box Height Comparison, Test No. 469467-3-1 (Bligh, Menges, and Kuhn 2018) and Updated Box Model (NHTSA n.d.)

### E-3.2 U-bolts

Capturing initial impact behavior is critical as it affects the vehicle's kinematic behavior thereafter. In previous studies, the SUT model was modified to not allow axle rotation, which resulted in significant front axle plastic deformation when used in a high-severity rigid barrier impact, as shown in Figure E-5. This degree of axle deformation was not observed in crash testing; instead, U-bolts or other connections fail and allow axle rotation. The lack of axle rotation and increased axle stiffness restricted the simulated vehicle's encroachment over the barrier.

To correct this, spot-weld connections between leaf springs were set to fail at a specified time, allowing the axle to rotate freely. However, the removal of this connection revealed the contact between beam elements against the shell edge did not function, and the front axle detached shortly after impact. To resolve this issue, CNRB connections were used between beam and shell nodes, as shown in Figure E-6. The U-bolt beams and surrounding shell elements were defined with failure criteria that allowed axle rotation at times similar to full-scale crash testing. Ultimately, the SUT model's ability to achieve ZOI values in simulations at the 36-in. barrier heights was moderately improved, with no change in accuracy at 42-in. barrier heights.

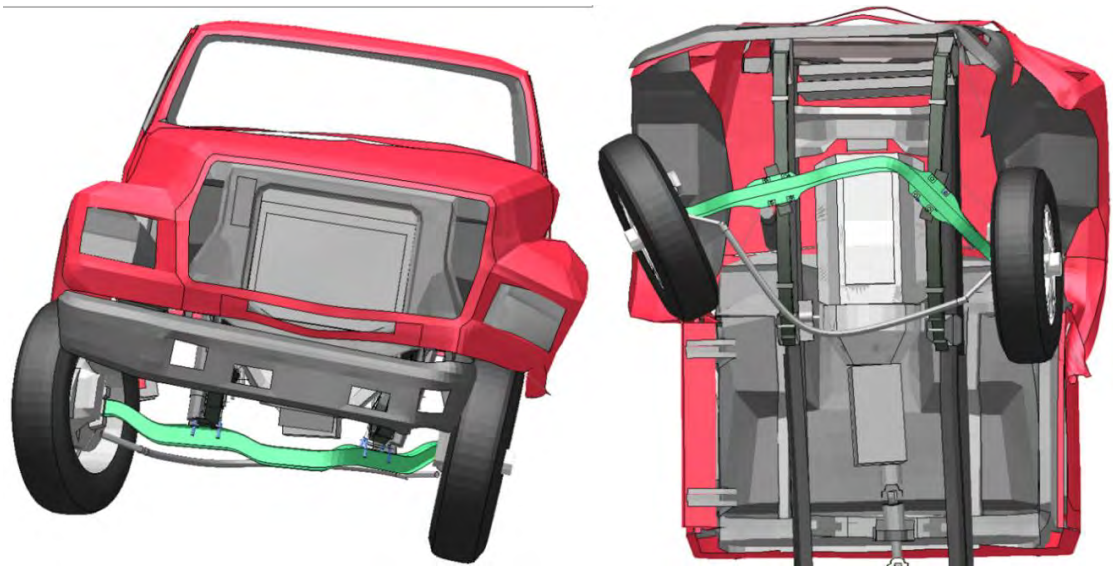

Figure E-5. SUT Model Axle Bending

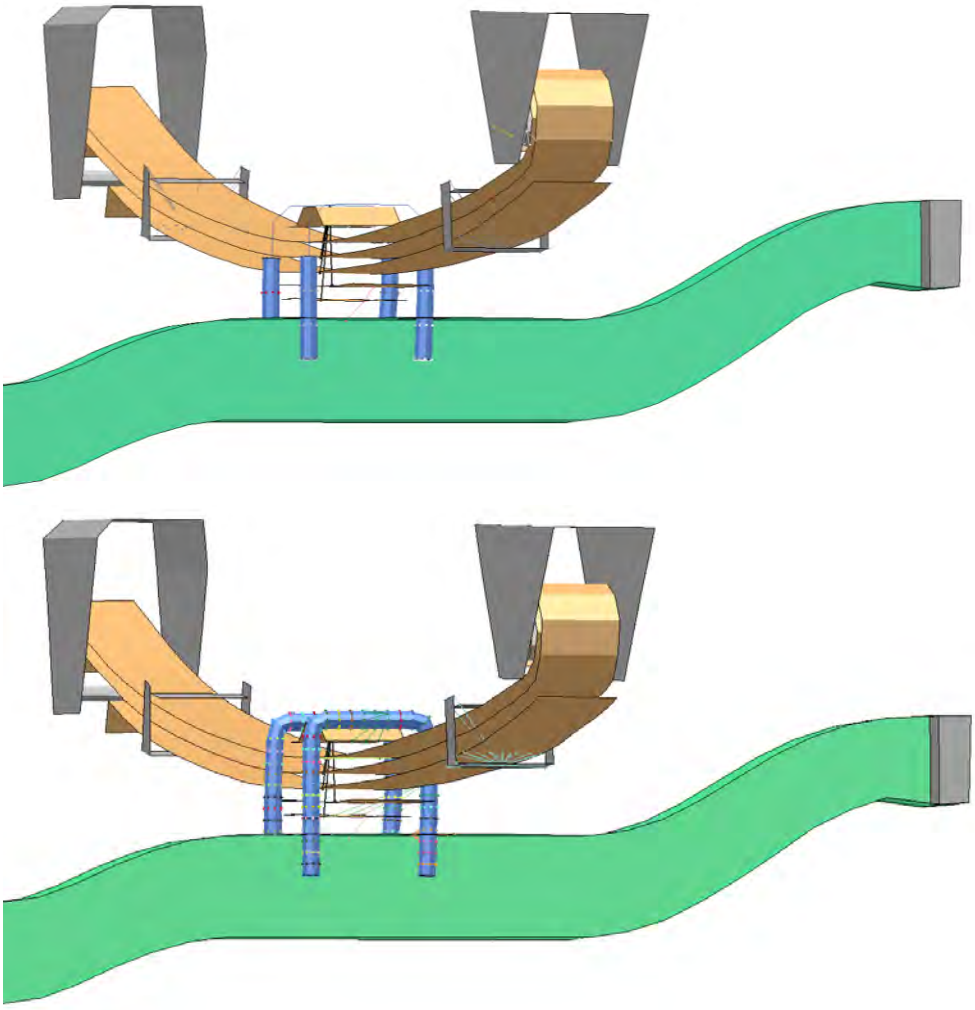

Figure E-6. SUT Model Original (top) and Updated U-bolts

### E-3.3 Cab-barrier Interaction

The encroachment of the vehicle over the barrier was limited by the SUT's gas tank. The gas tank model is very coarse, as shown in Figure 148, and affected encroachment by preventing axle rotation and by interacting with the barrier limited front-end crush. Therefore, the gas tank was removed since full-scale crash testing does not require an impact-side gas tank.

This significantly improved ZOI accuracy but also yielded model terminations. Since vehicle encroachment over the barrier increased, parts of the cab with a coarse mesh, as shown in Figure E-7, were interacting with the barrier. The first notable issues were snagging of cab nodes on the barrier and cab part-to-part snagging, both aggravated by coarse cab components. Automatic cab-to-barrier and cab-to-cab contact were defined with SOFT=2; it was believed truck self-contact was previously defined with SOFT=1 due to initial penetrations. Coarse cab components also generated out-of-range forces and subsequent error terminations. Re-meshing these coarse components would require additional modifications which could not be performed due to time constraints. Instead, the vehicle was repositioned for passenger-side impacts, since this side had additional components that limit cab-to-barrier interaction. This did not completely resolve model instability but reduced the frequency of error terminations.

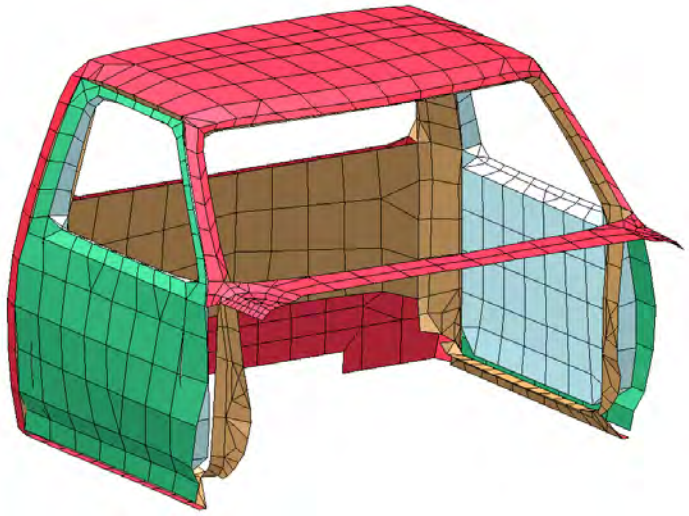

Figure E-7. SUT Model Cab Components with Coarse Mesh Density

## E-4 Friction Selection

Test no. 420020-9b (Sheikh, Bligh, and Menges 2011) was used for friction selection as it included a concrete barrier with a flat, continuous surface. Ridedown velocity plots, shown in Figure E-8, were studied to select friction values. Timing of key event occurrences, shown in Table E-1, was also considered when selecting friction values.

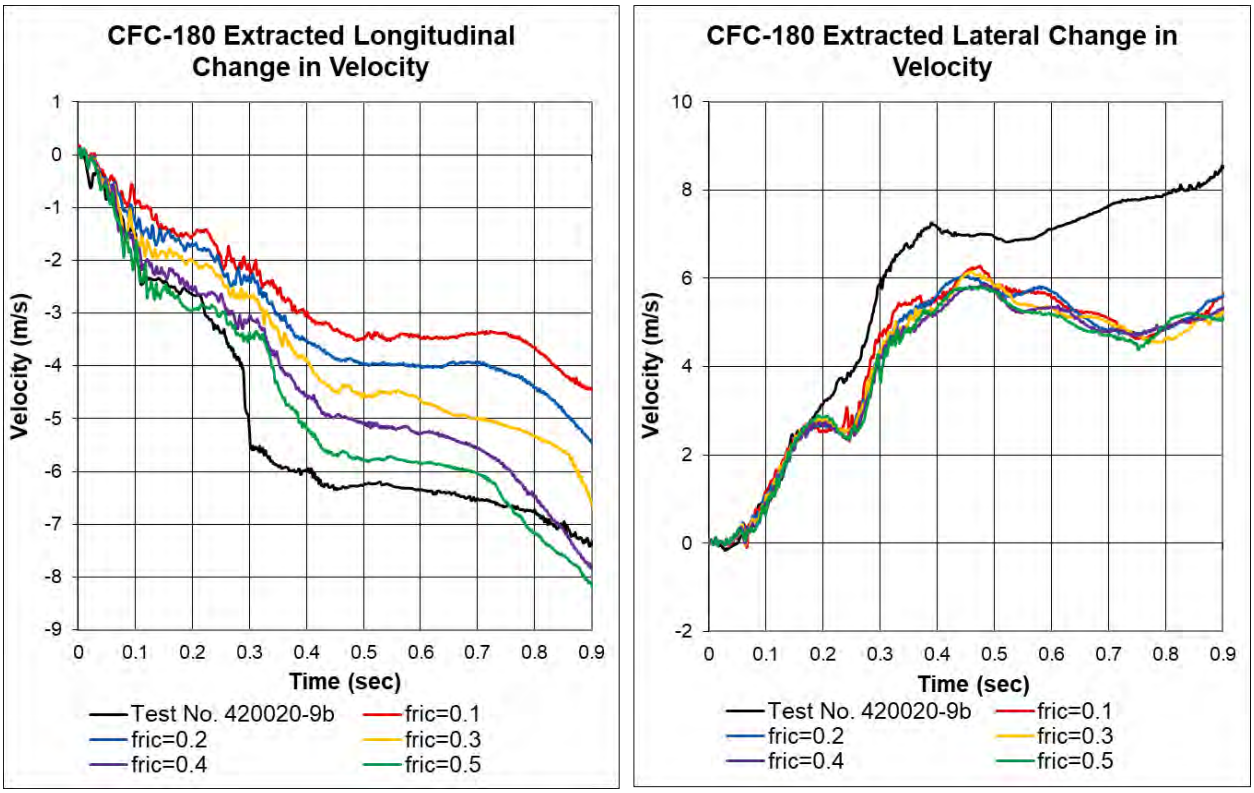


Figure E-8. Velocity Analysis for Varied Vehicle-barrier Friction

Tire-barrier friction was set to 0.4 during this friction study. Vehicle-barrier static and dynamic friction levels ranged from 0.1 to 0.5 with 0.1 increments. Increased friction produced better agreement between longitudinal velocity changes; reduced friction produced better agreement between lateral velocity changes. Although the model with vehicle-barrier friction set to 0.5 was most comparable to test no. 420020-9b in terms of longitudinal velocity change, it was least comparable in terms of maximum lateral extent. Maximum lateral extent was the most crucial parameter and therefore, vehicle-barrier friction of 0.4 was used in model validation.

Table E-1. Key Events with Varying Friction, Test No. 420020-9b (Sheikh, Bligh, and Menges 2011) and Simulation

| Event | Test No. 420020-9b | Simulated friction values | | | | |
|---|---|---|---|---|---|---|
| | | 0.1 | 0.2 | 0.3 | 0.4 | 0.5 |
| ZOI (in.) | 62.5 | 56.3 | 56.5 | 56.6 | 54.5 | 51.6 |
| ZOI relative difference (%) | - | 10.0 | 9.6 | 9.5 | 12.8 | 17.4 |
| Parallel time (ms) | 264 | 260 | 260 | 260 | 260 | 260 |
| Maximum ZOI time (ms) | 840 | 830 | 810 | 810 | 810 | 830 |

## E-5 Validation to Test No. 4CBR-1

### E-5.1 Test Setup

In MASH TL-4 full-scale crash test no. 4CBR-1 (Rosenbaugh et al. 2021), a 22,198-lb 2005 International 4300 impacted a 2.9 degree, 36-in. tall single-slope barrier at 57.6 mph and a 16.0-degree angle. In simulation, a 21,768-lb 1996 Ford F800 impacted a 2.9 degree, 36-in. tall single-slope barrier at 57.6 mph and a 16.0-degree angle. Test vehicle and simulation model dimensions and impact points are compared in Figure E-9. Test vehicle dimensions and simulated vehicle properties are compared in Figure E-10.

Figure E-9. Test No. 4CBR-1 (Rosenbaugh et al. 2021) and Simulation Vehicles

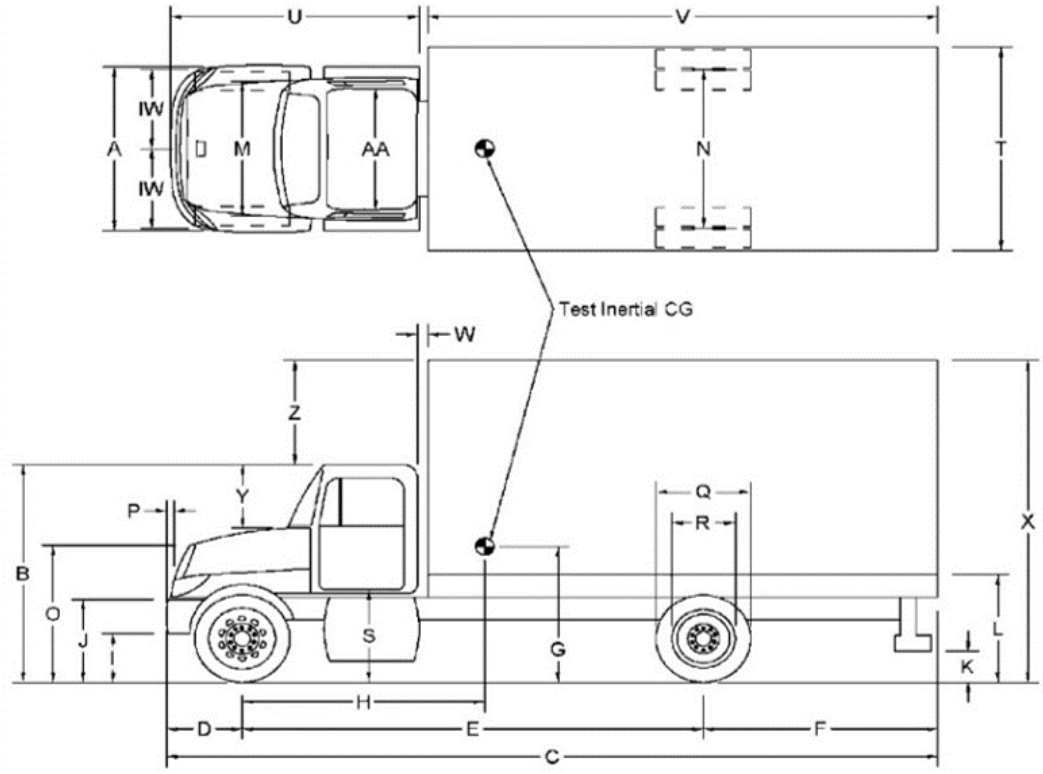


| Dimension (in.) | Test no. 4CBR-1 | FEA | Difference (%) |
|---|---|---|---|
| A | 92.5 | 93.1 | -0.6 |
| B | 98.9 | 87.9 | 11.1 |
| C | 334.0 | 338.0 | -1.2 |
| D | 82.5 | 90.2 | -9.3 |
| E | 229.5 | 208.2 | 9.3 |
| F | 41.0 | 34.0 | 17.2 |
| G | 50.6 | 51.5 | -1.8 |
| H | 140.5 | 133.5 | 5.0 |
| I | 20.8 | 20.3 | 2.4 |
| J | 35.3 | 33.0 | 6.4 |
| K | 23.0 | 18.3 | 20.3 |
| L | 48.5 | 50.3 | -3.8 |
| M | 79.8 | 80.6 | -1.0 |
| N | 72.8 | 72.4 | 0.5 |
| O | 59.0 | 62.5 | -6.0 |
| P | 1.0 | -0.8 | 177.8 |
| Q | 34.4 | 37.9 | -10.4 |
| R | 23.4 | 23.4 | 0 |
| S | 37.9 | 35.0 | 7.5 |
| T | 69.0 | 96.2 | 39.4 |

| Dimension (in.) | Test no. 4CBR-1 | FEA | Difference (%) |
|---|---|---|---|
| U | 106.8 | 102.6 | 3.9 |
| V | 223.0 | 226.4 | -1.5 |
| W | 4.0 | 3.3 | 18.3 |
| X | 146.1 | 134.1 | 8.2 |
| Y | 30.1 | 20.0 | 33.6 |
| Z | 47.5 | 46.3 | 2.6 |
| AA | 71.4 | 58.8 | 17.6 |
| Ballast height | 63.5 | 64.7 | -2.0 |
| | | | |
| **Weight (lb)** | | | |
| Test inertial | 22,198 | 21,768 | 1.9 |
| Ballast | 7,927 | 9,411 | -18.7 |
| | | | |
| **Accelerometer location (in.)** | | | |
| Longitudinal[1] | 142 | 142.3 | -0.2 |
| Lateral[2] | 0 | -0.6 | - |
| Above ground | 38 | 38.0 | 0 |
| [1]From front axle, positive rearward | | | |
| [2]From centerline, positive to passenger side | | | |

Figure E-10. Test No. 4CBR-1 (Rosenbaugh et al. 2021) Test Vehicle-Simulation Comparison

### E-5.2 ZOI and Key Events

The point of maximum intrusion during simulation is compared to the equivalent time step in test no. 4CBR-1 in Figure E-11. ZOI measurement from the test and simulation had a 12.6 percent relative difference. The model's ability to capture the ZOI from full-scale crash testing was deemed acceptable. Key events are summarized in Table E-2.

Figure E-11. Maximum Lateral Extent during Test No. 4CBR-1 (Rosenbaugh et al. 2021) and Simulation

Table E-2. Key Events Comparison, Test No. 4CBR-1 (Rosenbaugh et al. 2021) and Simulation

| Event | Test | FEA |
|---|---|---|
| ZOI measurement (in.) | 55.4 | 62.4 |
| ZOI time (ms) | 827 | 840 |
| Parallel time (ms) | 296 | 300 |

### E-5.3 Sequentials

Sequential Images of test no. 4CBR-1 and the simulation are compared in Figures E-12 through E-14. The basic kinematic response and sequence and timing of key events were generally comparable between the simulation and test no. 4CBR-1.

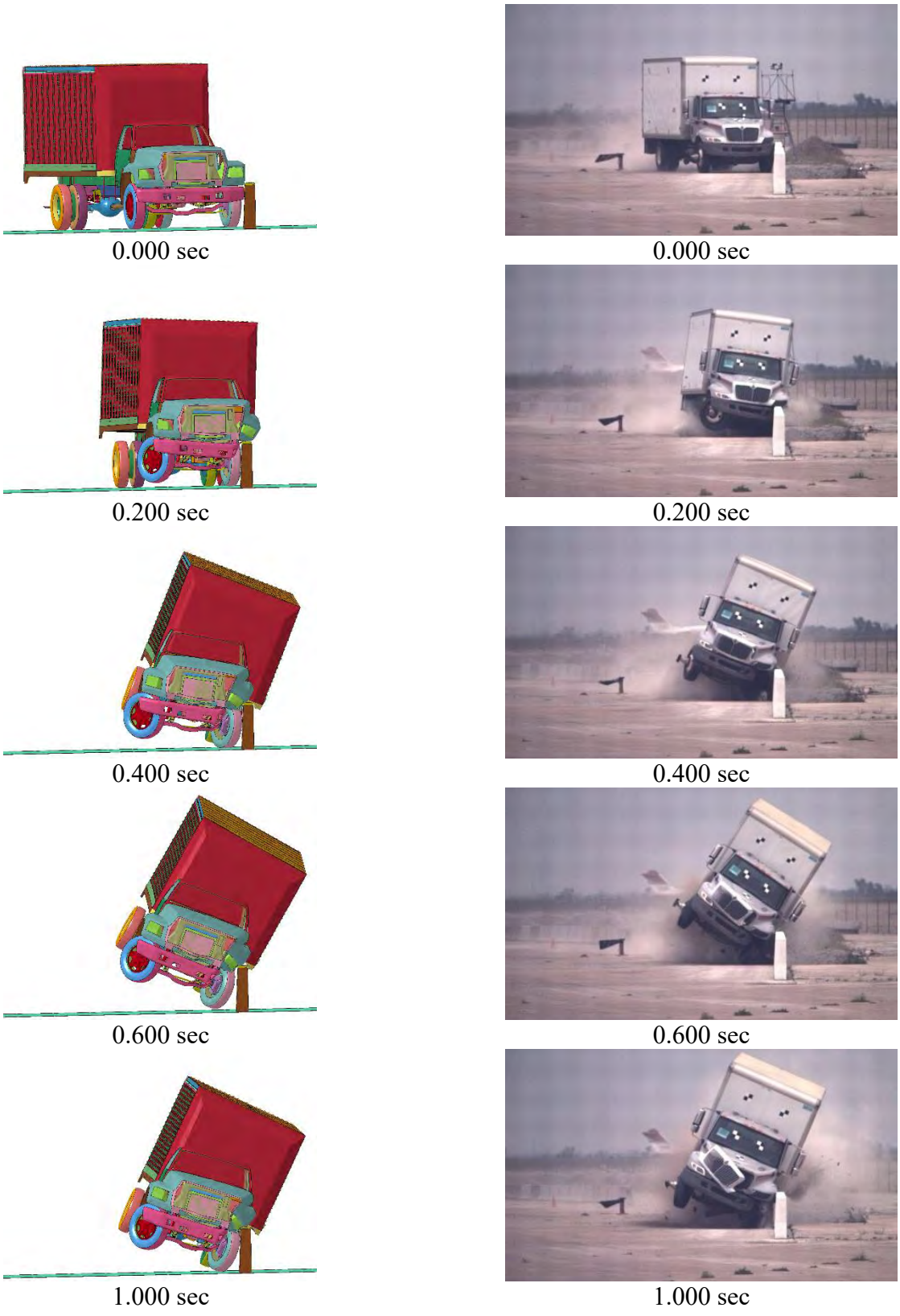


Figure E-12. Test No. 4CBR-1 (Rosenbaugh et al. 2021) and Simulation Downstream Sequential Images

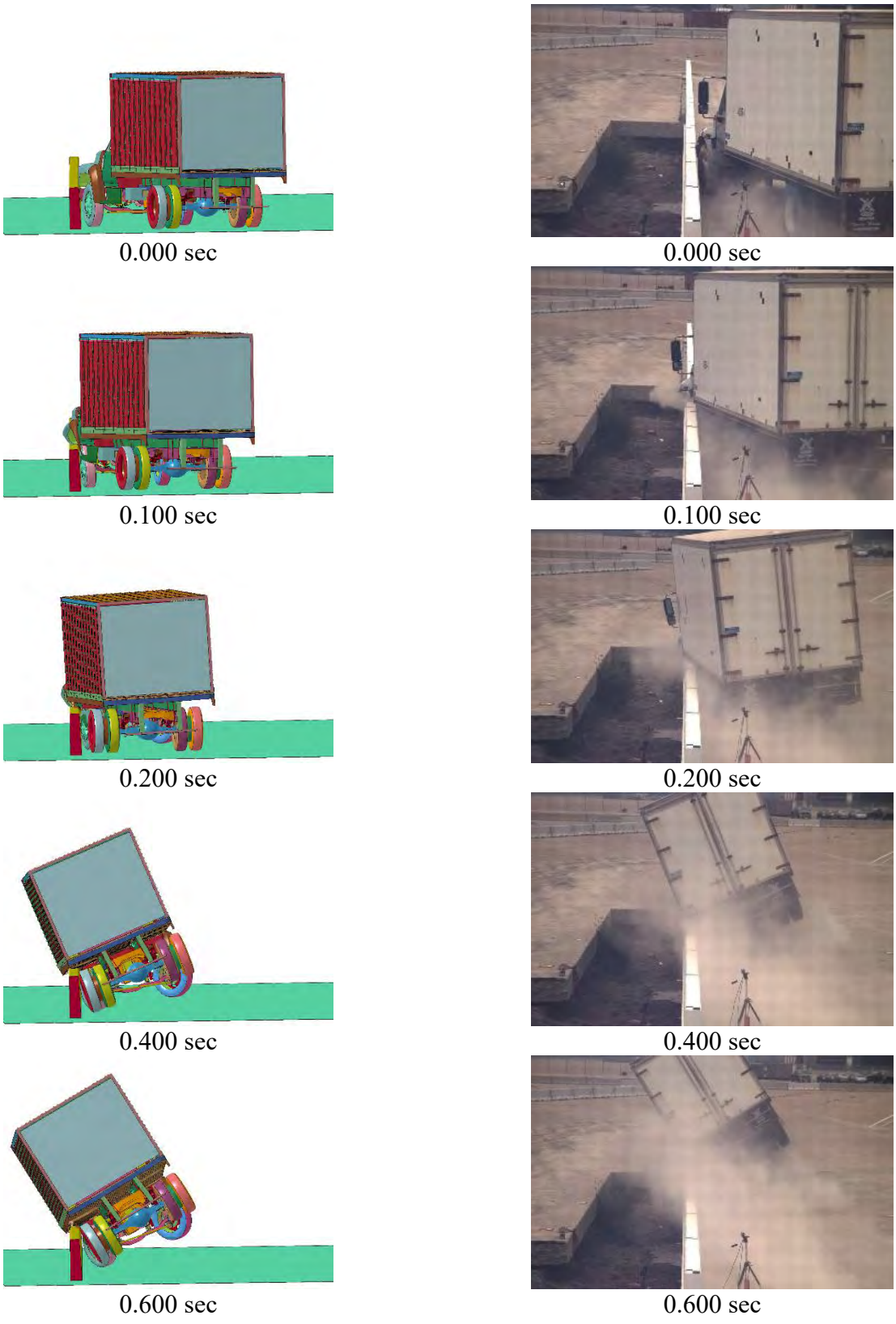


Figure E-13. Test No. 4CBR-1 (Rosenbaugh et al. 2021) and Simulation Upstream Sequential Images

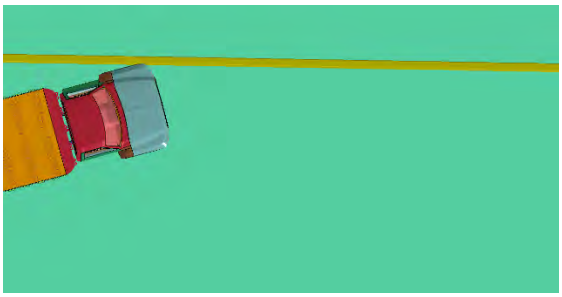

0.000 sec

0.000 sec

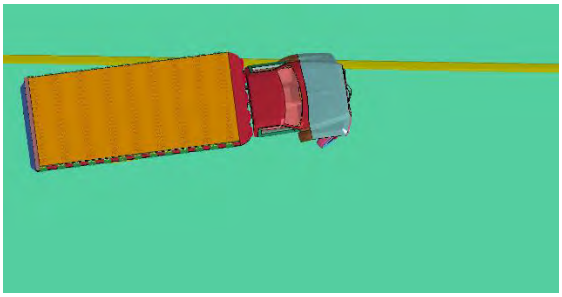

0.200 sec

0.200 sec

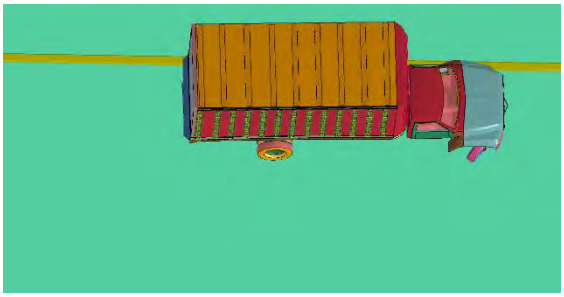

0.400 sec

0.400 sec

0.600 sec

0.600 sec

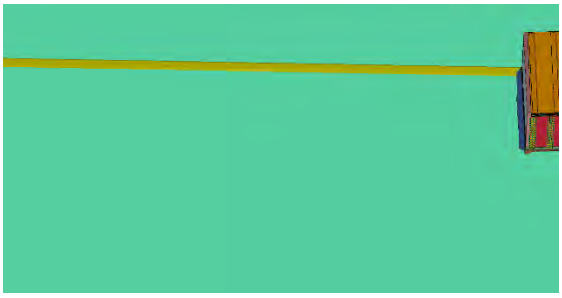

1.000 sec

1.000 sec

Figure E-14. Test No. 4CBR-1 (Rosenbaugh et al. 2021) and Simulation Overhead Sequential Images

## E-5.4 Time-dependent data

To validate overall dynamic performance of the crash test and simulation, acceleration, velocity, and displacements were compared, as shown in Figures E-15 through E-17. Accelerations were comparable, providing high confidence in the validation of the vehicle's dynamic ridedown performance.

Euler angles are compared in Figure E-18; pitch was slightly higher, and roll behavior was slightly lower in the test, primarily attributed to difficulties modeling front axle disengagement. The model's front axle slid back longidtuinally 10 ms after impact, causing pitch and subsequently resisting the vehicle's roll toward the barrier. This also reduced front suspension resistance and limited lateral loading, producing roll about the vehicle's longitudinal axis. The pitch could be affected by the tire, which was not deformed significantly in full-scale crash testing, wedging against the bottom of the cab model and producing lift. Front-end components, which cannot fail, contacting and riding up the barrier may also contribute to pitch.

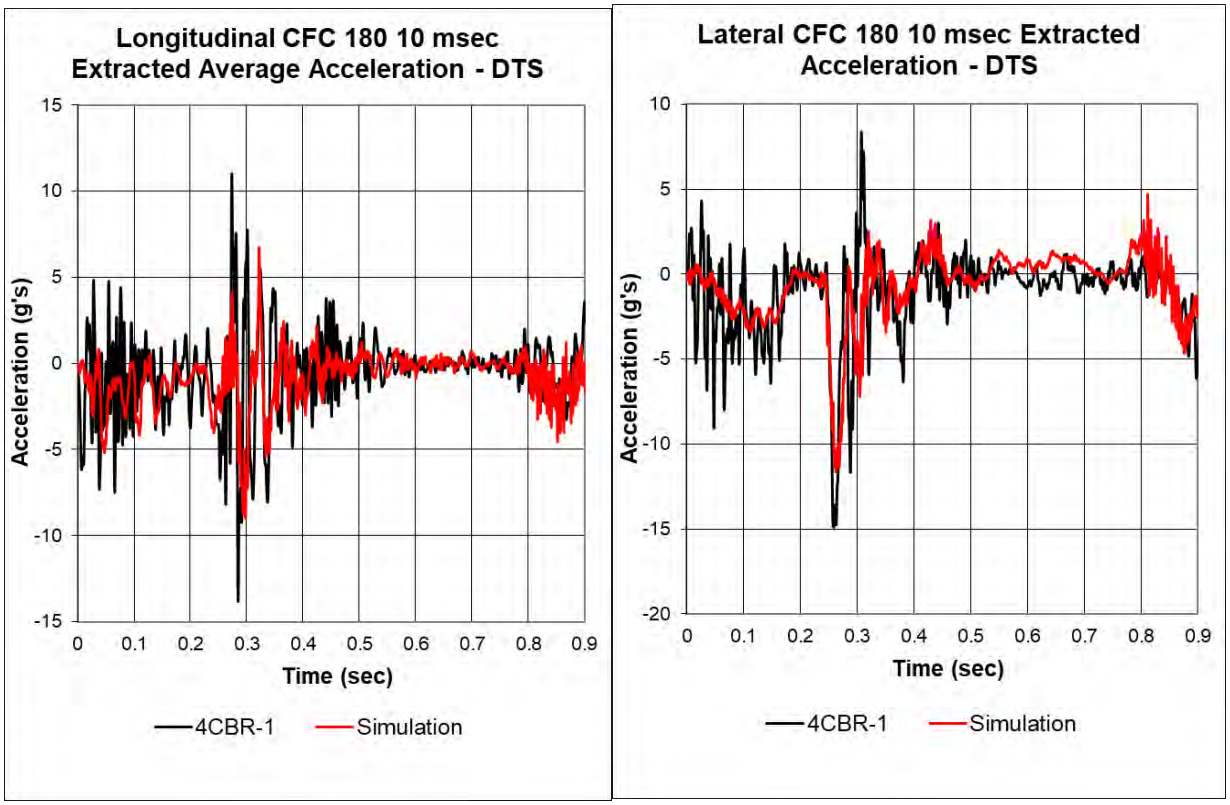


Figure E-15. Test No. 4CBR-1 (Rosenbaugh et al. 2021) and Simulation Acceleration

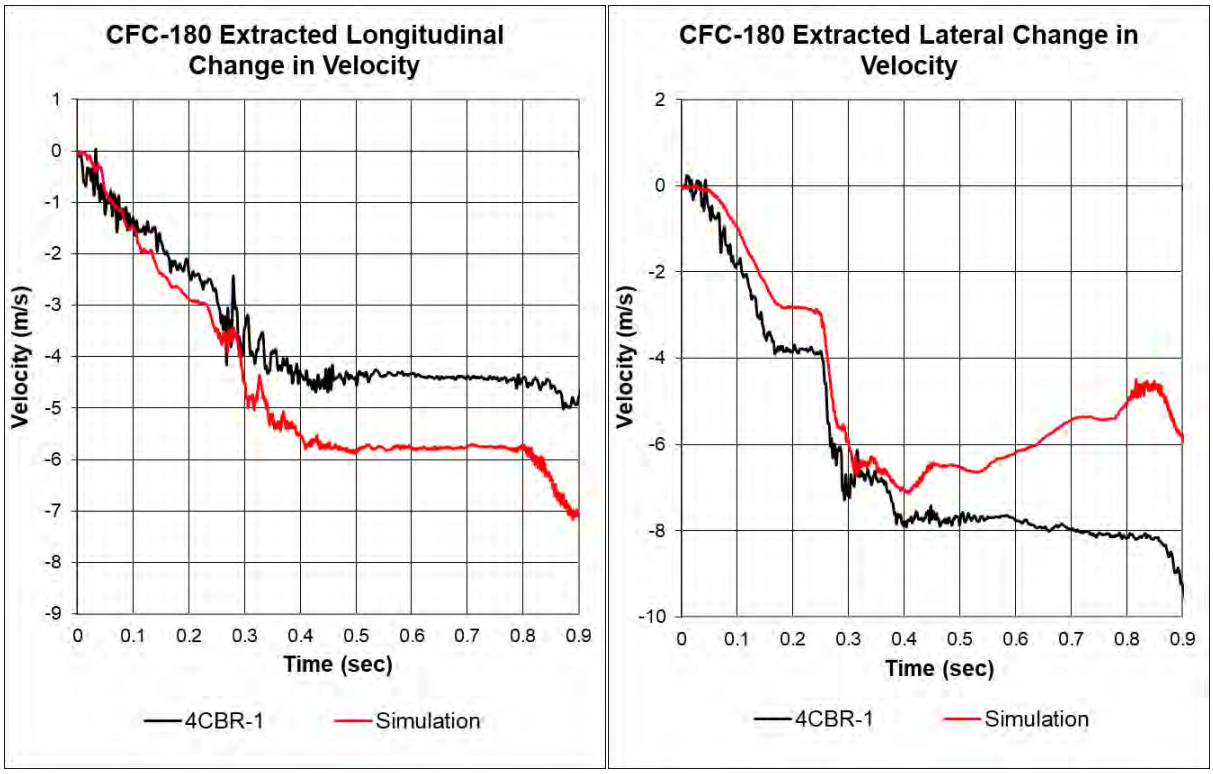


Figure E-16. Test No. 4CBR-1 (Rosenbaugh et al. 2021) and Simulation Velocity

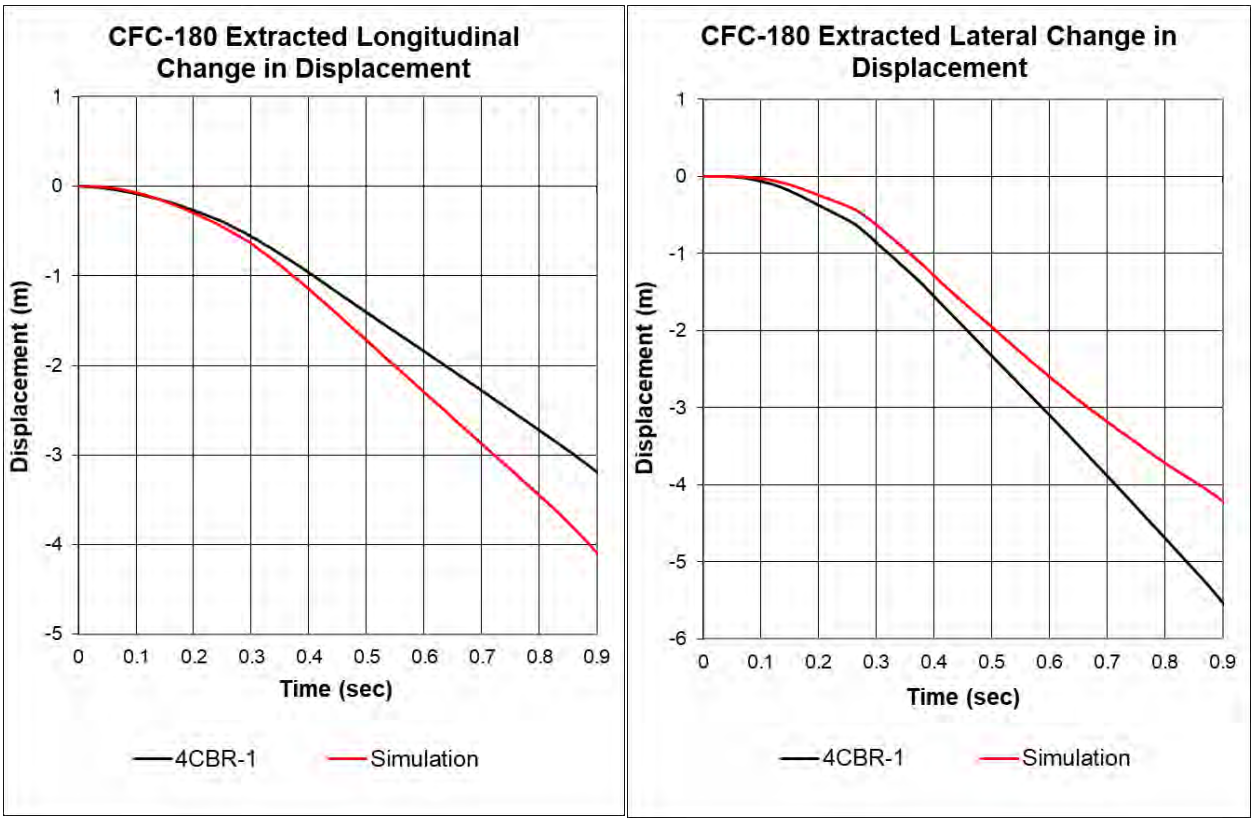


Figure E-17. Test No. 4CBR-1 (Rosenbaugh et al. 2021) and Simulation Displacement

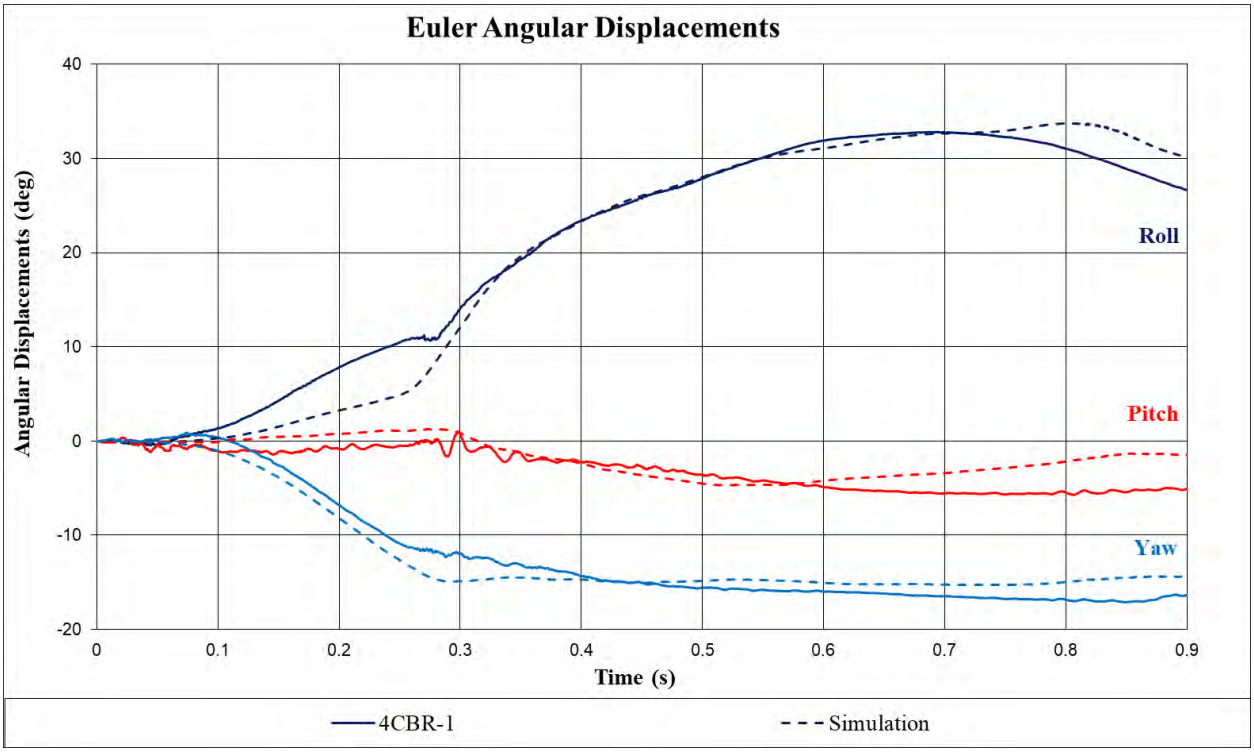


Figure E-18. Test No. 4CBR-1 (Rosenbaugh et al. 2021) and Simulation Euler Angles

### E-5.5 Solution Verification

To determine if the analysis produced a numerically stable result, global verification based on V&V criteria was performed and is summarized in Table E-3. The criteria of the part/material energy did not pass because of high hourglass energy. Parts with high changes in energy were the wheel wells and a box attached to the frame rail that did not contact the barrier or other components. These parts were deemed non-critical for energy absorption as they did not have a significant effect on the vehicle's kinematic response. Thus, they were excluded from evaluation criteria.

Additionally, total energy variation criteria did not pass V&V requirements. The system's kinetic energy spiked at the same time as U-bolt failure; to verify these were related, an additional model was run without U-bolt failure definition. Energy balance results, shown in Figures E-19 and E-20, verified the energy spike was related to U-bolt failure behavior and did not affect vehicle response during the simulation. To maximize potential for vehicle front-end engagement with the barrier, validation continued with U-bolt failure defined.

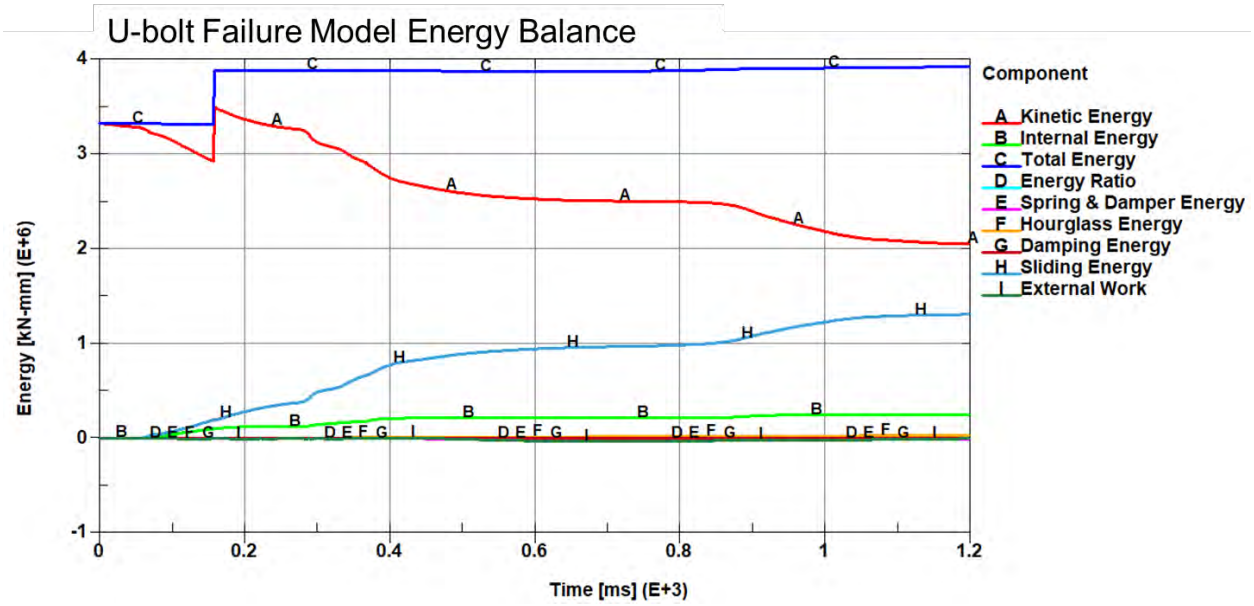


Figure E-19. Test No. 4CBR-1 Simulation Energy Balance with U-bolt Failure

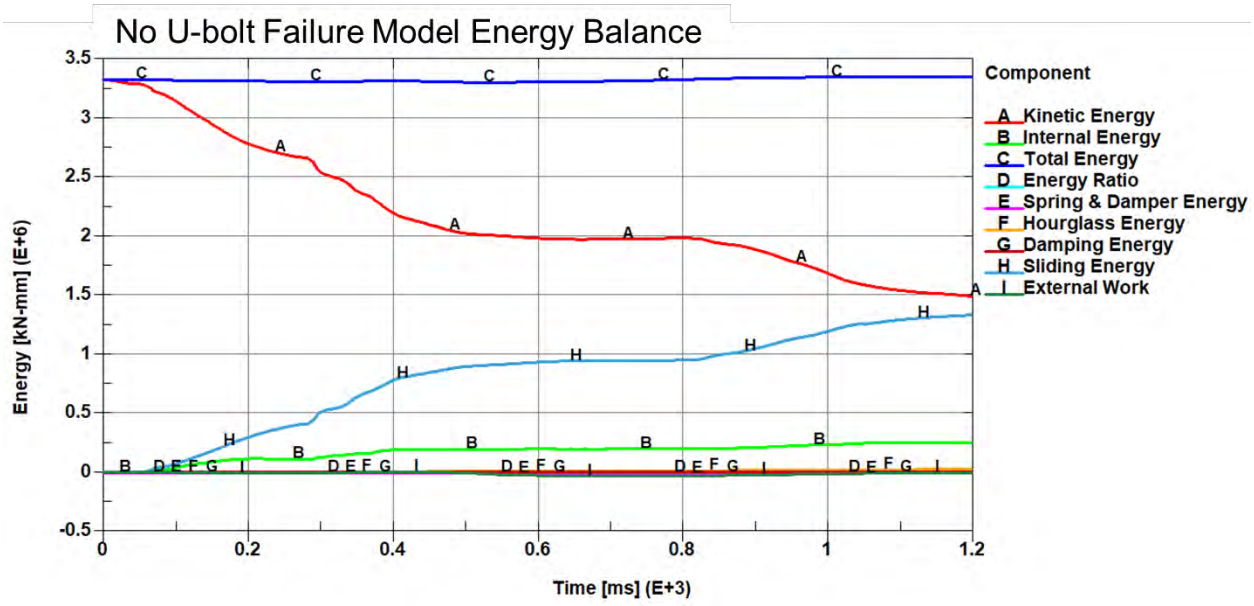


Figure E-20. Test No. 4CBR-1 Simulation Energy Balance without U-bolt Failure

Table E-3. Test No. 4CBR-1 Simulation Solution Verification

| Verification evaluation criteria | Change (%) | Pass? |
|---|---|---|
| ***Total energy*** of the simulation must not vary more than 10 percent from the beginning of the run to the end of the run | 15.6 | N |
| ***Hourglass energy*** at the end of the run is less than 5 percent of the total initial energy at the beginning of the run | 1.0 | Y |
| ***Hourglass energy*** at the end of the run is less than 10 percent of the total internal energy at the end of the run | 12.9 | N |
| The part/material with the most hourglass energy at the end of the run is less than 10 percent of the total internal energy of the part/material at the end of the run | 288.2 | N |
| Mass added to the total model is less than 5 percent of the total model mass at the beginning of the run | 0.0 | Y |
| The part/material with the most mass added had less than 10 percent of its initial mass added | 1.1 | Y |
| The moving parts/materials in the model have less than 5 percent of mass added to the initial moving mass of the model | 0.0 | Y |
| No shooting nodes in the solution | No | Y |
| No solid elements with negative volumes | No | Y |

### E-5.6 Time-history Validation

The TL-4 curves were evaluated over the approximately 0.9-s impact event. The default metric evaluation options in RSVVP were used, which included the Sprague & Geers and the ANOVA metrics. The default acceptance criteria for these metrics are 40% for the Sprague-Geers metrics, 5% for the ANOVA mean, and 35% for the ANOVA standard deviation of residuals. These acceptance criteria are based on comparison of repeated full-scale crash tests involving a small car impacting a rigid barrier (i.e., uni-body vehicle impact with short impact duration) and are likely too strict for this application, which involves a multi-body vehicle and a relatively long impact event. For this assessment, the V&V criteria were used to determine validity, while Sprague-Geers values less than or equal to 55 and standard deviation values less than or equal to 50 were deemed "borderline" acceptable.

#### E-5.6.1 Single-channel Assessment

Sprague-Geers and ANOVA metrics are shown in Table E-4 for x-, y-, and z- acceleration and yaw, roll, and pitch channels using RSVVP. Based on Sprague-Geers metrics, a comparison of the individual acceleration components indicated the simulation was in good agreement with the test for yaw and roll. The accelerations and pitch were in poor agreement with the test. ANOVA metrics indicated the mean residual error and standard deviation of the mean residual error were in agreement with the test for each metric.

Table E-4. Single-channel Time-history Comparison of Test No. 4CBR-1 (Rosenbaugh et al. 2021) and Simulation

| **Evaluation criteria (time interval [0 , 0.9444 s])** | | | | | | | | |
|---|---|---|---|---|---|---|---|---|
| O | ***Sprague-Geers***<br>Values less than or equal to 40 are acceptable | | | | | | | |
| | **Filter: CFC180<br>Sync.: None** | **RSVVP curve preprocessing** | | | | **M** | **P** | **Pass?** |
| | | **Shift** | | **Drift** | | | | |
| | | **True** | **Test** | **True** | **Test** | | | |
| | X-acceleration | **N** | N | **N** | N | -19.2 | 51 | B |
| | Y-acceleration | **N** | N | **N** | N | -5.2 | 46.2 | B |
| | Z-acceleration | **N** | N | **N** | N | -14.9 | 50.5 | B |
| | Roll | N | N | N | N | -6.6 | 39.4 | Y |
| | Pitch | N | N | N | N | -44.6 | 48.8 | B |
| | Yaw | N | N | N | N | -11.9 | 36.3 | Y |
| P | ***ANOVA***<br>Both criteria must be met:<br>• Mean residual error must be less than 5 percent of peak acceleration ($\bar{e} \le 0.05 \cdot a_{Peak}$)<br>• Standard deviation of the residuals must be less than 35 percent of peak acceleration ($\sigma \le 0.35 \cdot a_{Peak}$) | | | | | **Mean residual** | **Standard deviation of residuals** | **Pass?** |
| | X-acceleration (peak) | | | | | -0.3 | 14.1 | Y |
| | Y-acceleration (peak) | | | | | -0.6 | 16.6 | Y |
| | Z-acceleration (peak) | | | | | -0.6 | 17.6 | Y |
| | Roll | | | | | -0.3 | 8.5 | Y |
| | Pitch | | | | | 0.4 | 8 | Y |
| | Yaw | | | | | 0.1 | 6.9 | Y |

### E-5.6.2 Multi-channel Assessment

Since the individual data metrics did not satisfy all acceptance criteria, the multi-channel option in RSVVP was used to calculate weighted Sprague-Geer and ANOVA metrics for the six data channels, as shown in Table E-5. The resulting weight factors computed for each channel indicated the x-acceleration, y-acceleration, roll, and yaw controlled the kinematic behavior of the impact event. The velocity change in the z-direction was not as significant as the x- and y-directions, and pitch was less than roll and yaw. The weighted RSVVP metrics in the multi-channel mode did not all satisfy the acceptance criteria, and therefore the time-history comparison did not pass V&V criteria. However, this criteria was likely too strict for heavy-vehicle model validation, and the model passed the "borderline" acceptance criteria.

Table E-5. Multi-channel Time-history Comparison of Test No. 4CBR-1 (Rosenbaugh et al. 2021) and Simulation

| Evaluation criteria (time interval [0 , 0.9444 s]) | | | | |
|---|---|---|---|---|
| **Multi-channel weights:** Area II method | X-acceleration: 0.1490<br>Y-acceleration: 0.2686<br>Z-acceleration: 0.0824 | Yaw: 0.1470<br>Roll: 0.2687<br>Pitch: 0.0843 | | |
| O | ***Sprague-Geers***<br>Values less or equal to 40 are acceptable | **M** | **P** | **Pass?** |
| | | 19.2 | 51 | B |
| P | ***ANOVA***<br>Both criteria must be met:<br>• Mean residual error must be less than 5 percent of peak acceleration ($\bar{e} \le 0.05 \cdot a_{Peak}$)<br>• Standard deviation of the residuals must be less than 35 percent of peak acceleration ($\sigma \le 0.35 \cdot a_{Peak}$) | **Mean residual** | **Standard deviation of residuals** | **Pass?** |
| | | -0.29 | 14.12 | Y |

## E-6 Validation to Test No. 420020-9b

### E-6.1 Test Setup

In MASH TL-4 full-scale crash test no. 420020-9b (Sheikh, Bligh, and Menges 2011), a 22,150-lb 1991 International 4700 impacted a 36-in. tall, 10.9-degree single-slope barrier at 57.2 mph and a 16.1-degree. In simulation, a 21,768-lb 1996 Ford F800 impacted a 36-in. tall, 10.9-degree single-slope barrier at 57.2 mph and a 16.1-degree angle. Test vehicle and simulation model dimensions and impact points are compared in Figure E-21. Test vehicle dimensions and simulated vehicle properties are compared in Figure E-22.

Figure E-21. Test No. 420020-9b (Sheikh, Bligh, and Menges 2011) and Simulation Vehicles

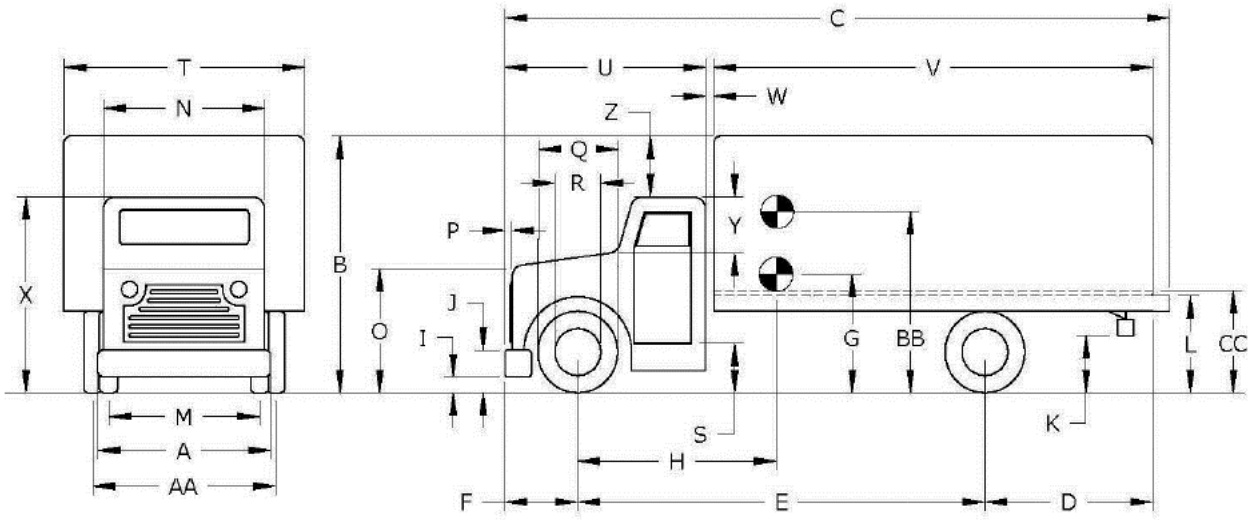


| Dimension (in.) | Test no. 420020-9b | FEA | Difference (%) |
|---|---|---|---|
| A | 95.3 | 93.1 | 2.3 |
| B | 133.0 | 134.1 | -0.8 |
| C | 274.0 | 338.0 | -23.4 |
| D | 56.0 | 90.2 | -61.1 |
| E | 187.5 | 208.2 | -11.0 |
| F | 30.5 | 34.0 | -11.4 |
| G | - | 51.5 | - |
| H | 103.9 | 133.5 | -28.5 |
| I | 19.0 | 20.3 | -6.6 |
| J | 30.5 | 33.0 | -8.2 |
| K | 27.5 | 18.3 | 33.3 |
| L | 48.0 | 41.2 | 14.2 |
| M | 80.5 | 80.6 | -0.1 |
| N | 73.0 | 58.8 | 19.5 |
| O | 61.5 | 62.5 | -1.7 |
| P | 2.0 | -0.8 | 138.9 |
| Q | 39.5 | 38.1 | 3.5 |
| R | 23.5 | 23.4 | 0.4 |
| S | 39.3 | 35.0 | 10.7 |
| T | 95.0 | 96.2 | -1.2 |

| Dimension (in.) | Test no. 420020-9b | FEA | Difference (%) |
|---|---|---|---|
| U | 97.0 | 102.6 | -5.8 |
| V | 173.5 | 226.4 | -30.5 |
| W | 1.0 | 3.3 | -226.7 |
| X | 96.0 | 87.9 | 8.5 |
| Y | 26.5 | 20.0 | 24.6 |
| Z | 33.5 | 46.3 | -38.2 |
| AA | 80.5 | 72.4 | 10.1 |
| Ballast height | - | 64.7 | - |
| **Weight (lb)** | | | |
| Test inertial | 22,150 | 21,768 | 1.7 |
| Ballast | 9,820 | 9,411 | 4.2 |
| **Accelerometer location (in.)** | | | |
| Longitudinal[1] | 109 | 109 | 0 |
| Lateral[2] | 0 | -0.59 | - |
| Above ground | 42 | 42 | 0 |
| [1]From front axle, positive rearward | | | |
| [2]From centerline, positive to passenger side | | | |

Figure E-22. Test No. 420020-9b (Sheikh, Bligh, and Menges 2011) Test Vehicle-simulation Comparison

### E-6.2 ZOI and Key Events

The point of maximum intrusion during simulation is compared to the equivalent time step in test no. 420020-9b in Figure E-23. ZOI measurement from the test and model had an 8.7 percent relative difference. The simulated model's ability to capture the ZOI from full-scale crash testing was deemed acceptable. Key events are summarized in Table E-6.

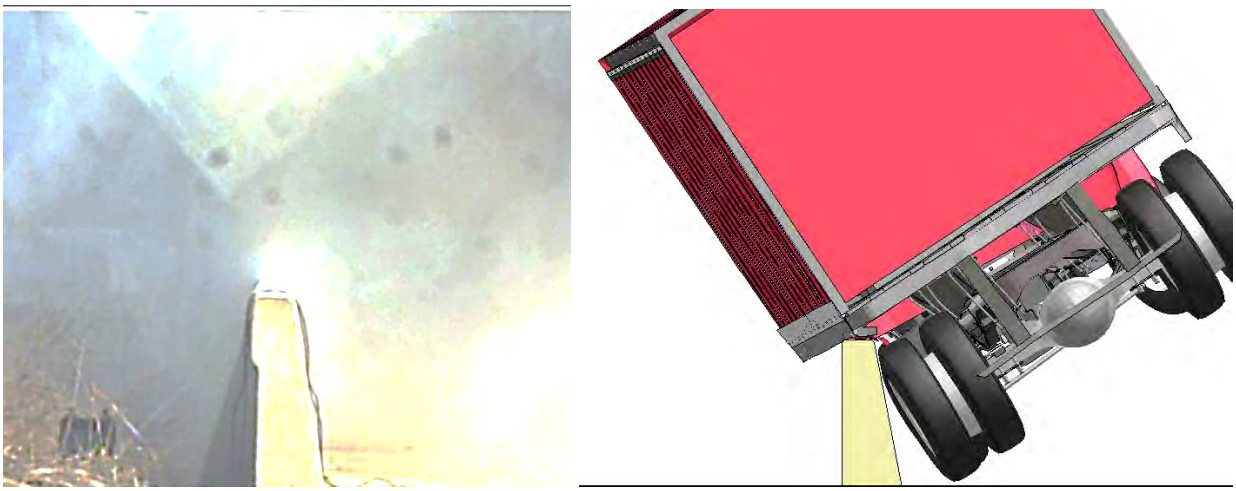

Figure E-23. Maximum Lateral Extent during Test No. 420020-9b (Sheikh, Bligh, and Menges 2011) and Simulation

Table E-6. Key Events Comparison, Test No. 420020-9b (Sheikh, Bligh, and Menges 2011) and Simulation

| Event | Test | FEA |
|---|---|---|
| ZOI measurement (in.) | 62.5 | 67.9 |
| ZOI time (ms) | 840 | 820 |
| Parallel time (ms) | 264 | 270 |

### E-6.3 Sequentials

Sequential images of test no. 420020-9b and the simulation are compared in Figures E-24 through E-28. The basic kinematic response and sequence and timing of key events were generally comparable between the simulation and test no. 420020-9b, though the simulated cab displayed much less roll than the test vehicle cab; the box behavior was very similar.

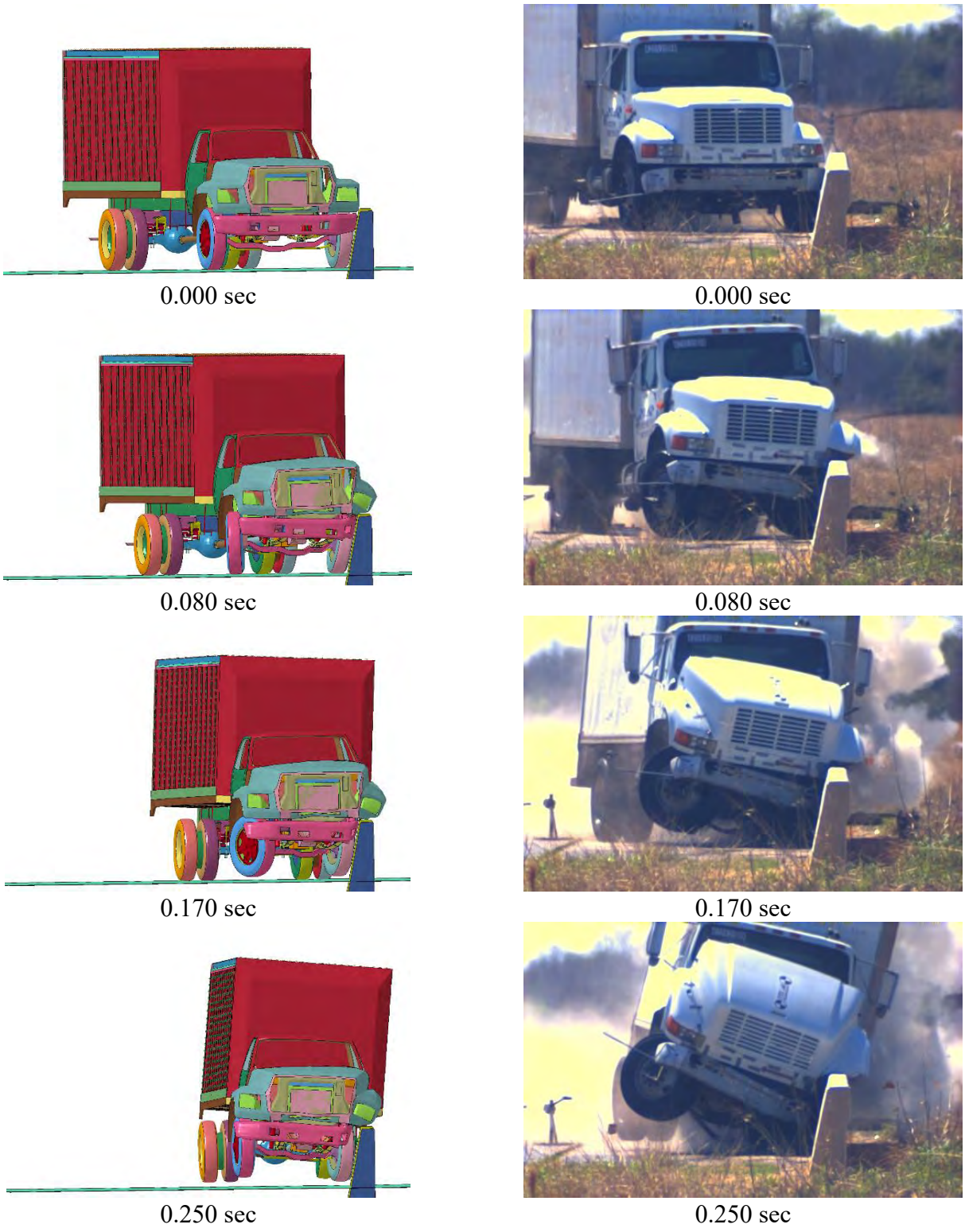


Figure E-24. Test No. 420020-9b (Sheikh, Bligh, and Menges 2011) and Simulation Downstream Sequential Images

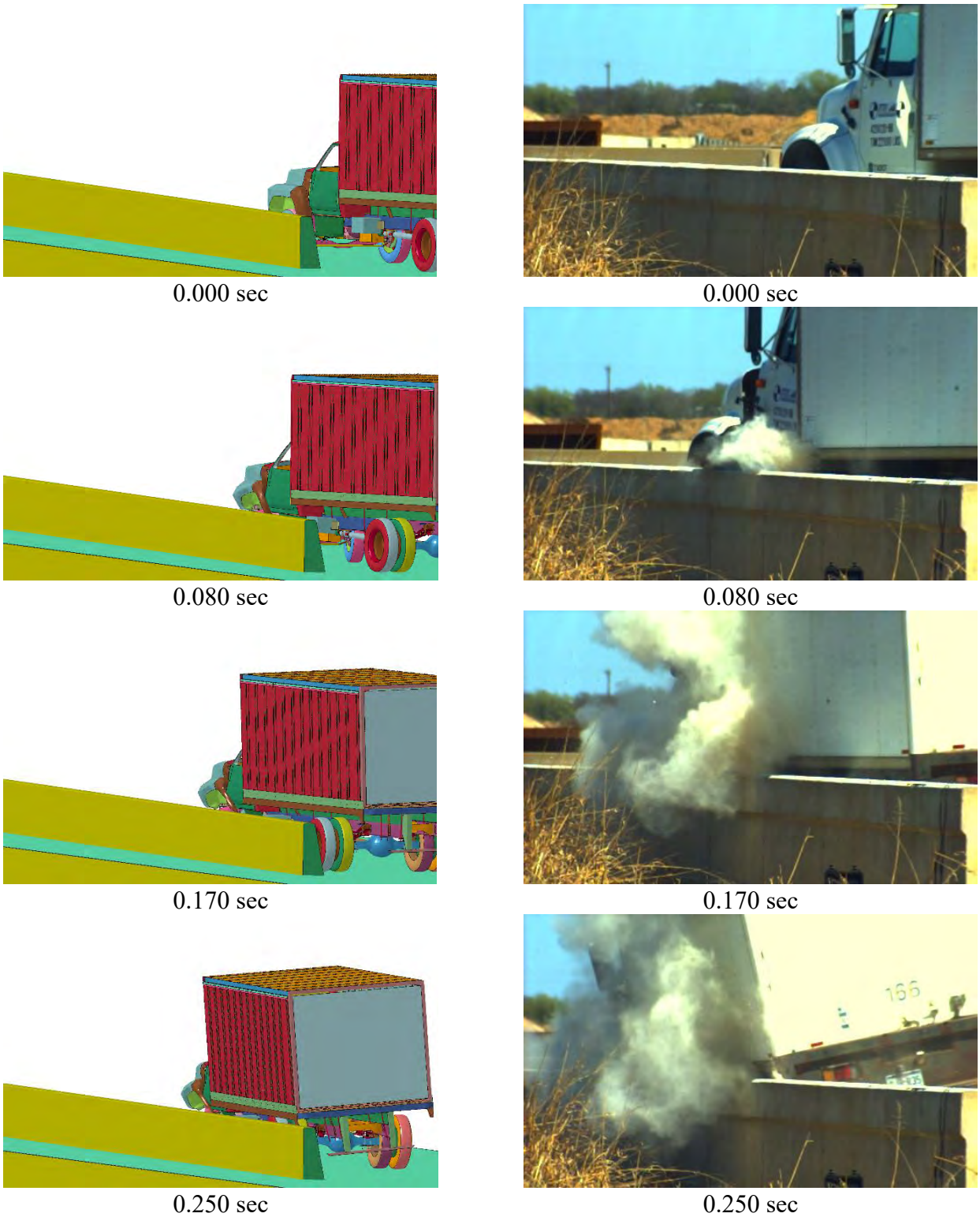


Figure E-25. Test No. 420020-9b (Sheikh, Bligh, and Menges 2011) and Simulation Upstream Sequential Images

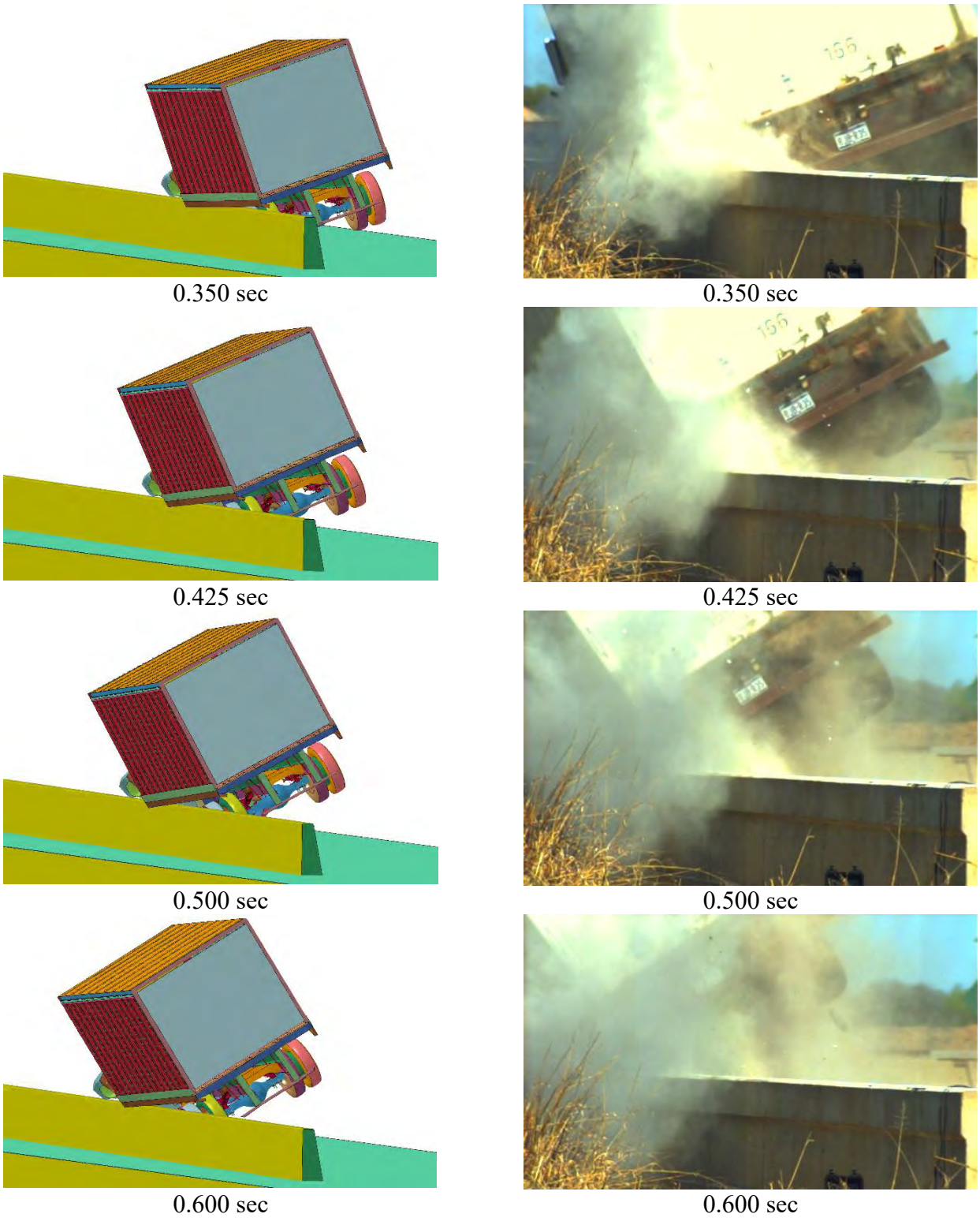


Figure E-26. Test No. 420020-9b (Sheikh, Bligh, and Menges 2011) and Simulation Upstream Sequential Images (continued)

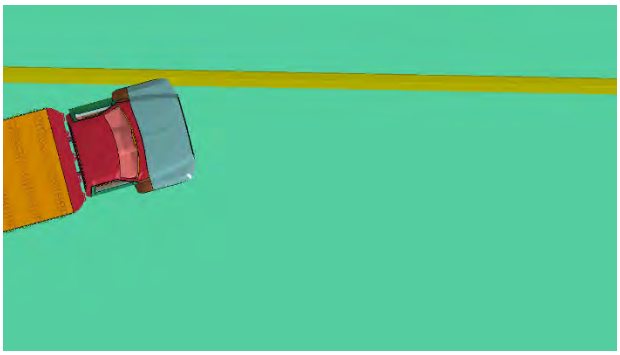

0.000 sec

0.000 sec

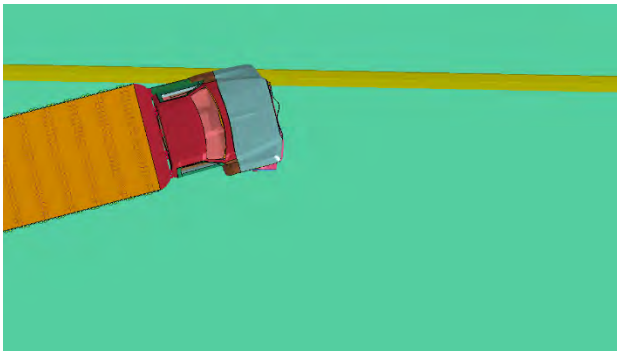

0.080 sec

0.080 sec

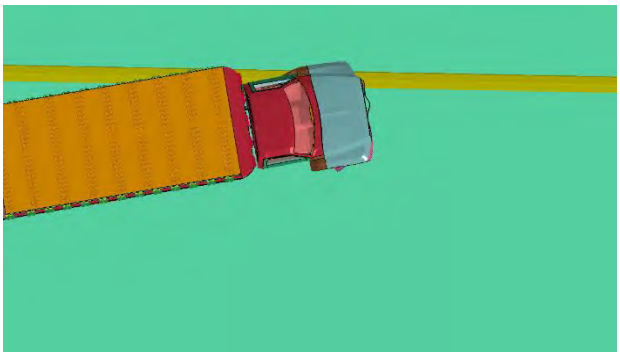

0.170 sec

0.170 sec

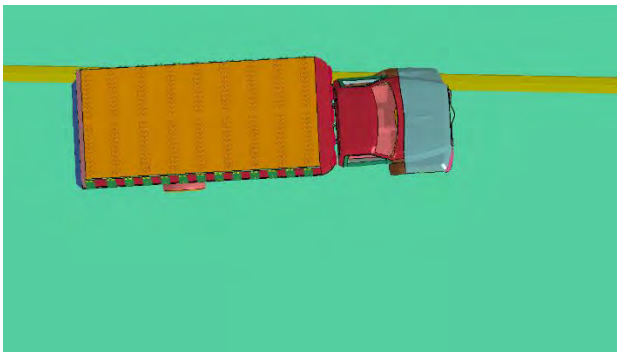

0.250 sec

0.250 sec

Figure E-27. Test No. 420020-9b (Sheikh, Bligh, and Menges 2011) and Simulation Overhead Sequential Images

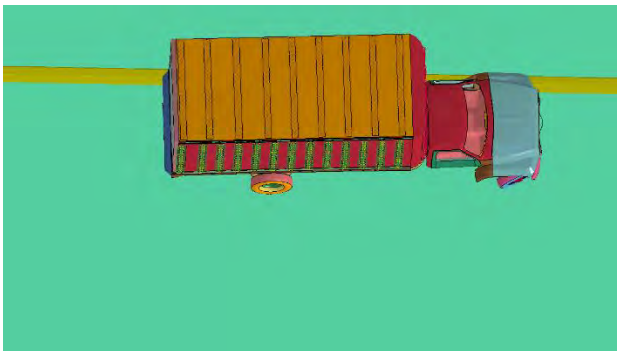

0.350 sec

0.350 sec

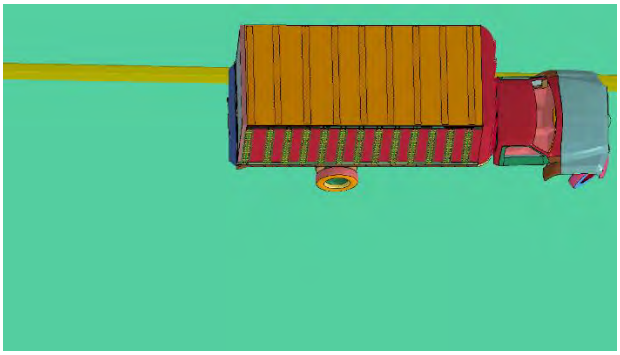

0.425 sec

0.425 sec

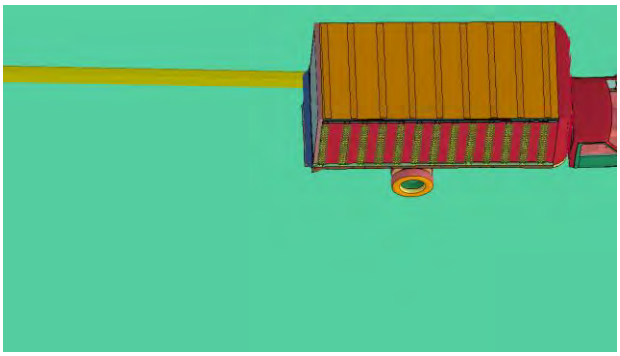

0.500 sec

0.500 sec

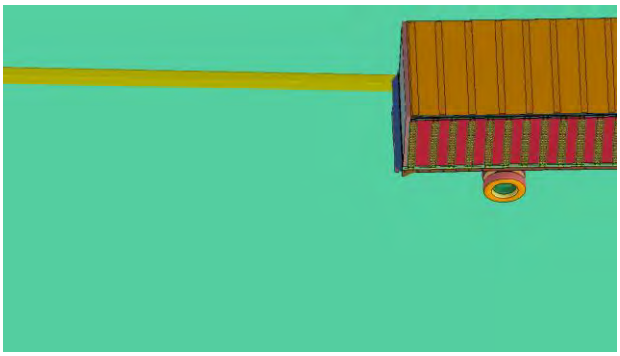

0.600 sec

0.600 sec

Figure E-28. Test No. 420020-9b (Sheikh, Bligh, and Menges 2011) and Simulation Overhead Sequential Images (continued)

## E-6.4 Time-dependent data

To validate overall dynamic performance of the crash test and simulation, acceleration, velocity, and displacements were compared, as shown in Figures E-29 through E-31. Accelerations were comparable, providing high confidence in the validation of the vehicle's dynamic ridedown performance. Discrepancies occurred at 0.1 and 0.3 seconds, where the model did not produce the longitudinal acceleration spikes seen in testing. Additionally, the simulation's lateral accelerations are out of phase from the test. Gyro sensors failed to record Euler angle data during testing.

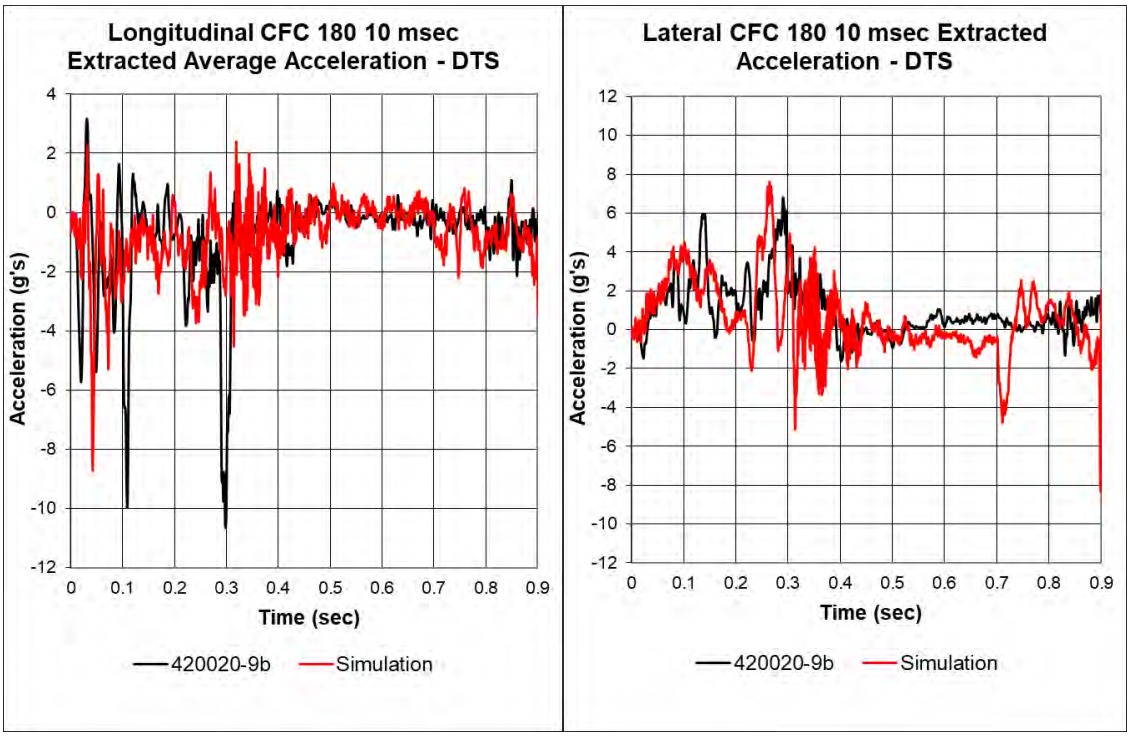


Figure E-29. Test No. 420020-9b (Sheikh, Bligh, and Menges 2011) and Simulation Acceleration

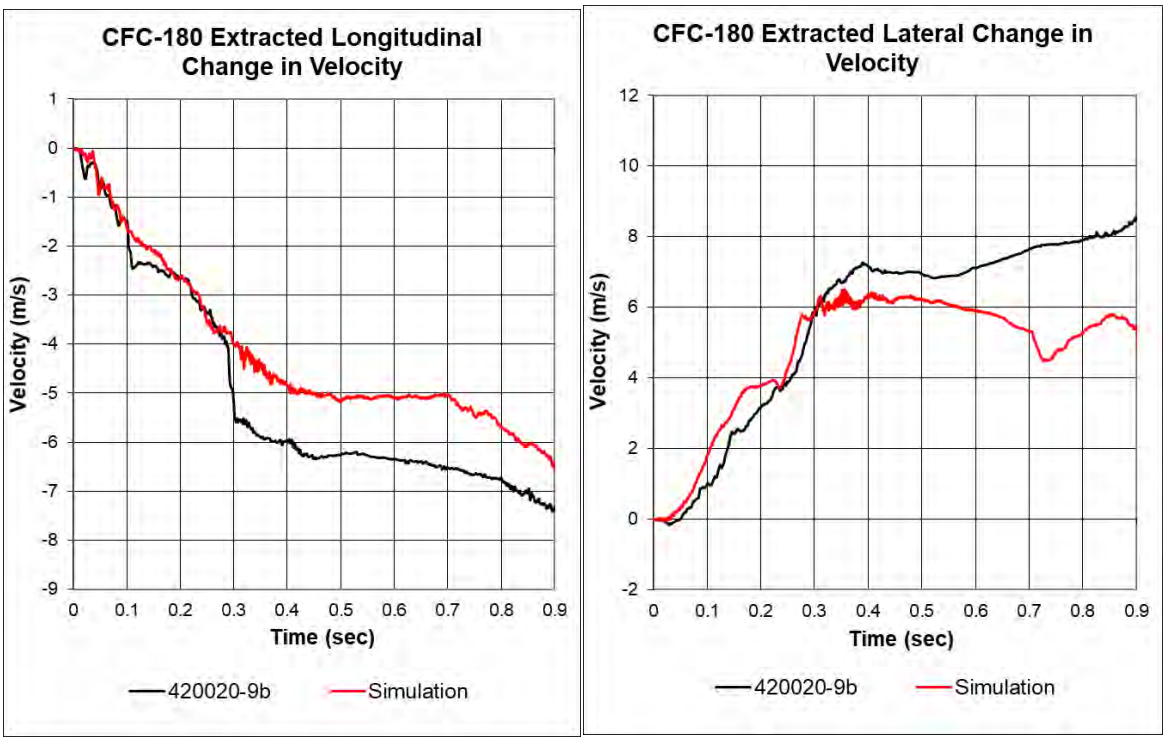


Figure E-30. Test No. 420020-9b (Sheikh, Bligh, and Menges 2011) and Simulation Velocity

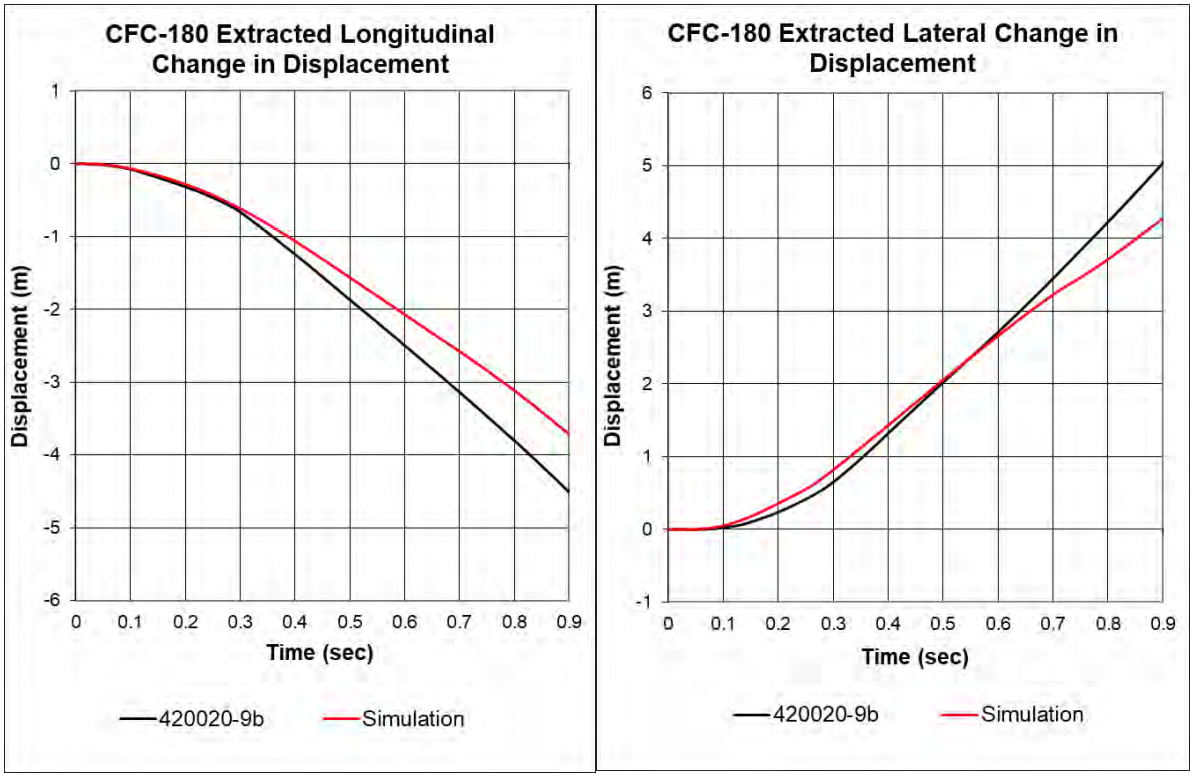


Figure E-31. Test No. 420020-9b (Sheikh, Bligh, and Menges 2011) and Simulation Displacement

### E-6.5 Solution Verification

To determine if the analysis solution produced a numerically stable result, the global verification assessment based on V&V criteria was performed and shown in Table E-7. The purpose of this assessment is to ensure that the numerical solution produces results that are numerically stable and conform to the conservation laws (e.g., results obey the conservation laws of energy, mass, and momentum). This is possible because the analysis was modeled as a closed system, in which the total energy should remain constant throughout the analysis and should be equal to the initial kinetic energy of the impacting vehicle. These indications do not necessarily mean that the result is a good comparison to the known solution. The criteria of the part/material energy did not pass because of a high hourglass energy due to the wheel well covers and a box attached to the frame rail that does not contact the barrier or other components. These parts were deemed as a non-critical components for energy absorption and were therefore excluded from the evaluation criteria.

Additionally, total energy variation criteria did not pass V&V requirements. This energy variation was investigated and yielded the same findings as that of the investigation conducted on the simulation validated against test no. 4CBR-1. Results indicate that the kinematic energy spike was related to the U-bolt failure behavior and did not affect the vehicle response during the simulation.

Table E-7. Test No. 420020-9b Simulation Solution Verification

| Verification evaluation criteria | Change (%) | Pass? |
|---|---|---|
| ***Total energy*** of the simulation must not vary more than 10 percent from the beginning of the run to the end of the run | 14.05 | N |
| ***Hourglass energy*** at the end of the run is less than 5 percent of the total initial energy at the beginning of the run | 0.59 | Y |
| ***Hourglass energy*** at the end of the run is less than 10 percent of the total internal energy at the end of the run | 5.97 | Y |
| The part/material with the most hourglass energy at the end of the run is less than 10 percent of the total internal energy of the part/material at the end of the run | 208.21 | N |
| Mass added to the total model is less than 5 percent of the total model mass at the beginning of the run | 0.00 | Y |
| The part/material with the most mass added had less than 10 percent of its initial mass added | 1.39 | Y |
| The moving parts/materials in the model have less than 5 percent of mass added to the initial moving mass of the model | 0.00 | Y |
| No shooting nodes in the solution | No | Y |
| No solid elements with negative volumes | No | Y |

### E-6.6 Time-history Validation

The curves were evaluated over 0.94 seconds of the impact event. The default metric evaluation options in RSVVP were used, which included the Sprague & Geers and the ANOVA metrics. The default acceptance criteria for these metrics are 40% for the Sprague-Geers metrics, 5% for the

ANOVA mean, and 35% for the ANOVA standard deviation of residuals. These acceptance criteria are based on comparison of repeated full-scale crash tests involving a small car impacting a rigid barrier (i.e., uni-body vehicle impact with short impact duration) and are likely too strict for this application, which involves a multi-body vehicle and a relatively long impact event. For this assessment, the V&V criteria were used to determine validity, while Sprague-Geers values less than or equal to 55 and standard deviation values less than or equal to 50 were deemed "borderline" acceptable.

### E-6.6.1 Single-channel Assessment

Sprague-Geers and ANOVA metrics are shown in Table E-8 for x-, y-, and z- acceleration and yaw, roll, and pitch channels using RSVVP. Based on Sprague-Geers metrics, a comparison of the individual acceleration components indicated the simulation was in poor agreement with the test ANOVA metrics indicated the mean residual error and standard deviation of the mean residual error were in agreement with the test for x- and z-acceleration; however, the y-acceleration showed poor correlation.

Table E-8. Single-channel Time-history Comparison of Test No. 420020-9b (Sheikh, Bligh, and Menges 2011) and Simulation

| **Evaluation criteria (time interval [0, 0.9483 s])** | | | | | | | | |
|---|---|---|---|---|---|---|---|---|
| O | ***Sprague-Geers***<br>Values less than or equal to 40 are acceptable | | | | | | | |
| | **Filter: CFC180 Sync.: None** | **RSVVP curve preprocessing** | | | | **M** | **P** | **Pass?** |
| | | **Shift** | | **Drift** | | | | |
| | | **True** | **Test** | **True** | **Test** | | | |
| | X-acceleration | N | N | N | N | 92 | 48.6 | N |
| | Y-acceleration | N | N | N | N | 250.9 | 48.7 | N |
| | Z-acceleration | N | N | N | N | 45.6 | 49.7 | B |
| P | ***ANOVA***<br>Both criteria must be met:<br>• Mean residual error must be less than 5 percent of peak acceleration ($\bar{e} \le 0.05 \cdot a_{Peak}$)<br>• Standard deviation of the residuals must be less than 35 percent of peak acceleration ($\sigma \le 0.35 \cdot a_{Peak}$) | | | | | **Mean residual** | **Standard deviation of residuals** | **Pass?** |
| | X-acceleration (peak) | | | | | 0.2 | 25.2 | Y |
| | Y-acceleration (peak) | | | | | -1.9 | 49.5 | B |
| | Z-acceleration (peak) | | | | | -2.8 | 27.8 | Y |

### E-6.6.2 Multi-channel Assessment

Since the individual data metrics did not satisfy all acceptance criteria, the multi-channel option in RSVVP was used to calculate weighted Sprague-Geer and ANOVA metrics for the six data channels, as shown in Table E-9. The weighted RSVVP metrics in the multi-channel mode did not

satisfy all acceptance criteria, and therefore the time-history comparison was not acceptable. This was primarily attributed to differences in acceleration between the test and simulation.

Table E-9. Multi-channel Time-history Comparison of Test No. 420020-9b (Sheikh, Bligh, and Menges 2011) and Simulation

| **Evaluation criteria (time interval [0 , 0.9483 s])** | | | | |
|---|---|---|---|---|
| **Multi-channel weights:**<br>Area II method | X-acceleration: 0.2742<br>Y-acceleration: 0.3337<br>Z-acceleration: 0.3921 | | | |
| O | ***Sprague-Geers***<br>Values less or equal to 40 are acceptable | **M** | **P** | **Pass?** |
| | | 90 | 48.6 | N |
| P | ***ANOVA***<br>Both criteria must be met:<br>• Mean residual error must be less than 5 percent of peak acceleration ($\bar{e} \leq 0.05 \cdot a_{Peak}$)<br>• Standard deviation of the residuals must be less than 35 percent of peak acceleration ($\sigma \leq 0.35 \cdot a_{Peak}$) | **Mean residual** | **Standard deviation of residuals** | **Pass?** |
| | | 0.23 | 25.19 | Y |

# Appendix F. Tractor-trailer Model Preparation and Validation

## F-1 Overview

The final model validated and adjusted as needed was the tractor-trailer model. Validation was conducted against test nos. MAN-1 (Rosenbaugh et al. 2016) and 510605-RYU1 (Buth and Menges 2012). This appendix discusses efforts to implement, expedite, and improve simulation stability, followed by a discussion of the validation results and model shortcomings.

## F-2 Preparation

The tractor-trailer model was repositioned for driver-side impacts at a 15-degree angle, allowing for simple replacement of barrier models for different simulation setups. Accelerations are affected by the recorded location, and therefore the model's accelerometer positioning was adjusted to match the mounting location used in full-scale crash testing. A non-impact, free-rolling vehicle model was defined to have an initial longitudinal velocity and used to conduct a qualitative energy balance check. This ensured the model's energy levels behaved properly in the absence of a rigid barrier impact.

All barriers were modeled rigidly with a Belytscho-Tsay element formulation and 30x30 mm shell elements. Single point constraints were applied to each node to fix the barrier in place.

## F-3 Modifications

The tractor-trailer model was too extensive and complex to make significant changes; instead, modifications were relatively minor to confirm the model satisfied ZOI targets. Simulation was initially performed using a 2017 tractor-trailer model; this was later replaced by a 2011 model as the 2011 model more accurately represented the ZOI from test no. MAN-1.

The tractor-trailer model initially displayed front axle stiffness which generated unrealistic impact behavior. A process similar to the one described in Appendix E-3.2 was used to model U-bolt failure as a timed spot-weld disengagement, which increased the accuracy of simulation. Additionally, a more compliant hitch was added to increase trailer roll.

## F-4 Friction Selection

Test no. MAN-1 was used for friction selection as it included a concrete barrier with a flat, continuous surface. Ridedown velocity plots, shown in Figure F-1, were studied to select friction values. Timing of key event occurrences, shown in Table F-1, was also considered when selecting friction values.

In initial simulation, the simulated tractor rolled toward the barrier on initial impact. When the 2011 model was used, the tractor rode up the barrier due to increased tire-barrier friction. Body- and tire-barrier friction values of 0.3 and 0.5, respectively, caused the trailer to achieve higher roll at approximately 0.05 sec. This agreed well with full-scale crash testing but adversely affected the box ZOI when impacting shorter barriers. None of the models yielded trailer pitch as observed in full-scale crash testing. This was attributed to the absence of contacts between the trailer and tractor

wheels, which allowed minor tire penetration and produced no trailer pitch. Due to time constraints, this was not corrected.

Run TL5-MAN-1-R7 was conducted using the 2017 tractor-trailer model; runs TL-5-B-MAN-1-R9-F0 and TL5-B-MAN-1-R9-F2 were conducted using the 2011 model. The 2011 model was significantly more comparable to test no. MAN-1 in terms of lateral velocity, particularly the second run, and therefore simulation was continued using the 2011 model.

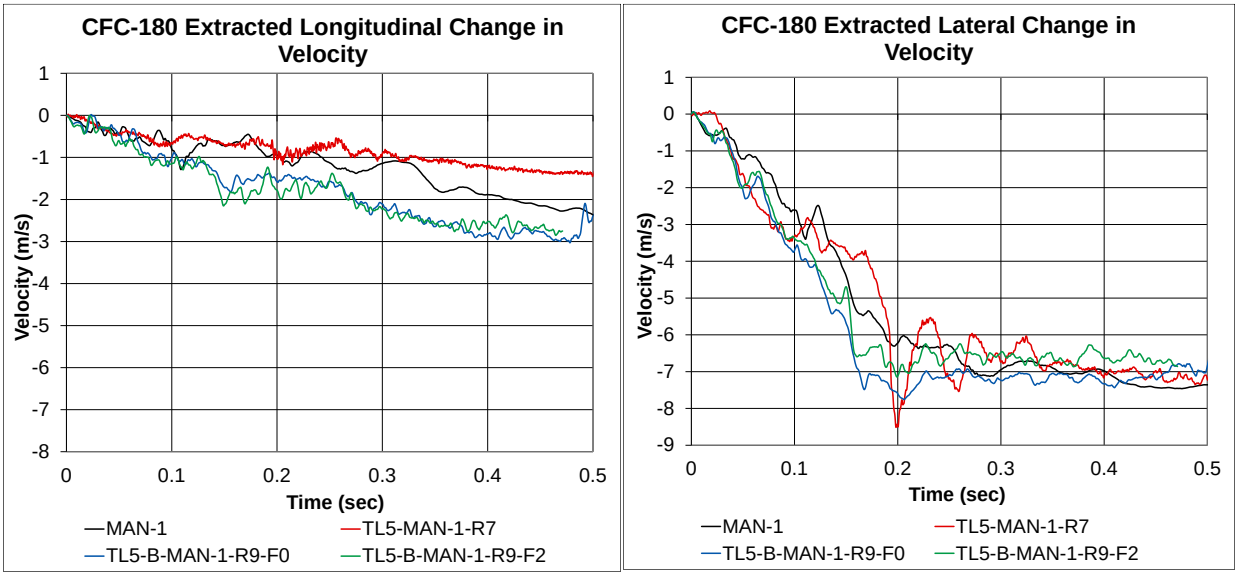


Figure F-1. Velocity Analysis for Varied Vehicle-barrier Friction

Tire- and vehicle-barrier friction values were evaluated with each ranging from 0.1 to 0.5, as shown in Table F-1. Run TL5-MAN-1-R7 included parameters consistent with other vehicle models used in this study and displayed good agreement with results from test no. MAN-1. Therefore, TL-5 validation was continued with tire- and vehicle-barrier friction values set to 0.4 and 0.1, respectively.

Table F-1. Key Events with Varying Friction, Test No. MAN-1 (Rosenbaugh et al. 2016) and Simulation

| Model | Friction | | ZOI (in.) | ZOI time (ms) | Parallel time (ms) | |
|---|---|---|---|---|---|---|
| | Vehicle-barrier | Tire-barrier | | | Tractor | Trailer |
| Test No. MAN-1 | N/A | N/A | 22.7 | 962 | 386 | 776 |
| TL5-MAN-1-R1 | 0.1 | 0.1 | 27.0 | 990 | 380 | 640 |
| TL5-MAN-1-R2 | 0.2 | 0.2 | 26.0 | 940 | 390 | 640 |
| TL5-MAN-1-R3 | 0.3 | 0.3 | 27.4 | 1030 | 500 | 680 |
| TL5-MAN-1-R4 | 0.4 | 0.4 | 15.7 | 880 | 890 | 670 |
| TL5-MAN-1-R5 | 0.5 | 0.5 | 15.3 | 9050 | 1010 | 680 |
| TL5-MAN-1-R6 | 0 | 0 | 26.1 | 980 | 380 | 630 |
| **TL5-MAN-1-R7** | **0.1** | **0.4** | **25.3** | **990** | **400** | **640** |
| TL5-MAN-1-R8 | 0.2 | 0.4 | 23.8 | 930 | 430 | 660 |
| TL5-MAN-1-R9 | 0.3 | 0.4 | 18.8 | 920 | 590 | 710 |

## F-5 Validation to Test No. MAN-1

### 6-2.1 Test Setup

In MASH TL-5 full-scale crash test no. MAN-1 (Rosenbaugh et al. 2016), an 80,076-lb 2004 International 9200 with 50,367 lb of ballast impacted a 49.25-in. tall, 9.85-in. thick 9.1-degree single-slope barrier at 51.7 mph and a 15.2-degree angle. In simulation, an 80,126-lb tractor-trailer with 50,516 lb of ballast impacted a 49.25-in. tall, 9.85-in. thick 9.1-degree single-slope barrier at 51.9 mph and a 15.2-degree angle. Test vehicle and simulation model dimensions and impact points are compared in Figure F-2.


Figure F-2. Test No. MAN-1 (Rosenbaugh et al. 2016) and Simulation Vehicles

## F-5.2 ZOI and Key Events

The point of maximum intrusion during simulation is compared to the equivalent time step in test no. MAN-1 in Figures F-3 and F-4. ZOIs from the test and FEA were 22.7 and 25.2 in., respectively, an 11.0 percent relative difference. Key events are summarized in Table F-2.

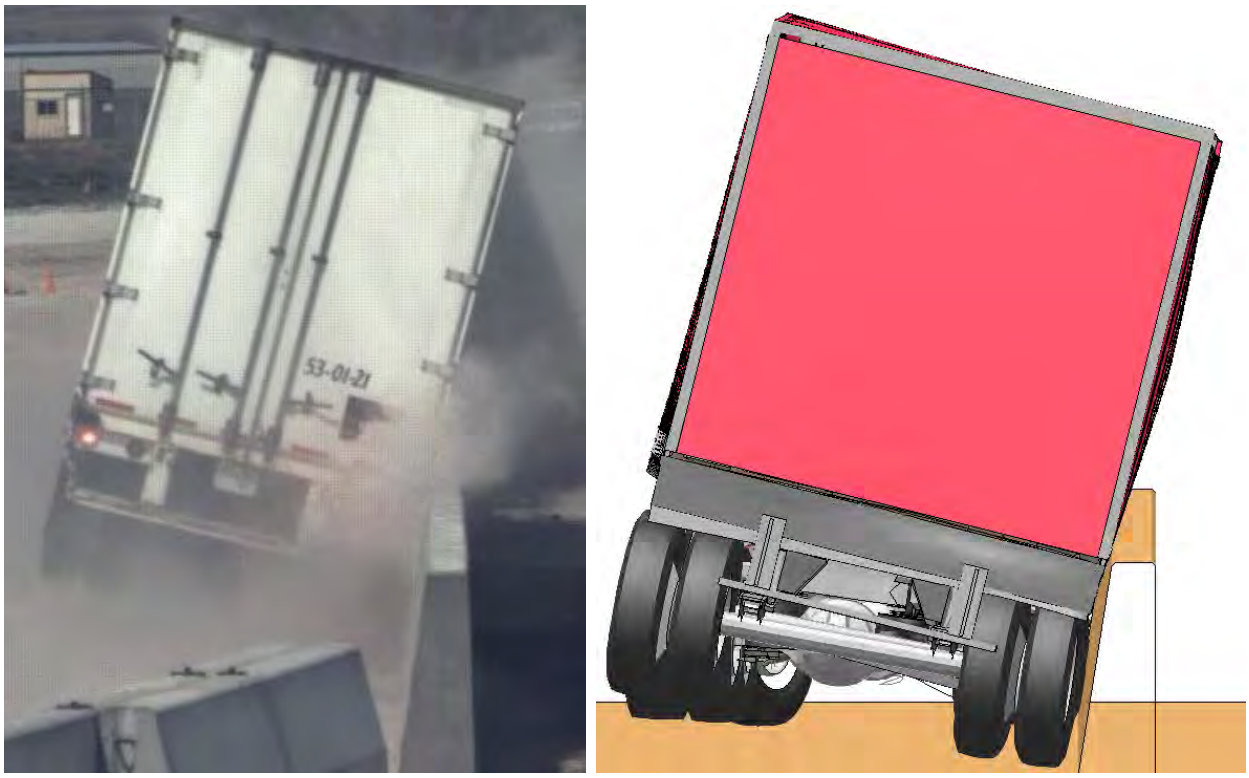

Figure F-3. Maximum lateral Extent during Test No. MAN-1 (Rosenbaugh et al. 2016) and Simulation

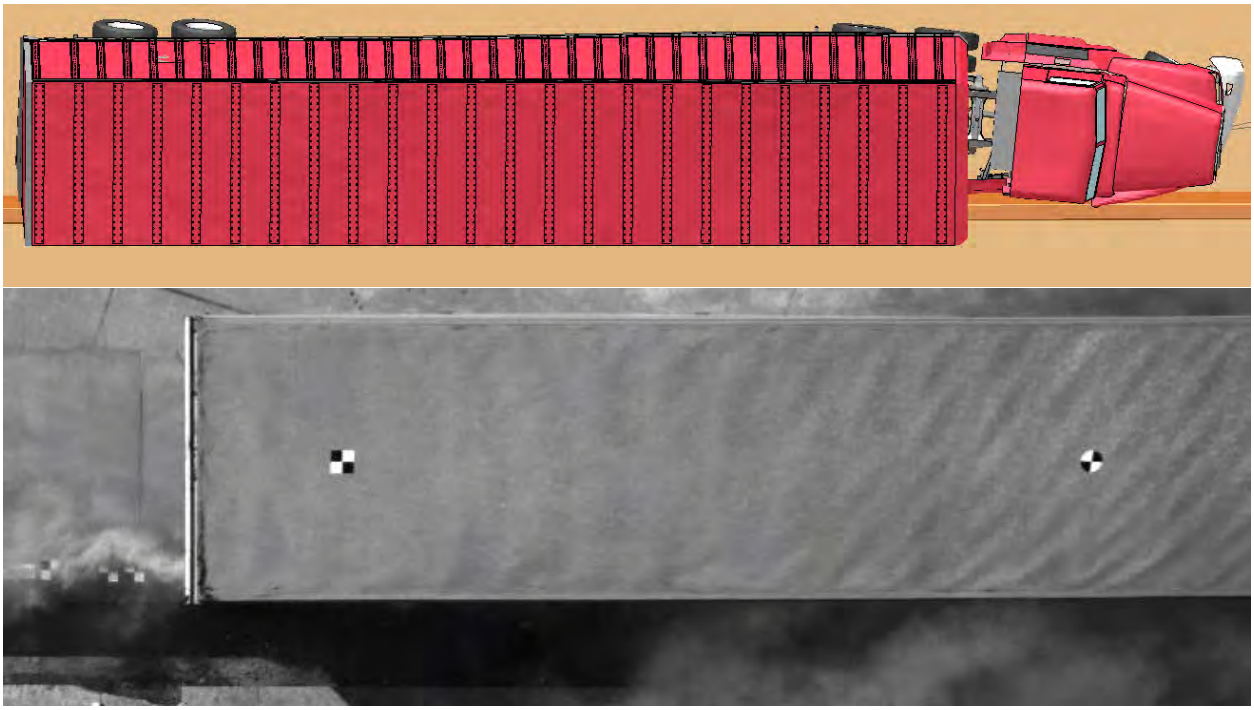

Figure F-4. Maximum Lateral Extent during Test No. MAN-1 (Rosenbaugh et al. 2016) and Simulation

Table F-2. Key Events Comparison, Test No. MAN-1 (Rosenbaugh et al. 2016) and Simulation

| Event | Test | FEA |
|---|---|---|
| ZOI measurement (in.) | 22.7 | 25.2 |
| ZOI time (ms) | 962 | 860 |
| Parallel time (ms) | 776 | 720 |
| Exit Time (ms) | 1768 | N/A[1] |

[1]Simulation terminated before vehicle exited the system.

### F-5.3 Sequentials

Sequential images test no. MAN-1 and the simulation are compared in Figures F-5 through F-7. The simulated vehicle behavior was fairly comparable to that of the test vehicle, though some differences were noted and believed to be attributable to increased front axle stiffness in the model, similar to what was seen in SUT simulation.

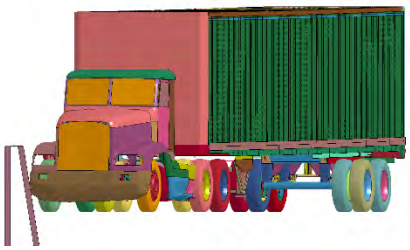

0.000 sec

0.000 sec

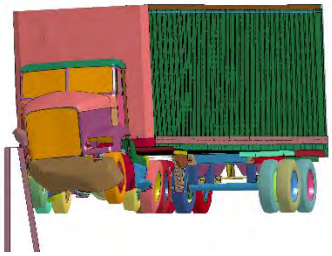

0.250 sec

0.250 sec

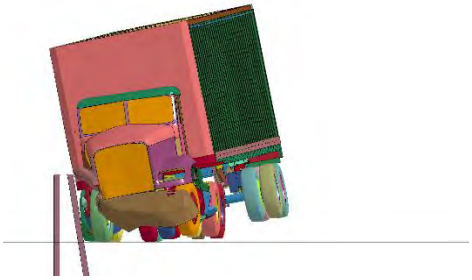

0.500 sec

0.500 sec

0.750 sec

0.750 sec

1.000 sec

1.000 sec

Figure F-5. Test No. MAN-1 (Rosenbaugh et al. 2016) and Simulation Downstream Sequential Images

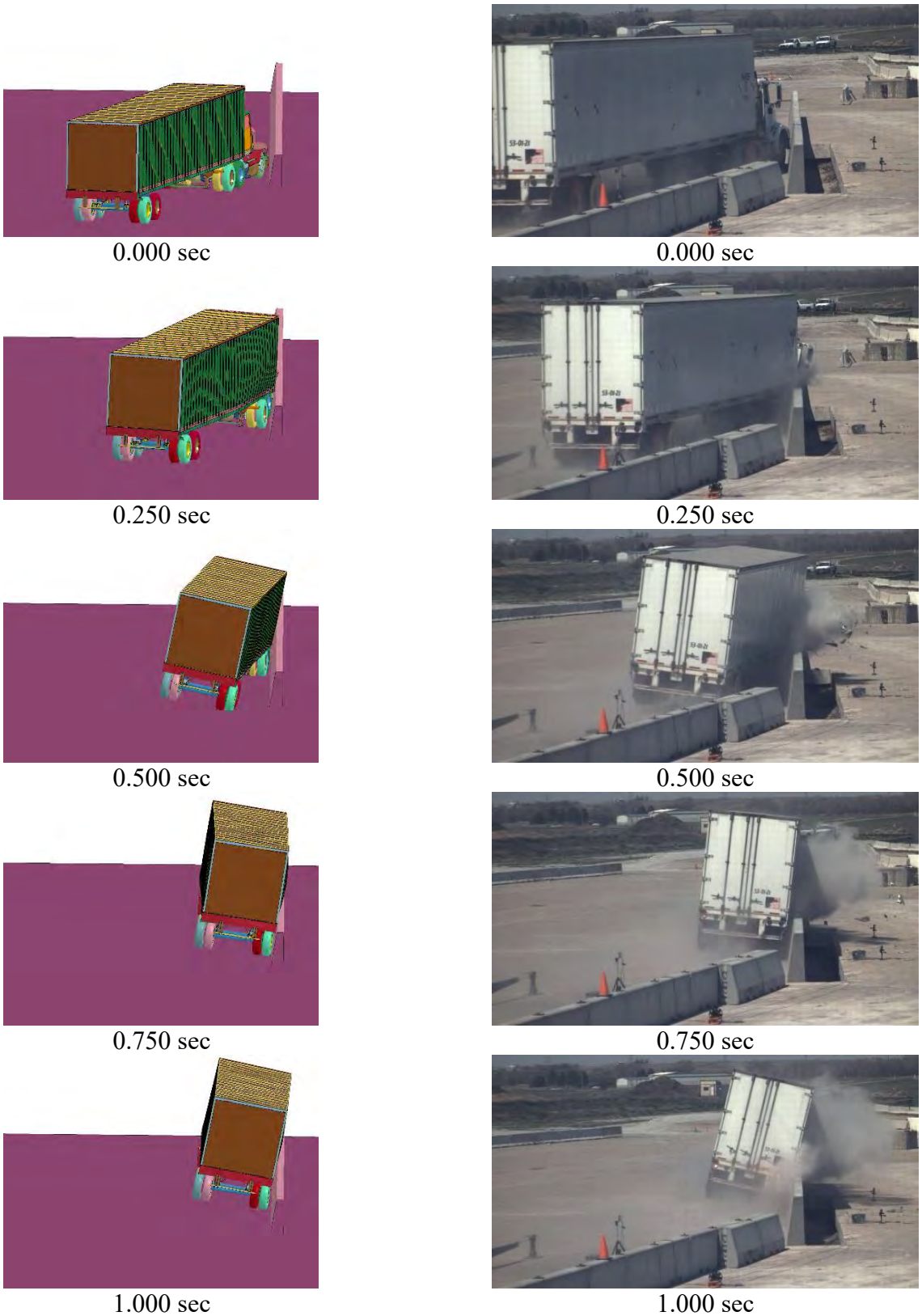


Figure F-6. Test No. MAN-1 (Rosenbaugh et al. 2016) and Simulation Upstream Sequential Images

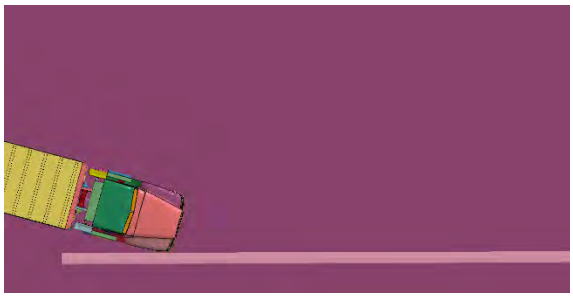

0.000 sec

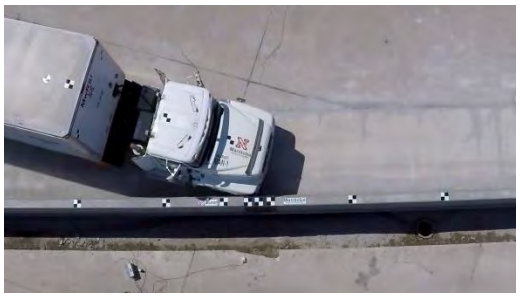

0.000 sec

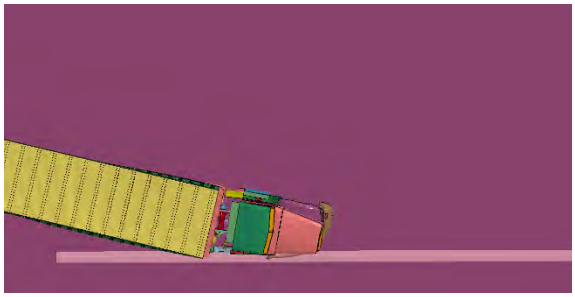

0.250 sec

0.250 sec

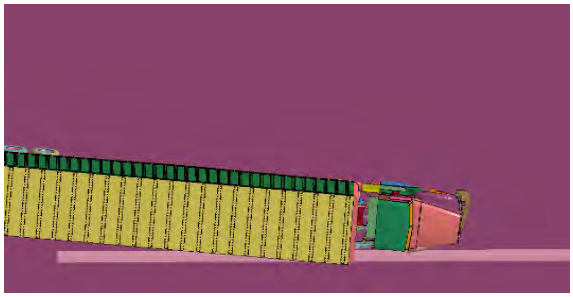

0.500 sec

0.500 sec

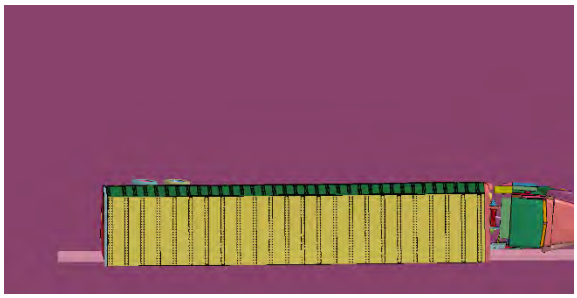

0.750 sec

0.750 sec

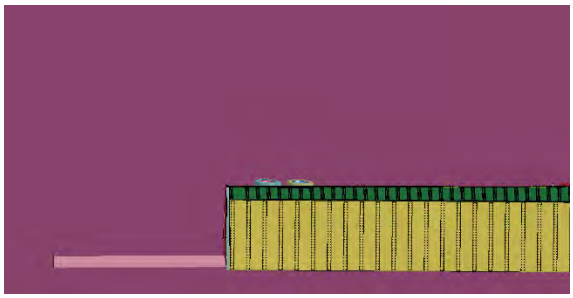

1.000 sec

1.000 sec

Figure F-7. Test No. MAN-1 (Rosenbaugh et al. 2016) and Simulation Overhead Sequential Images

## F-5.4 Time-dependent Data

To validate overall dynamic performance of the crash test and simulation, acceleration, velocity, and displacements of the cab were compared, as shown in Figures F-8 through F-10. Longitudinal acceleration varied between test and simulation from 0 to 0.2 s, producing velocity and displacement variations throughout the run; lateral accelerations were comparable.

Euler angles for the cab are compared in Figure F-11; initial roll was much higher in the test, while pitch and yaw were more comparable. It was believed the model's front axle stiffness may prevent vehicle roll at the outset of simulation.

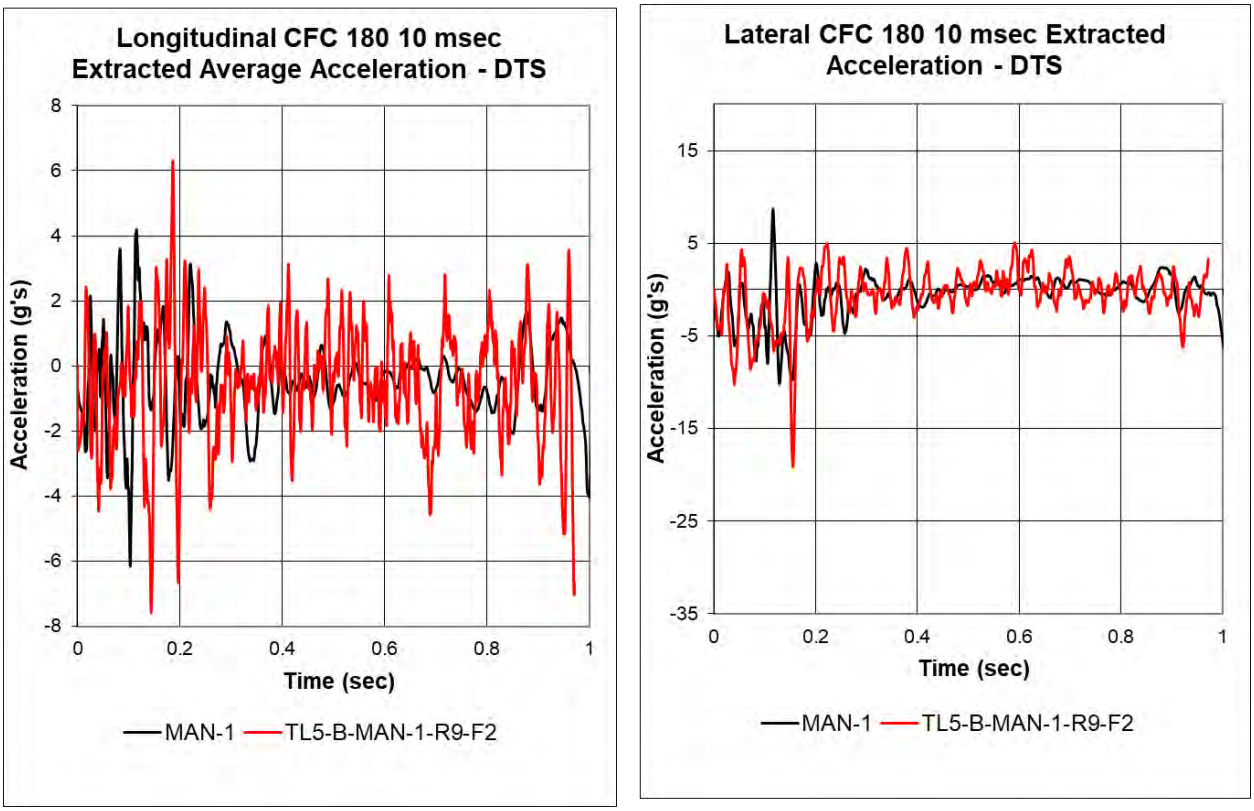


Figure F-8. Test No. MAN-1 (Rosenbaugh et al. 2016) and Simulation Cab Acceleration

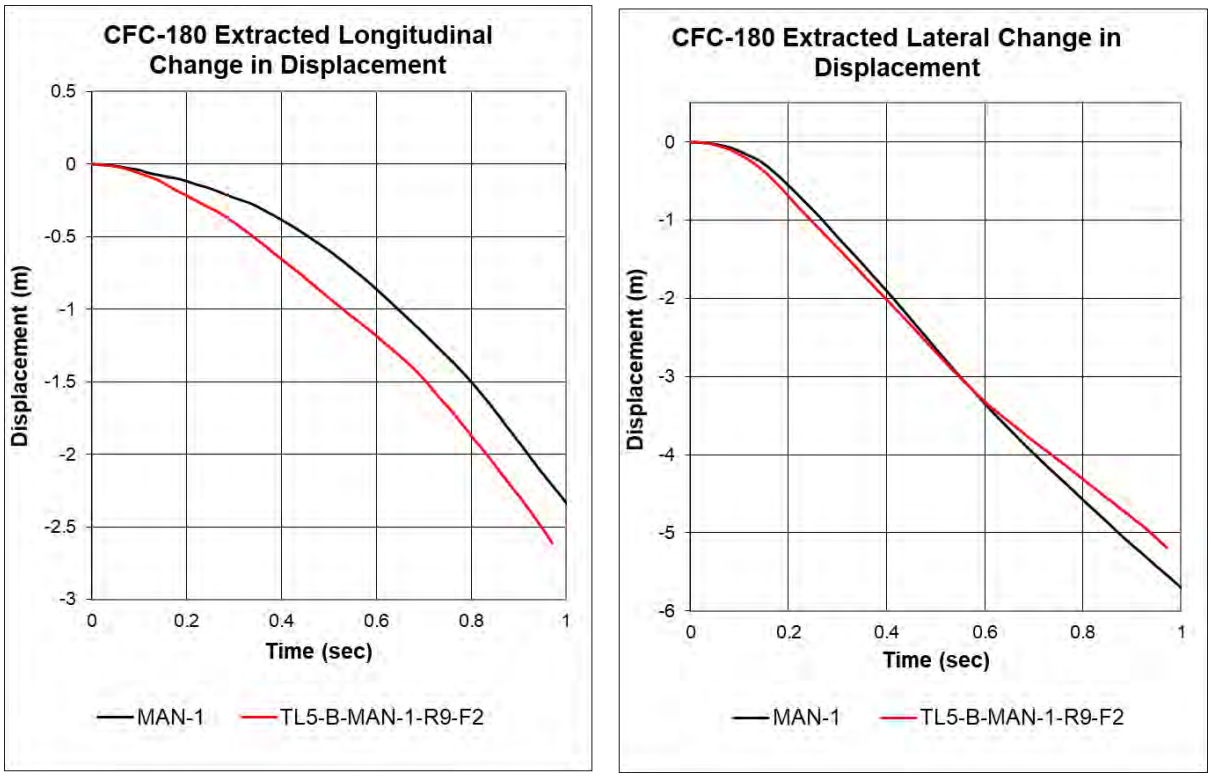


Figure F-9. Test No. MAN-1 (Rosenbaugh et al. 2016) and Simulation Cab Velocity

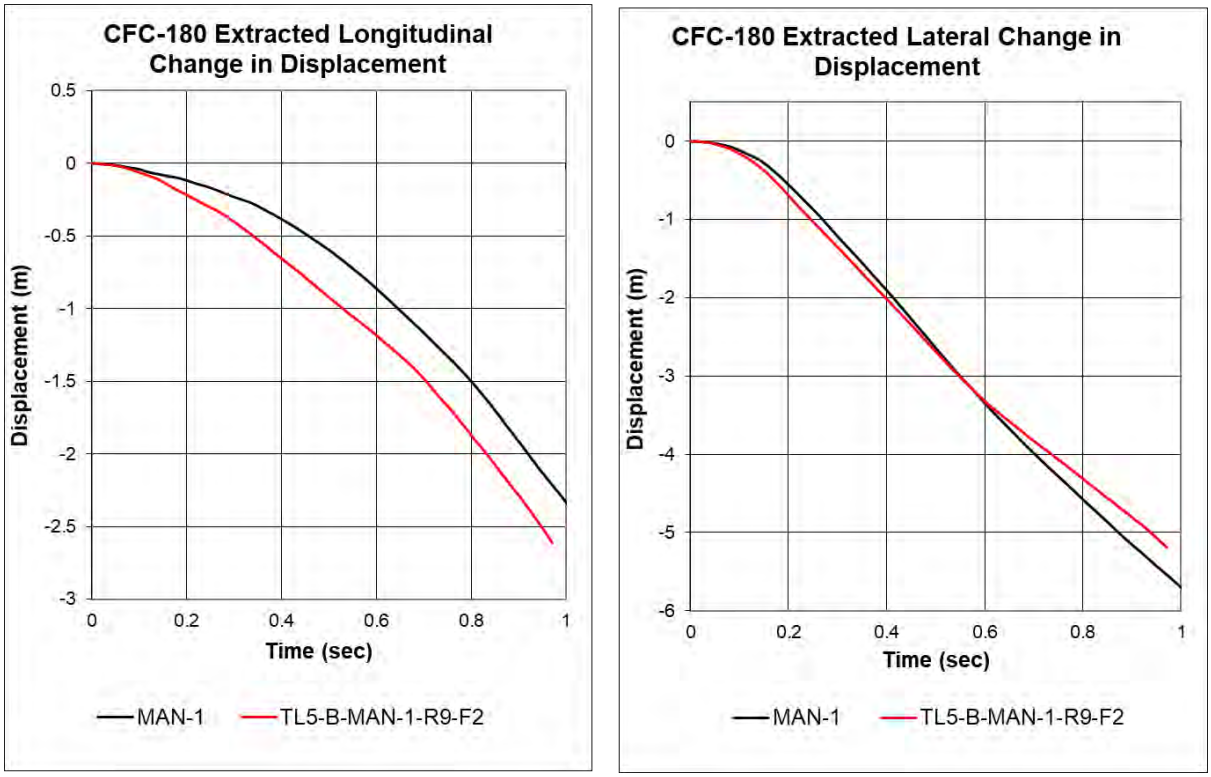


Figure F-10. Test No. MAN-1 (Rosenbaugh et al. 2016) and Simulation Cab Displacement

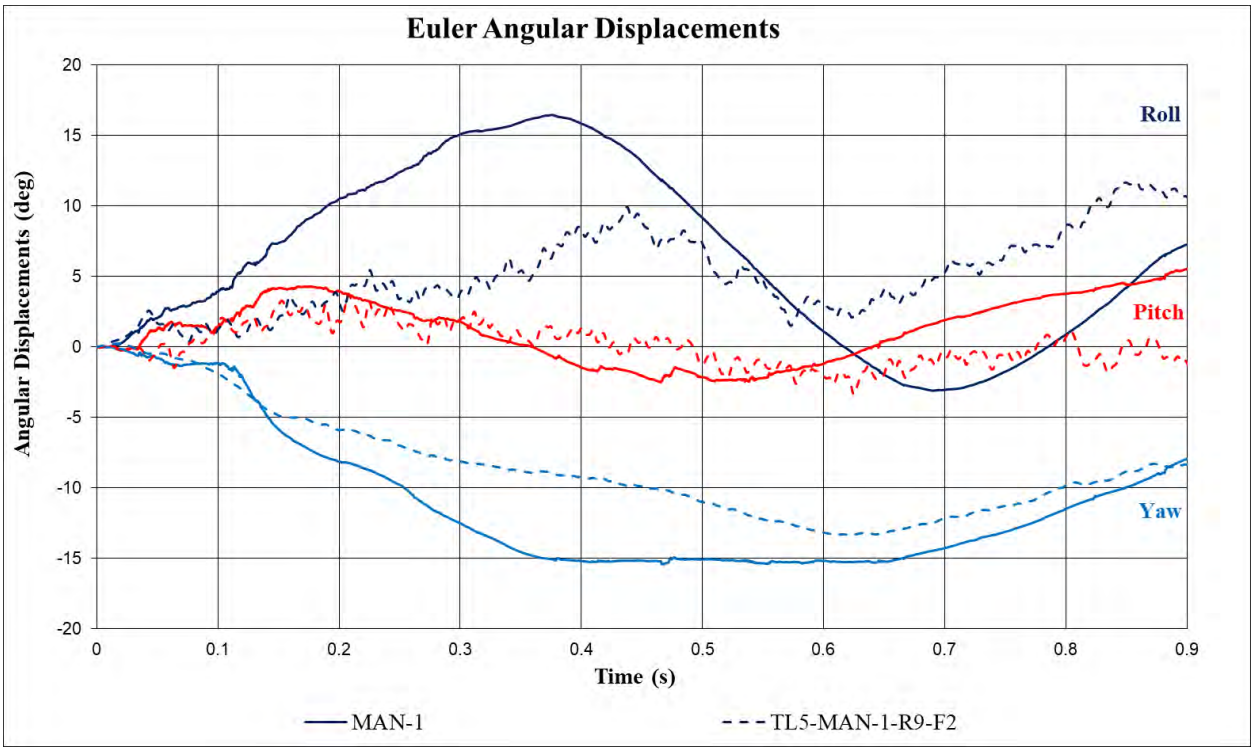


Figure F-11. Test No. MAN-1 (Rosenbaugh et al. 2016) and Simulation Cab Euler Angles

## F-6 Validation to Test No. 510605-RYU1

### F-6.1 Test Setup

In MASH TL-5 full-scale crash test no. 510605-RYU1 (Buth and Menges 2012), a 79,650-lb 1995 GM Tractor with 49,210 lb of ballast impacted a 41.3-in. tall, 8.9-in. thick Jersey barrier at 49.1 mph and a 14.6-degree angle. In simulation, a 79,982-lb tractor-trailer with 50,516 lb of ballast impacted a 41.3-in. tall, 9.85-in. thick Jersey barrier at 51.9 mph and a 14.6-degree angle. Test vehicle and simulation model dimensions and impact points are compared in Figure F-12.

Acceleration, velocity, and displacement data from the simulated tractor-trailer were not available. Gyro sensors failed to record Euler angle data during testing.

Figure F-12. Test No. 510605-RYU1 (Buth and Menges 2012) and Simulation Vehicles

### F-6.2 ZOI and Key Events

The point of maximum intrusion during simulation is compared to the equivalent time step in test no. 510605-RYU1 in Figure F-13. ZOIs from the test and FEA were 63.8 and 57.2 in., respectively, a 10.3 percent relative difference. The ZOI also occurs at a later time step in the test. Key events are summarized in Table F-3.

Figure F-13. Maximum Lateral Extent during Test No. 510605-RYU1 (Buth and Menges 2012) and Simulation

Table F-3. Table 24. Key Events Comparison, Test No. 510605-RYU1 (Buth and Menges 2012) and Simulation

| Event | Test | FEA |
|---|---|---|
| ZOI measurement (in.) | 63.8 | 57.2 |
| ZOI time (ms) | 1,453 | 920 |
| Parallel time (ms) | 840 | 700 |
| Exit Time (ms) | 408 | N/A[1] |

[1]Simulation terminated before vehicle exited the system.

### F-6.3 Sequentials

Sequential images of test no. 510605-RYU1 and the simulation are compared in Figures F-14 and F-15. The simulated vehicle behavior was fairly comparable to that of the test vehicle, though some differences were noted and believed to be attributable to increased front axle stiffness in the model, similar to what was seen in SUT simulation. Particularly, the left-front tire of the test tractor lifted off the ground much farther than the simulated model. The trailer was not fully visible in downstream camera views, as discussed in Section 8.1, but it was believed trailer behavior was comparable between the test and simulation.

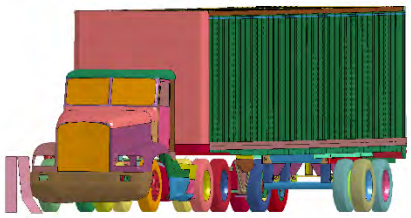

0.000 sec


0.000 sec

0.150 sec


0.150 sec

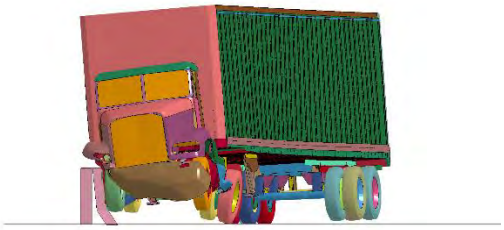

0.300 sec

0.300 sec

0.600 sec


0.600 sec

1.000 sec

1.000 sec

Figure F-14. Test No. 510605-RYU1 (Buth and Menges 2012) and Simulation Downstream Sequential Images

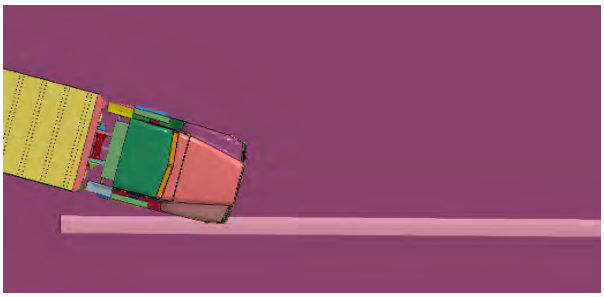

0.000 sec

0.000 sec

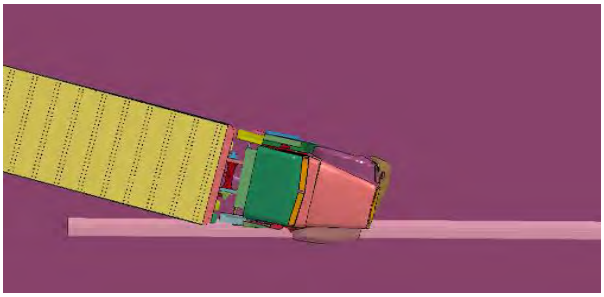

0.150 sec

0.150 sec

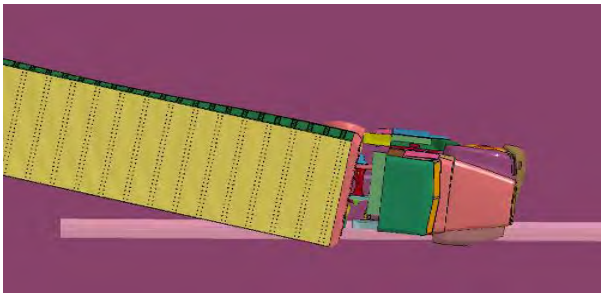

0.300 sec

0.300 sec

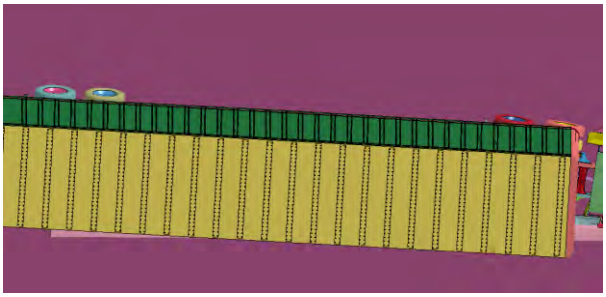

0.600 sec

0.600 sec

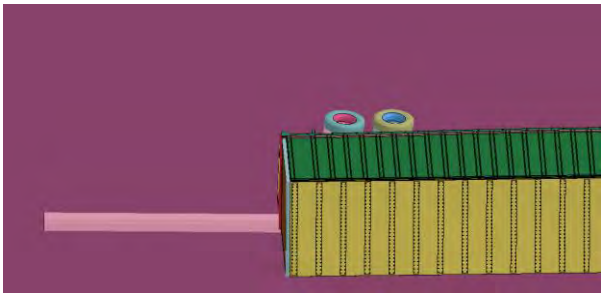

1.000 sec

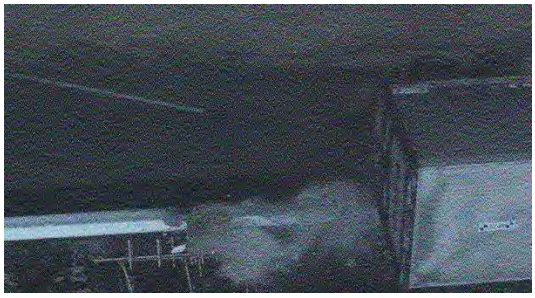

1.000 sec

Figure F-15. Test No. 510605-RYU1 (Buth and Menges 2012) and Simulation Overhead Sequential Images

## F-7 Discussion

As noted previously, the validation of the TL-5 tractor-trailer vehicle was more limited than the validation effort associated with the RAM data. Overall vehicle dynamics, timing, and ZOI intrusion values were similar for the simulation model compared to test data.

However, similar barrier shapes, geometries, and heights produced significantly different lateral ZOI encroachment windows. For example, 42-in. tall, vertical concrete parapets were evaluated in test nos. 405511-2, 469468-2-1, and 490025-2-1, which were associated with maximum lateral ZOI estimates extracted from high-speed digital video analysis of 73.5, 61.8, and 30.5 in., respectively. Calibrating the model to meet each of these ZOI encroachment values for similar barrier profiles and heights may be impossible. Moreover, results indicate that there may not be a clearly identifiable test that utilizes a test vehicle that is consistent with the modeled vehicle.

The objective of this research effort was to identify practical, maximum extents of the ZOI based on full-scale crash test and simulation data. Large uncertainty in simulation data means that it is therefore prudent to evaluate the ZOI predictions of the TL-5 simulation model above all other comparison metrics. For computer simulations evaluated in this study, an accurate transitional behavior was observed for a barrier height near 48 in. tall, in which the van-body trailer contacted the front face of the barrier but was allowed to slide over and pivot on the top surface of the barrier. Further, the predictive computer simulations had a similar behavior, in which the trailer pivoted around the front face of the barrier at a height of 54 in., but slid on top of the barrier surface at a height of 48 in. These behaviors were consistent with physical testing, and with few exceptions, simulation results indicated larger lateral and vertical extents of the TL-5 36000V vehicle.

Considerable uncertainty remains if the MASH TL-5 vehicle is representative of the worst-case impact conditions and ZOI estimates, or if full-scale testing of barriers with increased heights would indicate larger ZOI envelopes are necessary. Therefore, the limits presented in this study are recommended as “practical limits”, presented consistently with “practical worst-case” impact conditions selected for evaluating roadside hardware in MASH. The simulations of the TL-5 vehicle were therefore accepted based on trailer roll and ZOI predictions.

Due to the age and uncertainty of the large truck models, significant geometrical and stiffness differences between different truck makes, models, and production years, and minimal documentation available regarding damage to critical components including the fifth wheel, suspension structural components and attachments, ballast connections, and truck frame, it would be beneficial for an updated 36000V vehicle model to be developed which could improve confidence in results and take advantage of increases in computational power. Improved models of critical components would greatly increase confidence in output and could result in more accurate, predictive ZOI envelopes.

**Appendix G**

**Recommended Updates to the *Roadside Design Guide***
**G-1 RDG Section 5.5.2**

Appendix G is submitted for consideration by AASHTO to incorporate the research results in the next update of the *AASHTO Roadside Design Guide.*